Titre: Title:	Multi-Physics Modeling of Aerospace Composites Exposed to Fire
Auteur: Author:	Jean Langot
Date:	2020
Type:	Mémoire ou thèse / Dissertation or Thesis
Référence: Citation:	Langot, J. (2020). Multi-Physics Modeling of Aerospace Composites Exposed to Fire [Thèse de doctorat, Polytechnique Montréal]. PolyPublie. https://publications.polymtl.ca/5533/

POLYTECHNIQUE MONTRÉAL
affiliée à l'Université de Montréal

Multi-physics modeling of aerospace composites exposed to fire

JEAN LANGOT
Département de Génie Mécanique

Thèse présentée en vue de l'obtention du diplôme de *Philosophiæ Doctor*
Génie Mécanique

Novembre 2020

POLYTECHNIQUE MONTRÉAL
affiliée à l'Université de Montréal

Cette thèse intitulée :

Multi-physics modeling of aerospace composites exposed to fire

présentée par **Jean LANGOT**
en vue de l'obtention du diplôme de *Philosophiæ Doctor*
a été dûment acceptée par le jury d'examen constitué de :

Jean-Yves TRÉPANIER, président
Robert ÉTIENNE, membre et directeur de recherche
Martin LÉVESQUE, membre et codirecteur de recherche
Serge BOURBIGOT, membre
Nicholas DEMBSEY, membre externe

DEDICATION

Obtenir une thèse était un projet de vie qui me tenait à cœur. Non pas pour des raisons carriéristes, mais par passion pour la science. Je voulais apporter ma contribution, aussi modeste soit-elle, à l'édifice scientifique ; faire partie cette grande histoire des sciences, majoritairement constituée de graviers qui, empilés les uns sur les autres, forment une montagne. Cette thèse n'aurait jamais été un succès sans le support de mes directeurs de recherche, **Étienne Robert** et **Martin Lévesque**. Passionnés et passionnants, vous avez été capable de gérer brillamment le projet non seulement d'un point de vue technique, mais surtout humain ; ce qui, j'en suis convaincu, a permis de faire la différence dans les moments difficiles. En ce sens, vous représentez l'idéal de ce qu'un chef de projet doit être : un équilibre entre compétences rationnelles et émotionnelles. Je dois également beaucoup à mes collègues et amis des laboratoires LEMUR et LM2 de Polytechnique Montréal, tout particulièrement **Tanja Pelzmann**, **Pablo Chavez** et **Cristian Boanta**, pour leur aide dans mes travaux et pour leur joie de vivre qui a embelli mes années de doctorat.

Il faut aussi reconnaître les implications directes ou indirectes de mon entourage, de mes amis et de ma famille. Ma plus profonde gratitude revient tout d'abord à **Teddy Chapillon**, qui fut une véritable lanterne lors des périodes les plus sombres de cette dernière année. Je dois également beaucoup à l'indéfectible soutien que m'a apporté **Sophie Le Donne** dans la dernière ligne droite, ce qui m'a donné l'impulsion finale pour mener à bien mes travaux. Les parties de jeux vidéo et les apéros Skype avec les amis de toujours ont ensoleillé les périodes de confinement et de rédaction. Pour cela, je voudrais donc remercier **Matthieu Bardou**, **Gauthier Iung** ; ainsi que **Rémi Palandri**, avec qui j'avais d'une certaine façon démarré mon apprentissage en résistance au feu en tentant de fabriquer une fusée au chlorate de soude il y a une quinzaine d'années. Ma gratitude revient également et plus largement à toutes les belles personnes que j'ai rencontré ces dernières années, pour tous les bons moments passés ensemble et les discussions apaisantes : **Florence Nyssen**, **Thibault Draye**, **Laure Fossé**, **Chloé Mathelier**, **Marie Léger Saint-Jean**, **Nicolas Maignien** et bien d'autres. Mes excuses à ceux que je n'aurais injustement pas cité dans ce message, mais la place me manque et une thèse entière ne suffirait pas à reconnaître l'impact positif de chacun. Du côté de la famille, je souhaite remercier **Laure Leger** pour son support inébranlable, inconditionnel et intemporel. Je dois aussi reconnaître le rôle qu'ont joué **mes parents**, qui ont su m'enseigner la persévérance, qualité qui fut bien utile en cette fin de thèse. Et enfin, j'aimerais tout particulièrement remercier ma sœur **Marie Langot**, qui fut un modèle d'abnégation, de courage et de réussite tout au long de mes études.

ACKNOWLEDGEMENTS

I am grateful for the assistance and financial support from the Natural Sciences and Engineering Research Council of Canada (NSERC/CRSNG), through grant no. CRDPJ 478687-15, and the partners from CRIAQ ENV-708 project is acknowledged.

RÉSUMÉ

Les matériaux composites utilisés en aéronautique doivent réussir des tests de résistance au feu leur imposant de remplir leurs fonctions tout en étant exposé à une flamme durant un temps donné. Or, la combustion d'un matériau composite est un processus complexe impliquant l'interaction entre plusieurs phénomènes thermiques, chimiques et physiques. En particulier, certains phénomènes tel que l'inflammation des gaz issus de la pyrolyse du composite peuvent jouer un rôle crucial lors de sa dégradation. L'utilisation de modèles numériques permet d'étudier les différents processus agissant sur la dégradation du composite et d'aider au développement de nouveaux matériaux résistants au feu.

L'objectif de cette thèse est de modéliser la dégradation thermo-chimique d'un matériau composite exposé à une flamme. L'outil prédictif est composé de deux modèles couplés. Premièrement, un modèle thermo-chimique prédit la variation temporelle et spatiale de la température et de la densité du composite en fonction de ses propriétés et des conditions du test de résistance au feu. Ce modèle prend en compte les transferts de chaleur et les réactions chimiques dans l'épaisseur du composite. En particulier, plusieurs mécanismes de réactions chimiques sont proposés afin de modéliser la décomposition chimique de la phase solide en fonction de sa température. Les propriétés thermo-physiques du matériau sont mesurées lors d'expériences indépendantes afin d'être utilisées en tant que paramètres d'entrée dans le modèle. Ensuite, un modèle de cinétique chimique (Cantera) simule l'inflammation des gaz émis par les réactions chimiques en phase solide dans un environnement pauvre en oxygène. L'influence de cette source de chaleur supplémentaire sur la dégradation du matériau est étudiée. Le modèle global est validé à l'aide d'un test de feu à petite échelle, développé afin d'imiter les conditions rencontrées lors de tests de feu à plus grande échelle.

Le modèle numérique obtenu s'adapte à différentes conditions de test de feu et à différents matériaux. Il est capable de prédire l'évolution de la température du composite et le temps d'allumage de façon purement théorique, sans avoir recours à des paramètres empiriques propres à chaque test et matériau. En particulier, les résultats montrent que le flux de chaleur reçu par le matériau durant son inflammation est deux fois plus important que celui reçu du test de feu. Concernant la décomposition thermo-chimique du matériau, le mécanisme basés sur des réactions compétitives est le seul permettant de reproduire la masse résiduelle du matériau après exposition à de hautes températures, mais décrit la variation de masse avec moins de précision que les mécanismes basés sur des réactions consécutives ou parallèles.

ABSTRACT

Composites are widely used in the aerospace industry and must act as firewalls in some applications. Their flammability is assessed through standardized fire tests requiring the material to resist to a calibrated pilot flame during 15 minutes. The combustion of the composite is driven by the complex interactions of thermal, chemical and physical processes. In particular, the chemical degradation of the composite produces combustible gases that may ignite when they encounter the pilot flame, providing an additional heat source close to the surface and leading to the rapid destruction of the composite. Fire tests yield a pass or fail verdict but cannot provide insight of the phenomena at stake. The development of new numerical tools could help to understand the interactions of these complex phenomena and support the development of new fire resistant composites.

The objective of this thesis is to develop a multi-physics tool to predict the thermo-chemical degradation and ignition of a composite exposed to a pilot flame. An in-house pyrolysis model is developed to compute the material thermo-chemical degradation and coupled with a chemical kinetics software (Cantera) to model the gas-phase reactions. The solid-phase thermo-chemical model accounts for heat transfers, pyrolysis, oxidation and transport of mass through the composite thickness as a function of time. Several reaction schemes, including reactions of different nature (competitive, parallel, consecutive), are compared to model the solid-phase chemical reactions. The composite thermo-physical properties are measured through independent experiments and used as input parameters in the predictive tool. The model is validated against a small-scale test imitating the conditions encountered in large-scale fire tests.

The method developed here is versatile and does not depend on empirical parameters specific to the fire test conditions. The evolution of the backface temperature as a function of time and of the time-to-ignition for a composite exposed to fire are predicted with a good agreement. In particular, the simulations show that the heat flux received by the material approximately doubles when the pyrolysates ignite. The analysis of the thermo-chemical degradation showed that the schemes based on competitive reactions are the only models able to predict the variation of residual mass of the material exposed to heat as a function of the heating rate, but are less accurate than schemes based on parallel or consecutive reactions to represent the material mass loss rate.

TABLE OF CONTENTS

LIST OF TABLES

LIST OF FIGURES

LIST OF SYMBOLS AND ACRONYMS

1D	One Dimension
2D	Two Dimensions
3D	Three Dimensions
AC	Advisory Circular
CFD	Computational Fluid Dynamics
CS	Control Surface
CV	Control Volume
DSC	Differential Scanning Calorimetry
EASA	European Aircraft Safety Agency
FAA	Federal Aviation Administration
FDM	Finite Difference Method
FDS	Fire Dynamics Simulator
FEM	Finite Element Method
FTIR	Fourier Transform Infrared spectroscopy
FVM	Finite Volume Method
HRR	Heat Release Rate
ICAO	International Civil Aviation Organization
ISO	International Organization for Standardization
LIFT	Lateral Ignition and Flame Spread Test
MCC	Microscale Combustion Calorimeter
MS	Mass Spectrometer
OOA	Out-Of-Autoclave
PAN	Polyacrylonitrile
PEKK	Polyether-Ketone-Ketone
PMC	Advanced Polymer Matrix Composites
PPS	Polyphenylene Sulfide
SLPM	Standard Liter Per Minute
TGA	Thermogravimetric Analysis
TTI	Time-To-Ignition
XFA/LFA	Xenon/Laser Flash Analysis

LIST OF APPENDICES

Nomenclature

Greek Symbols

α Degradation degree $(-)$

β **Chapter 4**: intensive variable associated to the extensive variable B, for instance density ρ $(\mathrm{kg\,m^{-3}})$, specific enthalpy h $(\mathrm{J\,kg^{-1}})$. The unit depends on the application and is always expressed per unit mass.
Chapter 5: heating rate $(\mathrm{K\,min^{-1}})$

$\dot{\omega}_i$ Molar production rate of species i $(\mathrm{mol\,m^{-3}\,s^{-1}})$

ϵ Emissivity $(-)$

Γ_β Parameter associated to the flux $\underline{\boldsymbol{j}_\beta}$, which represents the capacity of a medium to transport β. For instance, Γ_β can be the thermal conductivity λ $(\mathrm{W\,m\,K^{-1}})$ or diffusion coefficient D $(\mathrm{m^2\,s^{-1}})$

κ Permeability $(\mathrm{m^2})$

Λ Pressure eigenvalue $(\mathrm{Pa\,m^{-2}})$

λ Thermal conductivity $(\mathrm{W\,m^{-1}\,K^{-1}})$

μ Dynamic viscosity $(\mathrm{Pa\,s^{-1}})$

ν Kinematic viscosity $(\mathrm{kg\,m^{-1}\,s^{-1}})$

Ω^e Finite element in the finite element method

ϕ Porosity $(\mathrm{m^3/m^3})$

ψ Approximation function used in Finite Element Method

ρ Density $(\mathrm{kg\,m^3})$

σ Stefan-Boltzmann constant $(\mathrm{W\,m^{-2}\,K^{-4}})$

Θ Parameter indicating the type of time differentiation method used in Finite Element Method $(-)$

θ Stoichiometric coefficient $(-)$

$\underline{\boldsymbol{\nabla}}$ Vector differential operator: $\underline{\boldsymbol{\nabla}} = \left(\frac{\partial}{\partial x_1}, ..., \frac{\partial}{\partial x_n}\right)$

Letters

$\dot{m}_g$ Mass flow rate of gaseous species ($\mathrm{kg\,m^{-2}\,s^{-1}}$)

$\mathbb{P}_i$ Material property. The unit depends on the application

$\underline{\underline{\boldsymbol{C}}}$ Element capacitance matrix

$\underline{\underline{\boldsymbol{K}}}$ Element coefficient matrix

$\underline{\boldsymbol{j}}_\beta$ Flux associated to the intensive variable β, for instance diffusion flux ($\mathrm{mol\,m^{-2}\,s^{-1}}$) or heat flux ($\mathrm{J\,m^{-2}\,s^{-1}}$)

$\underline{\boldsymbol{n}}$ Vector normal to a control surface ($-$)

A Pre-exponential factor ($\mathrm{s^{-1}}$)

a Acceleration ($\mathrm{m\,s^{-2}}$)

B Extensive variable describing a mass system, for instance mass m (kg), energy U (J), quantity of movement mv ($\mathrm{kg\,m\,s^{-1}}$)

C Constant used in polynomial interpolation or empirical formulas. The unit depends on the application

c_p Heat capacity ($\mathrm{J\,kg^{-1}\,K^{-1}}$)

D Diffusivity ($\mathrm{m^2\,s^{-1}}$)

E Activation energy ($\mathrm{J\,mol^{-1}}$)

F Force (N)

H Enthalpy (J)

h Specific enthalpy ($\mathrm{J\,kg^{-1}}$)

h_c Convection coefficient. The unit depends on the application

k Rate constant ($\mathrm{kg\,m^{-3}\,s^{-1}}$)

L Total thickness of the sample (m)

l Length of one element in the finite element method (m)

M Molecular mass ($\mathrm{kg\,mol^{-1}}$)

m Mass (kg)

N Total number of entities (homogeneous porous media) in the sample ($-$)

n Order of reaction ($-$)

N_e Total number of elements in the mesh ($-$)

N_g Total number of gaseous phases in the sample ($-$)

N_r Total number of chemical reactions ($-$)

N_s Total number of solid phases in the sample ($-$)

P Pressure (Pa)

Q Heat (J)

q Heat of reaction ($\mathrm{J\,kg^{-1}}$)

R Perfect gas constant ($\mathrm{J\,mol^{-1}\,K^{-1}}$)

R^2 Coefficient of determination ($-$)

S Surface ($\mathrm{m^2}$)

S_β Source term associated to the intensive variable β. The unit depends on the application, for instance mass production ($\mathrm{kg\,m^{-3}\,s^{-1}}$) or energy production ($\mathrm{J\,m^{-3}\,s^{-1}}$)

S_i Species involved in a chemical reaction

T Temperature (K)

t Time (s)

U Energy (J)

u,v Velocities ($\mathrm{m\,s^{-1}}$)

V **Chapter 4**: volume ($\mathrm{m^3}$)
Chapter 6: scaled radial velocity ($\mathrm{s^{-1}}$)

W Work (J)

W_F Weighting factor $(-)$

X Volume fraction (m^3/m^3)

x Space (m)

Y Mass fraction (kg/kg)

Subscripts

b Burner

bl Boundary layer

ch Char

$cold$ Cold face

exp Experimental

f Fibers

$flame$ Burner

g Gas phase

hot Hot face

i Entity i

ig Gas phase composing entity i

is Solid phase composing entity i

j Reaction j

m Matrix

num Numerical

pyr Pyrolysates

s Solid phase

tot Total

v Virgin

Superscripts

a	Approximation
e	Element e
T	Transpose

CHAPTER 1 INTRODUCTION

1.1 The use of composites in aerospace: an environmental and economical issue

Air pollution causes health and environmental damages and is nowadays a worldwide and ongoing challenge for humanity. In particular, the exposition to fine particle matters (diameter ≤ 2.5 μm) and O_3 from all ambient air pollution causes every year the loss of 8.8 million lives due to cardiovascular and respiratory diseases, which represents a global loss of life expectancy of 2.9 years per person, with 1.1 years due to fossil fuel emissions only [1]. Assuming that aircraft transport produces approximately 1% of surface O_3 and fine particle matters [2,3], 88000 deaths per year are attributable to aircraft emissions. Fuel consumption being directly related to the aircraft weight, approximately 3275 deaths could be avoided during the next decade for every reduction of 1% of mass of the aircraft in circulation (the details of the calculation are given in Appendix A). Moreover, aircraft also emit greenhouse gases such as CO_2 (2.4% of all human-induced emissions [4]) and therefore contributes to global warming, whose effects on human health are harder to quantify. Besides the environmental consequences of fossil fuel use for air transport, economic incentives are also pushing for decreasing use. The price of kerosene-type jet fuel used in aerospace increased from 18$/barrel in 1977 to 103$/barrel in 2019 [5]. This represents an augmentation of 472%, much more than the total inflation of the US dollar of 327% observed during the same period [6]. Knowing that fuel represents in average 40% of the direct operating costs of a flight and 22% of the total costs including advertisement, administration, etc, the reduction of specific fuel consumption could greatly improve the profitability of aircraft transport.

Technological innovations in the aeronautic sector during the last century concerned mainly the propulsion and aerodynamic efficiency. The reduction of the aircraft weight benefited from an important technology leap with the development of all-aluminum aircraft in the 1930's, but did not evolve significantly in the following decades because of the lack of lighter alternatives to aluminum alloys, until the recent development of composites [7]. A composite is a combination of at least two non-miscible materials, usually a matrix and a reinforcement (classical combinations of composites are introduced in Appendix B). The mechanical properties and density of composite materials and metal alloys are compared in Table 1.1. In general, their mass Young's modulus and tensile strength are much better than metal alloys, giving them a significant advantage in applications requiring light weight and good mechanical properties, such as aerospace. Since 1970, the proportion of composite materials in aircraft structural weight has exponentially increased from 5% for an A300 in 1972 to more

Properties	Metal alloys			Composites		
	Steel 35 NCD 16	Aluminum AU 4 SG	Titanium TA 6V	Carbon/epoxy	Glass/epoxy	Bore/aluminum
Density ρ ($\mathrm{g\,cm^{-3}}$)	7.9	2.8	4.45	1.5	2	2.7
Young Modulus E (GPa)	200	72	110	130	53	230
Mass Young Modulus $E/(\rho g)$ (km)	2500	2600	2500	8700	2650	8500
Tensile strength σ_m (MPa)	1850	500	1000	1000-1300	1800-2000	1250-1800
Mass tensile strength $\sigma_m/(\rho g)$ (km)	24	18	23	65-85	90-100	45-65

Table 1.1 Comparison of composite materials and metal alloys in terms of mechanical properties and weight. Table adapted from [8].

than 40% for an A350 in 2010 (Figure 1.1) from [9]. This trend is likely to continue in the coming years due to the constant design of new combinations of matrix and reinforcement. Figure 1.2 from [10] shows that a modern aircraft such as an A350 is nowadays a hybrid structure composed mostly of composite materials for the fuselage and metal allows in critical locations, such as the engine nacelles. In particular, carbon fibers reinforced composites occupy an important part of the fuselage. This composite has a good resistance to fatigue and corrosion and a light weight, but suffer from thermal decomposition at high temperature. Their is therefore a need to understand and circumvent their flammability limitations to reinforce the security of aircraft in case of fire.

1.2 The challenge of fire safety in the aerospace industry

1.2.1 Aircraft fires

According to the Federal Aviation Administration (FAA) [11], "*approximately twenty percent of the 1153 fatalities on U.S. transport airlines between 1981-1990 were caused by fire*". The number of casualties is expected to increase in the coming decade because of traffic growth. Most aircraft fires fall in three categories: ramp, inflight and post-crash fires [11]. Occurring when the aircraft is parked, ramp fires can be rapidly controlled and result only rarely in the loss of human lives, although some costly accidents have been reported. In 1985, the explosion of an engine before take off on a Boeing 737 operated by British Airtours (flight KT28M) trapped the passengers inside the plane as the fire spread rapidly to kerosene tanks and caused the loss of 55 lives among the 137 passengers, most of the deaths being due to smoke inhalation (Figure 1.3a). In-flight fires are significantly more problematic, particularly when they appear in inaccessible areas for the crew such as engines or fuselage. An aircraft can rapidly become uncontrollable once the engines or other critical systems are reached. These

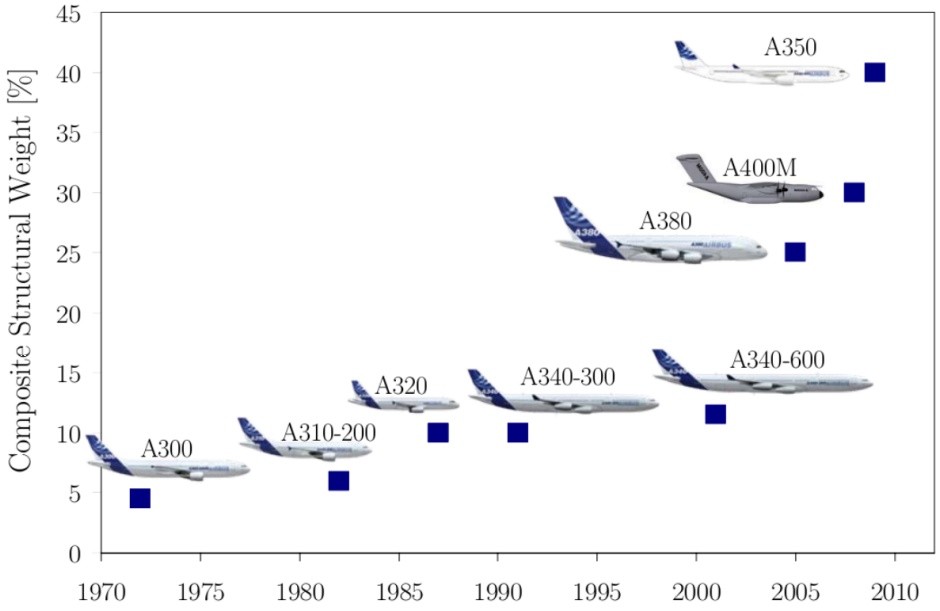

Figure 1.1 Composite structural weight over the last decades in Airbus planes [9].

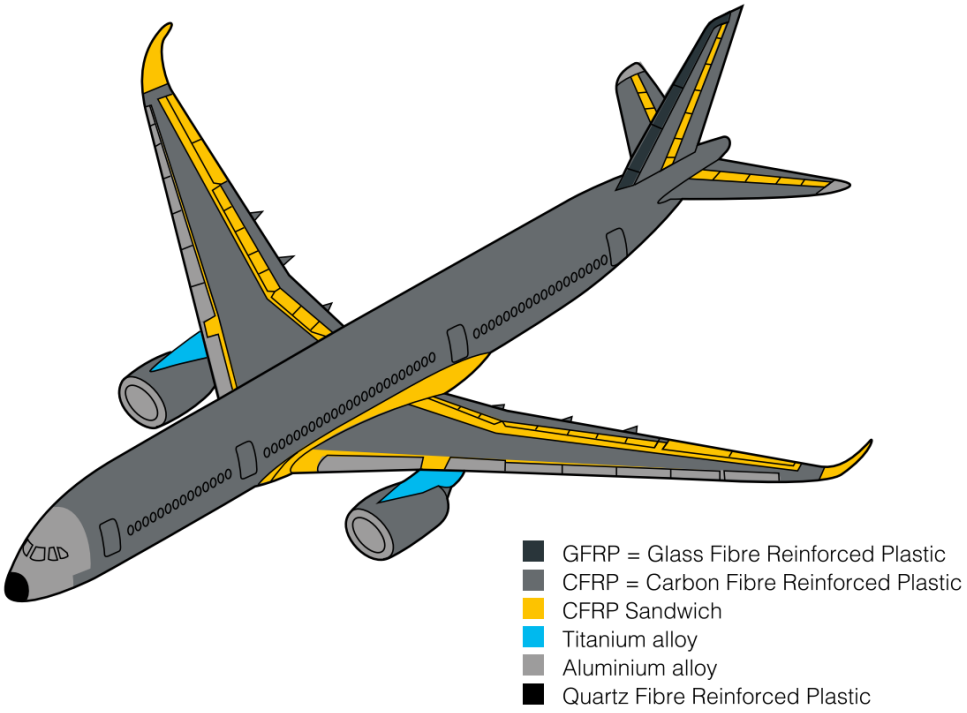

Figure 1.2 Materials composing an Airbus A350 [10].

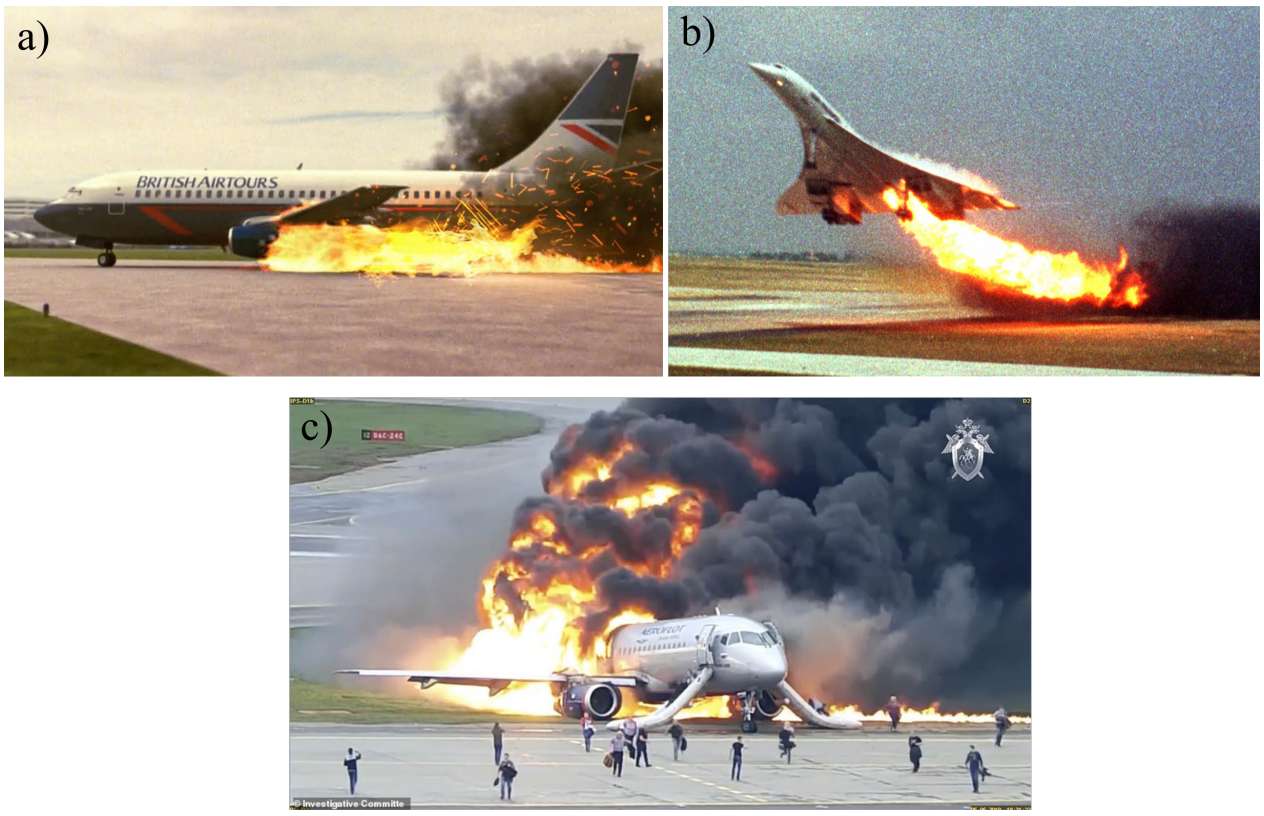

Figure 1.3 a) Boeing 737 operated by british Airtours (flight 28M) being victim of a fire before take-off. b) Concorde operated by Air France (flight 4590) being victim of a fire during take-off. c) Sukhoi RRJ-95B operated by Aeroflot being victim of a post crash fire.

fire are typically caused by short-circuit in an electrical system or overheated equipment, but can also be induced by external events very difficult to prevent. In 2000, a Concorde operated by Air France (flight 4590) ran over debris on the runway during takeoff (Figure 1.3b). The debris was projected into the fuel tank and damaged it, provoking a fire that rapidly spread to the landing gears and engines. The reduction of thrust and additional drag caused by the non-retracted gear led to the loss of control of the plane who crashed shortly after, killing all the passengers (113 persons). In total, in-flight fires have caused the loss of 339 lives between 1992 and 2001, becoming the fifth source of fatalities in aircraft accidents behind loss of control (2371 deaths), controlled flight into terrain (2152 deaths), unknown reasons (651 deaths) and mid-air collisions (506 deaths) [12]. Finally, post-crash fires are involved in the majority of death by fire; 40% of the passengers who survived an airplane crash subsequently die in the post-crash fire [11], mostly because of the inhalation of toxic smoke emitted by fuel combustion or the burning of combustible materials such as seat cushions. For instance, on 5 May 2019, the remaining fuel of a Sukhoi RRJ-95B operated by Aeroflot ignited after a failed landing, and the fire spread rapidly to the fuselage of the plane (Figure 1.3c). An emergency evacuation saved 32 passengers among the 73 occupants. In many aircraft accidents leading to uncontrollable fire, the time available to evacuation seems to be a critical factor and is directly correlated to the combustion rate of the material burning within the aircraft.

1.2.2 The fire certification in aerospace

An aircraft needs a certification specification to be allowed to fly, that must be verified every time its design is changed. The parts located in designated fire zones must meet requirements for the heat release rate, flame spread and burning rate, among others [13]. Most of the time, the certification requirement is assessed through standardized tests verifying if the materials are able to fulfill their functions when exposed to a fire environment during a defined period of time. The tests consist in exposing the material under evaluation to a pilot flame or radiant heater with variable conditions, depending on its function and location in the aircraft. The standards are defined by national/transnational organisations such as the FAA in the United States or EASA in Europe (European Union Aircraft Safety Agency), under the guidance of the ICAO (International Civil Aviation Organization). In particular, the FAA mandated the development of materials with improved fire resistance in 1987, with the objective of providing an additional $2-4$ minutes for evacuation in case of fire [11].
Figure 1.4 represents the acoustic liner investigated in this study, composed of a honeycomb core between two skins, both made of organic matrix composites. Its emplacement in the engine is showed in Figure 1.5. This panel is used in the inner part of the bypass duct and separates the bypass air flow from the technical compartment of the engine, where fuel and

oil are routed. Due to its location, this component must first act as an acoustic liner to damp the noise from the engine in operation. This is achieved with the honeycomb core and the perforated inner skin, which form a Helmholtz resonator and attenuates the sound. Moreover, the sandwich panel must also act as a firewall to prevent an external flame from spreading inside the engine and compromise its function. The bypass duct is indeed close to the nacelle and fuel handling system, whose ignition could create a fire propagating to the engine. In case of fire, the outer skin absorbs heat and loses rapidly its structural abilities, despite the convective cooling provided by the bypass flow. Under these conditions, the outer skin is unable to resist the static pressure imposed by the internal flow and tensile rupture of the fibers occurs rapidly.

The fire resistance of firewalls is assessed through standardized fire tests, according to Advisory Circular AC 20-135 [14] or the ISO 2685 standards [15]. These specify that the component must be able to perform its function when exposed to a 1366 K average flame temperature providing a 116 ± 10 kW m^{-2} heat flux for a minimum of 15 minutes, while withstanding the static pressure from the inside of the bypass duct (0.7 bar) for the first 5 minutes of the test. A kerosene burner is used to provide the pilot flame [16], whose temperature and heat flux are respectively calibrated with a thermocouple rake and a calorimeter.

The fireproofing strategies currently implemented often consist in thermal blankets, structurally integrated fire blankets or increased outer skin thickness. Each of these strategies is able to meet the fire test requirements but at the price of an additional weight, which increases the aircraft fuel consumption. The fire performance of the outer skin could also be improved while optimizing its weight by using different combinations of matrix and fibers and/or modify the matrix with the addition of inert fillers or fire retardant [17]. A better understanding of the fire behavior of composite materials is necessary to support the development of such new fire-resistant composites.

1.3 Objectives

The certification tests are expensive and consequently, aircraft engine manufacturer would like to perform a minimal number of them. Moreover, they yield only a pass/fail verdict, providing no information on the combustion process itself. However, a better understanding of the flammability of composites is essential to accelerate the development process of new parts reducing fire spread in critical applications, such as engine [11]. The use of numerical simulations to predict the decomposition of the material exposed to fire can significantly reduce the number of tests necessary to validate a new concept. It can also help to identify the key physical processes leading to composite decomposition and therefore support the

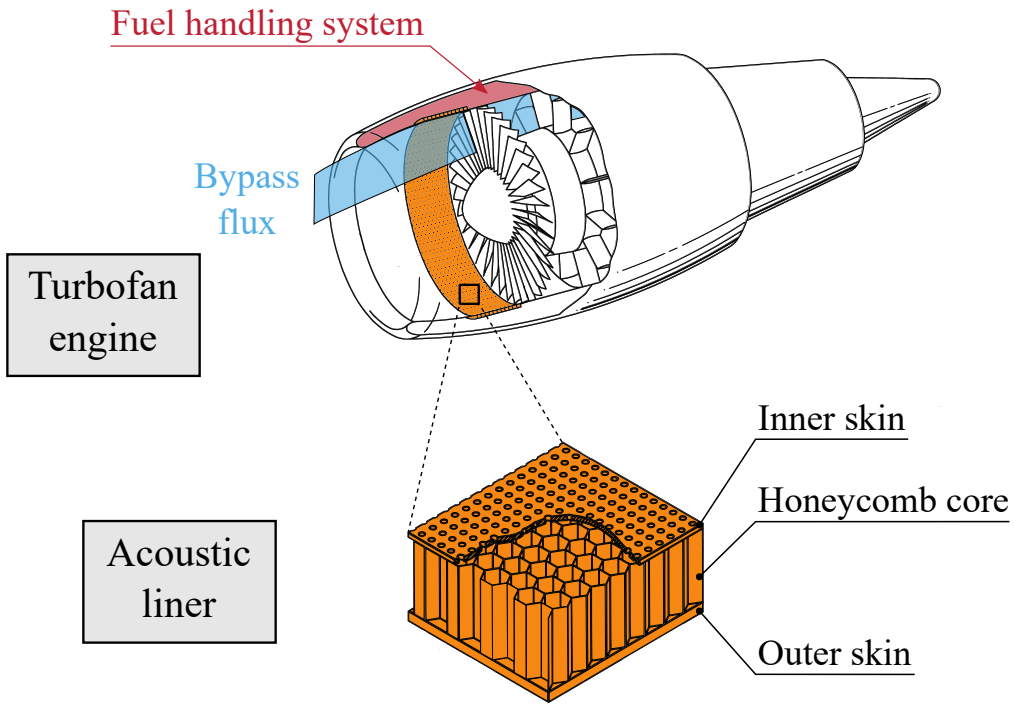

Figure 1.4 Honeycomb structure used as acoustic liner in turbofan engines.

development of new fire-resistant materials. Considering the number of physical, chemical and thermal processes involved simultaneously and interacting with each other during the composite thermal response, a multi-physics analysis is necessary to predict the behavior of such materials exposed to fire.

This study is part of a larger project whose overall objective is to investigate the behavior of composites exposed to a pilot flame in order to improve their fire resistance. This research project focuses on polymer matrix composite sandwich panels used as acoustics liners in the fan cases and bypass ducts of turbofan aircraft engines, as illustrated schematically in Figure 1.4. Several academic and industrial partners are involved and their contribution consists in identifying and testing candidate materials in small-scale experiments imitating the conditions encountered in a fire test. The research proposed here aims at developing a **multi-physics modeling of the fire test**. This predictive tool is intended to determine the time-dependent decomposition rate of the composite panel as a function of the fire test conditions and of the material properties. The gas-phase chemical reactions, heat transfer through the composite and chemical decomposition of the solid phases must be considered.

This thesis is divided as follow. First, Chapter 2 presents a literature review focused on the numerical modeling of composite fire resistance. A critical discussion of the literature review and the specific objectives of the thesis are introduced in Chapter 3. The mathematical and

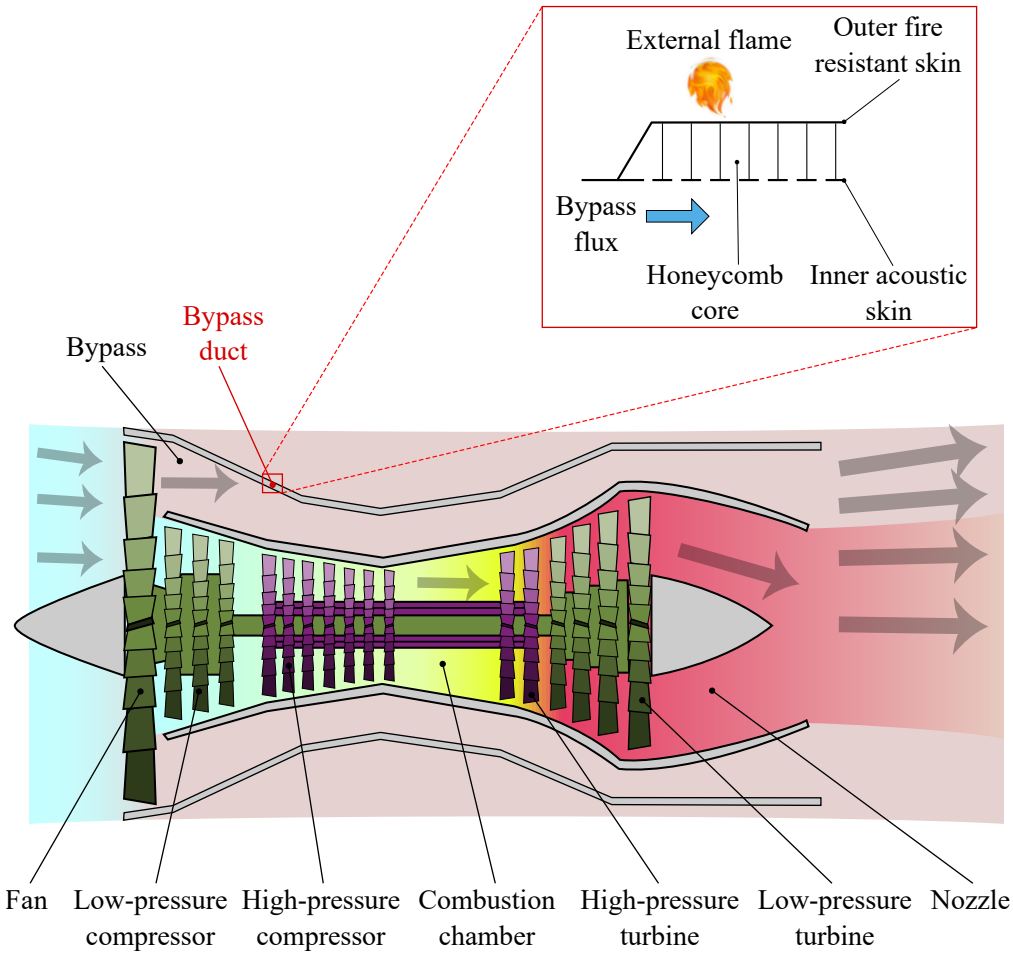

Figure 1.5 Localisation of the sandwich panel used as acoustic liner in the turbofan engine.

numerical developments of the solid phase model are presented in Chapter 4. The chemical decomposition of the material is described in Chapter 5. Finally, a carbon-epoxy composite is fully characterized and simulated in the context of a small-scale fire test in Chapter 6.

CHAPTER 2 LITERATURE REVIEW

2.1 Physics of composites combustion

Some composites start to decompose above 100 °C and release heat, smoke and gaseous products which can be toxic for humans [18]. The FAA estimated that the number of casualties caused by fire in aircraft accidents will grow every year by 4% because of the expected traffic growth, on one hand [19], and by another 1% because of the increasing part of lightweight and combustible materials in aircraft, on the other hand [11]. A number of literature reviews have been dedicated to the combustion of composites [20–25]. The term *combustion* here refers to the chain of processes that convert fuel into combustion products. Composite combustion involves thermal, chemical and physical processes in close interaction, that are represented in Figure 2.1 and explained with more details in the following.

2.1.1 Heat transfer from the pilot flame to the material

The heat is transmitted from the pilot flame through four different types of heat transfer: convection, thermochemical heat release, radiation and water vapor condensation [26]. The importance of the radiative heat transfer depends, among other factors, on the amount of soot produced by the flame. However, in the absence of a furnace enclosure, convection is expected to represent $70 - 90\%$ of the total heat transfer for flames up to 1700 K [27].
An impinging gas jet configuration, such as a pilot flame impinging a sample, is known to lead to high heat transfer and plays thus an important role in industrial applications [28]. However, in fire tests it results in a non-uniform convective heat transfer over the composite's surface, depending among other parameters on the flame geometry. Figure 2.2 represents the different flow regions typically considered in the analysis of impinging gas jets (here for a round nozzle) [29]:

The free jet region: the flow is most of the times turbulent in this area. The flow exchanges momentum with the surrounding environment, leading to the linear expansion of its boundaries. Although the overall flow decelerates in the free jet region, the axial velocity of the flow along the flame axis is constant in the *core length*. The length of the core depends on the turbulence level at the nozzle exit [30] and is typically on the order of four times the nozzle diameter on average [28].

The impingement region: the proximity of the solid surface causes the divergence of the streamlines away from the jet centerline. The flow decelerates when getting closer to

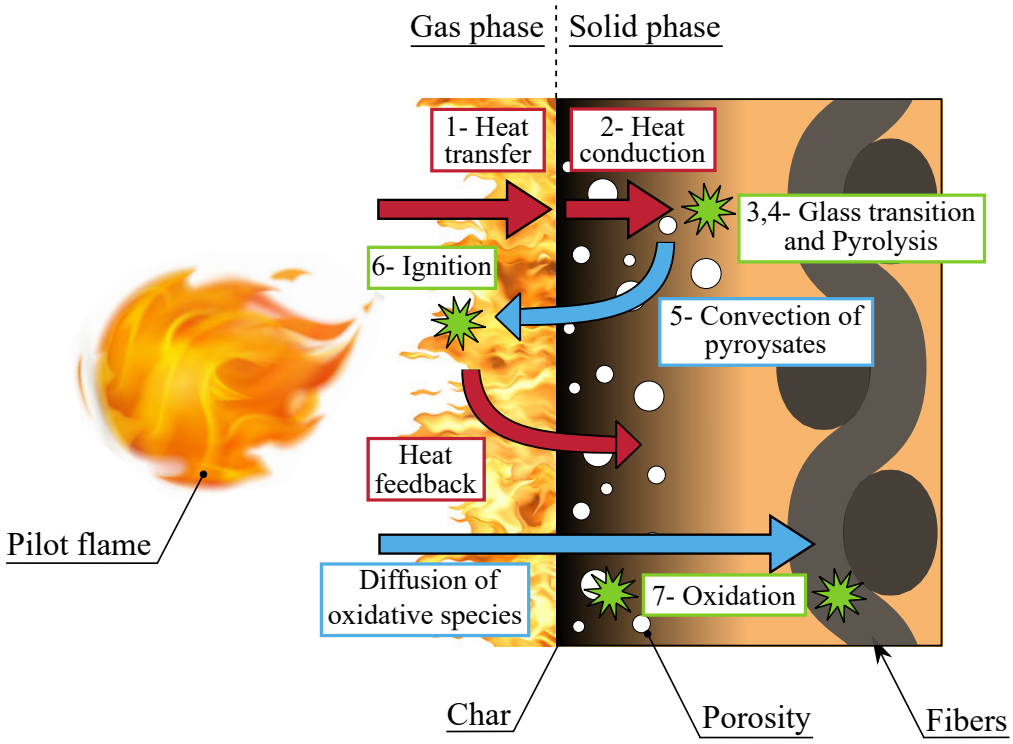

Figure 2.1 Thermal, chemical and physical processes encountered in composite combustion. Heat transfers are depicted in red ( ), mass transfers in blue ( ) and chemical reactions or phase change in green ( ). The virgin polymer matrix is depicted in orange ( ).

the stagnation point and accelerates when moving in the transverse direction [29]. The boundary layer has a relatively constant thickness (approximately 1% of the diameter [31]) and the flow is laminar in this region because of the stabilizing effect caused by the accelerating flow [30]. The width of the stagnation region is approximately 1.2 times the nozzle diameter [28].

The wall jet: the accelerated and laminar stagnation flow converts into a decelerated and turbulent flow in the wall jet region, parallel to the solid surface. The minimum thickness of this region is typically within 0.75-3 nozzle diameters and increases continually with the radius when going away from the impingement point [31].

The distribution of the convective heat flux over the material surface depends on the shape of the nozzle, its dimensions, the surface roughness and the radial distance from the stagnation point. In particular, the nozzle-to-sample distance appears to have an important influence [30]. Figure 2.3 from [30] represents the distribution of the local Nusselt number on a solid surface as a function of the dimensionless radial position. As a reminder, the convective heat transfer is directly proportional to the Nusselt number. If the core length is fully developed before the flame impinges the surface (approximately $H/D > 4$), the convective heat flux is maximum at the stagnation point and decreases monotonically thereafter [30]. However, if the core length is not fully developed, the convective heat transfer is maximum at the laminar-turbulent transition, some radial distance from the stagnation point. The heat transfer at different locations on the surface can be estimated with correlations [28, 30, 32], semi-analytical solutions [26] or CFD [33–37].

2.1.2 Heat conduction within the material

The heat propagates through the composite mainly by anisotropic heat conduction. In transient regimes, this phenomena is controlled by the composite thermal diffusivity, which is computed with its thermal conductivity, heat capacity and density. At constant temperature, the composite thermal conductivity is affected by moisture content, delamination, density, porosity, radiation across the porosity, microstructure and more generally by the composite manufacturing process. The imperfect bonding between matrix and reinforcement also adds a thermal resistance. Moreover, the geometry of the composite material and particularly the orientation of fibers with respect to the direction of heat transfer greatly affect the global thermal conductivity (and also the permeability, radiative absorption and Young's modulus). The matrix conductivity also increases with its crystallinity [38]. Lower and upper bonds of the thermal conductivity of the composite can be estimated from each phase

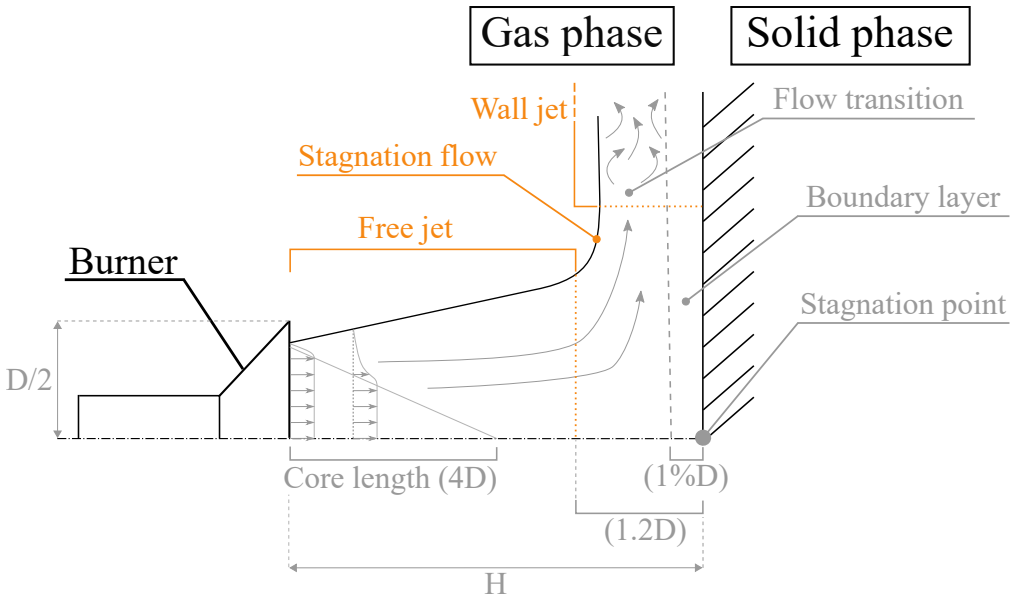

Figure 2.2 Geometry of an impinging gas jet.

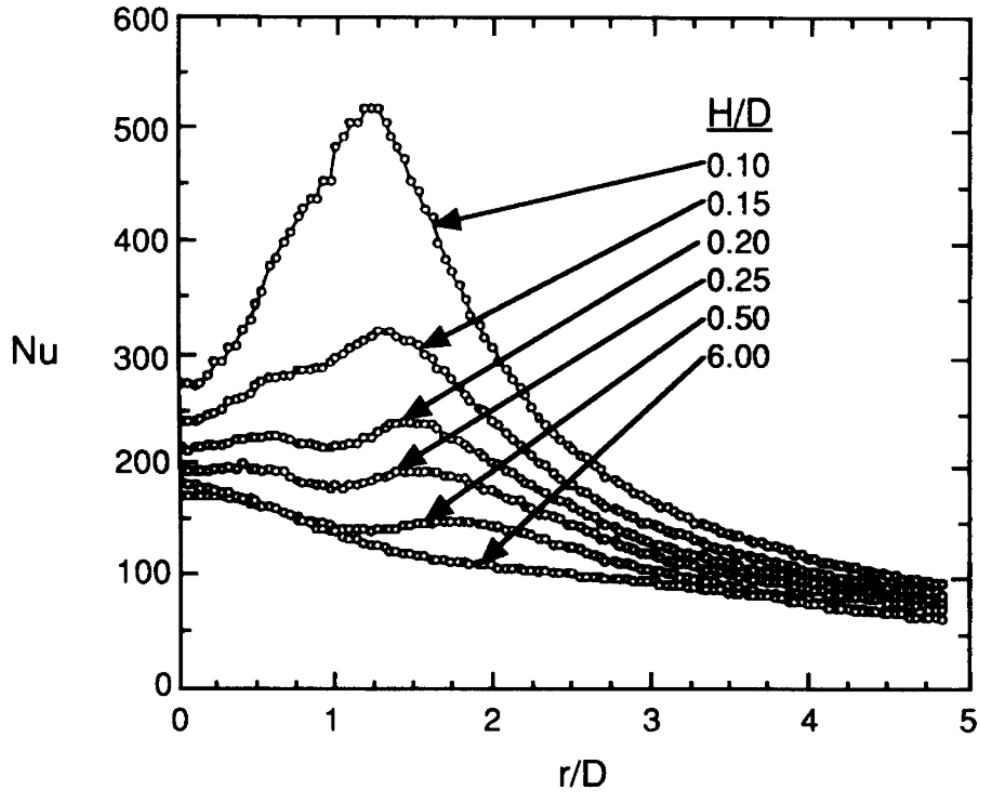

Figure 2.3 Radial variation of the local Nusselt number from the stagnation point in an impinging gas jet configuration (from [30]).

thermal conductivity with the Voigt and Reuss models. Other relations provide a better estimation, depending on the composite structure [39–41].
The thermal conductivity of the composite varies also as a function of temperature. First, because all the phase properties are temperature dependent. Then, because of chemical reactions occurring in the composite exposed to heat. As a result, the composite thermal conductivity may vary smoothly and monotonically in some temperature range but changes abruptly when chemical reactions occur with phase transitions. For instance, Figure 2.4a) from [23, 42] represents the variation of thermal conductivity of a glass/epoxy composite exposed to heat. First, the thermal conductivity increases with temperature and drops when a chemical reaction occurs around 300 C, then it increases again. The temperature dependence of each property can be measured experimentally and approximated using polynomial equations [43], typically of order 3 or 4 [23].

2.1.3 Matrix glass transition

The glass transition is a reversible transformation occurring in amorphous resins exposed to high temperatures, changing their solid and glassy state into a viscous and rubbery state. The matrix mechanical properties such as elastic modulus or strength are severely decreased, even if chemical reactions have not started yet. Figure 2.4b) from [18] shows a typical variation of a composite mechanical properties during glass transition. The glass transition temperature T_g is typically on the order of 350 K for epoxies [18].

2.1.4 Matrix pyrolysis

The term *pyrolysis* refers the thermal decomposition of an organic solid phase without the presence of oxygen. During pyrolysis, the molecules composing the solid are broken into smaller molecules through a very complex mechanism involving hundreds of intermediate reactions. Pyrolysis produces gas (pyrolysates), liquid (tar) and solid (char). In a fire resistance test, the decomposition of the matrix begins on the external surface once a critical temperature is reached. This temperature depends on the matrix composition and usually ranges from 500 to 700 K for polymer matrices [44]. Figure 2.5 from [23] shows a partially burned composite. A decomposition zone forms and progresses inside the material toward the cold face. The production of char increases the matrix porosity and results in a rise of the internal pressure because of the storage of gas in the pores. The increase in pressure can locally reach up to 15 times the atmospheric pressure for a phenolic matrix composite [45], which is sufficient to cause matrix-fiber debonding, delamination and matrix cracking [18]. The char contains a higher proportion of carbon than the original polymer (approximately 85 to 95%)

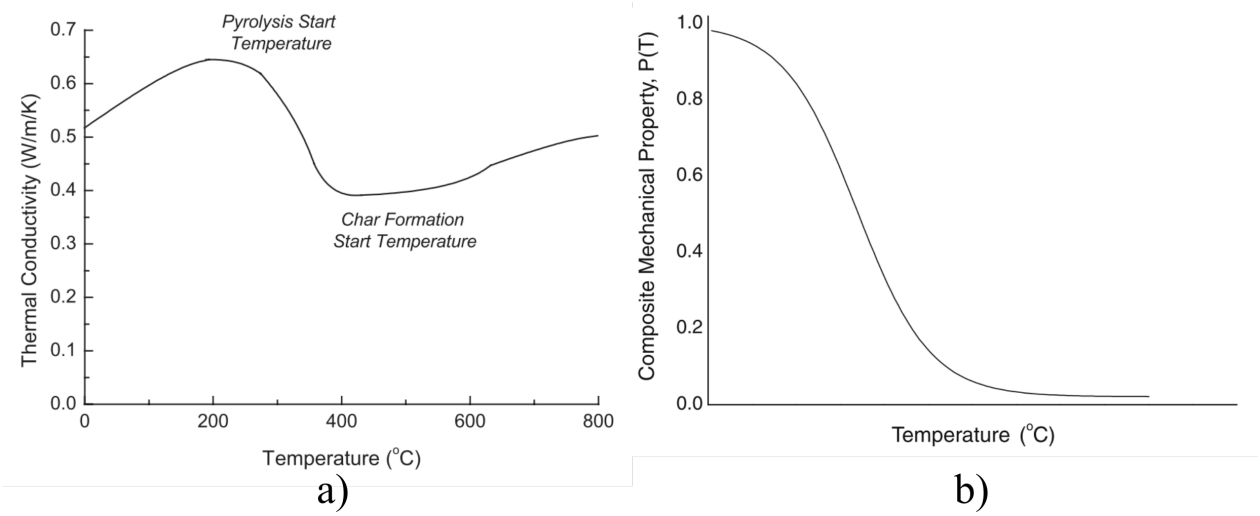

Figure 2.4 a) Through-thickness thermal conductivity of a glass/epoxy composite as a function of temperature (from [23,42]). b) Typical variation of a composite mechanical properties with an increasing temperature, because of the polymer matrix glass transition (from [18]).

in its crystalline or amorphous state, with traces of aromatic (molecules containing one or more rings of 6 carbon atoms) or aliphatic compouds [23]. The chemical process leading to char formation depends on the nature of the virgin matrix. In thermosets, random chain scissions fragment the molecular structure of the polymer, yielding very small quantities of char. Polyester, vynil esters and epoxies resin lose hydrogen atoms because of random chain scission, end-chain scission and chain stripping reactions, producing $5-20\%$ of char. Finally, polymers having a high proportion of aromatic rings produces higher quantities of char, up to $40-60\%$ for phenolic resins for instance. Figure 2.6 shows the linear relation existing between content of aromatic rings in polymers and the quantity of char formed. As the char is highly porous, its thermal diffusivity is low and having a high char yield contributes to reduce heat transfer to the remaining virgin material located further from the flame. Controlling and increasing char formation is therefore an important strategy in the development of new fire-resistant materials, such as those relying on intumescence (the formation of an expanding char layer). Moreover, pyrolysis consists mostly of endothermic reactions, which absorb energy from the pilot flame and therefore slows again the heat propagation in the material. Because of the combination of pyrolysis endothermicity and the formation of a low-diffusivity char layer, understanding pyrolysis is very important for the development of new fire-resistant materials. Pyrolysis kinetics can be modeled with the Arrhenius law, which in this case is often formulated to provide the variation of the density of the solid material as a function of temperature [46]. The parameters involved in the Arrhenius law, such as the

activation energy and the pre-exponential factor, can be measured with Thermogravimetric Analysis (TGA) using so-called *isoconversional methods* [47]. These methods rely on measuring the variation of mass as a function of temperature. Even if the global chemical process involves hundreds of reactions and intermediate species, it is most of the times simplified as a one-step, global reaction, in which the matrix decomposes into char and gas. However, multi-steps mechanisms can be necessary in several situations: (i) if TGA data reveals the presence of shoulders or inflexions in the curves depicting the variation of mass as a function of temperature, hinting at the presence of more than one major reaction; (ii) if the activation energy varies with the degree of material decomposition; (iii) if a microscopy analysis reveals the presence of several phases degrading independently [48]. The number and nature of reactions is then chosen to obtain the best fit against TGA data. A significant part of the present work addresses this critical issue and is presented in Chapter 5.

2.1.5 Convection of hot gases

If the connectivity of the pore network allows it, the gas produced by pyrolysis reactions migrates from the inside of the material toward the environment because of pressure gradients. Most of the time, these volatile species are forced to flow toward the heated side due to the higher permeability in this direction. As gas flows through the solid, heat is transferred from the solid to the gas and evacuated in the environment, causing a cooling effect and again slowing heat propagation [50]. If the permeability is too low, the exhaust gases are blocked within the composite and cannot escape, resulting in an important swelling. Hot volatile species can also migrate toward the cold side and condense in the virgin solid, modifying its properties before pyrolysis occurs. Moreover, the presence of hot volatiles within the virgin solid increases the solid temperature and favors flame spread [50]. The permeability of the matrix depends mainly on its state of decomposition, but also on the chemical structure of the polymer, its morphology, density and cristallinity [25].

2.1.6 Ignition of the material

The pyrolysate composition depends on the nature of the matrix but contains most of the times highly reactive species such as H_2 (59.4% and 19.9% for phenolic [51] and epoxy [52] pyrolysis, respectively) and CH_4 (14.9% and 1.9% for phenolic [51] and epoxy [53] pyrolysis, respectively). When the combustible pyrolysates encounter an oxidative atmosphere (for example containing O_2), they form a fuel-oxidizer mixture. The behavior of an explosive mixture is ruled by the following chemical reactions, where R, P and C indicate respectively the Reactants, stable Products and Chain carriers like radicals, and n and a are two integers:

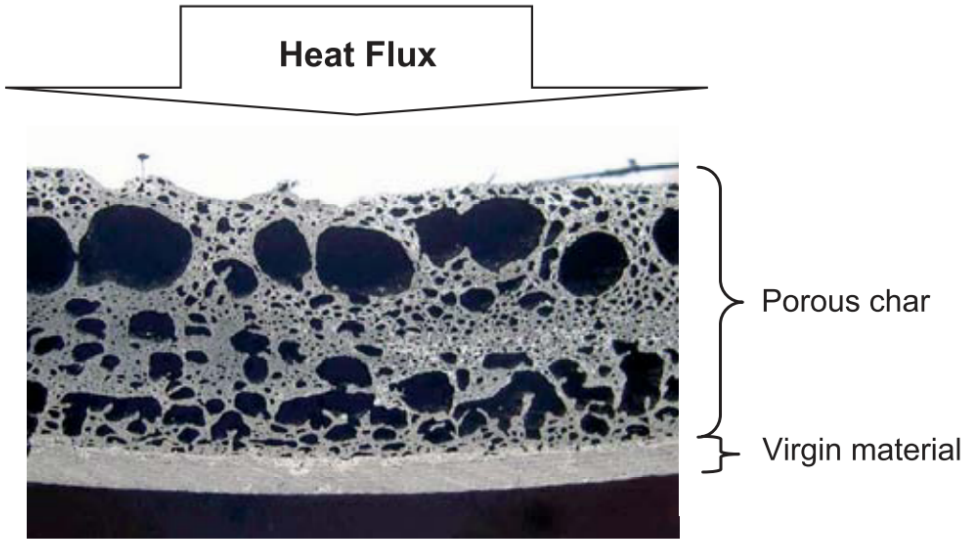

Figure 2.5 Section of a carbon/epoxy composite exposed to a heat source (from [23]).

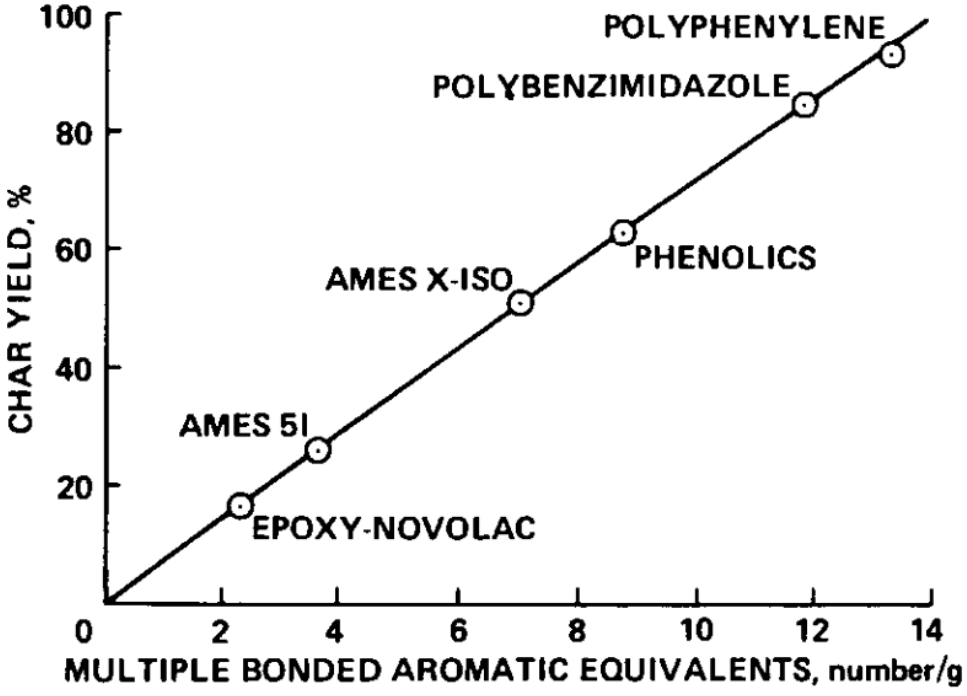

Figure 2.6 Linear relation between char yield and aromatic content in resins (from [49]).

$$nR = C \text{ (initiation)} \tag{2.1a}$$

$$R + C = aC + P \text{ (chain branching)} \tag{2.1b}$$

$$C + R + R = P \text{ (gas termination)} \tag{2.1c}$$

$$C = P \text{ (surface termination)} \tag{2.1d}$$

Ignition requires the creation of chain carriers, that are multiplied through branched-chain reactions, accelerating the overall reaction rate. Therefore, a pyrolysate-oxidizer mixture ignites if the heat generation exceeds heat losses through transport mechanisms, in which case the heat accumulated promotes the endothermic chain branching reactions, increasing the reaction rate and leading to thermal runaway [54].

In a fire test, the pyrolysates mix with the exhaust gases of the pilot flame which are poor in oxygen and whose composition varies with the type of fuel used in the burner and the calibration method. This homogeneous reaction may be delayed if the oxidizer flow velocity is high or if the oxygen concentration is very low [55]. The heat feedback from pyrolysate ignition increases again the composite temperature, promoting the production of pyrolysates and a positive feedback loop is created, leading rapidly to the complete decomposition of the composite. Moreover, the flames produced by pyrolysate ignition can heat other locations of the system and propagate the fire.

Therefore, the time-to-ignition (TTI) of polymer composites is a parameter of paramount importance in fire safety. It is usually assessed through standardized fire tests, performed for instance using cone calorimeter [13]. For instance, Figure 2.7a) represents the TTI of various carbon fibers composites exposed to 75 $\mathrm{kW\,m^{-2}}$ heat flux. It is interesting to note that the resins associated with the production of a high amount of char (Phenolic, PPS, PEKK) are also associated with a long TTI. The TTI depends among other factors on the composition and quantity of pyrolysates emitted during matrix pyrolysis. Therefore, a material yielding a low amount of char is susceptible to ignite more rapidly as it generates more volatils.

The capacity of a material to propagate fire is also related to its Heat Release Rate (HRR, in $\mathrm{kW\,m^{-2}}$), which describes the amount of heat released when the pyrolysates ignite. This heat is susceptible to be absorbed by other parts of the system and spread fire to the rest of the part under investigation. Figure 2.7b) presents different HRR for various composites. Regarding only TTI and HRR, carbon/PEKK seems to be a better material than carbon/epoxy in fire safety applications and has comparable density, but is also much more expensive (between $5 - 10$ \$/kg for epoxy resin and $25 - 76$ \$/kg for PEKK in 2020).

Time-to-ignition is most of the times modeled with empirical correlations based on parameters

related to the temperature of the solid phase, critical pyrolysate mass flow rate or critical heat flux [56]. These parameters are chosen to represent a specific set of material and fire test conditions and therefore their range of application is limited. The heat feedback from pyrolysate ignition is often neglected [35, 57] or modeled with empirical parameters [58] that are again valid only for a specific set of material and fire test conditions. Pyrolysis models have also been coupled to CFD models to simulate piloted ignition of solid materials [59–62], providing a more versatile tool than empirical correlations, able to simulate pyrolysate ignition in various conditions. However, they often rely on simplified chemical kinetics that cannot account for the mixing and ignition of pyrolysate in the exhaust gases of a pilot flame. This issue is addressed in Chapter 6.

2.1.7 Oxidation reactions

The increase of the matrix porosity allows oxidative species contained in the surrounding environment, such as water or oxygen, to diffuse into the composite in counterflow to the pyrolysate convection. They can then react with the carbonaceous species (typically the carbon fibers or the char layer) if the material's temperature is sufficiently high (around 620 and 720 K for respectively PAN and pitch based fibers [23]). Therefore, fiber oxidation only occurs when most of the matrix has pyrolysed and the exhaust gases have burnt [64]. It is also worth noting that the char layer usually oxidizes before the carbon fibers [65], therefore protecting them [23]. The oxidation being mostly an exothermic process, this heterogeneous reaction increases further the material's temperature [55]. Due to the high temperature required and the protective effect provided by the char, carbon fiber oxidation has often been neglected in previous modeling of fire tests [58], but is a major challenge in other situations such as rocket nozzle erosion [66–70]. However, Chelliah *et al.* [71] investigated the reaction rate of porous and non-porous graphite rods exposed to oxidizer flows. Figure 2.8 from [71] shows that combustion radicals such as OH or O can have a major impact on graphite erosion at elevated temperature. As these species are likely to be produced by the pilot flame, they could have an impact on the sample oxidation.

2.1.8 Other effects

Other effects may occur due to the high temperatures, such as delamination, crack formation or fiber-matrix debonding, and a reduction of the material mechanical properties. These phenomena increase the permeability of the material and thus reduce the residence time of the gas, altering the mechanisms of heat transfer by enhancing the convection cooling effect. Moreover, delamination could have an insulating effect because of the gas layer intruding be-

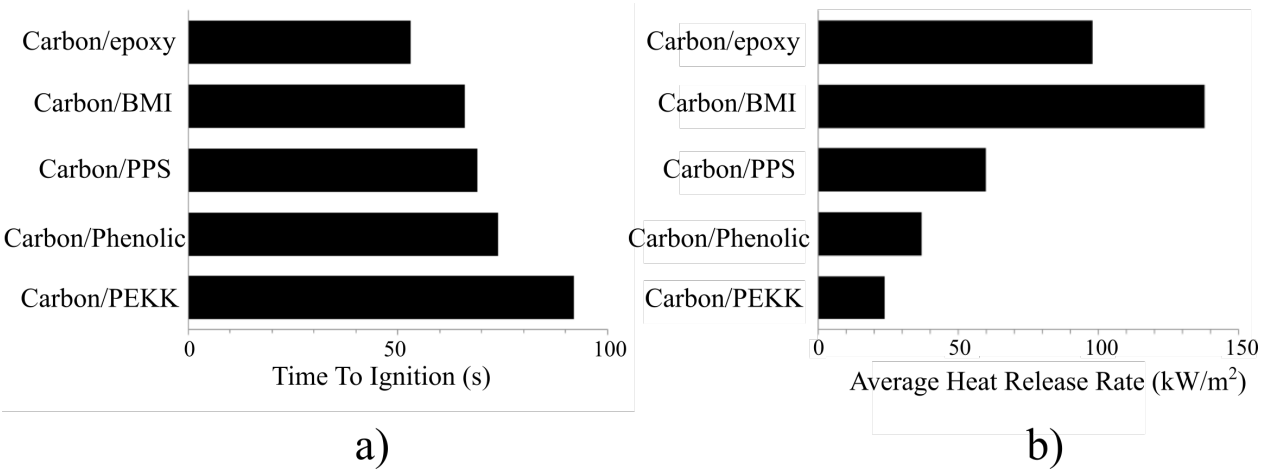

Figure 2.7 a) Time-to-ignition and b) heat release rate of various carbon fibers composites when exposed to a heat flux of 75 kW m^{-2} (from [63]).

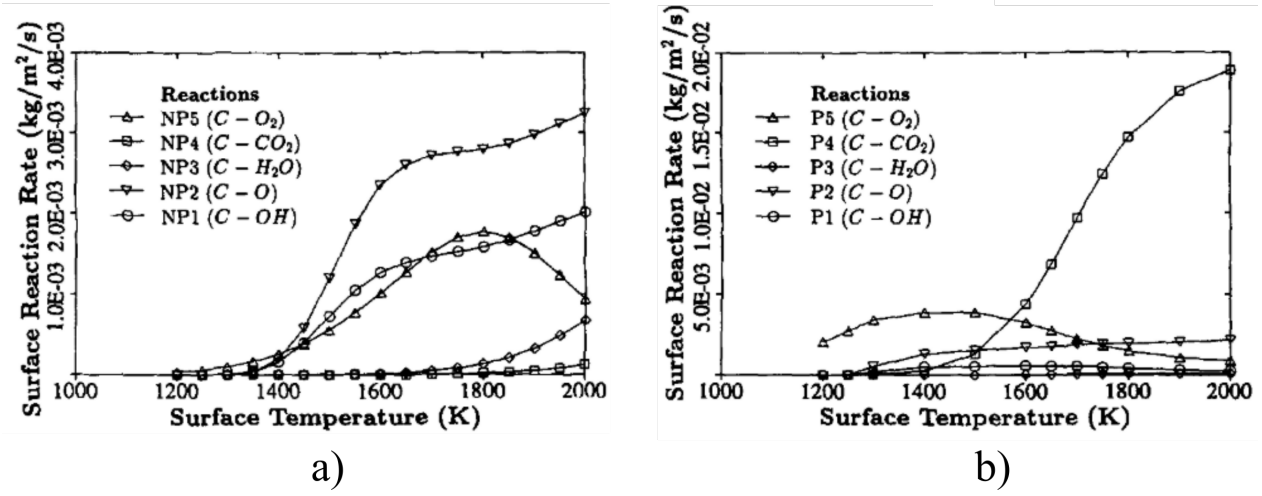

Figure 2.8 Numerical surface reaction rate as a function of temperature of non-porous (NP, Figure a) and porous (P, Figure b) graphite rods exposed to oxidizer stream at a strain rate of 200 s^{-1} (from [71]).

tween the composite plies. Delamination begins usually at the onset of matrix pyrolysis [72]. Moisture evaporation, often neglected in studies, can also impact the ignition time and CO production [25].

The processes listed above promote or reduce the composite thermal degradation, by influencing the material thermal properties or by absorbing or releasing heat from the pilot flame. However, the certification test cannot provide a detailed insight on the role of these different processes in composite combustion as such tests only provide a fail/pass verdict. Moreover, they are very expensive to conduct and time consuming. The prediction of an expected thermal response from a modeling effort has the potential to reduce the number of fire tests. A detailed numerical investigation is however necessary to understand how these processes interact.

2.2 The modeling of composite thermal degradation

Many authors have attempted to model the thermo-chemical degradation of heterogeneous solid combustible materials such as polymer composites [44, 55, 57, 62, 64, 73–79], wood [80–82] or solid rocket fuels [24, 83–85]. These models are often called *pyrolysis models* in the literature and have been the subject of several literature reviews [22, 23, 25, 50]. They require a mathematical description of the thermo-chemical processes. Most of these models can be divided in two categories. First, the semi-empirical approaches provide a macro-scale description of the outcome of a fire test, without considering the micro-scale phenomena occurring inside the sample. Then, the comprehensive approaches are based on conservation equations and model as many transport phenomena as possible.
Empirical approaches are introduced in Section 2.2.1. Then, Section 2.2.2 presents some of the most interesting comprehensive approaches.

2.2.1 The semi-empirical approaches

Semi-empirical approaches are the simplest way to model the pyrolysis of solid materials [74, 86–93]. They have been developed to describe the thermal degradation of composites for the first time by Griffis *et al.* [94] in 1981 and later by McManus *et al.* [95]. They have since been improved by Chen *et al.* [96]. These approaches have then been applied successfully to various fire resistance tests, including cone calorimeters [74, 86], Lateral Ignition and Flame spread Test (LIFT) [88] or small-scale fire test [87, 89, 90]. Semi-empirical approaches rely on assumptions and hypotheses specific to the standardized test, focussing on specific quantities of interest (time-to-ignition, heat release rate, mass loss rate, etc) with analyt-

ical solutions including empirical parameters. They are often based on a heat conduction equation with *apparent* thermal properties incorporating the effects associated with the solid chemical decomposition [91–93, 97]. An empirical law describes the variation of the thermal properties as a function of temperature, for instance with the heat capacity. Such a relation must capture the absorption or release of heat due to chemical reactions.

As an example, a semi-empirical approach was implemented by Quintiere [74] to predict the heat release rate of from materials submitted to a room-corner fire test exposure. Before the pyrolysis temperature is reached, the variation of temperature in the sample was computed with analytical solution of the heat equation, assuming that the sample was inert, semi-infinite and that its properties did not change with temperature. Then, the onset of pyrolysis was assumed to correspond exactly to the ignition of the composite and the solid temperature remained constant during its decomposition. The HRR is estimated with the heat of combustion (ΔH_c) and heat of gasification (ΔH_g), determined from bench-scale fire test data, with a method typically valid for the steady-state burning of thick non-charring ablative solids, which limits the range of application of the method [55]. The temperature of the upper gas layer was predicted with a correlation specific to corner fire situations [98].

The main advantage of empirical approaches lies in their simplicity of development as they do not rely on complicated numerical methods. Moreover, all input parameters required for these models can be directly obtained from existing bench-scale fire tests [55], avoiding the non-trivial measurement of the fundamental material properties from independent experiments requiring complex instrumentation. These approaches are perfectly well suited for materials having an excessively complicated fire behavior that cannot be grasped by a theoretical approach [99], such as composites. However, the extensive use of restrictive assumptions limits the range of validity of semi-empirical approaches to specific materials and test conditions with which the source experimental data was obtained. The input parameters must therefore be measured every time the material composition or the test conditions are changed. For instance, the empirical model previously described considers the ignition temperature as a material property, but in reality pyrolysates ignite when reaching their lower flammability limit, which depends among other on the intensity of the heat flux imposed on the material, as well as on the atmosphere composition, etc [100]. Pyrolysate ignition can be delayed because of a high strain rate in the gas layer [59]. Moreover, the solid temperature corresponding to pyrolysate ignition and pyrolysis onset are not necessarily the same. Therefore, the ignition temperature measured in a cone calorimeter cannot be used in a fire test. Finally, semi-empirical approaches do not always provide insight of the different phenomena in interaction in the solid phase. As a result, they are of limited use to provide understanding of the root cause of a material behavior under fire.

2.2.2 The comprehensive approaches

Comprehensive methods have been developed to provide a model for the thermal degradation based on the physical processes occurring within the material. They are based on the coupling of mass, energy and chemical models, described by conservation equations, and are intended to be versatile and valid for a broad range of test conditions. The models described in this section mainly differ by the assumptions and simplifications made to obtain a set of equations to solve. Some implement simple (single-step) or more complex reaction mechanisms (multi-step), model the solid porosity, take into account the flow resistance in the pores network, use detailed models to treat the transport phenomena and the effective thermal properties or describe the solid and gas phase with two different temperatures (no local thermal equilibrium). The models can be one-, two- or three-dimensional (respectively 1D, 2D or 3D) depending on the geometry assumed for the fire test. The main challenge for thermo-chemical modeling is to balance complexity and computational cost with the assumptions needed to simplify the model and limit the number of empirical parameters necessary, without compromising the ability of the code to capture effectively the physical behavior [55]. In general, comprehensive approaches follow a similar procedure. First, a thermal model provides the temperature profile as a function of the material properties and fire test conditions, using with the conservation of energy. Then, a chemical model computes the mass loss rate and heat release from chemical reactions with Arrhenius's law, as a function of the material temperature. Outputs from the chemical model, such as heat feedback and density variation, are used to update the material temperature and compute the transport of pyrolysates through the material porosity with the conservation of mass. A conservation of momentum is sometimes added to model the pressure rise in the porosity due to the production of gaseous species. The system of partial differential equations obtained is then discretized numerically using Finite Element, Finite Volume or Finite Difference Methods (respectively FEM, FVM and FDM). The material temperature and decomposition are sometimes used in a thermo-mechanical model to compute the mechanical properties of the composite or the thermal stress. These models usually focus on the solid phase and processes occurring in the gas phase are modeled with empirical formulations or with a CFD software coupled to the pyrolysis model.

The first comprehensive approaches were developed in 1946 to model wood pyrolysis [101] and have been applied to composite pyrolysis for the first time in 1985 [73]. Generalized comprehensive approaches, applicable to a wider range of materials and fire tests conditions, have then been developed since 2007 [55]. Finally, comprehensive approaches have been applied to composite exposed to a pilot flame in the context of a fire test in 2012 [35]. The different periods and most important works leading to the multi-physics modeling of com-

posite exposed to fire is represented on a timeline in Figure 2.9 and are introduced with more details in the following.

The modeling of wood pyrolysis

The first comprehensive pyrolysis models have been developed in the 1940s to investigate the pyrolysis of wood. Bamford *et al.* [101] modeled the combustion of wood with a one-dimensional transient heat equation with a source term accounting for the energy absorbed or released by chemical reactions. The material properties were considered constant. The model was straigthforward and easy to implement, although quite simple, when compared to the numerous processes occurring in wood combustion. Their model was later improved by Munson and Splinder [102] who considered thermal properties varying with the decomposition and gas flow through the porosity. Murty and Blackshear [103] used x-rays to measure simultaneously the heat and mass transfer in wood combustion and compared the measurement to numerical predictions, although the accuracy of 1D model suffered from 3D effects inherent to the experiments. Nonetheless, they drew a space-time map showing the location of the different processes occurring during wood combustion. They also showed that the endo/exothermicity of wood pyrolysis depends on the solid temperature and that char oxidation has a strong exothermic effect. Kung *et al.* [80] introduced the first truly comprehensive numerical approach that included transient conduction, internal convection of volatiles, Arrhenius-modeled decomposition of the matrix into volatiles and char, heat absorbed by the pyrolysis and variable thermo-physical properties. Their model was later improved by Kashiwagi [104] who investigated the decomposition of solid fuel exposed to a radiative heat source. Kashiwagi considered both gas-phase reactions and in-depth absorption of radiation in the composite. Kansa *et al.* [81] added a momentum equation to Kung's model to account for the resistance of the porous solid to gas motion and the resulting pressure rise. Miller and Ramohalli [105] introduced a parameter describing the fibers diameter to model the fibrous heterogeneity of wood. A 2D model of timber decomposition was developed by Fredlund [106] and the predictions of a 2D and 1D models to simulate the pyrolysis of lignocellulosic particles have been compared by DiBlasi [82], who showed that the chemical decomposition was faster and produced more volatiles with a 2D modeling.
Even if these models focused on wood combustion, the physical processes modeled could be applied to other charring materials and served as a basis to the modeling of composite combustion.

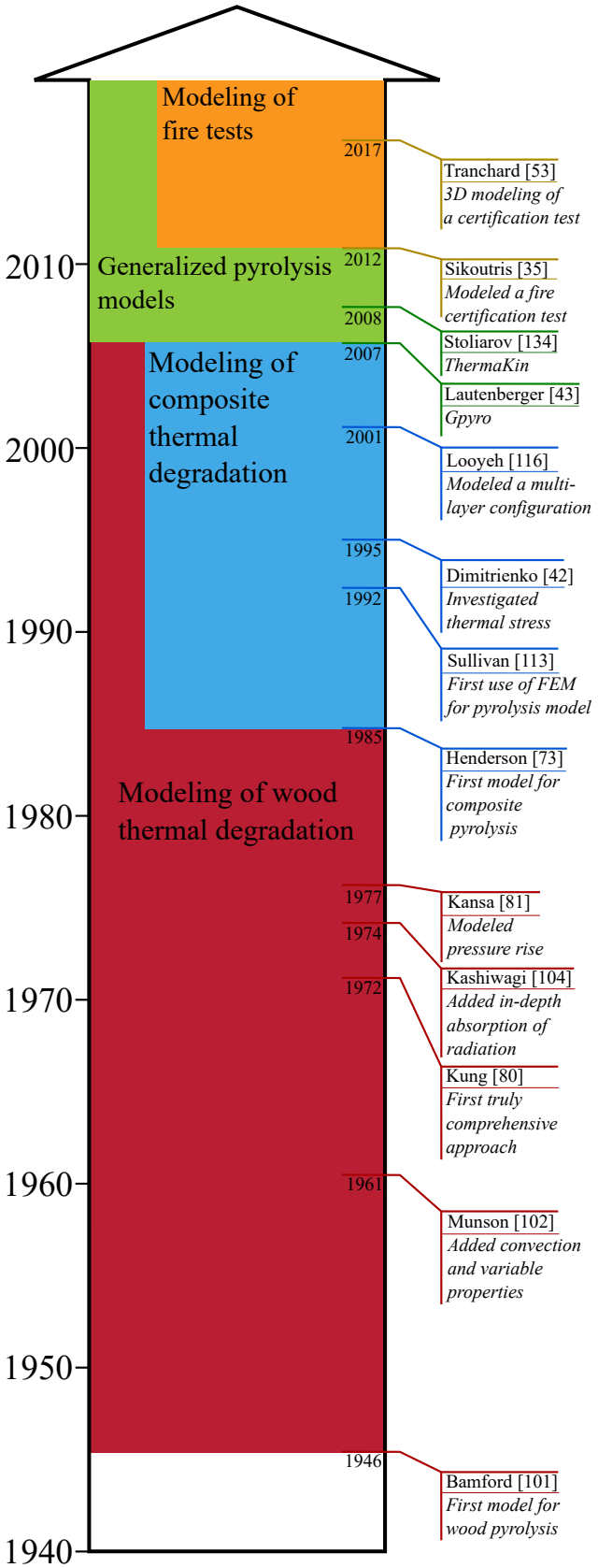

Figure 2.9 Timeline for the evolution of the pyrolysis models based on comprehensive approaches.

Pyrolysis models for composites

In 1985, Henderson *et al.* [73] were among the first to propose a truly comprehensive model for composite thermal degradation and their work has since been considered as a reference. With the knowledge gained in the modeling of wood pyrolysis, they modeled the thermal degradation of glass fiber polymer composites exposed to high temperatures. Their model included a detailed formulation for matrix pyrolysis and carbon-silica reactions [107]. In particular, they modeled the pyrolysis with two reactions to account for the complex shape of the curves representing the mass loss of the resin as a function of temperature. Their model also accounted for movement of gas through the char structure and comprised a complete material characterization to measure all its temperature dependent properties [108]. To investigate the validity of the hypothesis of local thermal equilibrium, they also used two different equations for the conservation of energy, to compute the temperature of the gas and solid phases. They demonstrated that the temperature difference between both phases could reach up to 200 K, despite the local temperature of the composite often considered uniform in the literature. In their case, the local thermal equilibrium assumption induced an error of 17% in the prediction of the material temperature against experimental data. This hypothesis has been later discussed by Zanoni *et al.* [109] for the smouldering combustion of organic liquids. They showed that the temperature difference between sand and liquid could reach 36% for the combustion of a hydrocarbon-contaminated soil. The so-called *Henderson's model* has since served as a reference for many of the upcoming studies.

The impact of the composite thermal degradation on its structure has been later investigated. The one-dimensional model of Henderson *et al.* was later extended to three-dimensions by Milke and Vizzini [110], with non-uniform boundary conditions to predict the cold face temperature of a carbon-epoxy composite exposed to a radiant heat source during 10 minutes. The agreement of their model with experimental data was good until the onset of composite delamination after 6 minutes of heat exposure, after which the cold face temperature was overestimated. This work highlighted the importance of accounting for the effect of chemical decomposition on the composite thermo-structural response. To address this issue, thermochemical expansion and internal pressurisation were introduced to Henderson's model [45,111,112]. In particular, Florio *et al.* [45] applied the Henderson's approach to a 0.03 m thick glass-phenolic sample exposed to a radiant heat flux of 279.7 kW m^{-2} and showed that the pore pressure could reach 10 times the atmospheric pressure. At these level of pressure, the composite is likely to undergo matrix cracking, fibre-matrix debonding and delamination damage. Sullivan and Salamon [113] investigated the influence of the pyrolysate production on the composite stress state with a coupled thermo-mechanical model. In particular, they modeled the variation in pore pressure because of solid deformation. They were also one

of the first researchers to use the FEM to solve the system of conservation equations in 2D geometries. Their efforts were continued by Looyeh *et al.* who also used FEM to model glass fibre reinforced panels exposed in a furnace [44, 75] and with complex 2D geometries [114], investigating later thermo-mechanical response of a composite exposed to heat source [115]. They were also one of the first to study the thermal degradation of a sandwich panel instead of a single-layer composite, taking into account the effect of thermal layer resistance in a multi-layer configuration [116]. Arguing that their work relied on empirical parameters because of simplifying assumptions and the use of apparent properties, Galgano *et al.* [117] proposed later another model for fibre-reinforced sandwich panels under fire conditions accounting for convective mass transfer, effective material properties, moisture evaporation and surface ablation. Dimitrienko *et al.* [42, 118–120] investigated thermal stress and evolution of thermo-mechanical properties of composites exposed to a heat source. In 1995, Gibson *et al.* [121] developed COMFIRE, a coupling between thermal, chemical and mechanical sub-models. COMFIRE has then been extensively used in many publications [122–127] to investigate the thermo-mechanical behavior of glass fiber reinforced polyester, vinylester and phenolic laminates. The thermo-mechanical analysis of composites exposed to heat source revealed that some mechanical processes, such as delamination, had an important influence on the composite thermal response by reducing heat transfer to the remaining virgin material. However, these processes remain very challenging to accurately model.

The thermal degradation of carbon epoxy composites has been modeled several times in the literature. Using the material properties measured by Quintiere *et al.* [128], McGurn *et al.* [129] predicted the one-dimensional thermal response of a carbon epoxy composite tested in a cone calorimeter to different radiant heat fluxes. They modeled both the pyrolysis of epoxy resin in the solid phase and pyrolysate combustion in the gas phase with a single-step reaction. They predicted the heat release rate with a good qualitative agreement, and argued that the remaining discrepancy between numerical and experimental data was due to three factors: (i) uncertainties related to the cold face boundary conditions, (ii) oversimplification of the gas-phase combustion reactions of pyrolysate and (iii) inadequate permeability model. Arguing that the non-one-dimensional heat transfer had not been investigated by McGurn *et al.* [129], McKinnon *et al.* [79] modeled the thermal response of a carbon/epoxy composite in two dimensions. They also modeled the epoxy pyrolysis with a four reactions mechanism instead of a single step reaction [128], which allowed them to greatly improve the accuracy in their model. They validated their approach by exposing the material to a radiant heat flux. Chippendale *et al.* [130] exposed a carbon/epoxy composite to very high radiant heat flux (0.38 $\mathrm{MW\,m^{-2}}$) emitted by a laser beam, to investigate thermal response of composite to lightning strike. The study of carbon/epoxy composites exposed to laser beams was later

continued by Biasi [52]. Other researchers developed more recently one-dimensional thermal degradation models for a composite submitted to a constant heat flux in a cone calorimeter [78, 131, 132].

The models cited above relied on many input parameters that had to be measured through independent experiments, as the number of unknown parameters increases rapidly with model complexity. Some of these parameters, such as the reaction scheme, are very difficult to measure experimentally but have a great influence on the model outcome. In order to identify the sources of inaccuracies, several authors analyzed the sensitivity of pyrolysis models to input parameters [132–135]. Krysl *et al.* [133] varied independently each property and showed that a perturbations of less than 5% of the pyrolysis activation energy, pyrolysate heat capacity or char thermal conductivity induced a temperature variation of 50 K on the cold face of a 11 mm thick polyester-glass heated at 1300 K during 1000 s. Stoliarov *et al.* [134] demonstrated that the rate and heat of decomposition, as well as the char yield, had a significant importance in the prediction of heat release rate. Chaos [135] estimated the sensitivity coefficient of each parameter as a function of time with a dynamic approach and confirmed results Stoliarov *et al.*'s [134] results when applied to non-charring materials. Batiot *et al.* [136] investigated specifically the sensitivity of the parameters describing the chemical decomposition and showed that variations of the activation energy and pre-exponential factor had more impact on mass loss rate than variations in the reaction order and char yield. They carried out their analyses on a single reaction scheme and did not investigate the influence of the number and nature of reactions used to represent the mechanism. Intermediate reactions were later added in chemical models to improve their predictive capabilities [137, 138], but very different mechanisms had already been developed for the same type of matrix [79, 139]. There is therefore a lack of discussions about the optimal number and nature of intermediate reactions that should be used in a reaction scheme. This issue is addressed in Chapter 5.

The development of generalized approaches

The assumptions allowing to derive a simplified set of governing equations from the conservation equations are often only valid for a specific class of material (thermoplastic, polymer, charring, intumescent, etc) and their mathematical formalism cannot be applied to other categories. To overcome this drawback, so-called *generalized approaches* have been developed since 2007. These methods are intended to be as versatile as possible and applicable to any kind of material. When compared to *classical* comprehensive approaches, their main characteristic is the use of an adaptable mathematical formalism, for instance accounting for a variable number of phases and chemical reactions. Since 2005, four generalized approaches have been developed: Fire Dynamics Simulator [140], Gpyro [55], ThermaKin [76]

and Pyropolis [64]. These models are based on nearly similar mathematical formulation, the difference between them lying in the details of some specific submodels.

The first generalized approach has been developed by Mc Grattan *et al.* [140]. The software Fire Dynamics Simulator (FDS) is a pyrolysis model coupled to a CFD software to simulate both the thermal degradation of a composite material and the gas-phase reactions. The condensed-phase model does not compute the mass transfer of pyrolysates through the solid porosity and the volatiles are instantaneously released in the gas phase. The conservation of momentum is not modeled so the pressure is considered constant in the solid phase. Local thermal equilibrium is assumed between the solid and gas contained in the porosities. The pyrolysis model accounts for heat conduction, temperature-dependent thermal properties, heat production and in-depth absorption of radiation. Solid phase reactions are computed with an Arrhenius equation with a n-order reaction model. Only a single reactant can be defined in chemical reactions, which is suitable to model pyrolysis but not oxidation. Heat transfers at the solid-gas interface are computed with a combination of forced and natural convection modeled with correlations. The formulation of chemical reactions in the gas phase is based on a straightforward lumped species approach and it is the responsibility of the user to define complex reaction mechanisms.

Lautenberger and Fernandez-Pello developed Gpyro in 2007 [43, 55]. This generalized approach solves the conservation of mass and energy in the solid phase and offers the possibility to model separately the gas and solid phases temperatures. Additionally, the conservation of momentum can be solved as an option to predict variations of pressure. The conservation of energy accounts for in-depth absorption of radiation, heat conduction, heat production from chemical reactions, heat convection and transport of volatiles through the porosity. Heterogeneous and homogeneous chemical reactions are modeled with Arrhenius equation and offer a wide variety of reaction models. Gpyro is coupled to optimization algorithms able to determine the best input parameters improving the agreement between predicted and experimental values. Conservation equations can be solved in one-, two-, or three-dimensions.

Developed in 2008 [134, 141], ThermaKin solves the conservation of mass and energy in a porous media. The movements of gas are driven by concentration gradients. It accounts for conductive heat transfers, heat production from chemical reactions and transport of pyrolysates through the porosity. The conservation of momentum is implicitly included in the gas flux formula. Penetration of external radiation is modeled with the Beer-Lambert law. Chemical reactions are modeled with Arrhenius law with first-order reaction model with one or two reactants. ThermaKin models one- or two-dimensional domains.

Snegirev *et al.* developped Pyropolis in 2013 [64]. It predicts the thermo-chemical behavior of charring and non-charring materials exposed to a radiant heat source and accounts for ma-

terial swelling. The model can be used for single-layer as well as multi-layer structures. Gas diffusion through the pore network is neglected and gas convection is driven by pressure gradients. Solid and gas phases are in local equilibrium and radiation through semi-transparent medium is neglected. The model accounts for intumescence, which means that the domain boundary can expand during the simulation. Pyropolis models one-dimensional domains. One of the main differences between Pyropolis and previous generalized approaches lies in the chemical model. In Pyropolis, no kinetic function is pre-assumed but is rather derived directly from TGA or MCC (Microscale Combustion Calorimeter) measurements. Several parallel reactions are then implemented in the reaction scheme to account for the complex shape observed in experimental data.

As the generalized approaches described above implement similar mathematical approaches, it appears that a consensus has been reached in the fire community about the processes that must be considered to simulate a composite exposed to fire. Most of these models allow to model matrix pyrolysis with complex chemical mechanisms, as this process has been identified as a major source of inaccuracies in previous comprehensive approaches [134, 135]. However, the choice of the reaction scheme is left to the user and the determination of an appropriate reaction scheme remains one of the main challenges [142]. Thermo-chemical models suffer from another limitation: the chemical models and material properties are based on experimental data very difficult to measure. For example, the properties of the char layer or the parameter defining the reaction kinetics are especially challenging to obtain [50]. Information related to different classes of materials can be found in the literature but this data cannot be generalized because: (i) the processing of materials is non-deterministic mainly due to the manufacturing specificities; (ii) there is no reference data on the properties of decomposition products, such as the char layer. Hence the material properties have to be thoroughly measured for each material system. It is also worth noting that all of these approaches have been solved with FVM or FDM but none of them has been solved with FEM, although this approach is often considered more appropriate for multi-physics modeling [143].

The modeling of composites exposed to fire

Most of the comprehensive approaches previously introduced described a composite exposed to radiative heat sources, which simplifies the modeling as the heat flux is well characterized and homogeneous over the composite surface. The modeling of the gas phase was also often decoupled from the solid phase and therefore the interaction between an external flame and the pyrolysates emitted by the composite was not considered in the simulations. As a result, the models assumed that the composite was exposed to a controlled and constant heat flux, neglecting the influence of pyrolysate ignition and flame spread. Yet, a reactive heat source

such as an external flame is much more realistic than a radiative heat source to address the requirements for composite fire walls. It provides a non-constant heat transfer over the composite surface and produces combustion products that influence the composite ignition and oxidation.

Comprehensive approaches have been applied to composites exposed to fire. In those cases, the flame was represented by different means. An oven with a temperature program intended to represent a hydrocarbon fire curve was sometimes used [117, 121, 125, 144, 145], for instance following the ISO 834 requirements [146–148]. A hydrocarbon fire curve is a time-dependent temperature program representative of small petroleum fires. Gibson *et al.* [121] applied the Henderson model to glass fiber reinforced polymer panels exposed to a reactive heat source using a hydrocarbon fire curve. This work was continued by Dodds *et al.* [125] and Wang [144], who modeled the fire behavior of a glass fibers panels exposed in a furnace programmed to follow the hydrocarbon fire curve.

A real pilot flame has more scarcely been used. McManus and Springer [149, 150] developed a one-dimensional thermo-mechanical model specifically developed for carbon-carbon and carbon-phenolic composites exposed to a propane torch. The flame heat flux was modeled as a uniform convective term on the sample surface, and the pyrolysate ignition and carbon species oxidation were not considered. Sikoutris *et al.* [35] modeled the thermo-chemical response of a flat panel exposed to propane burner according to the ISO 2685:1998 [15]. The non-uniform heat flux from the propane burner on a flat panel has been simulated by means of CFD. The flux was then considered as *frozen*, which means that its value did not vary during the entire test and corresponds to the maximum heat tranfer rate. The heat feedback from pyrolysate ignition was therefore neglected. This was intended to be a worst-case scenario as in reality the heat flux from the pilot flame to the composite decreases as the composite temperature increases. Gibson *et al.* [57] modeled the thermo-chemical behavior of thermoplastic and thermosetting composites exposed to a small-scale fire test. They validated their model with a calibrated propane burner yielding a heat flux of 50 $\mathrm{kW\,m^{-2}}$ on composites under tension or compression. The heat feedback from pyrolysate ignition was not modeled. Tranchard *et al.* [53, 58] developed a three-dimensional model predicting the heat transfer and degradation of a carbon-epoxy composite exposed to a propane flame. The convection coefficient accounting for heat transfer from the pilot flame to the composite was adjusted to represent the heat flux measured on the composite at the initial time step. Another term accounting for the inflammation of pyrolysates near the surface was included. The value of this heat feedback was empirically computed with the heat release rate measured under a Mass Loss Cone Calorimeter test.

Fully coupled solid-gas models have also been developed for the piloted ignition or flame

spread of combustible materials [52, 59–62, 151, 152] or gasification experiments in a cone calorimeter [62]. Lautenberger *et al.* [59] investigated the ignition of samples exposed to radiant heat flux in a convective oxidizer flow in microgravity with the CFD software Fire Dynamics Simulator (FDS) [140]. Xie and Desjardin [60] coupled CFD and pyrolysis models to investigate flame spread over composite samples for different inclination angles. The combustion of pyrolysate was modeled with a global one-step reaction. They showed that the heat flux received by the material varied with time because of pyrolysate combustion, although a common hypothesis in the literature is to assume that the heat flux is constant over the sample surface. Luo *et al.* [151] modeled the thermal response of a composite exposed to a pilot flame with a coupled CFD-pyrolysis modeling. Combustion reactions in the gas phase were modeled with single-step chemical kinetics. Their results showed that the heat feedback from pyrolysate ignition had an important influence on the heat transfer to the wall and therefore could not be neglected. Marquis *et al.* [152] used FDS to model glass fiber reinforced polyester sandwich composites exposed to fire. Pyrolysate combustion was again modeled with a global one-step reaction. A critical pyrolysate concentration was used to determine the time-to-ignition. Kacem *et al.* [61] studied open-air combustion by coupling a CFD code featuring turbulence, combustion and radiation with a thermo-chemical model, through a solid-gas interface. They showed that the correlations used in some CFD software to model the gas-solid interface led to inaccurate predictions because the specific situation modeled by correlations did not always represent the conditions of the fire test. The work of Boyer [62] is one of the most recent investigation of non-charring solid fuel ignition. Boyer predicted with a good agreement the mass loss rate and heat release rate of polymers exposed to a radiant heat flux in a cone calorimeter. The combustion of pyrolysate was modeled with a one-step global reaction of hydrocarbon oxidation, with an equivalent hydrocarbon fuel chosen to represent the species emitted by pyrolysis. His results showed that the heat feedback from pyrolysate combustion varied a lot with the nature of the considered material.

The works previously described recognized that the influence of the heat feedback from pyrolysate combustion on the composite thermal response cannot be neglected [60, 151] and depends on the nature of the material exposed to heat [62] and fire test conditions. In the context of a fire test, the pyrolysate combustion is also affected by the composition of the exhaust gases from the external flame, which in turn depends on the calibration method used to reach the heat flux and flame temperature specified in the certification test [15, 153]. The modeling of pyrolysate combustion must therefore be adaptive to different fire test conditions. However, pyrolysate combustion was often neglected [35, 57] or modeled with empirical parameters [58] that must be inferred experimentally for each set of test conditions and material composition. Pyrolysate combustion was sometimes modeled with simplified chemical

kinetics [60, 62, 151, 152], such as global one-step reactions. However, these methods cannot capture the numerous species and intermediate reactions involved in an atmosphere of complex composition, such as the exhaust gases from the pilot flame. Therefore, the use of global one-step reactions has to two consequences: first, it leads to an inaccurate prediction of the flame temperature from pyrolysate combustion. Indeed, global one-step reactions do not take into account the heat absorbed by the endothermic dissociation reactions or heating of other species not directly involved in the combustion. Second, the time-to-ignition cannot be directly modeled with a global one-step reaction and empirical methods are required [56], based for instance on a critical mass flow rate of pyrolysates [129], critical material temperature [74] or critical fuel mass fraction in the gas phase [59, 152]. These methods are therefore specific to the material under investigation and fire test conditions and lose their validity in another context, which is contradictory with the need to have a modeling of pyrolysate combustion adaptive to the calibration process for the pilot flame.

In reality, a mixture ignites when the heat generated by chemical reactions exceeds heat losses, which favors the creation of chain carriers leading to thermal runaway. This process involves hundreds of intermediate reactions, including chain branching reactions, which are the key to understand the ignition process [54]. More complex reaction mechanisms are available to model the pyrolysate combustion. For instance, GRI Mech 3.0 [154] has been developed for natural gas combustion and involves 53 species and 325 reactions, and is therefore able to model in great detail the composite ignition as a function of the atmosphere and pyrolysate composition. Other mechanisms are also available for more complex hydrocarbons [155–157]. These mechanisms could be implemented in two- or three-dimensional CFD simulations, but CFD modeling of combustion applications is a very complex task and most of the current simulations are limited to flames in simple configurations with no reacting solid phase [158, 159]. However, chemical kinetics software such as Cantera [160] model very complex reaction mechanisms in simplified one-dimensional CFD simulations, and therefore offer a good compromise between a detailed chemical kinetics and accurate CFD simulations. To the best of the author's knowledge, such tools have not been coupled to pyrolysis models in the context of a fire test.

2.2.3 Coupling strategies

In the works previously introduced, the modeling of composite exposed to fire requires the coupling of several sub-models: chemical model and thermal model in the solid phase, flame structure and pyrolysate ignition in the gas phase. Sometimes, a mechanical model is also used to predict the variation of mechanical properties as a function of temperature and decomposition degree. The term *coupling* indicates that some variables are involved simulta-

neously in several partial differential equations solved in different sub-models. The coupling strategy enables to treat different equations sharing the same variables at each time step. For instance, chemical reactions and thermal properties both depend on the solid temperature, derived from the conservation of energy whose source term comes from chemistry modeling. Furthermore, the convective heat transfer depends on the gas-phase flame structure but is also a boundary condition in the pyrolysis model. The term *coupling architecture* refers to the way in which different sub-models interact with each other and is related to several parameters: coupling level (strong or weak), nature of data exchanged (material properties, boundary conditions, source volume terms, geometry), data transfer direction and solution order (which equation must be solved first?).

Multi-physics problems fall into two categories, depending if the coupling level is strong or weak [143]. The term weak is used when it is not necessary to compute the interactions between two physical phenomena at every time step [143]. Two weakly coupled algorithms provide separate solution methods and exchange data periodically. This is for example the case for the flame-composite coupling if the influence of the solid on the gas flow is neglected. The flame reaches a stationary state while the solid temperature barely begins to increase and therefore it is not necessary to model the flame at each iteration: only the stationary state is computed at the first step and not updated hereafter. This modeling is straightforward and can be established with any CFD software, but does not capture the influence of the composite thermal decomposition on the flame, as needed for example to model the pyrolysate ignition.

The problem is said strongly coupled if all algorithms must be called at each solution step. This is the case for the thermo-chemical algorithms: pyrolysis and oxidation kinetics depend on the solid temperature, which is influenced by the heat released or absorbed by both chemical reactions. The problem implies therefore a volume source term on thermal side and a thermal interaction on chemical side [143].

The data transfer direction must also be considered. It can be unidirectional, if the data travels only from one algorithm to the other, or bidirectional, meaning the data are exchanged between the algorithms. Bidirectional data transfer is not always necessary, for example with the temperature-dependent mechanical properties computation. Thermodynamics strongly affects mechanical properties, but the effect of the latter on thermal profile is negligible [57, 123, 124]. On the contrary, the data transfer between thermal and chemical algorithms is bidirectional, because of the strong dependency of each algorithm on the outcomes of the other as seen above.

On the basis of the parameters described above, three coupling architecture can be chosen [143]:

1. **Fully coupled**: strongly coupled codes, for example thermo-chemical modeling, are solved simultaneously in a single algorithm. This approach implies solving coupled processes in a single matrix.

2. **Multiple modules**: several software packages or codes are coupled and controlled by a driver routine. Each physical phenomenon is controlled by one sub-model that exchange data with the driver routine and other sub-models at each iteration.

3. **Leader and followers modules**: this approach is close to the multiple modules method, except that the main algorithm ensures the role of driver routine and calls the other modules. This method is often used when several inputs of slave codes depend on the outcomes of another code, which becomes the main code.

CHAPTER 3 OBJECTIVES AND MOTIVATION

3.1 Critical discussion

Although the constant development of comprehensive approaches in the last 30 years led to major improvements in the modeling of the thermal response for a composite exposed to high temperatures, important points required more investigations:

- **Physics of composite combustion**: the thermal degradation of a composite exposed to a heat source is the result of the close interaction of chemical and thermal processes. In particular, solid phase chemical reactions such as pyrolysis and oxidation drives the loss of density of the composite, thus affecting thermal properties. The heat feedback from pyrolysate ignition also plays a major role in the composite degradation. Heat conduction in the solid phase and convection in the material porosity must be considered to develop a realistic model.

- **Modeling of the thermal degradation**: comprehensive methods based on the conservation of mass, energy and momentum in a porous medium can be used to model the thermal degradation of various classes of materials, such as composites. Even if these methods can account for a broad range of fire test conditions, they have been mostly applied to radiative heat source. Reactive heat sources such as pilot flames have been more scarcely investigated. In particular, the impact of the pilot flame operating parameters on the composite ignition and fire resistance has not been studied.

- **Material characterization**: pyrolysis models based on comprehensive methods have proved to be valuable tools, but are still extremely reliant on input parameters such as the material properties, which are challenging to measure at high temperatures. The number of parameters increases with the model complexity and most of the times, their value varies significantly with temperature. Each material simulated in a pyrolysis model must be thoroughly characterized.

- **Modeling of the reaction scheme**: although sensitivity analyses indicate that chemical reactions modeling has a significant influence on the prediction of the material decomposition rate, the complexity of the chemical kinetics implemented in state of the art models is still limited. As a result, kinetics models do not often capture the effect of intermediate steps, which can be significant. A more detailed modeling of the chemical

reactions has the potential to improve the prediction of the material decomposition rate. Several multi-steps reaction schemes must be developed and compared.

- **Modeling of pyrolysate ignition**: despite its potentially important impact on the material degradation, the pyrolysate ignition has been often neglected or modeled with empirical parameters. CFD software have been coupled to pyrolysis software, but they rely on simplified chemical kinetics that cannot represent the ignition of pyrolysates mixed with pilot flame exhaust gases. A better modeling of pyrolysate ignition in complex atmosphere is required to adequately model the outcomes of fire tests.

3.2 Objectives

The objective of this research is to develop a multi-physics modeling tool providing the material decomposition rate as a function of time and of the fire test conditions. This model must account for all relevant physical processes, while overcoming the limitations identified in the literature review. More specifically:

1. **Modeling of the thermal response of a composite material**: heat transfer through a composite exposed to a reactive heat source will be modeled to determine the thermal profile between the hot and cold faces, as well as the decomposition rate from pyrolysis and oxidation. The model will account for conduction in the solid phase, production and movement of pyrolysates through the material porosity, convective heat transfers and heat absorbed by chemical reactions. The different physical processes will be coupled into an in-house multi-physics tool, based on a comprehensive approach. The model will be developed with Finite Element Method. (Chapter 4).

2. **Modeling of the thermal decomposition and residual mass of a carbon fiber epoxy matrix composite with a phenomenological approach: effect of the reaction scheme**: the reaction mechanism describing the material pyrolysis and oxidation will be inferred from TGA with use of isoconversional methods. In particular, the optimal number and nature of chemical reactions describing the material decomposition will be discussed. The effect of the reaction scheme on the residual mass of the composite will be investigated (Chapter 5).

3. **Multi-physics modeling of the ignition of polymer matrix composite exposed to fire**: the pilot flame will be modeled with a chemical kinetics software to determine the composition of its exhaust gases in which the pyrolysate will mix and ignite. A novel architecture based on the coupling of the chemical kinetics software and the pyrolysis

model will be developed to address the mixing and ignition of the pyrolysates in the pilot flame exhaust gases (Chapter 6).

4. **Characterization of the thermal properties of a carbon/epoxy composite**: the material under investigation will be fully characterized and its temperature-dependent thermal properties measured, such as thermal conductivity, heat capacity, density (Chapter 6).

5. **Model validation against a small-scale fire test**: the outcomes of the model will be compared to a small-scale fire test mimicking the conditions encountered in a certification fire test. In particular, the numerical and experimental time-to-ignition and backface temperature will be compared (Chapter 6).

CHAPTER 4 MODELING OF THE THERMAL RESPONSE OF A COMPOSITE MATERIAL

A model is a simplified vision of reality. The objective of modeling is to predict the response of a system to an excitation, represented by source terms and boundary conditions. The response is the set of variables of interest describing the system over space and time, for instance mass, momentum and energy. Their variation is described by transport equations constituting the model, that are then discretized and solved by means of numerical methods [161].

First, the *conceptual model* developped here to investigate the fire resistance of composites is defined in Section 4.1, describing the assumptions on which the model is built, the transport processes considered and the composition and properties of the system. Then the *mathematical model* is defined in Section 4.2. It is the mathematical expression of the conceptual model; the equations constituting the model, fluxes influencing the transport of the variables and source terms and boundary conditions at the origin of the excitation of the system. Finally, the mathematical model is solved with numerical methods in Section 4.3.

4.1 Conceptual model

4.1.1 Model overview and assumptions

The predictive tool is intended to model heat transfer and thermo-chemical decomposition of a composite material exposed to fire. The model is developed with a *generalized* and *comprehensive* approach, which means empirical laws are avoided as much as possible and the model must be valid for a wide range of materials and conditions. To achieve this goal, the development is based on conservation of mass, momentum and energy, applied on a small volume at an arbitrary position inside the sample (referred to as the *control volume*) and as a function of the sample properties. The formulation is adaptable to a variable number of gaseous and solid phases, to different reaction mechanisms and offers different methods to compute its thermal properties.

The model implements (i) the temperature dependence of the sample properties, such as thermal conductivity, heat capacity, etc; (ii) conductive and convective heat transfer inside the material; (iii) convective and radiative heat flux on the hot face of the material; (iv) thermo-chemical decomposition of the solid components, for instance pyrolysis of the polymer matrix and oxidation of carboneceous species; (v) pressure rise because of the production of

gaseous species.
The model does not feature (i) material swelling and shrinkage, for instance because of intumescence, delamination or accumulation of gas in the sample; (ii) Creation and movement of liquid, for instance tar; (iii) Vaporization of liquid phases (water, tar); (iv) Radiation through semi-transparent medium.
The model is based on the following assumptions:

1. The moisture content of the sample is neglected.

2. The diffusivity D ($\mathrm{m^2\,s^{-1}}$) is assumed to be the same for all gaseous species and equal to the kinematic viscosity ν ($\mathrm{m^2\,s^{-1}}$) [43].

3. The control volume remains constant, which implies that the variation of mass and density are equivalent.

4. The sample is represented by a 1D domain, beginning at the point where the external flame impinges on the hot face of the sample and ending on the cold face. The domain is straight and orthogonal to the sample surface.

5. Solid and gas components are in local thermal equilibrium, which implies that both components have the same temperature in the control volume. This hypothesis is justified as long as the volumetric heat capacities of the solid species remain much larger than that of the gaseous species, which implies that the gas reaches very rapidly the solid temperature as it flows through it. This assumption avoids the need to solve separate energy conservation equations for both phases.

6. The gas behaves following the perfect gas law, which means that inter molecular attraction and molecular size are neglected. This law is appropriate for small molecules (for instance monoatomic gases) at low pressure and high temperatures, far from the critical point. It is worth noting that the gaseous species emitted during composite decomposition, for instance pyrolysates, can yet be complex and do not have a zero volume; moreover, the pressure increases because of gaseous species production and can reach several times the atmospheric pressure.

7. The entire void space contained in the composite, i.e. its pores, is interconnected. This implies that gaseous species may flow through the composite from pore to pore, which allows to be considered and treated numerically the composite as a porous medium.

4.1.2 Multi-components approach: preliminaries and definitions

A composite material is made up of several distinct solid phases, for instance matrix, fibers, or other reinforcement, but also contains gaseous species transported or stored in the initial porosity of the material, or appearing during its thermal decomposition. For instance, the char and its porosity constitute a distinct porous medium composed of both solid and gaseous species. Similarly, a tow of carbon fibers exposed to oxidation is also permeable to gaseous species, first because a tow is not perfectly impermeable to gas transport, and also because of the pores formed by the attack of oxidative species. In this regard, a composite material can be considered as an ensemble of several distinct porous media, in the sense that every small volume at the mesoscopic level always contains both solid and gas phases, in the form of a solid component with an interconnected network of pores [161, 162]. A convention is needed to represent a group of species that can conveniently be considered numerically as a single, homogeneous porous medium to compute their thermal properties. In this work, all species contained in the composite are modeled in groups referred to as *entities* or *phases*. A *phase* is a group of several distinct chemical species homogeneously distributed at the same state (solid or gas). An *entity* represents a combination of solid and gaseous *phases* that form one of the distinct porous medium constituting the composite; for instance the porous char layer, matrix or carbon fibers are all considered as *entities*. By assumption, the void space within each *entity* is distributed homogeneously at the mesoscopic scale.

Figure 4.1 represents a conceptual view of a control volume containing N different *entities* (a carbon-epoxy composite exposed to fire). The control volume is represented at the mesoscale, an intermediate scale between the microscopic (representing the microstructure of the material) and macroscopic scales (representing the material in its environment, i.e. the fire test). During fire exposure, the entity *porous matrix* decomposes through pyrolysis into the entity *porous char* that contains two phases: a solid phase (the char itself) and a gaseous phase (the gas contained in the porosity). Similarly, the entity *carbon fibers* contains two sub-phases, a solid phase (the carbonaceous compound) and a gaseous phase (the gas contained in the porosity), that appears during its oxidation. This figure is conceptual in the sense that it represents the material in the way a model *sees* it. It is not a zoom into the material, because in that case the distinction between phases would not be as clear as represented on the figure. This view allows to identify rapidly the different phases and entities, which is useful to estimate their volume or mass fractions. However, it does not provide information about the geometry of the different phases, which is primordial to estimate the thermal conductivity of the composite.

The distinction between entity and phase is important to compute the thermophysical properties as a function of the material decomposition. First of all, the volume fraction X_i of

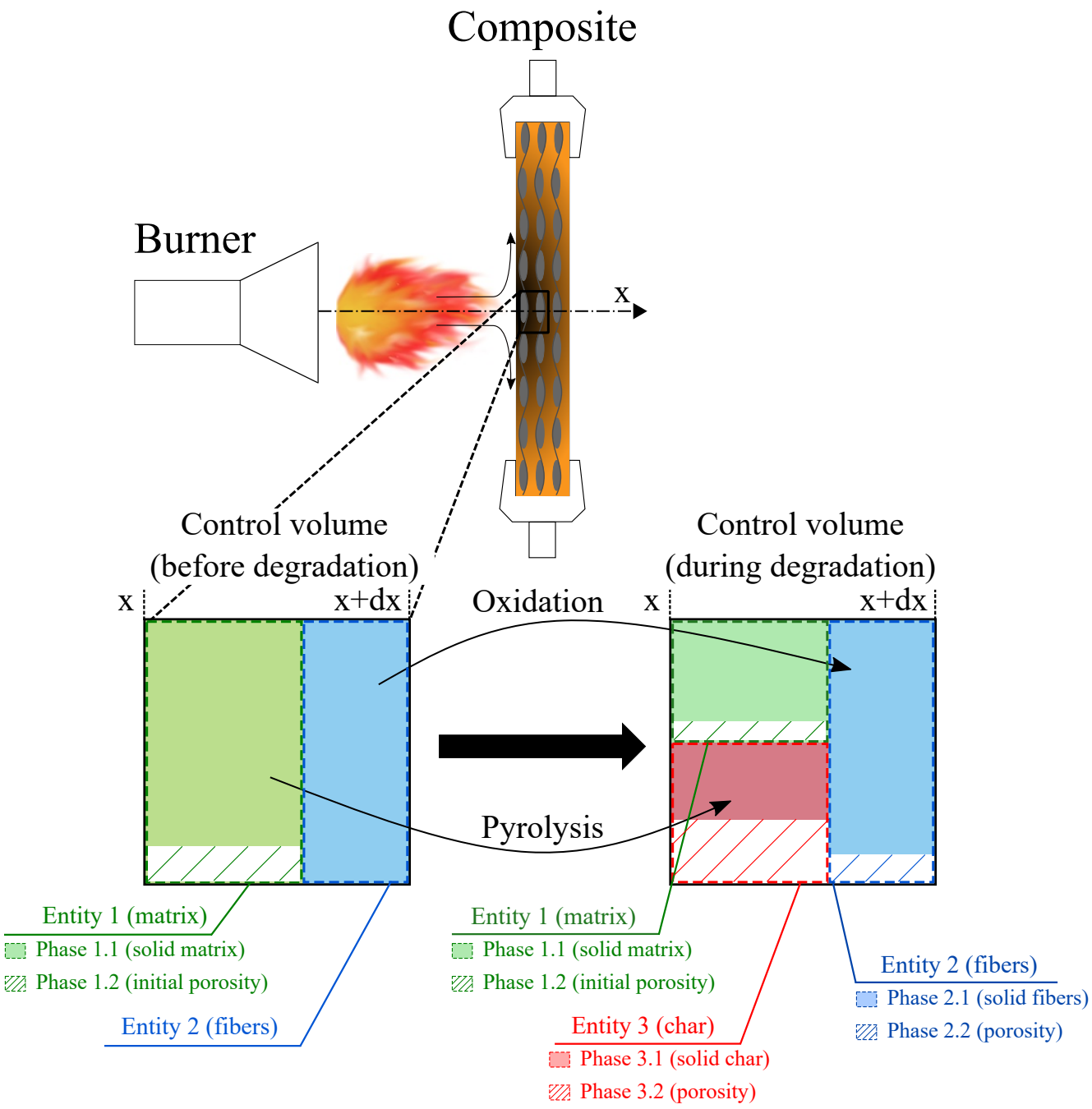

Figure 4.1 Illustration of a control volume containing several entities: a porous matrix, a porous char layer and non-porous carbon fibers. Although the domain is one-dimensional, the control volume has been drawn in 2D for better understanding.

each entity i is given by:

$$X_i = \frac{V_i}{V_{tot}} \tag{4.1}$$

where V_i is the volume of entity i and V_{tot} the total control volume. It is worth noting that $\sum_{i=1}^{N} X_i = 1$. This definition applies not only to the entity, but also to the phases constituting it. For instance, the volume fraction of the gaseous and solid phases composing the entity i are defined as:

$$X_{ip} = \frac{V_{ip}}{V_{tot}} \tag{4.2}$$

where the indexes ip denotes the solid ($p = s$) or gaseous ($p = g$) phase composing the entity i. Finally, the volume fraction can be defined not only with respect to the control volume but also with respect to the total solid or gaseous phases:

$$X_{ip,p} = \frac{V_{ip}}{\sum_{i=1}^{N_p} V_{ip}} \tag{4.3}$$

where N_p indicates the total number of solid or gaseous phases in the control volume. The index notation used in this work is summarized here:

- X_i: volume fraction of entity i
- X_{is}: volume fraction of the solid phase composing entity i
- X_{ig}: volume fraction of the gas phase composing entity i
- $X_{is,s}$: volume fraction of the solid phase composing entity i with respect to the total volume of all the solid phases
- $X_{ig,g}$: volume fraction of the gas phase composing entity i with respect to the total volume of all the gaseous phases

A distinction must also be made between the *absolute* density ρ_i, that is the density of a control volume containing only the entity i, and the *weighted bulk* or *effective* density $\bar{\rho}_i$, that is the density of entity i with respect to a control volume containing several different entities:

$$\bar{\rho}_i = \rho_i X_i \tag{4.4}$$

In the following, an overbar indicates *effective* quantities, defined with respect to the control volume. The total density $\bar{\rho}$ of the control volume is then given by:

$$\bar{\rho} = \sum_{i=1}^{N} X_i \rho_i = \sum_{i=1}^{N} \bar{\rho}_i \tag{4.5}$$

In the same manner, the effective density of all the gaseous or solid phases are represented by $\bar{\rho}_p$:

$$\bar{\rho}_p = \sum_{i=1}^{N_p} X_{ip} \rho_{ip} \tag{4.6}$$

Then, the mass fraction is defined as:

$$Y_i = \frac{m_i}{m_{tot}} = \frac{\bar{\rho}_i}{\bar{\rho}} = X_i \frac{\rho_i}{\bar{\rho}} \tag{4.7}$$

$$Y_{ip,p} = \frac{\bar{\rho}_{ip}}{\bar{\rho}_p} \tag{4.8}$$

where m_i and m_{tot} are respectively the mass of the phase i and of the sample. Again, $\sum_{i=1}^{N} Y_i = 1$.

The porosity represents the quantity of gas stored in pores appearing during the decomposition. It is defined as the volume fraction of void in each entity. The porosity ϕ_i is computed from each species bulk density as:

$$\phi_i = 1 - \frac{\bar{\rho}_i}{\bar{\rho}_{i,0}} = \frac{X_{ig}}{X_i} \tag{4.9}$$

where $\bar{\rho}_{i,0}$ corresponds to the effective density of the non-porous entity i over control volume. Finally, the total porosity is given by:

$$\bar{\phi} = \sum_{i=1}^{N} X_i \phi_i = \sum_{i=1}^{N} X_{ig} \tag{4.10}$$

Appendix C provides an example of application for all the equations introduced in this section.

4.1.3 Modeling of the thermophysical properties

The behavior of a material under fire attack depends on its thermal and physical properties, notably its thermal conductivity λ ($\mathrm{W\,m^{-1}\,K^{-1}}$), heat capacity c_p ($\mathrm{J\,kg^{-1}\,K^{-1}}$), sensible enthalpy h ($\mathrm{J\,kg^{-1}}$), permeability κ ($\mathrm{m^2}$), and emissivity ϵ ($-$), among others. The tempera-

ture dependence of each property $\mathbb{P}_i$ is defined in the model with a polynomial interpolation, typically of order 5 at the maximum:

$$\mathbb{P}_i(T) = \sum_{j=0}^{n} C_{ij} T^j \tag{4.11}$$

where C_{ij} is the jth polynomial coefficient of the ith thermo-physical property, and T is the temperature (K). The parameters C_{ij} are chosen empirically to fit experimental data representing the property $\mathbb{P}_i$ as a function of temperature.
Finally, the permeability is a function of the pore system, properties of gas mixture and porosity. It is calculated with the empirical formulation [106, 114]:

$$\kappa_i = \kappa_0 \exp(\kappa_1 \phi_i) \tag{4.12}$$

where κ_0 (m^2) is the inital porosity and κ_1 a curve fit coefficient. This equation was initially proposed by Fredlund for wood and was later used successfully by Looyeh [114] for composite combustion. Other formulations are also possible [64,162] but they are all based on empirical formulations. As the pore pressure depends on permeability, the curve fit coefficient can be computed with a prediction-correction method [144] to represent the pressure experimentally measured in the composite. In that case, the models do not really predict the pressure but rather use the pressure experimentally measured to provide a better estimation of gas flow through the material porosity.
Once the properties of each phase have been calculated as a function of temperature, the *effective* thermophysical properties of the entire control volume are computed with mass fraction Y_i (enthalpy h, heat capacity C_p) or volume fraction X_i (thermal conductivity λ, density ρ, porosity ϕ, radiative absorption ϵ, permeability κ, molecular mass M ($\mathrm{kg\,mol^{-1}}$) [55]:

$$\bar{\mathbb{P}} = \sum_{i=1}^{N} X_i . \mathbb{P}_i \tag{4.13}$$

$$\bar{\mathbb{P}} = \sum_{i=1}^{N} Y_i . \mathbb{P}_i \tag{4.14}$$

This method consisting in defining overall properties on the basis of mass or volume fraction is referred to as mixture rule in the following. This method is straightforward but does not provide information about the geometry of the phases and therefore cannot be used to compute the anisotropic thermal conductivity. The thermal conductivity of the control volume is computed as a function of the properties and geometries of its entities, following two main steps:

1. The conductivity of each entity i is computed as a function of its gaseous and solid phases ig and is, depending on the expected geometry of the pore distribution. If the porosity is assumed to consist of spheres homogeneously distributed in the solid phase, the conductivity of the porous medium is computed with Maxwell's model [163]:

$$\lambda_i = \lambda_{is} \left[\frac{\lambda_{ig} + 2\lambda_{is} + 2\phi_i(\lambda_{ig} - \lambda_{is})}{\lambda_{ig} + 2\lambda_{is} - \phi_i(\lambda_{ig} - \lambda_{is})} \right] \tag{4.15}$$

   This assumption is realistic for the porous char layer, as the influence of gaseous species on the matrix pyrolysis is neglected. In that case, the matrix decomposition is assumed to occur homogeneously inside the control volume as its temperature is constant. However, this assumption can be unrealistic when the decomposition of a solid phase depends on its exposition to another gaseous species, for instance the carbon fibers oxidation. In that case, the geometry of the porosity distribution can be influenced by the direction of diffusion of the oxidative species. For this reason, a second equation is defined and consists of a weighted sum of two extreme geometries, represented by the Voigt and Reuss models:

$$\lambda_i = W_F \left((1 - \phi_i)\lambda_{is} + \phi_i \lambda_{ig} \right) + (1 - W_F) \left(\frac{1 - \phi_i}{\lambda_{is}} + \frac{\phi_i}{\lambda_{ig}} \right)^{-1} \tag{4.16}$$

   where W_F is the user-chosen weighting factor that varies between 0 and 1 to represent the geometry of the pore distribution.

2. The conductivity of the composite depends on the geometry of its phases arrangement. Again, different methods have been implemented, depending on the composite geometry. First, a general equation consisting of the weighted sum of the Reuss and Voigt models was defined:

$$\bar{\lambda} = W_F \sum_{i=1}^{N} X_i \lambda_i + (1 - W_F) \sum_{i=1}^{N} \left(\frac{X_i}{\lambda_i} \right)^{-1} \tag{4.17}$$

   This equation has been implemented in the model to yield a versatile method, adaptable to many different configurations through the parameter W_F, as the model developped here is intended to be a generalized approach. However, some equations found in the literature are adapted to specific geometries. For instance, the Clayton model [164] is specifically developed for plain-weave composites, and is also implemented in the

following:

$$\bar{\lambda} = \frac{\lambda_m}{4}\left[\sqrt{(1-X_f)^2\left(\frac{\lambda_f}{\lambda_m}-1\right)^2+\frac{4\lambda_f}{\lambda_m}}-(1-X_f)\left(\frac{\lambda_f}{\lambda_m}-1\right)\right]^2 \tag{4.18}$$

where the index m and f refer to the matrix and fibers.

4.1.4 Modeling of the decomposition rate

Single reaction

Consider a single reaction during which a solid phase (S1) is consumed to produce another solid phase (S2) and gaseous species (GAS):

$$\mathrm{S1} = \theta_c \mathrm{S2} + (1-\theta_c)\mathrm{GAS} + q \tag{4.19}$$

where q is the heat of reaction and θ_c is the mass stoichiometric coefficient (kg/kg). For instance, in case of pyrolysis, S1 is the polymer matrix, S2 the char and GAS the pyrolysates. In case of oxidation, $\theta_c = 0$.
The rate of decomposition of this reaction ($\mathrm{kg\,m^{-3}\,s^{-1}}$) is given by:

$$\frac{\partial \rho_{S1}}{\partial t} = f(\rho_{S1}) A \exp\left(-\frac{E}{RT}\right) \tag{4.20}$$

A is the pre-exponential factor $\mathrm{s^{-1}}$, E the activation energy $\mathrm{J\,mol^{-1}}$, R the perfect gas constant $\mathrm{J\,mol^{-1}\,K^{-1}}$ and ρ_{S1} the density of the reactant $S1$. $f(\rho_{S1})$ represents the reaction model, i.e. the dependence of the reaction on the decomposition degree. The reaction model can take many different forms, whether the reaction is accelerating, decelerating or sigmoidal [47]. The most common reaction model is the n-order law, which provides:

$$k = (\bar{\rho}_{S1,0} - \bar{\rho}_{S1,\infty})\left[\frac{\bar{\rho}_{S1}(t) - \bar{\rho}_{S1,\infty}}{\bar{\rho}_{S1,0}(t) - \bar{\rho}_{S1,\infty}}\right]^n A \exp\left(-\frac{E}{RT}\right) \tag{4.21}$$

where n is the reaction order $(-)$, $\bar{\rho}_{S1,0}$ and $\bar{\rho}_{S1,\infty}$ are the initial and final (at the end of decomposition) densities of species $S1$ and n_j the order of the reaction $(-)$. In case of oxidation, Equation 4.21 is multiplied by the mass fraction of oxidizer [52]. The three parameters (A_j, E_j and n_j) form the so-called kinetic triplet. The reaction rate of the species

involved in reaction 4.19 is computed as [47]:

$$\frac{\partial \bar{\rho_{S1}}(t)}{\partial t} = -k \tag{4.22a}$$

$$\frac{\partial \bar{\rho_{S2}}(t)}{\partial t} = \theta_c k \tag{4.22b}$$

$$\frac{\partial \bar{\rho_{GAS}}(t)}{\partial t} = (1-\theta_c) k \tag{4.22c}$$

Generalization to a system of n reactions

Consider a system of reactions composed of N_r equations including N_i different species, occurring in the sample during fire exposure. The reaction rate of each reaction j is computed according to equation 4.21. Then, the consumption or production of each species i is given by:

$$\left.\frac{\partial \bar{\rho}_i}{\partial t}\right|_{net} = \sum_{j=1}^{N_r} \theta_{ij} k_j \tag{4.23}$$

The total density variation of gaseous or solid phase is computed as:

$$\left.\frac{\partial \bar{\rho}_p}{\partial t}\right|_{net} = \sum_{i=1}^{N_p} \left.\frac{\partial \bar{\rho}_{ip}}{\partial t}\right|_{net} = \sum_{i=1}^{N_p} \sum_{j=1}^{N_r} \theta_{ij} k_j \tag{4.24}$$

where the index p indicates solid ($p = s$) or gaseous ($p = g$) species.

4.2 Mathematical model

4.2.1 The conservation equation

The composite exposed to fire can be described by several extensive variables of interest, for instance the energy U, mass m and quantity of movement mv. The variation of these variables is obtained by global theoretical laws applied on a control mass, that is a system representing an arbitrary quantity of matter constituting the entire composite or exposed to fire [165], as depicted in Figure 4.2. It is worth noting that the control mass represents the initial mass of the composite (matrix and fibers) and all products from the decomposition of the solid phase (pyrolysates); the control mass is, by definition, constant:

$$\frac{\partial m_{syst}}{\partial t} = 0 \tag{4.25}$$

Then, the variation of momentum is given by the Newton's second law:

$$\sum \underline{\boldsymbol{F}} = m\underline{\boldsymbol{a}} = \frac{\partial m\underline{\boldsymbol{v}}}{\partial t} \tag{4.26}$$

Finally, the variation of energy is given by the first law of thermodynamics:

$$\frac{\partial Q}{\partial t} - \frac{\partial W}{\partial t} = \frac{\partial U}{\partial t} \tag{4.27}$$

These laws act on the control mass and describe the global state of the entire material at an arbitrary moment. However, they cannot provide insight on the processes occurring inside the composite during its thermal degradation. Local equations valid for every small volume inside the composite are required.

The Reynolds Transport Theorem, which is a 3D generalization of the Leibniz integral rule, allows to convert the mathematics of the global theoretical laws so that they can be applied to a control volume (a small volume at a specific location, through which mass and energy may cross) instead of a control mass (a quantity of mass exchanging only energy with its surrounding). Consider a system described by an extensive property B, i.e. proportional to the quantity of matter in the system. This extensive variable can be converted to its intensive form by $\beta = \partial B/\partial m$, where ∂m is a small variation of mass. The Reynolds Transport Theorem provides a relation between the extensive and intensive variables [165]:

$$\left.\frac{\partial B}{\partial t}\right|_{CM} = \frac{\partial}{\partial t}\int_{CV} \beta\rho dV + \int_{CS} \beta\rho(\underline{\boldsymbol{v}} \cdot \underline{\boldsymbol{n}})dS \tag{4.28}$$

where the indexes CM and CV refer to the control mass and the control volume, with CS the control surface, i.e. the boundary of the control volume. ρ is the density, V the volume of the control volume and S the surface of the control surface, $\underline{\boldsymbol{v}}$ the flow velocity at the control surface with respect to the control surface normal $\underline{\boldsymbol{n}}$, pointing outward. The variation of an extensive property can be written in a general form as a sum of a source term and a diffusive term:

$$\left.\frac{\partial B}{\partial t}\right|_{CM} = \int_{CS} \underline{\boldsymbol{j}}_\beta \cdot \underline{\boldsymbol{n}} dS + \int_{CV} S_\beta dV \tag{4.29}$$

where S_β represents the source term, that is the creation or absorption of β inside the control volume, and $\underline{\boldsymbol{j}}_\beta$ represents the diffusive flux of B through the boundaries. The flux $\underline{\boldsymbol{j}}_\beta$ is defined by the product of the *generalized force* driving the flux, i.e. the gradient of the variable β, by the parameter Γ_β that represents the capacity of the medium to transport β [166]:

$$\underline{\boldsymbol{j}}_\beta = \Gamma_\beta \times \underline{\boldsymbol{\nabla}}(\beta) \tag{4.30}$$

Of course, the gradient of the dependent variable β is not the only force driving the fluxes acting on the system, but the objective is to develop a general equation adaptable to different situations. For instance, γ_β and β can be the diffusion coefficient D and concentration in the Fick's first law. If another flux driven by the gradient of another variable is acting on the system, it can be expressed as a part of the source term. If there is no diffusive term in a particular situation, Γ_β can be set to 0 [166]. Finally, equations 4.28 and 4.29 contain surface integrals that can be transformed into volume integrals with the Gauss-Ostrogradsky theorem:

$$\int_{CS} \underline{\boldsymbol{j}}_\beta \cdot \underline{\boldsymbol{n}}\, dS = \int_{CV} \underline{\boldsymbol{\nabla}} \cdot \underline{\boldsymbol{j}}_\beta\, dV \tag{4.31}$$

Combining Equations 4.28, 4.29, 4.30 and 4.31 provides the integral form of the generalized conservation equation of the intensive property β:

$$\frac{\partial}{\partial t}\int_{CV} \beta\rho\, dV + \int_{CS} \beta\rho(\underline{\boldsymbol{v}} \cdot \underline{\boldsymbol{n}})\, dS = \int_{CS} \underline{\boldsymbol{j}}_\beta \cdot \underline{\boldsymbol{n}}\, dS + \int_{CV} S_\beta\, dV \tag{4.32}$$

The integral form of the conservation equation is not suitable for a numerical analysis. Other assumptions are required to derive the local form of Equation 4.32. First, the sample is assumed to behave as a continuum, which means that its properties do not vary significantly over distances of the order of magnitude of the mean free path, as it would be the case if shock waves were present or for an extremely diluted gas. Then, the local equilibrium is assumed, i.e. the global equilibrium is verified on each point of the control volume [167]. These two hypotheses allow to write the conservation equation in their local form, here in 1D [166]:

$$\frac{\partial \rho\beta}{\partial t} + \frac{\partial \rho v \beta}{\partial x} = \frac{\partial}{\partial x}\left(\Gamma_\beta \frac{\partial \beta}{\partial x}\right) + S_\beta \tag{4.33}$$

The first term on the left hand side is the *storage term*, which accounts for the variation of β inside the control volume. The second term on the left hand side is the *convective term*, representing the flux of β by transport of matter, with $\rho v = \dot{m}$. The first term on the right hand side is the *diffusive term*, which accounts for the flux of β without transport of matter. The second term on the right hand side is the *source term*, accounting for the production or consumption of β, when applicable. The advantage of developing a general form for the conservation equation is to manipulate any differential equation useful for the problem so that it meets to the standard form assumed in numerical studies, which simplifies the modeling of conservation equations derived in new configurations, such as the one treated here. It is worth noting that when Equation 4.33 is applied to a control volume containing both gas

and solid phases, the convective term applies only to the gas phase, therefore:

$$\frac{\partial \rho\beta}{\partial t} + \frac{\partial \rho_g v_g \beta}{\partial x} = \frac{\partial}{\partial x}\left(\Gamma_\beta \frac{\partial \beta}{\partial x}\right) + S_\beta \tag{4.34}$$

If applied to the entire control volume, this last equation can further be simplified. Expanding the first two derivatives provides [143]:

$$\beta\left(\frac{\partial \rho}{\partial t} + \frac{\partial \rho_g v_g}{\partial x}\right) + \rho\frac{\partial \beta}{\partial t} + \rho_g v_g \frac{\partial \beta}{\partial x} = \frac{\partial}{\partial x}\left(\Gamma_\beta \frac{\partial \beta}{\partial x}\right) + S_\beta \tag{4.35}$$

The first term on the left hand side represents mass conservation or continuity. If the conservation equation is applied to the entire control volume (including both gas and solid phases), this term is 0, as the variation of mass in a fixed volume equals the net flow across its surface. This allow to simplify the conservation equation to:

$$\rho\frac{\partial \beta}{\partial t} + \rho_g v_g \frac{\partial \beta}{\partial x} = \frac{\partial}{\partial x}\left(\Gamma_\beta \frac{\partial \beta}{\partial x}\right) + S_\beta \tag{4.36}$$

One initial and two boundary and conditions are required to compute the transport of β. The initial conditions consist in defining the value taken by β at the first time step. The boundary conditions depend on the way the environment is acting on the sample on each face. Three possibilities have been implemented (illustrated here on the hot face of the pyrolysis model domain, i.e. $x = 0$):

- **Dirichlet boundary conditions**: the value of β is imposed on the extremity of the domain and does not vary:

$$\beta(x = 0) = \beta_0 \tag{4.37}$$

- **Neumann boundary conditions**: the flux of β is imposed on the extremities of the domain. This condition can be used to represent, for instance, impermeable surfaces to heat of mass transfers:

$$\left.\frac{\partial \beta}{\partial x}\right|_{x=0} = j_{\beta,0} \tag{4.38}$$

- **Robin boundary conditions**: the flux of β is imposed, with a retroactive parameter h_c updated at each iteration to represent the evolution of the interactions between the sample and the environment.

$$\left.\frac{\partial \beta}{\partial x}\right|_{x=0} = h_c(\beta_{env} - \beta_0) \tag{4.39}$$

In the following, the general conservation equation is applied on different variables and control volumes, that are described in Appendix D.

4.2.2 Conservation of solid species

First, the general equation of conservation 4.33 is applied to the solid phase is of the composite. The solid part of the control volume is isolated ($\rho = \bar{\rho}_s$, $m = m_s$) and the extensive variable defining the mass of the solid species is is: $B = m_{is} = m_s Y_{is,s}$. Therefore, the intensive variable associated to B is $\beta = \partial(m_s Y_{is,s})/\partial m_s = Y_{is,s}$ By assumption, only gaseous phases can cross the control volume boundaries, which implies that the diffusive and convective terms of equation 4.34 are zero: $\Gamma_\beta = 0$ and $v = 0$. The source term is defined as the net variation of mass of species is:

$$S_{Y_{is}} = \sum_{j=1}^{N_r} \theta_{ij} k_j \tag{4.40}$$

As the conservation equation is applied on a control volume containing the solid phase only, Equation 4.34 cannot be used and Equation 4.36 must be used instead. It provides:

$$\frac{\partial \bar{\rho}_s Y_{is,s}}{\partial t} = \sum_{j=1}^{N_r} \theta_{ij} k_j \tag{4.41}$$

Considering that $\bar{\rho}_s Y_{is,s} = \bar{\rho}_s \bar{\rho}_{is}/\bar{\rho}_s = \bar{\rho}_{is}$, this equation can be written in a more compact form:

$$\frac{\partial \bar{\rho}_{is}}{\partial t} = \sum_{j=1}^{N_r} \theta_{ij} k_j \tag{4.42}$$

At the initial state, $\frac{\partial \bar{\rho}_{is}}{\partial t} = 0$.

4.2.3 Conservation of gas phase mass

Equation 4.33 is applied to the total gas phase ($\rho = \bar{\rho}_g$ and $m = m_g$). The extensive variable of interest is the total mass of the gas phase: $B = m_g$ and $\beta = \partial m_g/\partial m_g = 1$. The gaseous species contained in the material may flow toward the environment or be stored within the porosity of the material. The only flux acting on the control volume is the convective flux as gaseous species are transported by the flow of gas through the porosity. However, the net total diffusive flux of gaseous species is 0, as each gaseous species diffuses into another. The

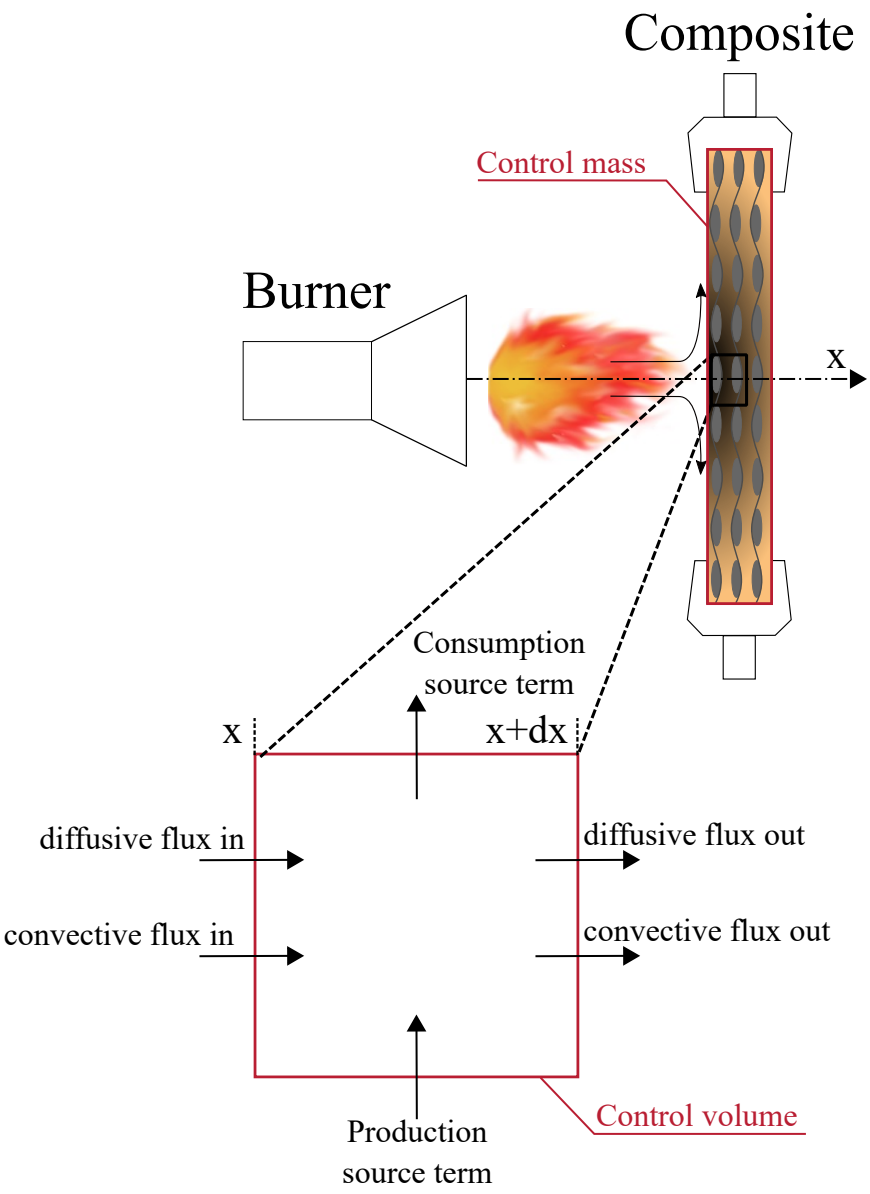

Figure 4.2 Illustration of the difference between control volume, i.e. a small volume whose boundaries are permeable to mass and energy transfers, and control mass, i.e. an arbitrary amount of mass, permeable only to energy transfers. The horizontal arrows on the control volume indicate flux in and out. The vertical arrows indicate source terms, which are the production or consumption of the variable of interest inside the control volume.

source term is defined as the total variation of mass of all the gaseous species:

$$S_g = \sum_{i=1}^{N_g} \left.\frac{\partial \bar{\rho}_{ig}}{\partial t}\right|_{net} = \sum_{i=1}^{N_g}\sum_{j=1}^{N_r} \theta_{ij} k_j \tag{4.43}$$

As the conservation equation is applied on a control volume containing the gas phase only, Equation 4.36 must be used, providing:

$$\frac{\partial \bar{\rho}_g}{\partial t} + \frac{\partial \bar{\rho}_g v}{\partial x} = \sum_{i=1}^{N_g}\sum_{j=1}^{N_r} \theta_{ij} k_j \tag{4.44}$$

It is worth noting that $\bar{\rho}_g = \sum_{i=1}^{N_g} X_{ig}\rho_{ig}$. The pores being all interconnected, the density of every gaseous phase is assumed to be the same, therefore $\rho_{1g} = \rho_{2g} = ... = \rho_g$. As $\bar{\phi} = \sum_{i=1}^{N_g} X_{ig}$, which leads to:

$$\bar{\rho}_g = \bar{\phi}\rho_g \tag{4.45}$$

The gas density is computed with the perfect gas law:

$$\rho_g = \frac{P\bar{M}}{RT} \tag{4.46}$$

Injecting Equation 4.46 into Equation 4.44 yields the equation for the conservation of gas phase mass:

$$\frac{\partial \rho_g \bar{\phi}}{\partial t} + \frac{\partial \rho_g \bar{\phi} v}{\partial x} = \sum_{i=1}^{N_p}\sum_{j=1}^{N_r} \theta_{ij} k_j \tag{4.47}$$

If the gaseous species are assumed to flow through the composite with no resistance, the pore pressure remains constant and the mass flow rate can be directly computed from the conservation of mass by integrating Equation 4.47. It provides:

$$\dot{m}_g = \rho_g \bar{\phi} v = \int_{x_{cv}}^{L} \left(\sum_{i=1}^{N_p}\sum_{j=1}^{N_r} \theta_{ij} k_j - \frac{\partial \rho_g \bar{\phi}}{\partial t} \right) dx \tag{4.48}$$

where L is the composite thickness and x_{cv} the location of the control volume on the x-axis. It is worth noting that the second term in Equation 4.48, representing the accumulation of gas inside the porosity, can be neglected most of the times. At the initial state, $\frac{\partial \bar{\rho}_{is}}{\partial t} = 0$. If the system should also be solved for pressure, another method is required to calculate $\dot{m}_g$, as will be seen in the following.

4.2.4 Conservation of gaseous species

Equation 4.34 is applied to the gas phase ($\rho = \bar{\rho}_g$ and $m = m_g$). The variable of interest is the partial mass of the gaseous species ig ($B = m_{ig} = Y_{ig,g} m_g$), and its intensive variable form is therefore $\beta = \partial(Y_{ig,g} m_g)/\partial m_g = Y_{ig,g}$. Both convective and diffusive fluxes must be considered, as well as the net creation of species ig:

$$S_{ig} = \sum_{j=1}^{N_r} \theta_{ij} k_j \tag{4.49}$$

Assuming that the gas can be treated as a continuum, the diffusion flux depends on the concentration gradient of species ig and is calculated with Fick's law ($\Gamma_\beta = \bar{\rho}_g D$):

$$j_{Y_{ig,g}} = -\bar{\rho}_g D \frac{\partial Y_{ig,g}}{\partial x} \tag{4.50}$$

where $J_{D,j}$ is the diffusive flux of gaseous species j ($\mathrm{kg\,m^2\,s^{-1}}$) and D the diffusivity ($\mathrm{m^2\,s^{-1}}$). Injecting Equations 4.45, 4.48 and 4.50 in Equation 4.34 yields:

$$\frac{\partial \bar{\phi} \rho_g Y_{ig,g}}{\partial t} + \frac{\partial \dot{m}_g Y_{ig,g}}{\partial x} = -\frac{\partial}{\partial x}\left(\bar{\phi} \rho_g D \frac{\partial Y_{ig,g}}{\partial x}\right) + \sum_{j=1}^{N_r} \theta_{ij} k_j \tag{4.51}$$

Neglecting the time and space derivative of $\phi \rho_g$ and $\dot{m}_g$, when compared to that of $Y_{ig,g}$, the conservation of mass reduces to:

$$\bar{\phi} \rho_g \frac{\partial Y_{ig,g}}{\partial t} + \dot{m}_g \frac{\partial Y_{ig,g}}{\partial x} = \frac{\partial}{\partial x}\left(\bar{\phi} \rho_g D \frac{\partial Y_{ig,g}}{\partial x}\right) + \sum_{j=1}^{N_r} \theta_{ij} k_j \tag{4.52}$$

One initial value and two boundary conditions are required to solve this equation. At the initial state, $Y_{ig,g} = 0$ in the whole computational domain. The mass flux of the gaseous species ig is defined with the heat transfer analogy [55]:

$$j_{Y_{ig,g}}\Big|_{x=0} = \frac{h_{c,0}}{\bar{c}_{pg}} \left(Y_{ig,g}|_\infty - Y_{ig,g}|_{x=0}\right) \tag{4.53}$$

$$j_{Y_{ig,g}}\Big|_{x=L} = \frac{h_{c,L}}{\bar{c}_{pg}} \left(Y_{ig,g}|_\infty - Y_{ig,g}|_{x=L}\right) \tag{4.54}$$

4.2.5 Conservation of energy

The conservation of energy is applied simultaneously to all phases of the sample, as gas and solid are assumed to be in local thermal equilibrium (hypothesis 5), leading to $\rho = \bar{\rho}$ and $m = m_{cv}$ in Equation 4.36. The enthalpy is the extensive variable of interest ($\beta = H$). For

solids, liquids and ideal gases (hypothesis 6), the enthalpy and specific enthalpy are given by:

$$dH = m_{cv}\bar{c}_p dT \tag{4.55}$$

$$dh = \bar{c}_p dT \tag{4.56}$$

Assuming that $d\bar{c_p}$ is negligible when compared to dT, the $H(T)$ equations simplify into [166]:

$$H = m_{cv}\bar{c}_p T = B \tag{4.57}$$

$$h = \bar{c}_p T = \beta \tag{4.58}$$

Convection and conduction are both transporting heat into the system. The diffusive term is modeled with Fourier's law:

$$j_h = \lambda \frac{\partial T}{\partial x} \tag{4.59}$$

Therefore, $\Gamma_\beta = \lambda / c_p$ in Equation 4.30 [166]. Finally, the source term S_β corresponds to the total heat absorbed or released by the chemical reactions occurring in the control volume:

$$S_h = \sum_{j=1}^{N_r} k_j q_j \tag{4.60}$$

The injection of B, β, Γ_β and S_β into Equation 4.36 yields:

$$\bar{\rho}\frac{\partial \bar{c}_p T}{\partial t} + \bar{\rho}_g v \frac{\partial \bar{c}_{pg} T}{\partial x} = \frac{\partial}{\partial x}\left(\frac{\bar{\lambda}}{\bar{c}_p}\frac{\partial c_p T}{\partial x}\right) + \sum_{j=1}^{N_r} k_j q_j \tag{4.61}$$

Neglecting the spatial and temporal variation of $\bar{c}_p$ compared to those of T, the equation can be simplified as:

$$\bar{\rho}\bar{c}_p\frac{\partial T}{\partial t} + \dot{m}_g \bar{c}_{pg}\frac{\partial T}{\partial x} = \frac{\partial}{\partial x}\left(\bar{\lambda}\frac{\partial T}{\partial x}\right) + \sum_{j=1}^{N_r} k_j q_j \tag{4.62}$$

One initial condition and two boundary conditions are required to solve this equation. At the initial state, the temperature is equal to the environment temperature in the whole computational domain. The heat flux is defined with a Robin boundary condition to account for the convective heat transfer on both hot and cold faces:

$$j_h|_{x=0} = h_{c,0}\left(T|_{\infty,0} - T|_{x=0}\right) \tag{4.63}$$

$$j_h|_{x=L} = h_{c,L}\left(T|_{\infty,L} - T|_{x=L}\right) \tag{4.64}$$

4.2.6 Conservation of gas phase momentum

A last equation describing the pressure rise inside the composite is required. The modeling of pressure rise is optional in the code presented here. If the pressure is not computed and assumed to be constantly equal to the environment pressure, Equation 4.48 is used to determine $\dot{m}_g$. This choice corresponds to a situation in which the gas flows through the composite without resistance. However, in reality, the resistance of the pore network to gas flow provokes a pressure rise inside the porosity, and the pressure gradient drives the mass flow rate. If this pressure rise is considered, Equation 4.34 is again applied to the total gas phase ($B = m_g$ and $\beta = 1$), but the gas phase density is computed using the ideal gas law:

$$\rho_g = \frac{P\bar{M}}{RT} \tag{4.65}$$

Moreover, the effect of the pressure rise must be considered to model the mass flow rate through the porosity. If the pressure is computed, $\dot{m}_g$ is calculated with the Darcian law:

$$\dot{m}_g = -\frac{\bar{\kappa}}{\nu}\frac{\partial P}{\partial x} \tag{4.66}$$

Injecting Equations 4.46 and 4.66 into Equation 4.47 yields:

$$\frac{\partial \frac{P\bar{M}\bar{\phi}}{RT}}{\partial t} = \frac{\partial}{\partial x}\left(\frac{\bar{\kappa}}{\nu}\frac{\partial P}{\partial x}\right) + \sum_{i=1}^{N_p}\sum_{j=1}^{N_r}\theta_{ij}k_j \tag{4.67}$$

One initial condition and two boundary conditions are required to solve this equation. At the initial state, the pressure is equal to the environment pressure P_0 in the whole computational domain. The pressure is then fixed on the extremities of the domain with a Dirichlet Boundary condition:

$$P|_{x=0} = P_0 \tag{4.68}$$

$$P|_{x=L} = P_0 \tag{4.69}$$

4.3 Numerical method

In this section, the numerical method used to solve simultaneously the conservation equations derived in the previous section are introduced. First, the finite element formulation is derived and the time step resolution is introduced. Finally, the complete code algorithm is presented.

4.3.1 Finite Element Formulation

The finite element method consists in subdividing the computational domain into n subdomains, also called *finite element*. Each element Ω_e is constituted of two nodes to which a value of β is assigned. Between two nodes, $\beta(x,t)$ is approximated by an interpolation, represented by an approximation function $\underline{\boldsymbol{\psi}}^e(x)$:

$$\beta(x,t) \approx \beta^e(x,t) = \underline{\boldsymbol{\beta}}^e(t)\underline{\boldsymbol{\psi}}^e(x) = \sum_{j=1}^{2} \beta_j^e(t)\psi_j^e(x) \tag{4.70a}$$

$$\frac{\partial \beta(x,t)}{\partial x} \approx \frac{\partial \beta^e(x,t)}{\partial x} = \underline{\boldsymbol{\beta}}^e(t)\frac{\partial \underline{\boldsymbol{\psi}}^e(x)}{\partial x} = \sum_{j=1}^{2} \beta_j^e(t)\frac{\partial \psi_j^e(x)}{\partial x} \tag{4.70b}$$

$$\frac{\partial \beta(x,t)}{\partial t} \approx \frac{\partial \beta^e(x,t)}{\partial t} = \frac{\partial \underline{\boldsymbol{\beta}}^e(t)}{\partial t}\underline{\boldsymbol{\psi}}^e(x) = \sum_{j=1}^{2} \frac{\partial \beta_j^e(t)}{\partial t}\psi_j^e(x) \tag{4.70c}$$

where β^e is an approximation of β over the element Ω^e, $\underline{\boldsymbol{\psi}}^e(x)$ is the approximation function vector, $\psi_j^e(x)$ the jth term of the approximation function and $\beta_j^e(t)$ the jth term of the dependent variable vector.

The Finite Element formulation is applied to the general conservation Equation 4.36. First, all the terms of Equation 4.36 are regrouped on one side of the equality and multiplied by a weight function w. Then, the expression is integrated over the element domain Ω_e, yielding the *weighted-residual* statement of Equation 4.36:

$$0 = \int_{\Omega_e} w\left[\rho^e\frac{\partial \beta^e}{\partial t} + \dot{m}_g^e\frac{\partial \beta^e}{\partial x} - \frac{\partial}{\partial x}\left(\Gamma_\beta^e\frac{\partial \beta^e}{\partial x}\right) - S_\beta^e\right]dx \tag{4.71}$$

This equation contains a second derivative of β^e with respect to x, which requires ψ_j^e to be twice differentiable with respect to x. This requirement can be weakened by using an integration by parts on the second derivative term:

$$\int_{\Omega_e} w\frac{\partial}{\partial x}\left(\Gamma_\beta^e\frac{\partial \beta^e}{\partial x}\right)dx = \left[w\Gamma_\beta^e\frac{\partial \beta^e}{\partial x}\right]_{\Omega_e} - \int_{\Omega_e}\frac{\partial w}{\partial x}\Gamma_\beta^e\frac{\partial \beta^e}{\partial x}dx \tag{4.72}$$

Injecting Equation 4.72 into Equation 4.71 yields the *weak formulation*:

$$\int_{\Omega_e} w\rho^e\frac{\partial \beta^e}{\partial t}dx + \int_{\Omega_e} w\dot{m}_g^e\frac{\partial \beta^e}{\partial x}dx + \int_{\Omega_e}\frac{\partial w}{\partial x}\Gamma_\beta^e\frac{\partial \beta^e}{\partial x}dx = \left[w\Gamma_\beta^e\frac{\partial \beta^e}{\partial x}\right]_{\Omega_e} + \int_{\Omega_e} wS_\beta^e dx \tag{4.73}$$

According to the Bubnov-Galerkin method, the weight function ϕ is chosen to be equal to the approximation function ψ. As two independent algebraic equations are required to solve

for the two unknown dependent variables on each element, two independent functions are chosen for w: $w = \psi_1^e$, $w = \psi_2^e$. Injecting Equations 4.70a to 4.70c into Equation 4.73 yields the ith equation on the ith node of element Ω^e:

$$\sum_{j=1}^{2}\left[\int_{\Omega^e}\psi_i^e(x)\rho^e\psi_j^e(x)dx\right]\frac{\partial\beta_j^e(t)}{\partial t} + \sum_{j=1}^{2}\left[\int_{\Omega^e}\psi_i^e(x)\dot{m}_g^e\frac{\partial\psi_j^e(x)}{\partial x}dx + \int_{\Omega^e}\frac{\partial\psi_i^e(x)}{\partial x}\Gamma_\beta^e\frac{\partial\psi_j^e(x)}{\partial x}dx\right]\beta_j^e(t) = \left[\psi_i^e(x)\Gamma_\beta^e\frac{\partial\beta^e}{\partial x}\right]_{\Omega^e} + \int_{\Omega^e}\psi_i^e(x)S_\beta^e dx \quad (4.74)$$

The other advantage of the integration by parts is to introduce naturally the boundary conditions, which appear in the first term on the right side of Equation 4.74. This term can be evaluated on each node composing one element of length l using equation 4.30:

$$\textbf{First node} \quad \left[\psi_1^e(x)\Gamma_\beta^e\frac{\partial\beta^e}{\partial x}\right]_0^l = \psi_1^e(l)\left(\Gamma_\beta^e\frac{\partial\beta^e}{\partial x}\right)_l - \psi_1^e(0)\left(\Gamma_\beta^e\frac{\partial\beta^e}{\partial x}\right)_0 = -\underline{\boldsymbol{j}}_\beta^e(0) \quad (4.75)$$

$$\textbf{Second node} \quad \left[\psi_2^e(x)\Gamma_\beta^e\frac{\partial\beta^e}{\partial x}\right]_0^l = \psi_2^e(l)\left(\Gamma_\beta^e\frac{\partial\beta^e}{\partial x}\right)_l - \psi_2^e(0)\left(\Gamma_\beta^e\frac{\partial\beta^e}{\partial x}\right)_0 = \underline{\boldsymbol{j}}_\beta^e(l) \quad (4.76)$$

Injecting Equations 4.75 and 4.76 into Equation 4.74 and regrouping all the terms, it provides the *finite element model*:

$$\underline{\underline{\boldsymbol{C}}}^e\underline{\dot{\boldsymbol{\beta}}}^e + \underline{\underline{\boldsymbol{K}}}^e\underline{\boldsymbol{\beta}}^e = \underline{\boldsymbol{F}}^e \quad (4.77)$$

With:

$$\underline{\underline{\boldsymbol{C}}}^e = \int_0^l \underline{\boldsymbol{\psi}}^{eT}(x)\rho^e\underline{\boldsymbol{\psi}}^e(x)\,dx \quad (4.78a)$$

$$\underline{\underline{\boldsymbol{K}}}^e = \underline{\underline{\boldsymbol{K}}}_1^e + \underline{\underline{\boldsymbol{K}}}_2^e = \int_0^l \underline{\boldsymbol{\psi}}^{eT}(x)\dot{m}_g^e\frac{\partial\underline{\boldsymbol{\psi}}^e(x)}{\partial x}\,dx + \int_0^l \frac{\partial\underline{\boldsymbol{\psi}}^{eT}(x)}{\partial x}\Gamma_\beta^e\frac{\partial\underline{\boldsymbol{\psi}}^e(x)}{\partial x}\,dx \quad (4.78b)$$

$$\underline{\boldsymbol{F}}^e = \underline{\boldsymbol{F}}_1^e - \underline{\boldsymbol{F}}_2^e = \begin{bmatrix}-\underline{\boldsymbol{j}}_\beta^e(0)\\ \underline{\boldsymbol{j}}_\beta^e(l)\end{bmatrix} - \int_0^l \underline{\boldsymbol{\psi}}^{eT}(x)S_\beta^e\,dx \quad (4.78c)$$

where $\underline{\boldsymbol{\psi}}^{eT}$ is the transpose of $\underline{\boldsymbol{\psi}}^e$. $\underline{\underline{\boldsymbol{C}}}^e$ and $\underline{\underline{\boldsymbol{K}}}^e$ are called the *capacitance* and *coefficient* matrices. It is worth noting that their terms depend on the element properties (ρ^e, Γ_β^e, etc), which in turn depend most of time on the intensive parameter β^e or its derivative. Therefore, an intermediate value of β must first be estimated to calculate the element matrices before predicting the actual value of β with Equation 4.77 [143].

The simplest definition of the approximation function $\underline{\boldsymbol{\psi}}^e(x)$ is a linear interpolation, defined on each element Ω_e such as:

$$\underline{\boldsymbol{\psi}}^e(x) = \begin{bmatrix} \frac{l-x}{l} & \frac{x}{l} \end{bmatrix} \tag{4.79a}$$

$$\frac{\partial \underline{\boldsymbol{\psi}}^e(x)}{\partial x} = \begin{bmatrix} \frac{-1}{l} & \frac{1}{l} \end{bmatrix} \tag{4.79b}$$

Once the element matrices have been defined for the general form of the conservation equation, they are computed for each conservation equation constituting the model, as shown in Appendix E.

The element matrices $\underline{\underline{\boldsymbol{C}}}^e$, $\underline{\underline{\boldsymbol{K}}}^e$ and $\underline{\boldsymbol{F}}^e$ must then be assembled to give the global matrices $\underline{\underline{\boldsymbol{C}}}$, $\underline{\underline{\boldsymbol{K}}}$ and $\underline{\boldsymbol{F}}$ covering the entire computational domain. This step must obey two rules: first, the dependent variable β must be continuous. Then, the fluxes must be balanced between consecutive elements [143]. This implies that the *interior fluxes* $-\underline{\boldsymbol{j}}_\beta(0)$ and $\underline{\boldsymbol{j}}_\beta(l)$ between two elements cancel each other. The only remaining terms in $\underline{\boldsymbol{F}}$ are the fluxes on each extremity of the computational domain, i.e the Neumann or Robin boundary conditions. The assembly is achieved by the following algorithm [114]:

$$\underline{\underline{\boldsymbol{C}}} = \sum_{e=1}^{N_e} \underline{\underline{\boldsymbol{C}}}^e \tag{4.80a}$$

$$\underline{\underline{\boldsymbol{K}}} = \sum_{e=1}^{N_e} \underline{\underline{\boldsymbol{K}}}^e \tag{4.80b}$$

$$\underline{\boldsymbol{F}} = \sum_{e=1}^{N_e} \underline{\boldsymbol{F}}^e \tag{4.80c}$$

4.3.2 Time-step algorithm

The differential equation 4.77 can be used to predict the evolution of temperature over time. The duration of the fire test is divided into m discrete time steps and the duration of an interval is $\Delta t = t^{n+1} - t^n$, where n indicates the time step number. The variation of β in one time step is described by [143]:

$$\frac{\partial \underline{\boldsymbol{\beta}}^a}{\partial t} = \frac{\underline{\boldsymbol{\beta}}^{n+1} - \underline{\boldsymbol{\beta}}^n}{\Delta t} \tag{4.81a}$$

$$\underline{\boldsymbol{\beta}}^a = (1-\Theta)\underline{\boldsymbol{\beta}}^n + \Theta \underline{\boldsymbol{\beta}}^{n+1} \tag{4.81b}$$

where the superscript a denotes the approximation of β used to compute the element matrices and θ a parameter varying between 0 and 1, indicating the type of differentiation method

used. Injecting in Equation 4.77 and regrouping all the terms provides:

$$\underline{\boldsymbol{\beta}}^{n+1} = \left[\frac{\underline{\underline{\boldsymbol{C}}}(\underline{\boldsymbol{\beta}}^a)}{\Delta t} + \Theta\underline{\underline{\boldsymbol{K}}}(\underline{\boldsymbol{\beta}}^a)\right]^{-1} \underline{\boldsymbol{F}}(\underline{\boldsymbol{\beta}}^a) + \left[\frac{\underline{\underline{\boldsymbol{C}}}(\underline{\boldsymbol{\beta}}^a)}{\Delta t} + \Theta\underline{\underline{\boldsymbol{K}}}(\underline{\boldsymbol{\beta}}^a)\right]^{-1} \left[\frac{\underline{\underline{\boldsymbol{C}}}(\underline{\boldsymbol{\beta}}^a)}{\Delta t} + (\Theta-1)\underline{\underline{\boldsymbol{K}}}(\underline{\boldsymbol{\beta}}^a)\right] \underline{\boldsymbol{\beta}^{\boldsymbol{n}}} \quad (4.82)$$

If $\Theta = 0$, the temperature temporal derivative is approximated with the *forward difference method*, which requires few computer resources but implies stability conditions on the time step Δt. $\Theta = 0.5$ is the *Crank-Nicholson* approximation, which is unconditionally stable and second-order accurate but is affected by noise if the time step exceeds a critical threshold. Finally, $\Theta = 1$ is the *backward difference method*, unconditionally stable [143]. The choice of the differentiation method is let to the user and can be changed depending on the situation. Due to the non-linearity of Equation 4.77, the fixed point method is set up to investigate the convergence of the code. Convergence is achieved when the variation of the model variables changes by less than a user-chosen threshold between two iterations. A relative convergence criterion is defined by [55]:

$$\frac{\beta^j - \beta^{j-1}}{min(\beta^{j-1}, \epsilon)} < rtol \quad (4.83)$$

where j is the iteration number, ϵ is a small value to avoid dividing by zero and $rtol$ the relative tolerance desired (typically 10^{-5}). Finally, Figure 4.3 represents the code algorithm.

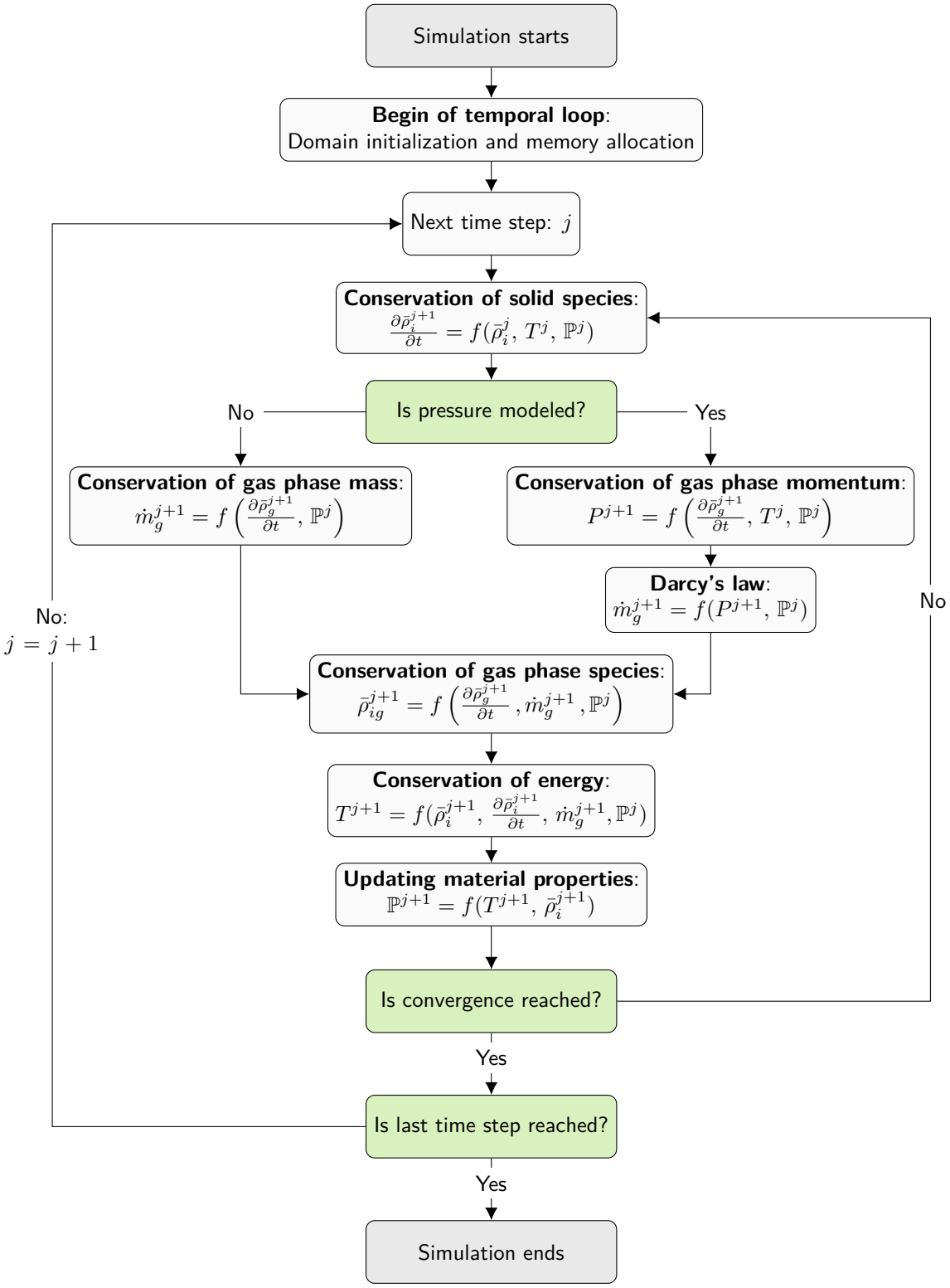

Figure 4.3 Algorithm representing the simulation steps.

CHAPTER 5 ARTICLE 1: MODELING THE THERMAL DECOMPOSITION AND RESIDUAL MASS OF A CARBON FIBER EPOXY MATRIX COMPOSITE WITH A PHENOMENOLOGICAL APPROACH: EFFECT OF THE REACTION SCHEME

Jean Langot, Pablo Chávez-Gómez, Martin Lévesque, Etienne Robert (Polytechnique Montréal, Canada)

Submitted to Fire and Materials on October 5th 2020

Abstract

The thermal decomposition of Polymer Matrix Composites (PMCs) is a complex process involving hundreds of reactions and species which is often modeled with simplified one-step schemes. These schemes can be improved by adding intermediate reactions of different nature (competitive, parallel, consecutive). However, the optimal number and nature of intermediate reactions is rarely discussed. In this paper, several reaction schemes of increasing complexity have been developed to model the decomposition of a carbon/epoxy composite. The kinetic parameters describing each reaction have been extracted from Thermogravimetric Analysis (TGA) by means of isoconversional methods. The composite mass loss rate and residual mass have been modeled and compared to TGA and tube furnace data. This research shows that adding parallel or consecutive intermediate reactions improves the agreement against TGA data compared to a single-step model, but only competitive reactions can account for the variation of the residual mass observed in the tube furnace when the heating rate is varied.

Keywords: *isoconversional methods, pyrolysis, oxidation, reaction mechanism, carbon/epoxy laminate, Polymer Matrix Composite (PMC), Thermogravimetric Analysis (TGA)*

5.1 Introduction

Polymer Matrix Composites (PMCs), and more specifically carbon/epoxy composites, are extensively used in modern aircrafts [7], from cabin to primary and secondary structures, including the engines' "cold zone". For this test application, some powerplant components need to act as firewalls and must meet strict certification guidelines to ensure airworthiness [15]. Composites used in this context undergo thermal degradation, a complex phenomenon driven by several closely coupled thermal, chemical and physical processes [18]. Comprehensive py-

rolysis models [43, 64, 76, 140] have been developed to improve the understanding of composite degradation at high temperatures and support the design of new fire-resistant materials. These models are more versatile than empirical approaches, insofar as they are based on the conservation of mass, energy and momentum. However, comprehensive pyrolysis models require extensive material characterization, to estimate input parameters for the material properties as well as for the chemical reactions leading to the material decomposition.

Inaccuracies on input parameters can drastically reduce the model agreement against experimental data. However, sensitivity analyses have shown that the reaction scheme itself used to model the composite chemical decomposition has the most significant influence on its overall thermal behavior and more specifically on the material ignition, which leads rapidly to the complete degradation of the samples [134,135]. In particular, the four parameters having the most influence on the average mass loss rate of a polymer exposed to a heat source are the activation energy, the pre-exponential factor, the heat of reaction and the char yield. Unfortunately, detailed reaction schemes are not available, as the thermal decomposition of a carbon/epoxy composites involves hundreds of reactions and intermediate species [168], that will vary with the composites chemical composition. This difficulty is compounded when considering the thermal decomposition of resins which constituents can change significantly between manufacturers. The lack of knowledge of the exact resin composition imposes the use of phenomenological approaches, based on mathematical interpretation of experimental data taking into account the nature of the phenomena at play rather than strictly chemical and physical considerations. There is therefore a need to identify the appropriate level of complexity to implement in thermochemical decomposition models to improve their accuracy, taking into account the material properties that can conveniently be obtained experimentally for model inputs.

The complete reaction scheme is often summarized into one or a few global one-step reactions, in which the polymeric matrix decomposes into char and gas through pyrolysis [129,130,169–173]. This reaction can then be characterized with Thermogravimetric Analysis (TGA) or Differential Scanning Calorimetry (DSC) under an inert atmosphere using so-called isoconversional methods [47]. Several authors [79, 137–139] improved their reaction scheme by adding intermediate reactions even if the real detailed mechanism remains partially, or totally, unknown. The intermediate reactions can either be competitive, parallel or consecutive [174]. For instance, Rein *et al.* [137] developed a five-step scheme composed of a combination of competitive and consecutive reactions to model the smoldering combustion of polyurethane foam. Lautenberger and Fernandez-Pello [175] modeled the oxidative pyrolysis of wood with a scheme composed of 4 consecutive heterogeneous reactions and 2 homogeneous reactions. Kim *et al.* [138] evaluated several reaction schemes describing the decomposition of fiberglass

composites and concluded that increasing the complexity of the reaction scheme is sometimes unjustified. There is therefore a need to assess the ideal mechanism complexity as a function of the composite constituents.

For carbon/epoxy composites, McKinnon *et al.* [79] modeled the thermo-chemical decomposition of a laminate using TGA data, with consecutive reactions used to fit the complex shape of the single peak visible in the mass loss rate curve. Tranchard *et al.* [139] modeled the pyrolysis of an epoxy-based system with two main competitive reactions, to account for the variable residual mass observed when the heating rate is changed. In the aforementioned schemes, the knowledge of the chemical processes at play is only partial, which justifies the use of phenomenological approaches based on easily accessible experimental data. However, in most cases, the influence of the nature and number of the reactions used has not been discussed. The existence of two fundamentally different schemes describing the thermo-chemical decomposition of the same type of matrix (i.e. epoxy resins) demonstrates that there is a need to systematically compare different phenomenological modeling approaches.

Moukhina [174] recently showed that several different reduced reaction schemes can capture the mass loss curve with a good agreement at specific heating rates, even if they are very different from the complete reaction scheme. The same author however pointed out that differences between models could increase when the heating rate is varied, in particular for the residual mass after thermal decomposition. This parameter depends directly on the char yield, which is very important in fire test simulation as it directly influences the quantity of insulating char formed on the hot face of the sample, protecting the composite from further heat transfer. The char yield also directly controls the proportion of combustible pyrolysates emitted to the surface and potentially leading to composite ignition, and is therefore a key parameter to predict the material mass loss rate in fire test [134]. Considering the difference of heating rates encountered in TGA ($1-50\,\mathrm{K\,min^{-1}}$) and in a real fire test ($>500\,\mathrm{K\,min^{-1}}$), there is a need to optimize the reaction scheme not only in terms of mass loss rate but also residual mass. Unfortunately, the residual mass of a composite sample is subject to high variability in TGA because of the small size of the sample that cannot ensure a consistent matrix volume fraction in each sample, representative of the actual material composition. The volume fraction of each phase varies indeed locally in a composite [176, 177]. The use of an equipment able to degrade bigger samples, such as a tube furnace, can overcome this difficulty. In the literature, tube furnaces and TGA have already been used in combination to investigate plastic pyrolysis [178] or coal combustion [179].

The objective of this work is to investigate the influence of the nature and number of intermediate reactions on the ability of phenomenological thermal decomposition models to capture the mass loss rate and residual mass of PMCs. First, the theory of reaction rates in solids

and isoconversional methods is reviewed and theoretical expressions for schemes involving a variable number of intermediate reactions of different nature are derived. Then, kinetic parameters are obtained from TGA measurements with the isoconversional methods and used to develop schemes of increasing complexity. Finally, the choice of the nature and number of intermediate reactions in the reaction scheme is discussed by comparing the model outcomes to TGA and residual mass data. A carbon/epoxy material system is used as an example in this study, but the method developed here is intended to be generalized on a wide variety of polymer composites evaluated in fire tests.

5.2 Theory

5.2.1 Background on reaction rate in solids

The decomposition rate of a solid exposed to a heat source is often represented by the degree of decomposition α, which is a parameter varying from 0 (material not degraded) to 1 (fully degraded material) as:

$$\alpha = \frac{m(t) - m_0}{m_\infty - m_0} \tag{5.1}$$

where $m(t)$, m_0, m_∞ are the current, initial and final mass of the sample (kg). The reaction rate in solids can be calculated as a function of the temperature T (K), decomposition degree α and pressure P (Pa) as [47]:

$$\frac{d\alpha}{dt} = k(T) f(\alpha) h(P) \tag{5.2}$$

with $k(T)$ (s^{-1}) being the temperature-dependent decomposition rate. Assuming that the gaseous products are continuously evacuated, the pressure dependence can be neglected and $h(P) = 1$. The influence of the decomposition degree is accounted for by the reaction model $f(\alpha)$, which can take many different forms, whether the reaction is accelerating, decelerating or sigmoidal [47]. The most common reaction model is the n-order law $f(\alpha) = (1 - \alpha)^n$, where n is the reaction order $(-)$. Finally, the temperature dependence is represented by the Arrhenius equation:

$$k(T) = A \exp\left(-\frac{E}{RT}\right) \tag{5.3}$$

where A is the pre-exponential factor (s^{-1}), E the activation energy ($J\,mol^{-1}$) and R the ideal

gas constant ($\mathrm{J\,K^{-1}\,mol^{-1}}$). Combining Eqs. 5.2 and 5.3 provides the equation commonly used in kinetic analysis of solids exposed to heat as:

$$\frac{d\alpha}{dt} = \beta\frac{d\alpha}{dT} = f(\alpha)A\exp\left(-\frac{E}{RT}\right) \tag{5.4}$$

where β is the heating rate ($\mathrm{K\,s^{-1}}$) obtained by the chain rule. The accuracy of the reaction scheme depends strongly on the kinetic triplet (A,E,n) that must be inferred experimentally, typically through Thermogravimetric Analysis (TGA) or Differential Scanning Calorimetry (DSC).

5.2.2 Background on isoconversional methods

The isoconversional principle states that the reaction rate at a constant extent of conversion is only a function of temperature, allowing the determination of the activation energy independently of the reaction model $f(\alpha)$. Isoconversional methods are divided in two categories: differential and integral methods, whether the analysis is performed on differential (DSC) or integral (TGA) data [47].
The differential isoconversional methods consist in taking the logarithm of Equation 5.4:

$$\ln\left(\beta\frac{d\alpha}{dT}\right)_{\alpha,\beta} = \ln(f(\alpha)A_\alpha) - \frac{E_\alpha}{RT_\alpha} \tag{5.5}$$

where the indices (α,β) denote respectively the specific decomposition degree and the heating rate at which the calculation is done. Then, assuming that $f(\alpha)$ is constant for each decomposition degree, the slope of the curve of $\ln\left(\beta\frac{d\alpha}{dT}\right)_{\alpha,\beta}$ plotted against $\frac{1}{T_\alpha}$ provides $-\frac{E_\alpha}{R}$. This method advantageously avoids the use of mathematical approximations or assumptions about the form taken by $f(\alpha)$, but the application of the differential method to integral data requires numerical differentiation that induces noise, leading to inaccuracies [47].
The integral isoconversional methods are based on the direct analysis of integral data such as those provided by TGA. The integration of Equation 5.4 yields:

$$\int_0^\alpha \frac{d\alpha}{f(\alpha)} = \frac{A}{\beta}\int_0^T \exp\left(-\frac{E}{RT}\right)dT \tag{5.6}$$

Introducing the change of variable: $T = \frac{E}{Ry} \Rightarrow dT = -\frac{E}{Ry^2}dy$ leads to:

$$\int_0^\alpha \frac{d\alpha}{f(\alpha)} = -\frac{EA}{R\beta}\int_{+\infty}^{\frac{E}{RT}} \frac{\exp(-y)}{y^2}dy \tag{5.7}$$

The integral $p(y_f) = \int_{y_f}^{\infty} \frac{\exp(-y)}{y^2} dy$ (with $y_f = E/RT$) can be approximated by several methods after an integration by parts [180]. Starink [181] demonstrated that all mathematical approximations of Equation 5.7 can be summarized by the following general equation:

$$\ln\left(\frac{\beta}{T_\alpha^{k_1}}\right) = -k_2 \frac{E}{RT_\alpha} + k_3 \tag{5.8}$$

where the constants k_1 and k_2 depend on the integral approximation used. For instance, $(k_1\,;\,k_2) = (2\,;\,1)$ in [182], $(k_1\,;\,k_2) = (0\,;\,1.052)$ in [183, 184], $(k_1\,;\,k_2) = (1\,;\,1)$ in [185] and $(k_1\,;\,k_2) = (1.92\,;\,1.0008)$ in [181]. Flynn [186] insisted on the necessity to use an adequate approximation for the range considered for y_f. These approximations lose accuracy if y_f is small, typically $y_f < 15$ [181]. For epoxy pyrolysis, previous studies reported an activation energy close to 180 $\mathrm{kJ\,mol^{-1}}$ [128, 169], which yields an y_f varying from 18 to 70. For this range, the Starink parameters offer the best accuracy and are thus used in this study. Depending on the values taken by the parameters E and A, several reaction models $f(\alpha)$ can describe a single experimental curve in cases of complex decomposition, where a linear relation exists between the apparent values of E and A [187]:

$$\ln(A_{\alpha,j}) = \frac{E_{\alpha,j}}{RT} + \ln\left[\frac{\beta d\alpha/dT}{f(\alpha)}\right]_{\alpha,j} = a_\beta + b_\beta E_{\alpha,j} \tag{5.9}$$

with $A_{\alpha,j}$ and $E_{\alpha,j}$ being the apparent Arrhenius parameters for each j reaction model and a_β and b_β constants depending on the heating rate β. In other words, Equation 5.9 states that a linear relation exists between $A_{\alpha,j}$ and $E_{\alpha,j}$, represented by so-called compensation lines of slope b_β in a semi-log of $ln\,(A_{\alpha,j})$ as a function of $E_{\alpha,j}$. Once E_α has been determined by isoconversional methods, the corresponding value of A_α can be computed with this compensation principle. If the decomposition is described by a single-step reaction scheme, all the compensation lines intersect at the exact value of E and A. It is worth noting that this compensation approach is valid regardless of the reaction model that has been used to establish the linear relationship between E and A.

Then, the reaction model $f(\alpha)$ can be obtained by substituting different forms of $f(\alpha)$ into Equation 5.6 and comparing the curves obtained to experimental results.

Another method consists in assuming a general form for the reaction model, for instance $f(\alpha) = (1-\alpha)^n$, and then finding n by mathematical optimization with a least-square algorithm. In that case, the square of the difference between measured and calculated data is minimized simultaneously for all the heating rates for which experimental data is available and for different values of n, until an optimal value is found providing the smallest

residual [47]:

$$\text{Residue} = \sum_{i=1}^{M} \left[(x_{exp,i} - x_{num,i})^2 \right] \tag{5.10}$$

where M is the number of different heating rates and x the variable on which the optimization is carried out, for instance α, or more frequently $d\alpha/dT$, owing to the high variations of this variable with time. This method provides a good quality of fit when optimizing smooth and regular peaks, but is less advantageous for irregular curves resulting from the overlapping of several peaks taking their origin in distinct chemical reactions. Numerical optimization can also be used to improve the values of E and A to be in better agreement with experimental data, starting from the values obtained by isoconversional methods as initial guesses.

5.2.3 Development of multi-step schemes

It is generally admitted that the material decomposition can be modeled by a one-step scheme if the activation energy E_α, computed by means of isoconversional methods, varies by less than 10% with respect to the decomposition degree. However, a strong variation of E_α with respect to α reveals the presence of multi-step decomposition kinetics involving several reactions [174]. If several peaks are visible on the mass loss rate curve over temperature, they can be analyzed separately assuming that one peak represents one reaction. However, this is not always the case and several reactions can be overlapped into a single peak, making the analysis even more challenging. In that case, it can be difficult to determine if the reaction scheme is composed of competitive, consecutive, or parallel reactions (several schemes are represented on Figure 5.1 as an example), without prior knowledge of the complete chemical scheme which is in general unknown. Two very different schemes can model an experimental mass loss curve with a very good agreement at some heating rates, but differ when the heating rate is varied, which influences the residual mass after thermal decomposition [174]. For this reason, it is desirable to test different schemes involving a variable number of reactions of different nature, and observe the impact on the predicted residual mass.
A systematic equation accounting for a variable number of reactions can help tackle this difficulty. Equation 5.4 can be modified to account for multi-step reactions, provided that $f(\alpha)$ is known. However, as the number of reactions used to describe the composite decomposition is increased to consider multi-steps reaction schemes, it would be very difficult to use a different reaction model for each of these reactions.

For this reason, the reaction model is assumed to follow a n-order law in this study.
Multi-steps schemes have already been derived for parallel reactions [47, 187], but as the

equations developped in these works do not involve the char yield they therefore cannot be used to determine the residual mass after decomposition. Different equations describing the reaction rate of multiple reactions have been developed here, based on the variation of density instead of the decomposition degree in order to explicitly obtain the char yield θ_i. It is worth noting that in our approach the sample volume is assumed to remain constant. Equation 5.1 and 5.4 can be combined to compute the density variation of a species i associated with a single reaction j, assuming that each phase degrades completely (therefore $\bar{\rho}_{i,\infty} = 0$) as:

$$\left.\frac{d\bar{\rho}_i(t)}{dt}\right|_j = -\bar{\rho}_{i,0}\left[\frac{\bar{\rho}_i(t)}{\bar{\rho}_{i,0}(t)}\right]^{n_j} A_j \exp\left(-\frac{E_j}{RT}\right) \tag{5.11}$$

where ρ_i represents the density of species i ($\mathrm{kg\,m^{-3}}$). The bar above the density indicates that the quantity is defined as a spatial average over the control volume. The total density change for a variable number of competitive, parallel and consecutive reactions can then be calculated with different methods, depending on the nature of the reaction scheme.
In the following, several theoretical formulations describing the density variation of a matrix decomposing with competitive, consecutive and parallel reactions are derived on an arbitrary control volume. The equations are first developed for a simple case involving only two reactions, as represented on Figure 5.1, and are then generalized to N equations.

Competitive reactions

A solid phase is composed of a single species A that can be decomposed following exposure to heat into species C_1 and C_2, both representative of the char, through two independent competitive reactions, as shown schematically in Figure 5.1a). The total density is given by:

$$\rho_{tot} = \bar{\rho}_A + \bar{\rho}_{C1} + \bar{\rho}_{C2} \tag{5.12}$$

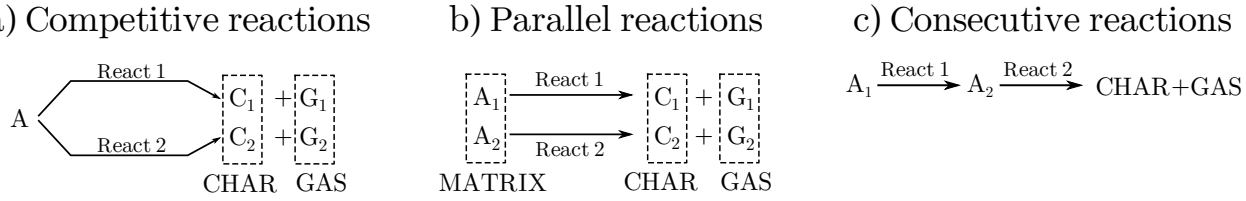

Figure 5.1 Examples of how two reactions can be arranged to form a simple reaction scheme involving a) competitive, b) parallel or c) consecutive reactions.

which leads to:

$$\frac{d\rho_{tot}}{dt} = \frac{d\bar{\rho}_A}{dt} + \frac{d\bar{\rho}_{C1}}{dt} + \frac{d\bar{\rho}_{C2}}{dt} \tag{5.13}$$

Substituting Equation 5.11 into Equation 5.13 yields:

$$\begin{aligned}
\frac{d\rho_{tot}}{dt} &= -\bar{\rho}_{A,0}\left(\frac{\bar{\rho}_A}{\bar{\rho}_{A,0}}\right)^{n_1} k_1(T) + \theta_1\bar{\rho}_{A,0}\left(\frac{\bar{\rho}_A}{\bar{\rho}_{A,0}}\right)^{n_1} k_1(T) \\
&\quad -\bar{\rho}_{A,0}\left(\frac{\bar{\rho}_A}{\bar{\rho}_{A,0}}\right)^{n_2} k_2(T) + \theta_2\bar{\rho}_{A,0}\left(\frac{\bar{\rho}_A}{\bar{\rho}_{A,0}}\right)^{n_2} k_2(T) \\
&= \bar{\rho}_{A,0}\left[(\theta_1 - 1)\left(\frac{\bar{\rho}_A}{\bar{\rho}_{A,0}}\right)^{n_1} k_1(T) + (\theta_2 - 1)\left(\frac{\bar{\rho}_A}{\bar{\rho}_{A,0}}\right)^{n_2} k_2(T)\right]
\end{aligned} \tag{5.14}$$

Equation 5.14 can be generalized to N reactions as:

$$\frac{d\rho_{tot}}{dt} = \bar{\rho}_{A,0}\sum_{i=1}^{N}(\theta_i - 1)\left[\left(\frac{\bar{\rho_A}}{\bar{\rho}_{A,0}}\right)^{n_i} k_i(T)\right] \tag{5.15}$$

Parallel reactions

A solid phase is composed of two species A_1 and A_2, with a volume fraction of respectively $X_{A,1}$ and $X_{A,2}$. When the material is exposed to heat, A_1 and A_2 decomposes into species C_1 and C_2 through two independent parallel reactions, as represented in Figure 5.1b). The total density is given by:

$$\begin{aligned}
\rho_{tot} &= X_{A1}(\rho_{A1} + \rho_{C1}) + X_{A2}(\rho_{A2} + \rho_{C2}) \\
&= (\bar{\rho}_{A1} + \bar{\rho}_{C1}) + (\bar{\rho}_{A2} + \bar{\rho}_{C2})
\end{aligned} \tag{5.16}$$

Equation 5.16 can be differentiated with respect to time to obtain the mass loss rate as:

$$\frac{d\rho_{tot}}{dt} = \left(\frac{d\bar{\rho}_{A1}}{dt} + \frac{d\bar{\rho}_{C1}}{dt}\right) + \left(\frac{d\bar{\rho}_{A2}}{dt} + \frac{d\bar{\rho}_{C2}}{dt}\right) \tag{5.17}$$

Substituting Equation 5.11 into Equation 5.17 yields:

$$\begin{aligned}\frac{d\rho_{tot}}{dt} &= \left(-\bar{\rho}_{A1,0}\left(\frac{\bar{\rho}_{A1}}{\bar{\rho}_{A1,0}}\right)^{n_1} k_1(T) + \theta_1\bar{\rho}_{A1,0}\left(\frac{\bar{\rho}_{A1}}{\bar{\rho}_{A1,0}}\right)^{n_1} k_1(T)\right) \\ &\quad + \left(-\bar{\rho}_{A2,0}\left(\frac{\bar{\rho}_{A2}}{\bar{\rho}_{A2,0}}\right)^{n_2} k_2(T) + \theta_2\bar{\rho}_{A2,0}\left(\frac{\bar{\rho}_{A2}}{\bar{\rho}_{A2,0}}\right)^{n_2} k_2(T)\right) \\ &= (\theta_1 - 1)\left[\bar{\rho}_{A1,0}\left(\frac{\bar{\rho}_{A1}}{\bar{\rho}_{A1,0}}\right)^{n_1} k_1(T)\right] + (\theta_2 - 1)\left[\bar{\rho}_{A2,0}\left(\frac{\bar{\rho}_{A2}}{\bar{\rho}_{A2,0}}\right)^{n_2} k_2(T)\right] \quad (5.18)\end{aligned}$$

Equation 5.18 can be generalized to N reactions as:

$$\frac{d\rho_{tot}}{dt} = \sum_{i=1}^{N}(\theta_i - 1)\left[\bar{\rho}_{i,0}\left(\frac{\bar{\rho}_i}{\bar{\rho}_{i,0}}\right)^{n_i} k_i(T)\right] \quad (5.19)$$

Consecutive reactions

Consider a solid phase composed of a single species A_1. When the material is exposed to heat, A_1 decomposes into species A_2, and then A_2 decomposes into C, as represented in Figure 5.1c). The total density is given by:

$$\rho_{tot} = \bar{\rho}_{A_1} + \bar{\rho}_{A_2} + \bar{\rho}_C \quad (5.20)$$

which leads to:

$$\frac{d\rho_{tot}}{dt} = \frac{d\bar{\rho}_{A_1}}{dt} + \frac{d\bar{\rho}_{A_2}}{dt} + \frac{d\bar{\rho}_C}{dt} \quad (5.21)$$

Substituting Equation 5.11 into Equation 5.21 yields:

$$\begin{aligned}\frac{d\rho_{tot}}{dt} = -\bar{\rho}_{A_1,0}\left(\frac{\bar{\rho}_{A_1}}{\bar{\rho}_{A_1,0}}\right)^{n_1} k_1(T) + \theta_1\bar{\rho}_{A_1,0}\left(\frac{\bar{\rho}_{A_1}}{\bar{\rho}_{A_1,0}}\right)^{n_1} k_1(T) \\ - \bar{\rho}_{A_2,0}\left(\frac{\bar{\rho}_{A_2}}{\bar{\rho}_{A_2,0}}\right)^{n_2} k_2(T) + \theta_2\bar{\rho}_{A_2,0}\left(\frac{\bar{\rho}_{A_2}}{\bar{\rho}_{A_2,0}}\right)^{n_2} k_2(T) \quad (5.22)\end{aligned}$$

$\bar{\rho}_{A_2,0}$ represents the density of the intermediate specie A_2 with respect to the control volume, whose value is unknown. It is assumed in this work that $\bar{\rho}_{A_2,0}$ and $\bar{\rho}_{C,0}$ can be computed from the density of the initial species through the char yield θ: $\bar{\rho}_{A_2,0} = \theta_1\bar{\rho}_{A_1,0}$ and $\bar{\rho}_{C,0} = \theta_2\bar{\rho}_{A_2,0} = \theta_1\theta_2\bar{\rho}_{A_1,0}$. This assumption yields:

$$\frac{d\rho_{tot}}{dt} = \bar{\rho}_{A_1,0}\left[(\theta_1 - 1)\left(\frac{\bar{\rho}_{A_1}}{\bar{\rho}_{A_1,0}}\right)^{n_1} k_1(T) + \theta_1(\theta_2 - 1)\left(\frac{\bar{\rho}_{A_2}}{\theta_1\bar{\rho}_{A_1,0}}\right)^{n_2} k_2(T)\right] \tag{5.23}$$

Equation 5.23 can be generalized to N reactions as:

$$\frac{d\rho_{tot}}{dt} = \bar{\rho}_{A_1,0}\left[\sum_{i=1}^{N} \gamma_i(\theta_i - 1)\left(\frac{\bar{\rho}_i}{\gamma_i\bar{\rho}_{A_1,0}}\right)^{n_i} k_i(T)\right] \tag{5.24}$$

with $\gamma_i = 1$ if $i = 1$ and $\gamma_i = \prod_{j=1}^{i-1}\theta_i$ the rest of time.

5.3 Experimental methods

5.3.1 Materials

The material studied is a 1.6 mm-thick, quasi-isotropic laminate fabricated from an aerospace-grade carbon/epoxy pre-preg system (reinforcement: woven carbon fiber HTS40 E13 3K PW), procured from Solvay (formerly CYTEC, Tulsa, OK). Samples for TGA and tube furnace tests were extracted therefrom considering its full thickness. The matrix represents 41.76% of the total weight. The exact composition of the epoxy resin system is a trade secret and, therefore, could not be obtained from the manufacturer, which forces the use of phenomenological approaches to characterize its decomposition.

5.3.2 Thermogravimetric Analysis & Differential Scanning Calorimetry

Simultaneous Differential Scanning Calorimetry (DSC) and TGA measurements have been performed using a TGA/DSC 1 apparatus (Mettler-Toledo, Columbus, OH) in both inert (N2, 60 ml min^{-1}) and oxidative (air, 60 ml min^{-1}) environments, under atmospheric pressure. The samples were placed in 70 μl open alumina crucibles and exposed to three different heating rates of 5, 10 and 25 K min^{-1}, as platinum may act as a catalyst on the oxidation of carbon fibers [188]. The heating rates and the corresponding sample mass are reported in Table 5.1.

5.3.3 Tube furnace

The residual mass relative to the initial value of a composite sample is difficult to assess using TGA, from the high variability between runs, as the small size of the sample does not ensure a consistent volume fraction for each constituent of the composite [52, 189]. For this reason, a tube furnace (Carbolite Gero STF furnace tube) was selected as a complementary

Apparatus	Heating rate ($K\,min^{-1}$)	Sample mass (mg)			
		N_2		Air	
STA	5	10.6980		10.3630	
	10	14.9319		15.2581	
	25	12.0205		11.0230	
		N_2			
Tube furnace	1	899.7	893.9	780.0	792.3
	3	768.6	768.0	901.0	782.0
	5	539.2	563.4	555.1	557.4

Table 5.1 Heating rates and mass of the samples used in STA and tube furnace runs.

approach to TGA to estimate the composite residual mass after decomposition, to overcome the limitations of the finite sample size. This instrument allows the pyrolysis of samples an order of magnitude heavier ($500 - 900$ mg) than those used in TGA ($10 - 20$ mg), while placed in an open alumina pan. The three sets of 4 samples were heated at different rates until reaching 1000 °C, then kept at constant temperature for one hour, before letting the sample cool naturally. The maximum heating rate is however much lower than in a TGA, limited to 5 $K\,min^{-1}$ by the capability of the equipment. Once the samples reach room temperature, they were weighed with a high precision scale (10^{-4} g). Inert environment was ensured by a constant Argon flow (1317 $ml\,min^{-1}$). No residue is observed in the pan at the end of the experiment, suggesting that the inert flow is high enough to efficiently evacuate the gasses emitted by chemical reactions.

5.4 Results and Discussions

5.4.1 Experimental results

TGA / DSC

Figure 5.2 shows the variation of the sample mass as a function of temperature for three different heating rates obtained from the TGA under inert (Figure 5.2a) and oxidative atmospheres (Figure 5.2d). The variation of the degree of decomposition $d\alpha/dT$ is also shown as a function of temperature under inert (Figure 5.2b) and oxidative atmospheres (Figure 5.2e). Figure 5.2c) represents the heat flow transmitted to the sample as a function of temperature under an inert atmosphere for a single heating rate (10 $K\,min^{-1}$), with the corresponding $d\alpha/dT$ curve. The hatched area corresponds to the heat absorbed or released by chemical reactions or physical changes occurring in the sample during its decomposition.
Under an inert atmosphere, the composite decomposition starts at 500 K and is complete above 900 K, accompanied by a mass loss of approximately 26.5%. This reaction is typically associated with pyrolysis as it does not require the presence of reactive species. The resin

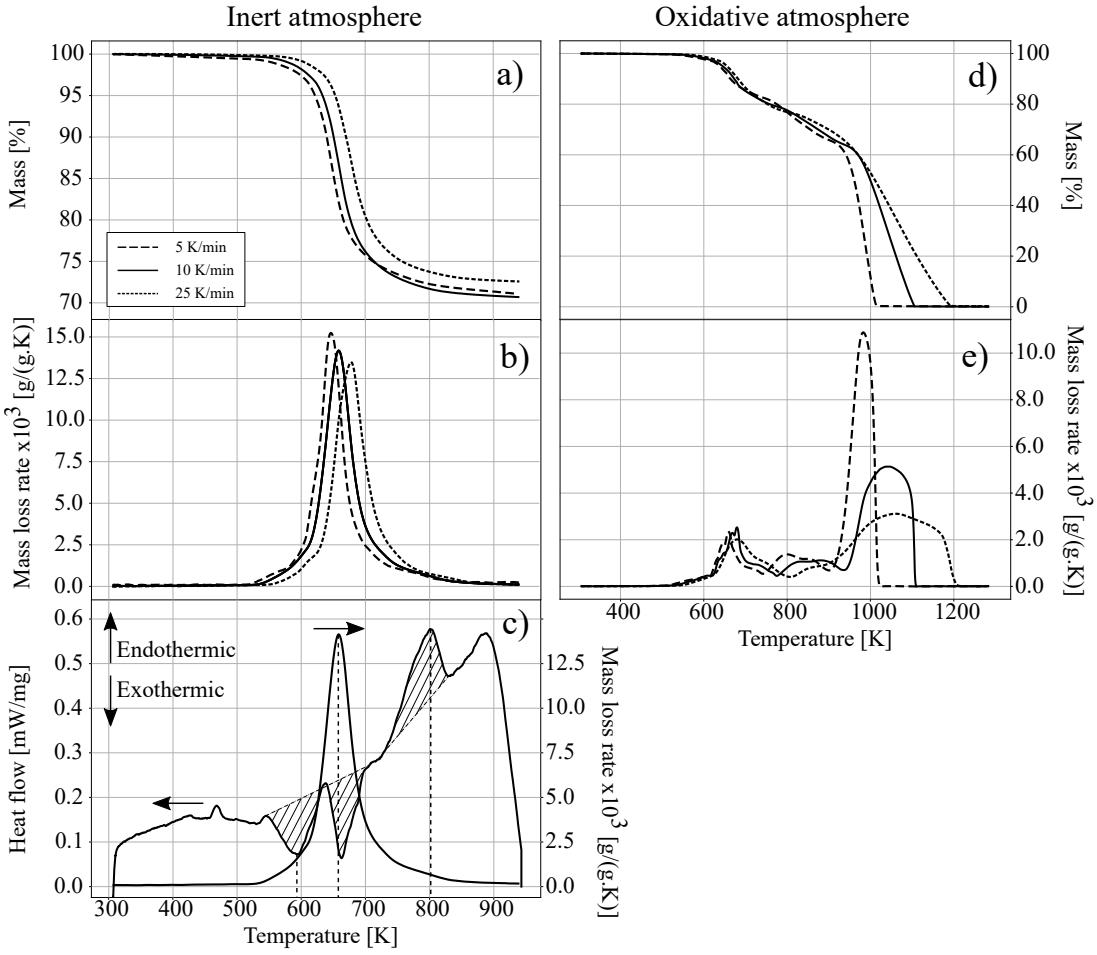

Figure 5.2 Variation of mass, mass loss rate and heat flow per unit mass as a function of temperature under inert a)-b)-c) and oxidative d)-e) atmospheres. The heating rate for c) is 10 K min^{-1}.

represents 41.76% of the total composite weight, with the remaining mass corresponding to the sum of the fibers, which are non-reactive under an inert atmosphere, and the residues (char) from resin decomposition. The variations in residual mass observed between runs in Figure 5.2a) are mostly the result of the small size of the sample used for TGA, that cannot ensure a composition representative of the actual composite. As a consequence, it is not possible to clearly identify a trend in the variations of residual mass (*i.e.* a monotonic variation). This justifies the use of bigger samples in a tube furnace to measure the residual mass. A single peak is visible on Figure 5.2b), shifting to the right as the heating rate is increased. This shifted single peak suggests that, under inert atmosphere, the phenomena at play can be captured by a single reaction. However, at least three reactions absorbing/releasing heat can be observed in the corresponding DSC data of Figure 5.2c). This demonstrates that several reactions are overlapped into the single TGA peak, highlighting the need to develop multi-steps reaction schemes. It must be emphasized that the measurements provided by the DSC are qualitative and not quantitative, as the DSC was not calibrated to measure the heat of reaction.

Figure 5.2e) shows three different peaks in the TGA curves, hinting at the presence of at least three different reactions under an oxidative atmosphere. The first occurs between 500 and 800 K, and is associated with matrix pyrolysis. The two other peaks correspond to the char and fiber oxidation, which requires the presence of oxygen diffusing within the porous sample. The different peaks are very irregular, when compared to those obtained under an inert atmosphere, making data analysis challenging. The temperature ranges of each peak are reported in Table 5.2.

Tube furnace

Figure 5.3 presents the residual mass means after treatment in the tube furnace for three different heating rates: 1, 3 and 5 $\mathrm{K\,min^{-1}}$. The variation of residual mass observed in the tube furnace (72.5 and 74.6%) is quantitatively similar to the one observed in TGA (71 and 73%); however, contrary to the results obtained with TGA, the residual mass decreases monotonically with an increasing heating rate. This again reveals that several reactions are

Heating rate	Matrix pyrolysis (K)		Char oxidation (K)		Fiber oxidation (K)	
($\mathrm{K\,min^{-1}}$)	Range	Peak	Range	Peak	Range	Peak
5	500 – 740	660	740 – 900	679	900 – 1013	681
10	500 – 773	800	773 – 935	840	935 – 1103	860
25	500 – 805	983	808 – 936	1045	936 – 1189	1061

Table 5.2 For each decomposition step isolated from the curves of Figure 5.2, temperature range over which they occur and temperature at the peak.

at play, as a single decomposition step is associated to a unique char yield and therefore cannot provide different residual masses when the heating rate is changed. Therefore, the tube furnace provides useful information about the actual reaction mechanism. The variation of residual mass remains quantitatively low, but could increase at higher heating rates.
The error bars on Figure 5.3 show the 95% confidence intervals (CI) using Student's t-distribution, appropriate for small data sets. Data show limited error because of the important size of the samples that ensures a similar volume fraction of each constituent in all samples. The error increases slightly for $\beta = 5\ \mathrm{K\,min^{-1}}$, possibly because of the smaller sample size (see Table 5.1), or because of equipment limitations at higher heating rates. Upon visual examination, there is an overlap of CIs between data from 3 and 5 $\mathrm{K\,min^{-1}}$; therefore, a t-test was performed ($t = 3.327$, $p = 0.0159$). Thus, the residual mass means of the aforementioned heating rates can be considered statistically different at a 95% CI. The low data error suggests that tube furnaces could be more appropriate than TGA to estimate the residual mass of a composite sample after thermal decomposition due to variation of matrix volume fraction which depending on the location of the sample extraction, as demonstrated for woven configurations [176].

5.4.2 Thermochemical parameters

Isoconversional methods have been used to infer the activation energy and pre-exponential factor from TGA measurements, following to the method described in Section 5.2.2. Figure 5.4a) reveals the evolution of the activation energy as a function of the decomposition degree, under an inert atmosphere. The activation energy increases rapidly from almost 0 at $\alpha = 0$ to 185 $\mathrm{kJ\,mol^{-1}}$ at $\alpha = 0.3$. A plateau is subsequently reached and the activation energy remains almost constant until $\alpha = 0.7$. This plateau most likely corresponds to the main pyrolysis step of epoxy decomposition. The activation energy at the plateau is in agreement with previous values reported in the literature for other types of epoxy resins [129, 130, 169–171]. The activation energy increases again above $\alpha = 0.7$, reaching a peak of $E = 447\ \mathrm{kJ\,mol^{-1}}$ for $\alpha = 0.92$ and sharply decreasing thereafter. An activation energy increasing with decomposition degree is a typical behavior observed several times for epoxy matrices [139, 169]. Very reactive species, i.e. with low activation energies, react first whereas the less reactive species react react only later as the temperature becomes sufficiently high. Only the very weakly reactive species remain at the end of the decomposition process, which explains the peak observed at $\alpha = 0.92$ on Figure 5.4a). The value reached at the peak and the decrease after $\alpha = 0.92$ have limited physical meaning and could be caused by a loss of validity of the isoconversional methods for high decomposition degree, *i.e.* above $\alpha = 0.9$. Nevertheless, the pyrolysis process can be modeled as a one-step reaction if the activation

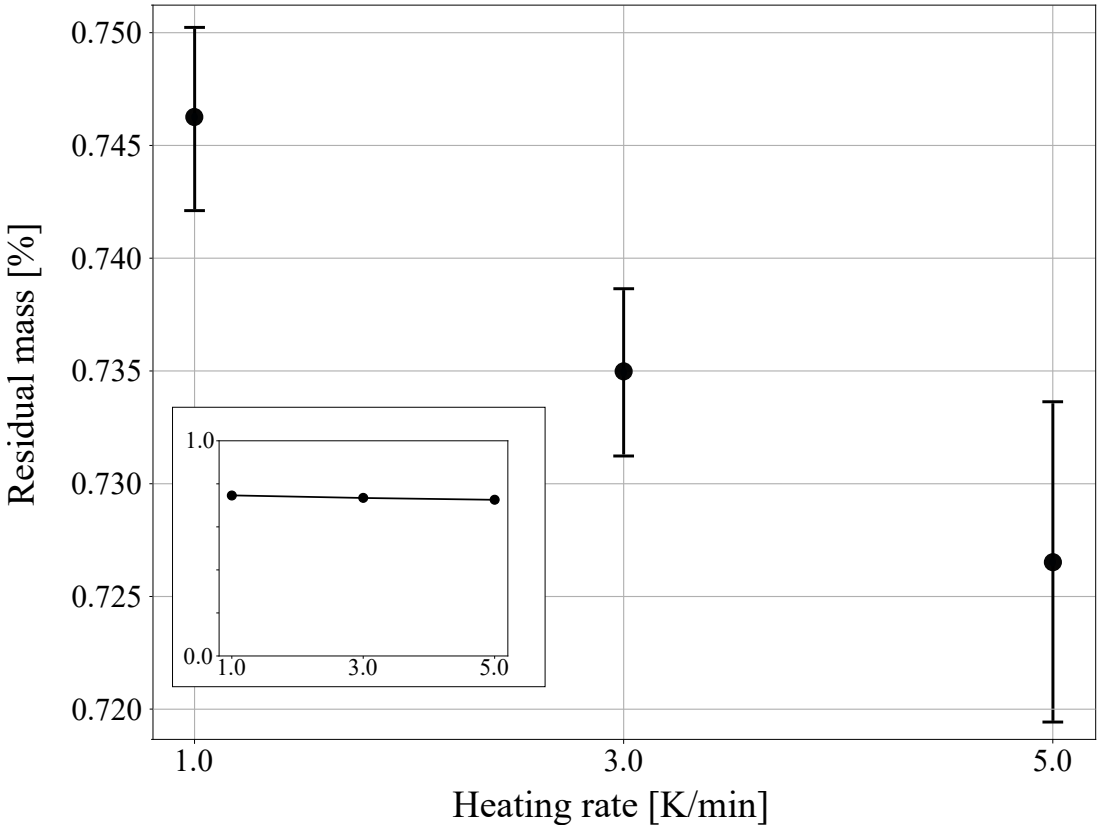

Figure 5.3 Residual mass means obtained after decomposition in a tube furnace at three different heating rates: 1, 3 and 5 $\mathrm{K\,min^{-1}}$. Error bars show the 95% confidence intervals considering Student's t-distribution.

energy is almost constant (less than 10% of variation) over a wide range of decomposition degrees [46]. This is not the case here as strong variations of E can be observed for $\alpha \leq 0.3$ and $\alpha \geq 0.7$, further motivating the need of implementing more complex reaction schemes. Figure 5.4b) represents the evolution of the pre-exponential factor as a function of the activation energy. The dots represent the different reaction models for which the couple (E, A) has been calculated. Four n-order reaction model have been evaluated with a reaction order n successively equal to 1, 2, 3, and 4. With this approach, it is generally admitted that if the thermo-chemical decomposition can be summarized as a single-step reaction, the compensation lines cross each other at a single point, whose coordinates (E, A) provide the activation energy and pre-exponential factor of the reaction. Here, the compensation lines do not cross at a single point, which again motivates the need to develop multi-step reaction schemes.
As the decomposition is much more complicated under oxidative atmosphere, the activation energy has been computed independently for each of the three peaks observed on Figure 5.2e), according to the ranges reported in Table 5.2. Figure 5.5a), 5.5c) and 5.5e) show the evolution of the activation energy as a function of a normalized decomposition degree under an oxidative atmosphere, for each step (matrix pyrolysis, char oxidation, fiber oxidation). It can be observed that the activation energy of the matrix pyrolysis is significantly lower under an oxidative atmosphere than under an inert one. This phenomenon has already been observed for epoxy resins in previous studies [52, 190] and could be related to an early pre-oxidation of highly reactive epoxy resin components before the onset of pyrolysis [52, 191]. This could also be the result of the activation energy for the char oxidation at low conversion degree (112 kJ mol^{-1} on Figure 5.5) being lower than than the activation energy of the matrix pyrolysis under inert atmosphere (185 kJ mol^{-1}). Consequently, the char can be oxidized as soon as it is formed, reducing the activation energy of the composite when considered as a whole, for low decomposition degrees. The pyrolysis activation energy reported on Figure 5.5a) could thus be a weighted mean of the activation energies related to matrix pyrolysis and early char oxidation. As the decomposition degree progresses, the activation energy for matrix pyrolysis under an oxidative atmosphere seems to reach a plateau of approximately 185 kJ mol^{-1} for $\alpha = 0.2$ but decreases after $\alpha = 0.5$, further supporting this hypothesis. However, it is difficult to reach a definitive conclusion because of the irregularity of the first and second peaks on Figure 5.2e), making the calculation of the activation energy inaccurate, particularly for char oxidation. Finally, Figure 5.5e) represents the activation energy for fiber oxidation. It starts at a high value ($E = 315$ kJ mol^{-1}) and decreases regularly thereafter, until reaching 75 kJ mol^{-1} at the end of the decomposition. This behavior could be explained by the typical structure of PAN-based carbon fibers, which have a turbostratic/graphitic outer skin that protects the amorphous and more reactive core [192]. Another explanation is the heteroge-

neous nature of carbon-oxygen kinetics [193, 194]. Halbig *et al.* [194] performed TGA runs on T-300 carbon fibers at different temperatures and suggested the existence of two regimes: (i) a low temperature regime (720-1150K) associated with high activation energy, where oxidative species are in excess; (ii) a high temperature regime (870-1700K) associated with low activation energy, where the reaction rate is controlled by the diffusion of oxidative species. Each of these regimes could be modeled with a specific reaction model $f(\alpha)$. However, the two regimes are likely to coexist in our case because of the large temperature range encountered in both fire test and TGA. The decreasing of the activation energy of carbon fiber oxidation observed on Figure 5.5e) tends to confirm the existence of a transition between the two regimes. For this reason, a more versatile n-order reaction model will be used to develop an aerobic reaction scheme in Section 5.4.3, because of the lack of a reaction model describing simultaneously these two regimes.
Figure 5.5b), 5.5d) and 5.5f) represent the evolution of the pre-exponential factor as a function of the activation energy. For all reactions considered, it is difficult to define a particular point where the compensation lines cross, although for pyrolysis it appears to be positionned at high values for the (E, A) pair. For both char and fiber oxidation, this crossing point is likely located near the lower bounds of the (E, A) range obtained.

5.4.3 Numerical results

Single-step schemes: anaerobic decomposition

Mathematical optimization was used to identify the order of reaction n as well as to optimize the activation energy E and the pre-exponential factor A. First, an average value E_{av} was computed from the values reported in Figure 5.4a). A corresponding pre-exponential factor A_{av} was calculated using the compensation parameters determined from Figure 5.4b). The data set (E_{av}, A_{av}) was used as an initial guess in the optimization process. E and A were optimized within a range centered on (E_{av}, A_{av}): E was varied between $0.8E_{av}$ and $1.2E_{av}$, and A was varied between $10^{-3}A_{av}$ to $10^{3}A_{av}$. The reaction order n was optimized between 1.0 and 5.0.
The residue (Equation 5.10) was computed using two different methods for the pyrolysis: with $x = \alpha$ and with $x = d\alpha/dT$, to compare both methods. The residue was minimized to find optimal values for (E, A, n) with the least-squared algorithm method, using the package "LMFIT" in Python [195]. In order to avoid misinterpreting a local minimum, the initial value E_{av} was varied to verify if the solution is valid regardless of the initial guess. Finally, once the complete kinetic triplet is identified, the char yield is calculated by minimizing the difference between numerical and experimental residual mass over all the heating rates used

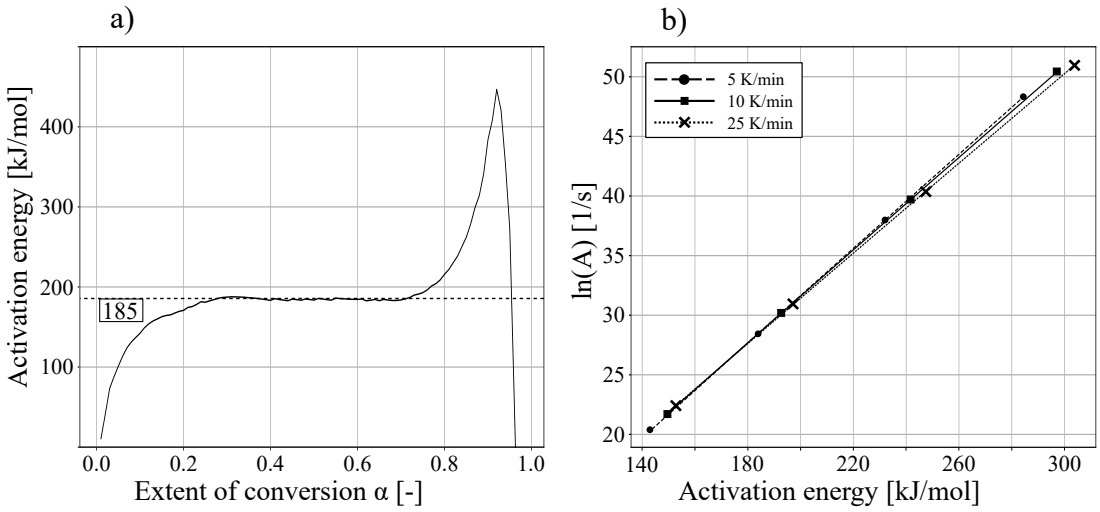

Figure 5.4 a) Evolution under inert atmosphere of the activation energy as a function of the extent of conversion, as evaluated using isoconversional methods and b) pre-exponential factor as a function of the activation energy, from the compensation principle.

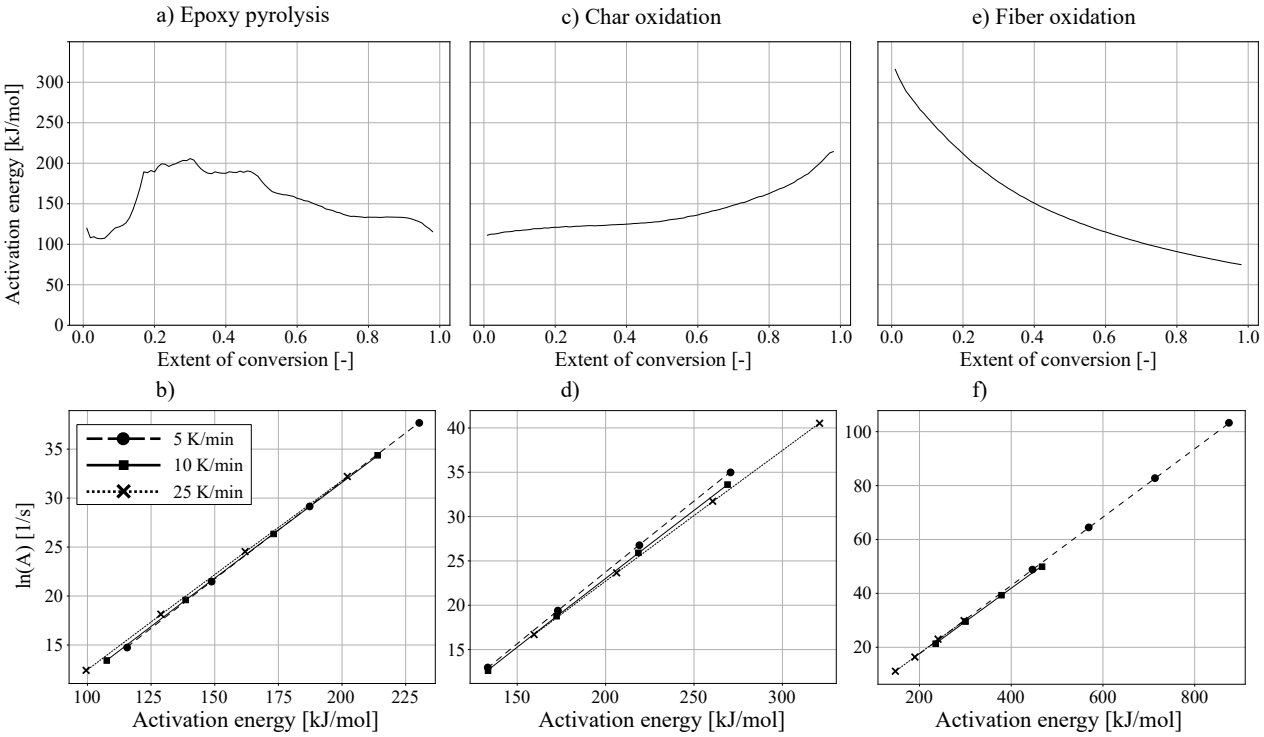

Figure 5.5 a), c), e): Evolution under oxidative atmosphere of the activation energy as a function of the extent of conversion for respectively epoxy pyrolysis, char oxidation and fiber oxidation. b), d), f): evolution of the pre-exponential factor as a function of the activation energy for respectively epoxy pyrolysis, char oxidation and fiber oxidation.

in the tube furnace, with the char yield θ varying from 0 to 1.

The single-step schemes accounting for matrix pyrolysis under an inert atmosphere are reported in Table 5.3. The coefficient of determination R^2 indicates the quality of fit between the experimental and numerical values of the quantity optimized (α or $d\alpha/dT$) for all the heating rates. The two schemes obtained by optimizing α and $d\alpha/dT$ are very similar; however, the optimization based on α provides a better coefficient of determination than that based on $d\alpha/dT$. There is no clear threshold of R^2 stating that a numerical reaction scheme can or model depict the actual decomposition, but previous studies aimed at maximizing this coefficient to choose their reaction scheme. When modeling pyrolysis, R^2 typically ranges from 0.95 to 0.99 [173], and optimizing the reaction scheme with α instead of $d\alpha/dT$ improved the R^2 from 0.96 to 0.99. This reveals that the integral value is easier to fit than its derivative, probably due to the strong variations of $d\alpha/dT$ on Figure 5.2b). The value obtained for E is also slightly larger than the initial guess E_{av} for both schemes. The char yield θ calculated here corresponds to an averaged residual mass over the three heating rates used in the tube furnace, as it is impossible to obtain a residual mass that varies as a function of the heating rate with a single-step scheme. This shows that despite the good mathematical agreement obtained with TGA data, a single-step scheme cannot capture the variations of residual mass observed as a function of the heating rate and therefore misses some information inherent to the actual mechanism.

Multi-steps schemes: aerobic decomposition

From the experimental data collected for thermal decomposition under an oxidative atmosphere, the multi-step mechanism leading to the material aerobic decomposition has been modeled with three single step reactions, obtained from distinct peaks in the TGA data. From these single-step reactions, one can then build a multi-step scheme with 2 consecutive reactions and 1 parallel reaction, as shown schematically on Figure 5.6, to account for matrix pyrolysis, char oxidation and fiber oxidation. The method used to infer the kinetic triplet is similar to the one developed in Section 5.4.3: average values (E_{av}, A_{av}) are computed for each reaction on Figure 5.5 and are optimized in a narrowed range ($\pm 20\%$). The only difference being on the choice of the variable optimized with Equation 5.10: because of the irregularity

Reaction	Quantity minimized	E (kJ mol^{-1})	A (s^{-1})	n (-)	θ (-)	R^2 (-)
Pyrolysis	α	193	2.20×10^{13}	3.03	0.3678	0.9983
	$d\alpha/dT$	199.17	5.26×10^{13}	2.43	0.3678	0.9614

Table 5.3 Reaction scheme of a carbon fiber epoxy matrix composite exposed to an inert atmosphere for heating rates $\beta = 5, 10, 25$ K min^{-1}.

of the mass loss rate peaks on Figure 5.2e), the residue was calculated solely with $x = \alpha$ for the reactions under an oxidative atmosphere.
The kinetic triplet for each reaction are reported in Table 5.4. Globally, the optimization confirmed the previous estimation of E and A obtained from isoconversional methods, except for the activation energy related to fiber oxidation which is more important than its average value on Figure 5.5c).

Multi-steps schemes: anaerobic decomposition

Section 5.4.3 revealed that a single-step reaction scheme can model the mass loss rate of the epoxy resin with a good agreement against TGA data, but is unable to capture the variation of residual mass observed in the tube furnace. For this reason, several reaction schemes specifically developed for epoxy pyrolysis are proposed in this section, including intermediate reactions of different nature: competitive, parallel or consecutive. The initial values of activation energy E_i are first distributed in the range observed on Figure 5.4, i being the reaction number. Then, the corresponding values of pre-exponential factor A_i are calculated with the compensation principle. Finally, the density variation is computed with Equations 5.15, 5.19, 5.24 and each set of parameters (E_i, A_i, n_i) is optimized simultaneously by minimizing the residue calculated using Equation 5.10. For instance, the initial activation energies of three-parallel intermediate reactions are $[E_1, E_2, E_3]$=[80, 160, 220] kJ mol^{-1}, and then these values are optimized in the range $[80 \pm 20\%, 160 \pm 20\%, 220 \pm 20\%]$. Therefore, the activation energies of the multi-steps schemes is distributed in the entire range observed on Figure 4a). Moreover, the initial values $[E_1, E_2, E_3]$ were varied to avoid misinterpreting local minimum. It is worth noting that the optimization is carried out in this section on $x = d\alpha/dT$ only, because the complex shape of $d\alpha/dT$ allows a more accurate optimization when several reactions are at play. E_i is varied between $0.8 \times E_i$ and $1.2 \times E_i$, A_i between $A_i \times 10^{-3}$ and $A_i \times 10^3$ and n_i between 0 to 5. If the scheme includes parallel reactions, another parameter X_i varying between 0 and 1 describing the volume fraction of the sub-phases composing the matrix is also optimized simultaneously, with the constraint $\sum_{i=1}^{N} X_i = 1$. Then, an optimal value of the char yield θ_i between 0 and 1 is obtained in a second step by minimizing the residue calculated using Equation 5.10 with x being the residual mass at the end of the test.

Thermo-Oxidative Decomposition	Quantity minimized	E (kJ mol^{-1})	A (s^{-1})	n (-)	θ (-)	R^2
Pyrolysis	α	148	2.26×10^9	3.13	0.3678	0.9955
Char oxidation	α	112	1.7×10^4	1.76	-	0.9938
Fiber oxidation	α	260	4.93×10^{10}	4.83	-	0.9907

Table 5.4 Scheme composed of single-step reactions of a carbon fiber epoxy matrix composite exposed to an oxidative atmosphere for heating rates $\beta = 5, 10, 25$ K min^{-1}.

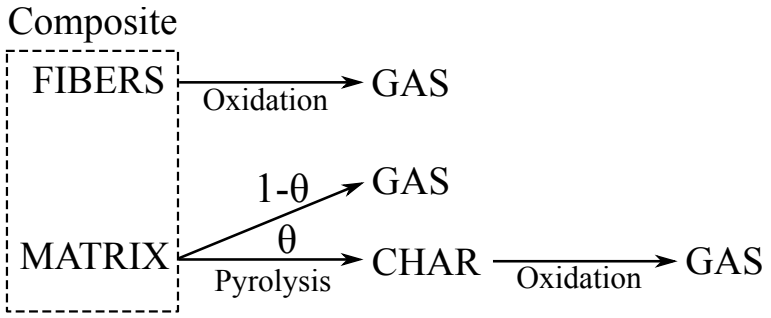

Figure 5.6 Reaction scheme describing the chemical decomposition of a carbon epoxy composite exposed to an oxidative atmosphere.

Figure 5.7 represents the quality of fit of the numerical mass loss rate $d\alpha/dT$ against TGA data for each scheme (competitive, parallel, consecutive). The x-axis is the number of reactions and the y-axis is the evolution of the coefficient of determination R^2. Figure 5.9 shows a comparison between numerical and experimental mass loss rate for $\beta = 10\ \mathrm{K\,min^{-1}}$ for four different reaction schemes: single-step, three competitive, three consecutive, three parallel. The scheme composed of parallel reactions offers the best agreement against experimental $d\alpha/dT$ data when the number of reactions is increased, followed by the reaction scheme composed of consecutive reactions. As the parallel reaction scheme consists in adding independent reactions, and because the optimization is realized on 4 different parameters (E_i, A_i, n_i, X_i), the parallel reaction scheme is less constrained than the consecutive and competitive schemes. Therefore, the better agreement obtained with the parallel scheme could be the result of the lack of constraints on the scheme, and therefore the good quality of fit could be due to mathematical causes rather than physical considerations. R^2 roughly stagnates for competitive reactions, showing that adding this type of reactions does not improve the model agreement against experimental mass loss rates.

Figure 5.8 represents the residual mass as a function of heating rates for all the schemes. The coefficient of determination has been added on Figure 5.8 to ease the comparison of the curves. It shows that the reaction schemes composed of parallel and consecutive reactions all provide a constant residual mass when the heating rate is changed, and therefore cannot accurately model the variation of residual mass observed in the tube furnace, even if these two schemes offered very good agreement against mass loss rate data. The competitive reaction models are the only ones capable of properly modeling a variable residual mass. This can be explained because a different char yield is associated with each competitive reaction. In such a scheme, some reactions can be promoted to the detriment of other reactions for low or high heating rates. Therefore, the global char yield varies for each heating rate, as it tends to the value provided by the dominant reaction. To summarize, reaction schemes composed

of competitive reactions do not capture mass loss rate data as well as those composed of consecutive or parallel reactions, but are the only one able to properly capture the variation of residual mass as a function of heating rate. Having three competitive reactions instead of two decreases simultaneously the agreement against experimental mass loss rate ($R^2 = 0.9573$ vs $R^2 = 0.9631$) and residual mass ($R^2 = 0.80$ vs $R^2 = 0.92$), showing that the optimum number of competitive reactions is two. Figure 5.10 shows the variation of mass as a function of time under inert atmosphere. The measurements obtained from TGA (continuous line) are compared to the outcomes obtained with the reaction scheme composed of two competitive reactions in Table 5.5 (dashed line). The residual mass obtained with the two-competitive scheme is in the same range than the one obtained in TGA, which shows that the model is able to provide a realistic value of the residual mass even beyond the heating rates of the tube furnace. Moreover, contrary to the TGA data, the residual mass obtained with the two-competitive scheme decreases monotonically with the heating rate, with a variation of 3% for $\beta = 5 - 25$ K min^{-1}. This variation could be even more important in a fire test $\beta > 500$ K min^{-1}.

These results confirm the tendency observed in the literature that adding intermediate reactions can improve the agreement against mass loss rate data. However, it also shows that a reaction scheme can simultaneously capture the mass loss rate with a good quality of fit, but not the residual mass. In the literature, reaction schemes are typically chosen to maximize the agreement against mass loss rate data. In that case, the reaction scheme composed of parallel reactions should be the best, as it provides the best coefficient of determination; however, this parallel reaction scheme is unable to model the variation of residual mass observed in the tube furnace. The char yield controls the quantity of protective char and combustible gases formed during the pyrolysis, and therefore influences the material thermal decomposition. In some cases, the reaction rate and char yield can have an almost comparable influence on the thermal response of a composite exposed to heat source [76]. The differences of residual mass observed in this study remain low in absolute terms for the composite as a whole, but are more significant relative to the char-forming fraction of the material (matrix). Moreover, these differences could rise with higher heating rates, or with different polymers. Consequently, optimizing a reaction scheme to obtain a best fit against experimental mass loss rate only, as usually done in the literature, could lead to inaccurate predictions if the reaction scheme is intended to be used in a composite pyrolysis model. However, a need remains to investigate the effect of optimizing the mass loss rate at the expense of the residual mass.

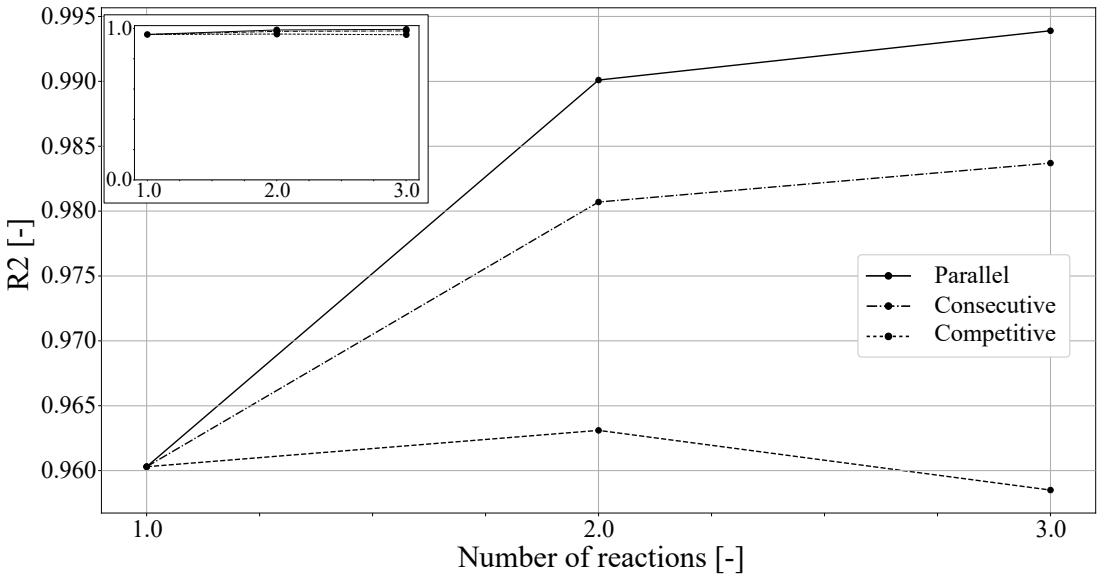

Figure 5.7 Evolution of the coefficient of determination (R^2) as a function of the number and nature of intermediate reactions used in the reaction scheme under an inert atmosphere.

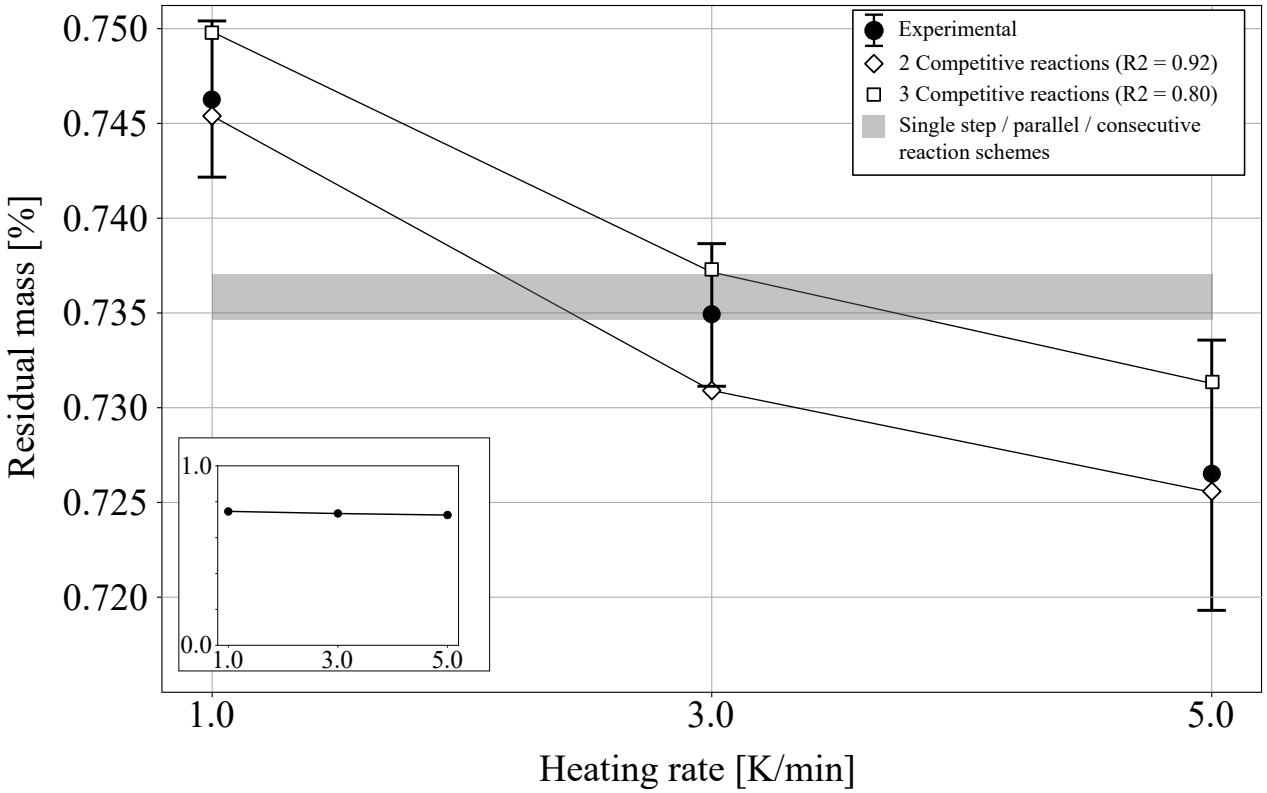

Figure 5.8 Evolution of the residual mass as a function of the heating rate for anaerobic pyrolysis of carbon/epoxy composite, comparing experimentally obtained values to the modeling results using different reaction schemes.

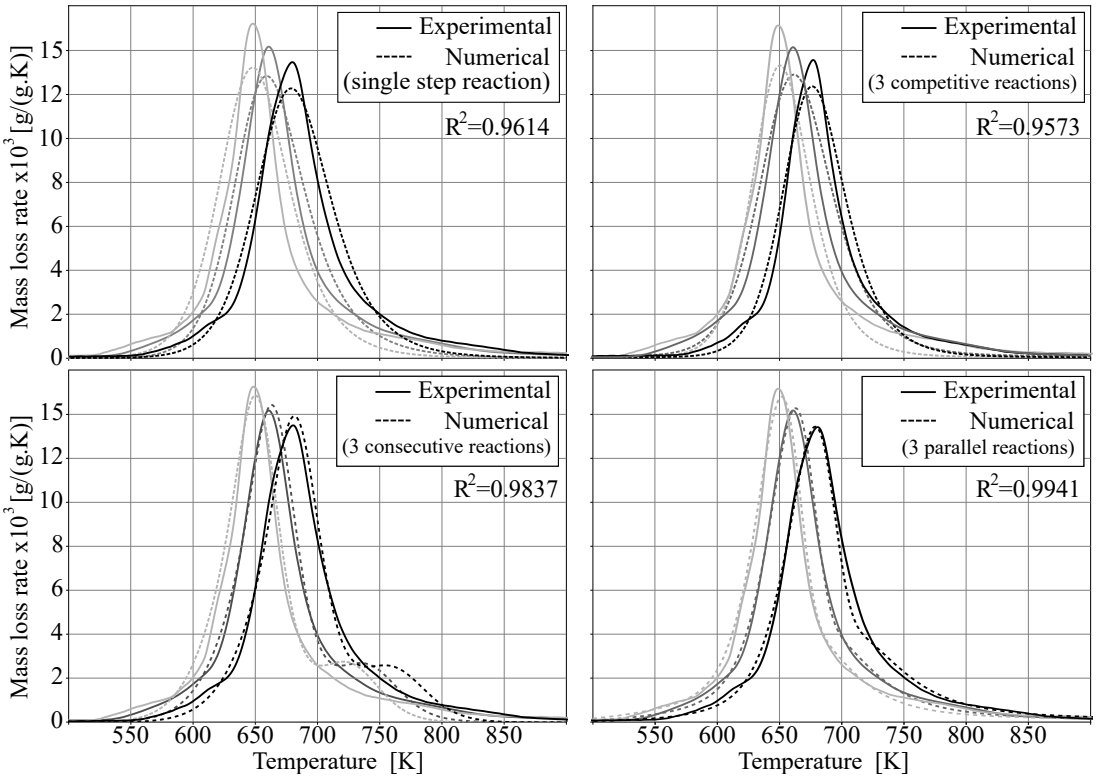

Figure 5.9 Comparison between mass loss rates from anaerobic TGA experiments and kinetic modeling for different reaction schemes. (□): $\beta = 5$ K min^{-1}, (■): $\beta = 10$ K min^{-1}, (■): $\beta = 25$ K min^{-1}.

Type	N	X_i (m^3 m^{-3})	E (kJ mol^{-1})	A (s^{-1})	n (-)	θ_i (-)	R^2 (-)
Single-step	1	-	199.17	5.26×10^{13}	2.43	0.3687	0.9614
Competitive	2	-	80	1.71×10^{3}	1.37	0.44	0.9631
		-	241	1.21×10^{17}	2.45	0.3	
	3	-	153	2.47×10^{9}	1.89	0.62	0.9573
		-	178	3.09×10^{11}	2.20	0.53	
		-	203	3.96×10^{13}	2.17	3.9×10^{-9}	
Parallel	2	0.67	120	7.46×10^{6}	2.79	0.55	0.9900
		0.33	214	7.90×10^{14}	1.16	8.92×10^{-8}	
	3	0.48	73.4	3.24×10^{3}	4.79	0.734	0.9941
		0.23	152	2.94×10^{9}	2.09	2.57×10^{-8}	
		0.29	215	9.36×10^{14}	1.06	2.20×10^{-8}	
Consecutive	2	-	185	2.13×10^{13}	2.5	0.81	0.9807
		-	200	1.49×10^{14}	2.49	0.45	
	3	-	170	4.99×10^{11}	1.5	0.787	0.9837
		-	190	1.35×10^{13}	1.5	0.606	
		-	200	1.015×10^{12}	1.5	0.770	

Table 5.5 Single-step and multi-step reaction scheme describing the pyrolysis of an epoxy resin exposed to an inert atmosphere for heating rates $\beta = 5, 10, 25$ K min^{-1}. The residue (Equation 5.10) is calculated with $x = \alpha$ for all the schemes.

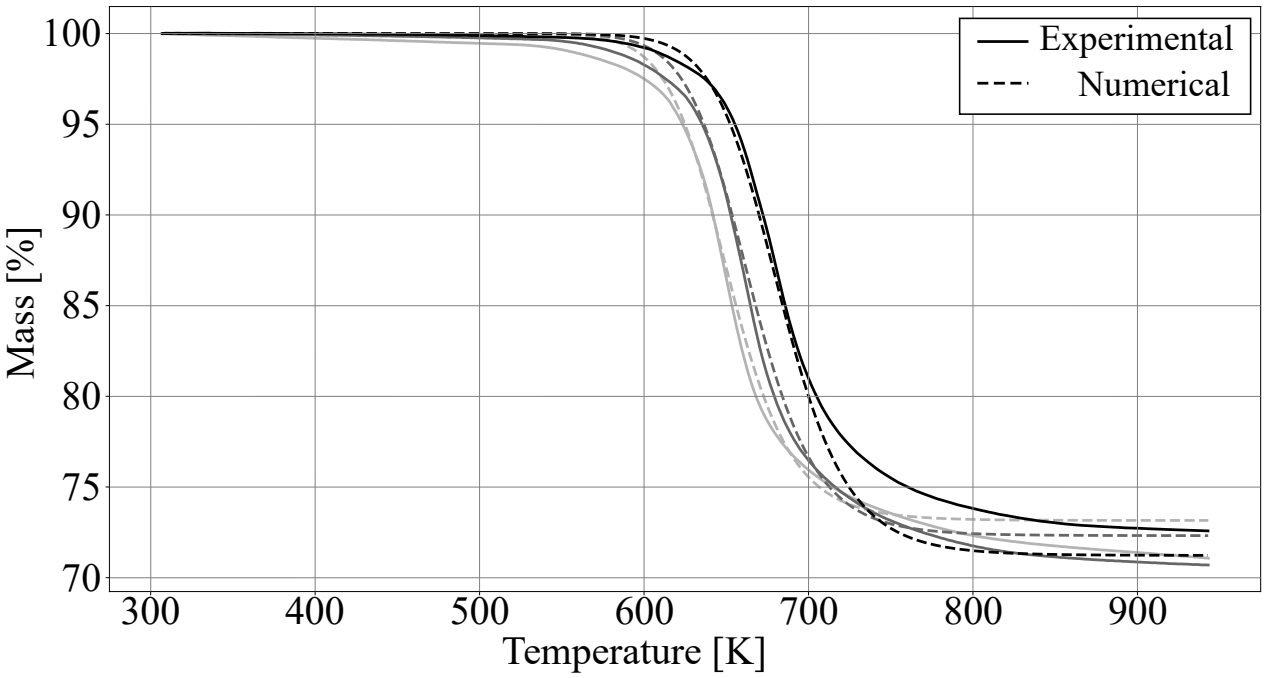

Figure 5.10 Variation of mass as a function of time under inert atmosphere. The dashed lines depict the numerical data obtained with the reaction scheme composed of 2 competitive reactions (Table 5.5) and the continuous lines represents the mass measured with TGA. (▭): $\beta = 5\ \mathrm{K\,min^{-1}}$, (▭): $\beta = 10\ \mathrm{K\,min^{-1}}$, (▭): $\beta = 25\ \mathrm{K\,min^{-1}}$.

5.5 Conclusion

Pyrolysis models are widely used to predict the behavior of composites exposed to high temperatures. Due to the sensitivity of these predictive tools to the thermo-chemical decomposition of the resin, different reaction schemes of increasing complexity are implemented in the literature to best represent TGA data. A popular strategy consists in adding intermediate reactions of different nature (parallel, competitive, consecutive) to obtain the best fit with the experimental mass loss rate. However, the optimal number and nature of intermediate reactions is rarely discussed.

In this paper, the thermo-chemical parameters (E, A and n) describing the pyrolysis of an epoxy resin, as well as the oxidation of char and carbon fibers have been extracted from TGA data using isoconversional methods. Several reaction schemes of variable complexity are proposed and assessed. A first single-step scheme modeled the mass loss rate observed in TGA with a very good agreement, but was unable to model the variation of residual mass observed in a tube furnace when the heating rate is changed. For this reason, several multi-steps schemes have been developed and compared, with an increasing number of reactions of different nature. Results show that even if the addition of parallel or consecutive reactions improves the agreement against TGA data, these schemes are unable to account for the variation of residual mass observed in a tube furnace. Although, adding competitive reactions does not improve the agreement with TGA data compared to a single-step scheme, only this type of reaction allows to model the variation of residual mass with a very good agreement. More research is needed to test reaction schemes including simultaneously competitive, consecutive and parallel intermediate reactions.

This research suggests that contrary to what is commonly done in the literature, obtaining a best fit between experimental and numerical TGA data is not sufficient to build a realistic reaction scheme. Considering the influence of the char yield in heat transfer processes, the residual mass should also be considered when developing a reaction scheme that is intended to be implemented in a pyrolysis model. The variation of residual mass of the carbon-epoxy composite studied here remains low but could be more important for other materials. Further research is needed to find the right balance between accurate modeling of E/A and accurate modeling of θ, if a good agreement cannot be obtained simultaneously on these two variables. This issue could be addressed by investigating the sensitivity of pyrolysis models to reaction schemes of different nature, for different classes of materials.

Conflict of interest statement

No conflict of interest needs to be reported.

Acknowledgments

We are grateful for the assistance and financial support from the Natural Sciences and Engineering Research Council of Canada (NSERC/CRSNG), through grant no. CRDPJ 478687-15, and the partners from CRIAQ ENV-708 project is acknowledged. One of the authors (PCG) is grateful to the National Science and Technology Council of Mexico (CONACYT) for his doctoral scholarship.

CHAPTER 6 ARTICLE 2: MULTI-PHYSICS MODELING OF THE IGNITION OF POLYMER MATRIX COMPOSITE EXPOSED TO FIRE

Jean Langot, Tanja Pelzmann, Pablo Chávez-Gómez, Cristian Stefan Boanta, Martin Lévesque, Etienne Robert (Polytechnique Montréal, Canada)
Julian Karsten, Bodo Fiedler (Hamburg University of Technology)

Submitted to Fire Safety Journal on October 13th 2020

Abstract

Advanced polymer matrix composites (PMCs) are widely used in modern aircraft and as such have to withstand fire to comply with safety regulations. The thermal degradation of these lightweight materials is a complex process involving chemical reactions in the solid and gas phases, potentially leading to flaming combustion. Here, we numerically investigate the heat feedback from the ignition of outgassing at the surface of a structural polymer matrix composite exposed to a pilot flame. Our model couples the thermal, physical and chemical processes in the solid phase to compute the composite degradation, as well as the production and movements of pyrolysates. A counterflow diffusion flame is used to model the ignition of the combustible effluent close to the sample surface, where the hot jet of the pilot flame impinges. The predictive capabilities of the method are demonstrated considering a carbon/epoxy composite exposed to small-scale fire test. As input and validation data for our model, material properties have been measured for virgin and partially burned samples via Differential Scanning Calorimetry, Xenon Flash Analysis and Thermogravimetric Analysis. The model is able to predict the backface temperature and time-to-ignition of the composite sample exposed to a flame with a good accuracy.

***Keywords**: pyrolysate combustion, pyrolysis model, chemical kinetics model, GRI-Mech 3.0, fire test, heat feedback, time-to-ignition, carbon-epoxy composite*

6.1 Introduction

Polymer matrix composites (PMC) are extensively used in the aerospace industry due to their light weight and versatility [7]. However, owing to their inherent flammability, their usage is mostly limited to applications where temperatures do not reach their glass transition T_g or decomposition temperatures [196]. To decrease aircraft weight, there is an incentive

to use these materials in location where they must act as firewalls, such as in and around powerplants. In such cases, their fire resistance is assessed through standardized certification tests requiring the material to maintain its functions while containing fire when exposed to a 1366 K (2000 °F) pilot flame for 15 minutes [15]. To increase the understanding of failure modes and improve the design process of PMC-based aircraft powerplant firewalls, this paper presents a multi-physics model for the thermo-chemical degradation processes associated with a carbon/epoxy composite subjected to conditions representative of certification tests [15]. When exposed to fire, a PMC undergoes several closely-coupled thermal, chemical and physical processes [18, 65]. As the matrix exceeds its T_g (for amorphous polymers) and the decomposition temperature is reached, it first degrades through pyrolysis, locally decreasing the material density and affecting its thermo-physical properties. The formation of a low-density porous char layer on the surface may protect the remaining matrix from further heat transfer, thus slowing its degradation. Gaseous pyrolysis products (henceforth referred to as *pyrolysates*) migrate from the inside of the material toward the hot face as a consequence of pressure gradients and higher permeability in this direction. The combustible effluent exiting the sample meets the hot exhaust jet produced by the pilot flame close to the surface. The pilot burner is operated lean to achieve the desired temperature. Consequently, the gaseous exhaust effluent contains non-negligible amounts of oxygen. Moreover, as the pilot flame itself approaches the surface, other oxidative species besides O_2 as well as radicals are available to mix with and ignite the pyrolysate escaping the surface. This reactive mixture ignites as the lower flammability limit is reached and gives rise to a diffusion flame which in turn provides a heat feedback further promoting the material degradation. The ignition of the composite is defined as the onset of self-sustained combustion, potentially leading to the appearance of large flames that may contribute to spread fire. Consequently, the time-to-ignition is an important parameter in fire safety science [23]. The temperature of the flame produced by this additional heat source depends on the pyrolysate composition and fire test conditions. The thermal feedback loop is also a crucial factor in the fire resistance of combustible solids and its accurate modeling is paramount to achieve quantitative predictions. Finally, the char and, subsequently, carbon fibers are oxidized, increasing again the material porosity and providing an additional heat source due to the exothermic nature of these oxidation reactions. So-called *pyrolysis models* aim at modeling the interactions between these processes [43, 64, 140, 141]. The thermal degradation of PMCs has been studied considering materials exposed to both non-reactive and reactive heat sources [35, 52, 57, 58, 79, 130, 132]. Non-reactive heat sources are often lasers [52, 130] or radiant heaters [79, 132]. The models considering these heat sources usually offer good agreement with experimental data since a non-reactive source is often simpler to model than a reactive one. Indeed, the source heat flux is typically homo-

geneous and the atmosphere can be controlled to prevent oxidation or pyrolysate ignition, which considerably limits the number and complexity of phenomena that must be modeled. By contrast, the modeling of reactive heat sources, such as pilot flames, is much more challenging [35, 57, 58], notably because the interactions between the flame and the pyrolysate strongly affect the composite ignition.

The thermal degradation of composites is sensitive to the heat feedback from pyrolysate combustion [60, 151], which depends on the nature of the material exposed to heat [62]. In the context of a fire test, the pyrolysate combustion for a given material is also affected by the composition of the exhaust gases from the pilot flame, which in turn depends on burner operation parameters [15, 153]. In previous modeling of a fire test, pyrolysate combustion was often neglected [35, 57] or modeled with empirical parameters [58] that must be inferred experimentally for each set of test conditions and material composition. Fully coupled solid-gas models have also been developed for the piloted ignition of combustible materials [52, 59, 60, 62, 151, 152], but they often relied on simplified chemical kinetics, i.e. global one-step reactions, that cannot capture the effect of composition in the exhaust gases of a burner used for certification testing. This simplification has two consequences; first, it can lead to an overestimation of the flame temperature from pyrolysate combustion, as global one-step reactions do not consider the heat absorbed by the endothermic dissociation reactions. Second, the pyrolysate time-to-ignition cannot be modeled with a global one-step reaction. A mixture ignites when the heat generated by chemical reactions exceeds heat losses, favoring the creation of chain carriers leading to thermal runaway. As a consequence, chemical kinetics based on global one-step reaction relies again on empirical parameters to estimate the time-to-ignition [56], usually related to a critical pyrolysate mass flow rate [129] or material surface temperature [74].

Available general purpose complex reaction mechanisms are suitable to model pyrolysate ignition and combustion. For instance, GRI-Mech 3.0 has been developed for natural gas combustion and involves 53 species, including hydrocarbons up to C3, and 325 reactions [154]. These mechanisms can be implemented in two- or three-dimensional Computational Fluid Dynamics (CFD) simulations, but such modeling in practical combustion applications is a very complex task, with most current simulations limited to flames in simple configurations, with no reacting solid phase [158, 159]. Chemical kinetics software such as Cantera [160] however allows for the use of complex reaction mechanisms in simple one-dimensional CFD simulations, and therefore offer a good compromise between detailed chemical kinetics and accurate CFD simulations. A chemical kinetics software has been coupled to a pyrolysis model by Li *et al.* [197] to investigate the surface ablation of charring composites, but to the best of the authors knowledge the work presented here is the first occurrence that this

approach is used to model the heat feedback from pyrolysate ignition in the context of a fire test.

This paper presents a multi-physics model for the heat feedback and time-to-ignition from gas phase reactions at the surface of a composite subjected to a one-sided reactive heat flux. This predictive tool is based on a novel coupling architecture between a pyrolysis model and a chemical kinetics model. To validate this approach, numerical predictions are compared against fire test conducted on a carbon/epoxy composite exposed to a methane flame. For this purpose, a novel small-scale fire test [153] has been developed to mimic the conditions encountered in large-scale fire certification [15]. The material has also been characterized extensively to obtain its thermal and chemical properties, both in the virgin state and following thermal degradation. A sensitivity analysis has been done to investigate the effect of variations in material properties, solid-phase chemical reactions and gas-phase chemical reactions. The novelty of this study lies in the coupling architecture of a chemical kinetics software with a pyrolysis model, that has never been done in the context of a fire certification test. This approach allows a purely theoretical prediction of the time-to-ignition and heat feedback from the combustion of pyrolysates mixed with a pilot flame exhaust gases.

6.2 Background

6.2.1 Modeling

Pyrolysis models

The degradation of composite materials results from the complex interaction of physical, chemical and thermal processes. This degradation can be modeled empirically [86], but the validity of the model obtained is limited to the conditions of the specific fire test for which it was developed and becomes obsolete if these test conditions are changed. An analytical modeling approach is also possible [198], but it relies on many assumptions, typically restricting its range of application to semi-infinite and non-reactive solids [199]. In contrast, comprehensive models based on the conservation of mass, energy and sometimes momentum [43, 52, 64, 140, 141] have a wider range of application, and are adaptable to changes in fire test conditions. However, they require a large number of material properties and parameters that must be inferred from specialized experiments in simple configurations rather than fire tests. As the predictive tool developed in this work is intended to be adaptable to different fire test conditions, a comprehensive approach is adopted.

Chemical kinetics model

The ignition of combustible materials is driven by chemical reactions occurring in both solid and gas phases. Solid phase reactions are often modeled with global simplified reactions as the chemical species involved are mostly unknown. Gas phase reactions can be modeled with more detailed reaction model such as Cantera, as the pyrolysate composition can be measured [52, 53]. Cantera is an open-source suite of tools, developed for problems involving thermodynamics, transport processes and chemical kinetics [160]. It models flames that are stabilized in an axisymmetric stagnation flow, and computes the solution along the stagnation streamline ($r = 0$), using a similarity solution to reduce the three-dimensional governing equations to a single dimension. In particular, the counterflow diffusion flame sub-model (class *CounterflowDiffusionFlame* in Python) is governed by the conservation of mass, radial momentum, energy and species, which reads:

$$\frac{\partial \rho u}{\partial x} + 2\rho V = 0 \tag{6.1a}$$

$$\rho u \frac{\partial V}{\partial x} + \rho V^2 = -\Lambda + \frac{\partial}{\partial x}\left(\mu \frac{\partial V}{\partial x}\right) \tag{6.1b}$$

$$\rho c_p u \frac{\partial T}{\partial x} = \frac{\partial}{\partial x}\left(\lambda \frac{\partial T}{\partial x}\right) - \sum_i j_i c_{p,i} \frac{\partial T}{\partial x} - \sum_i h_i M_i \dot{\omega}_i \tag{6.1c}$$

$$\rho u \frac{\partial Y_i}{\partial x} = -\frac{\partial j_i}{\partial x} + M_i \dot{\omega}_i \tag{6.1d}$$

where ρ is the density ($\mathrm{kg\,m^{-3}}$), u and v are the axial and radial velocities ($\mathrm{m\,s^{-1}}$), $V = v/r$ the scaled radial velocity, Λ the pressure eigenvalue ($\mathrm{Pa\,m^{-2}}$), μ the dynamic viscosity ($\mathrm{Pa\,s}$), T the temperature (K), λ the thermal conductivity ($\mathrm{W\,K^{-1}\,m^{-1}}$), Y_i the mass fraction of species i $(-)$, $c_{p,i}$ the specific heat capacity of species i ($\mathrm{J\,kg^{-1}\,K^{-1}}$), h_i the enthalpy of species i ($\mathrm{J\,kg^{-1}}$), M_i the molecular weight of species i ($\mathrm{kg\,mol^{-1}}$) and $\dot{\omega}_i$ the molar production rate of species i ($\mathrm{mol\,m^{-3}\,s^{-1}}$). j_i is the diffusive mass flux of species i ($\mathrm{kg\,m^{-2}\,s^{-1}}$) and is computed with a mixture-averaged formulation. The gases are treated as ideal for the calculation of their thermodynamic properties, following a mixture rule, with polynomial fits used to capture their temperature-dependence. These conservation equations model the transport of matter and heat in the reaction zone. Sin *et al.* [200] showed that similarity solutions can successfully predict velocity profile of a two-dimensional stagnation point flow, even at high aspect ratio (when the distance between inlet and solid surface is 5 times the lateral distance of the problem).

Gas combustion is modeled with the GRI-Mech 3.0. The reaction rates are represented with Arrhenius equations and the chemical equilibrium is modeled with a non-stoichiometric

solver [201], yielding the temperature and species distribution in the reaction zone.

6.2.2 Material characterization

Thermo-physical properties

Each species i contained in the composite (gaseous or solid) needs to be described by at least three thermo-physical properties, depending on the complexity of the pyrolysis model: ρ_i, $c_{p,i}$ and λ_i. Ideally, these properties must be measured as a function of temperature in the range of interest from 300K to 1000K. These temperature-dependent properties are rarely provided by the manufacturer or the literature and an extensive characterization work is therefore necessary. Two different approaches are available to obtain them.

First, the apparent properties of the composite can be used in the predictive tool, without distinction of the different phases [53], reducing the number of thermo-physical properties that must be measured. This method allows the direct use of the properties measured without additional calculation or hypotheses, but cannot provide insight on the properties or degradation of each phase.

The second method consists in calculating the properties of each sub-phases independently from experiments performed on the composite [52, 132], increasing the number of thermo-physical properties that must be measured. This forces the use of conventions and hypotheses to derive all the unknown parameters from a limited number of experiments carried out on the entire composite. The global or *effective* composite properties $\bar{\mathbb{P}}$ can then be determined with a rule of mixture weighted by mass or volume (X_i) fraction:

$$\bar{\mathbb{P}} = \sum_{i=1}^{N} X_i \bar{\mathbb{P}}_i \tag{6.2a}$$

$$\bar{\mathbb{P}} = \sum_{i=1}^{N} Y_i \bar{\mathbb{P}}_i \tag{6.2b}$$

where N is the total number of species in the control volume. The mixture rule is the simplest approach to model the composite properties, although it does not account for the geometrical aspects or interactions between phases. Other approaches consider the geometry of the composite with various level of precision. For instance, upper- and lower-bounds of the composite thermal conductivity can be estimated with the Voigt and Reuss models. The Maxwell's model [163] provides the thermal conductivity of a random distribution of spheres into a homogeneous porous media. The Clayton model [164] has been specifically developed and validated [202] for plain-weave composites. Nevertheless, the method consisting in calculating the composite properties as a function of each phase properties increases

the complexity of the material characterization, but provides a more detailed insight of the phase contribution to the overall material degradation. Therefore, the second method is preferred in this work. Then, the temperature-dependent thermal conductivities and heat capacities can be measured respectively with Laser/Xenon Flash Analysis (LFA/XFA) [203] and Differential Scanning Calorimetry (DSC) [199].

Kinetic analysis

When exposed to heat, a carbon/epoxy composite degrades through matrix pyrolysis, char oxidation and carbon fiber oxidation. Sensitivity analyses have shown that the matrix pyrolysis plays a dominant role in the composite thermal behavior as char and carbon fibers are comparatively much less reactive [135]. For this reason, among others, char and fibers oxidation were most of the time neglected in composite pyrolysis models [58]. However, in the context of firewall certification testing considered here, a pilot flame can produce species with a high oxidative potential, notably combustion radicals, that can play a significant role in carbon oxidation [71]. Therefore, char and carbon fiber oxidation are included in this work. The reaction rate associated with each chemical reaction is usually computed with the Arrhenius law in pyrolysis models [43, 64, 141]:

$$\frac{\partial \alpha}{\partial t} = f(\alpha) A \exp\left(-\frac{E}{RT}\right) \tag{6.3}$$

where $\alpha = \frac{m(t)-m_0}{m_\infty - m_0}$ is the degree of advancement of the reaction, m_0 and m_∞ are respectively the initial and final mass of the sample exposed in Thermogravimetric Analysis (TGA) (kg), A is the pre-exponential factor (s^{-1}), E the activation energy ($\mathrm{J\,mol}^{-1}$), R the perfect gas constant ($\mathrm{J\,mol}^{-1}\,\mathrm{K}^{-1}$). $f(\alpha)$ is the reaction model and represents the dependence of the reaction on the degree of advancement. The reaction model is assumed to follow the n-order law $f(\alpha) = (1-\alpha)^n$ in most pyrolysis models [35, 53, 204], where n is the reaction order ($-$). With this assumption, 3 parameters (A, E, n) must be measured for each reaction, plus a parameter q ($\mathrm{J\,kg}^{-1}$) describing the heat released or absorbed by the chemical reaction. These parameters are usually inferred through TGA or DSC using the so-called *isoconversional principle*, which states that the reaction rate at a constant extent of conversion is only a function of temperature [46].

The pyrolysate composition must also be known to model the material ignition. Several authors attempted to measure the composition of the outgassing emitted by an epoxy resin with Mass Spectrometry (MS) [52, 205, 206] or Fourier Transform Infrared spectroscopy (FTIR) [53, 206–208] and most of them reported the emission of water and some combustible gases such as CH_4 or H_2. However, a qualitative measurement is not sufficient to model the

pyrolysate ignition and a quantitative composition is required as input parameter in Cantera. To the best of our knowledge, only two authors provided a quantitative composition of the pyrolysates emitted by the degradation of an epoxy resin, via MS [52] and FTIR [53], respectively. It is worth noting that FTIR did not allow to detect H_2, although this species has probably a major influence in pyrolysate ignition because of its reactivity. Jiang *et al.* [205] identified H_2O, H_2 and C_2H_2 as the main species present in the pyrolysates with mass spectrometry, using soft ionisation with an electron energy of 15 eV to prevent the fragmentation of hydrocarbons. Pyrolysates are therefore mainly composed of low molecular weight hydrocarbons, which supports the choice of GRI-Mech 3.0 to model their ignition. From the mass spectrum obtained, Biasi [52] quantified the molar fraction of each of the main species based on the maximum relative intensities of the peaks, therefore considering that the sensitivity of the instrument was identical for all species, an assumption that should be verified through extensive calibration [209]. Although very approximative, the pyrolysate composition obtained is the only one found in the literature for epoxy. It is shown in Table 6.1 and used in this work. The influence of inaccuracies in pyrolysate composition on the modeling of material degradation will be discussed later. Pyrolysates are assumed to be a mixture of ideal gases, so that the volume fraction is equal to the molar composition.

6.3 Small-scale fire test

Figure 6.1 represents the small-scale test bench used to reproduce the conditions present in large-scale fire-resistance certification tests [153]. The test considered here is intended for structural components that must act as firewalls and is described in the FAA AC 20-135 [14] and in ISO 2685 [15] standards. The flame is required to have an average temperature of approximately 1100 °C (2000 °F) and a heat flux density of 116 ± 10 kW m^{-2} at the sample location. Although a kerosene burner is traditionally used in certification tests, the flame is produced in this work by a more simple methane burner, as the modeling developed here cannot account for phenomena specific to liquid fuel burners such as droplet projection that could create local hot spots on the sample. The parameters that yield the desired flame conditions are calibrated using a water-calorimeter and a Gardon heat gauge. The sample (25 mm wide and 300 mm long) is held from the top and bottom, with no mechanical

Species	H_2O	H_2	C_2H_2
Volume fraction (−)	0.706	0.199	0.095

Table 6.1 Composition of the pyrolysates emitted by the pyrolysis of a M21 epoxy resin measured with Mass Spectrometry (from [52]).

stress applied. Since the flame width (approximately 50 mm) exceeds the sample width, two ceramic shields are placed along the sample sides to prevent the flame from wrapping around the edges. The backside temperature opposite to the impinging point is measured continuously using a K-type thermocouple with a spring-loaded joint to maintain steady surface contact. The temperature on the front face is probed only for short times to avoid altering the flame dynamics using a S-type thermocouple, with the exposed wire protected by a ceramic coating. Furthermore, the samples are monitored with video cameras during the entire test duration to identify precisely the ignition onset and the flame quenching at the front face. The small-scale test rig was mounted in an approximately 1 cubic meter enclosure, separated into a hot side where the flame impinges on the sample and the cold side where weak outgassing of the sample and natural convection dominated.

6.4 Modeling

6.4.1 Coupling architecture

The modeling approach implemented here consists of three coupled sub-models. First, a zero-dimensional chemical kinetics model computes the pilot flame chemical equilibrium as a function of the oxidizer and fuel composition (sub-model 1). This model provides the composition of the pilot flame exhaust gases X_b, mass flow rate $\dot{m}_b$ ($\mathrm{kg\,m^{-2}\,s^{-1}}$) and temperature T_b, that are used as input parameters for sub-models 2 and 3. Then, a one-dimensional pyrolysis model computes the thermal degradation of the composite during fire exposure as a function of the heat flux $\dot{q}_b$ ($\mathrm{W\,m^{-2}}$) received from the pilot flame and pyrolysate ignition at its surface (sub-model 3). This model provides the pyrolysate composition $X_{g,pyr}$, mass flow rate $\dot{m}_{g,pyr}$ and temperature $T_{g,pyr}$. The one-dimensional computational domain is oriented along the composite sample thickness and co-linear with the pilot flame axis, beginning at the stagnation point of the flame impinging on the hot face and ending on the cold face. The use of a one-dimensional domain in the solid phase is reasonable as the size of the zone of approximately constant heat transfer on the hot face on the order of the pilot flame diameter (50 mm) and the sample width (25 mm) are both much greater than the composite thickness (1.6 mm). Therefore, the lateral dimension of the domain is more than 15 times greater than the axial dimension (along the flame axis), which is greater than the minimum factor of 3 traditionally used to justify the use of one-dimensional domains. In the literature, one-dimensional pyrolysis models have been used successfully to predict the degradation of composites in similar geometrical configurations, exposed to pilot flame [57] or radiant heat flux [73, 132]. Finally, when the pyrolysates flow out of the solid phase and encounter the pilot flame exhaust gases, they form a combustible mixture that can potentially ignite as

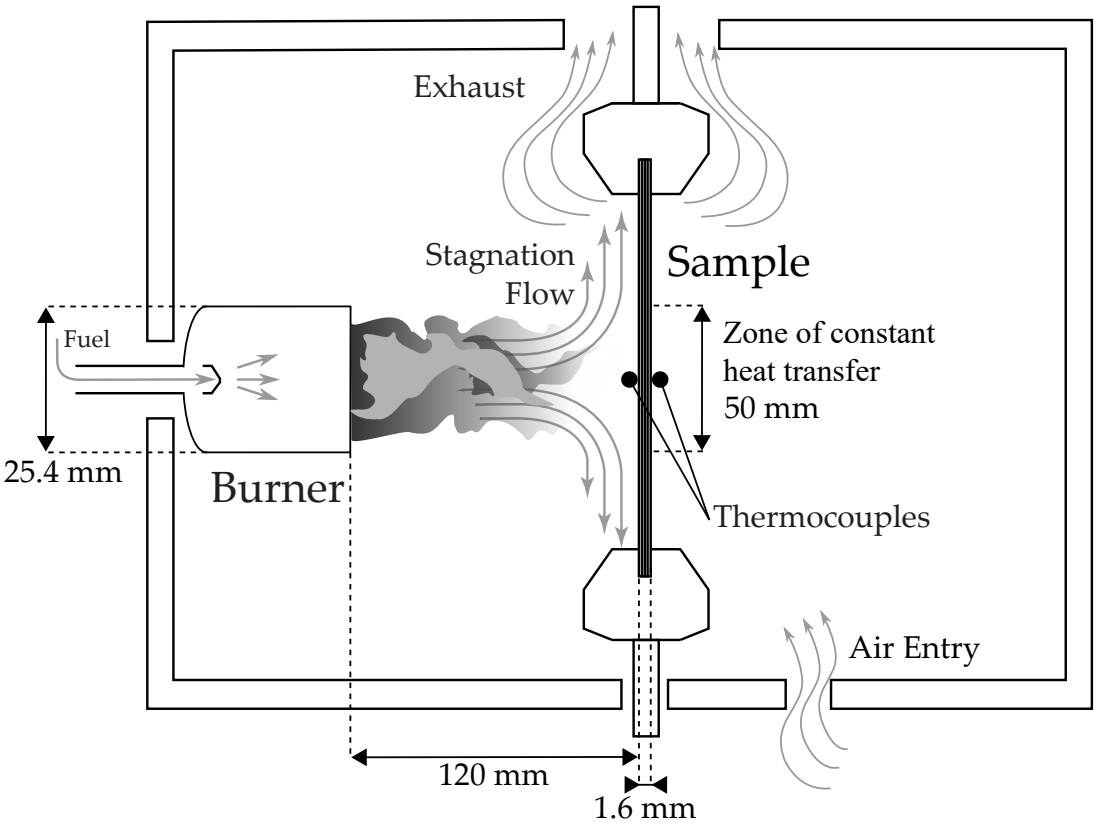

Figure 6.1 Small-scale test used to reproduce the conditions encountered in real full-scale certification tests.

an axisymmetric non-premixed counterflow flame. A one-dimensional counterflow diffusion flame model is therefore used to identify ignition conditions and provides the flame temperature T_{fl}, which is then used to update the heat flux received by the material $\dot{q}_b$ (sub-model 2). The computational domain for this sub-model begins at the burner exit and ends on the material surface. It is worth noting that similarity solutions reducing a three-dimensional problem to a single dimension have already been used successfully to predict the velocity profile of a two-dimensional stagnation point flow in a close configuration [200].
Pyrolysate ignition and heat feedback are modeled as a function of time. The total duration of the fire test is therefore divided into time steps, during which all sub-models exchange data. The pilot flame rapidly reaches steady state and this equilibrium is assumed to be independent from processes in the solid sample or in the thin layer close to the surface where pyrolysates burn. This hypothesis is reasonable as chemical equilibrium is typically reached in the order of magnitude of 10^{-6} s for methane combustion, which is much faster than the time required to attain the sample surface (in the order of magnitude of 10^{-2} s) or the duration of a time step (not less than 10^{-3} s). The pilot flame sub-model is therefore called only once at the first time step and is not updated thereafter. The chemical processes in the gas phase in the vicinity of the sample surface are assumed to occur very fast relative to the processes in the solid phase, such that the pyrolysate ignition model is computed in steady state, whereas the pyrolysis model in the solid phase is computed in transient state. Therefore, the counter-flow diffusion flame and pyrolysis sub-models are called at every time step because, as the material degrades, pyrolysate mass flow rate and temperature evolve over time. The solid and gas phase modeling are combined through a master-slave strong coupling. The solid phase code provides the pyrolysate mass flow rate and temperature on the hot face and calls the counterflow diffusion flame model at each iteration. Figure 6.2 represents the modeling approach implemented here as well as the data exchanged.

6.4.2 Pilot flame modeling (sub-model 1)

The pilot flame is modeled with the chemical kinetics software Cantera [160], providing the composition and temperature of the exhaust gases at chemical equilibrium. This is achieved using the GRI-MECH 3.0 mechanism (53 species and 325 reactions) with a non-stoechiometric solver, holding pressure and enthalpy fixed (function *equilibrate* in Python). The burner used in this work is a partially premixed methane burner. Both oxidizer (O_2) and fuel are diluted with 55% volume CO_2 to achieve the conditions specified in the certification test procedure in terms of flame temperature and heat flux. The flow rate is 7 Standard Liter Per Minute (SLPM) for both fuel and oxidant, yielding $\dot{m}_b \approx 0.23\ \mathrm{kg\,m^{-2}\,s^{-1}}$. Air is added to the mixture in Cantera to account for mixing with the atmosphere to reach a flame temperature

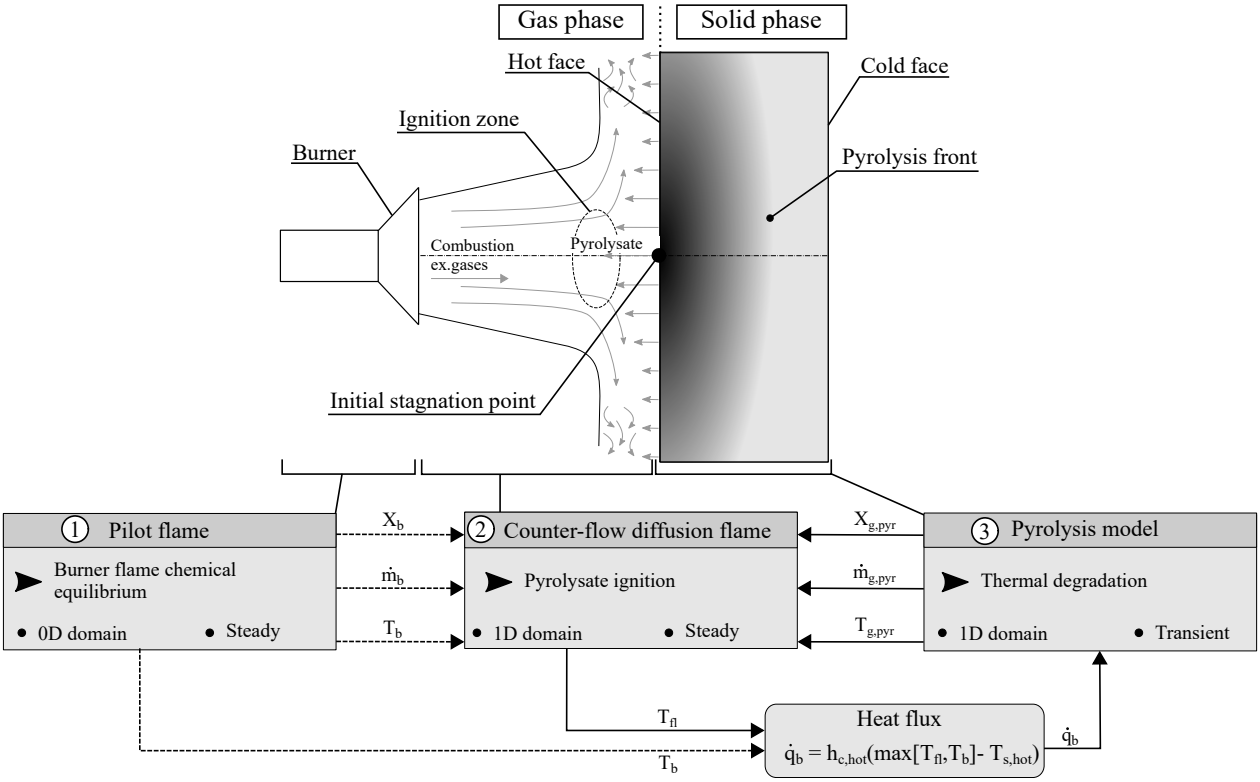

Figure 6.2 Architecture of the coupled approach, which consists of three sub-models coupled together. The temperature and composition of the pilot flame impinging on the composite are modeled in zero-dimension at stationary state with Cantera (sub-model 1). The pyrolysate composition, mass flow rate and temperature are computed with a one-dimensional transient pyrolysis model (sub-model 2). The mixing of pyrolysate with pilot flame exhaust gases and their ignition are modeled with a one-dimensional stationary counter-flow diffusion flame model in Cantera (sub-model 3). The arrows represent data fluxes. Dashed arrows depict weak coupling (variables computed only once) and solid arrows depict strong coupling (variables updated at each iteration).

of 1366 K. The composition of the pilot flame exhaust gases computed by Cantera is provided in Table 6.2.

6.4.3 Counterflow diffusion flame modeling (sub-model 2)

The counterflow diffusion flame model provided by Cantera [160] (class *CounterflowDiffusionFlame* in Python) is used to calculate the pyrolysate ignition. Three boundary conditions were defined on each side: the mass flow rate $\dot{m}_b$, temperature T_b and composition X_b of the exhaust gases on the burner side, and the pyrolysate mass flow rate $\dot{m}_{g,pyr}$, temperature $T_{g,pyr}$ and composition $X_{g,pyr}$ on the material side. The calculation of the temperature profile is then performed in a one-dimensional domain going from the burner exit to the material surface. Material ignition is defined here as the moment at which the boundary layer temperature exceeds the temperature of the exhaust gases of the pilot flame. This is a practical criterion as the objective of this study is to determine when the heat feedback from pyrolysate ignition outreaches the heat flux provided by the calibrated pilot flame.

6.4.4 Solid phase modeling (sub-model 3)

This section aims at developing a generalized and comprehensive pyrolysis model. First, the multi-components approach used to compute the composite properties as a function of the properties of its phases is introduced. Then, the modeling of the degradation rate is described. Finally, a mathematical model based on conservation equations is developed. Finally, the finite element formulation and time-step integration are introduced. The model is based on the following assumptions:

- The control volume remains constant, which implies that the variation of mass and density are equivalent. Swelling and delamination are neglected [35].
- The gas behave accordingly to the perfect gas law [43].
- The entire void space contained in the composite, i.e. its pores, is interconnected [161].
- The diffusivity D ($\mathrm{m^2\,s^{-1}}$) is assumed to be the same for all gaseous species and equal to their kinematic viscosity ν ($\mathrm{m^2\,s^{-1}}$) [43].

Species	N	CO_2	O_2	H_2O
Molar composition (−)	0.62	0.16	0.12	0.09

Table 6.2 Composition of the exhaust gases emitted by the partially premixed methane burner used in the small-scale fire test. Only the main species (≥ 0.09 mol mol^{-1}) are reported here.

- The pyrolysate vapors are assumed to be in thermal equilibrium with the solid phase [109] and flow toward the hot face through the porous media with no resistance [44, 73]. Gas migration toward the cold face is not modeled, since the cold face is considered impermeable until the matrix is consumed.

Multi-components approach

A composite material undergoing thermal decomposition is composed of several distinct porous media, in the sense that every small volume at the mesoscopic level always contains both solid and gas phases, in the form of a solid component with an interconnected network of pores [161, 162]. Figure 6.3 presents a conceptual view of a control volume containing matrix, fibers, char and porosity, for a carbon-epoxy composite exposed to fire. The volume fraction X_i of each phase i is given by:

$$X_i = \frac{V_i}{V_{tot}} \tag{6.4}$$

where V_i is the volume of phase i and V_{tot} the total control volume. The volume fraction can be defined not only with respect to the control volume but also with respect to the total solid or gaseous phases as:

$$X_{i,p} = \frac{V_i}{\sum_{i=1}^{N_p} V_i} \tag{6.5}$$

where p represents the phase of interest ($p = s$ and $p = g$ for respectively solid and gaseous phases) and N_p indicates the total number of solid or gaseous phases in the control volume. A distinction must be made between the *absolute* density ρ_i, that is the density of a control volume containing only the phase i, and the *weighted bulk* or *effective* density $\bar{\rho}_i$, that is the density of phase i with respect to a control volume containing several different phases. These quantities are related to each other as

$$\bar{\rho}_i = \rho_i X_i \tag{6.6}$$

Next, parameters with an overbar indicate *effective* quantities, defined with respect to the control volume. The total density of the control volume $\bar{\rho}$ is given by:

$$\bar{\rho} = \sum_{i=1}^{N} \bar{\rho}_i = \sum_{i=1}^{N} X_i \rho_i \tag{6.7}$$

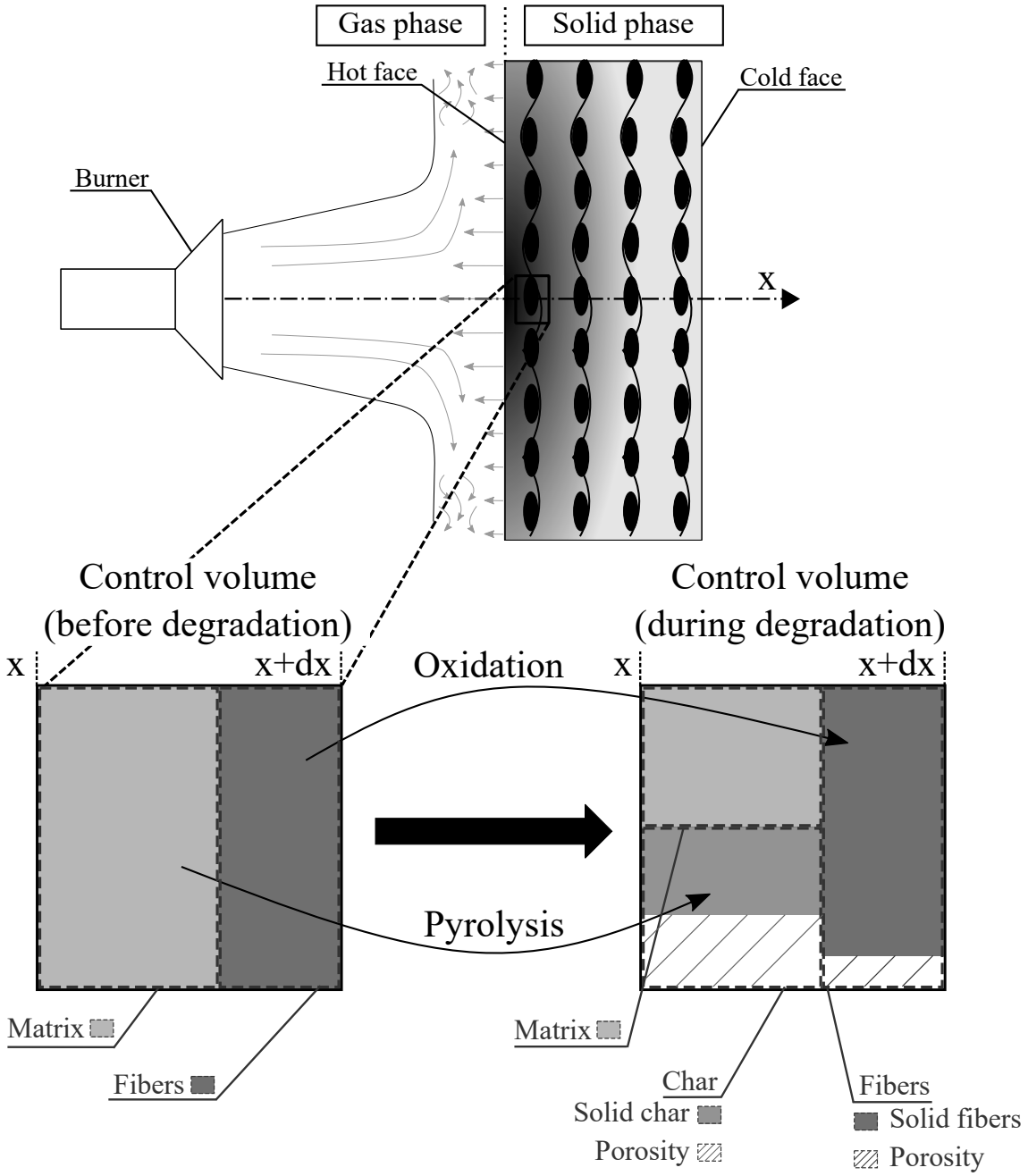

Figure 6.3 Illustration of a control volume containing several phases: matrix, char layer and carbon fibers. Although the domain is one-dimensional, the control volume has been drawn as a two-dimensional conceptual view for better understanding.

Then, the mass fraction is defined as:

$$Y_i = \frac{m_i}{m_{tot}} = \frac{\bar{\rho}_i}{\bar{\rho}} = X_i \frac{\rho_i}{\bar{\rho}} \tag{6.8}$$

The porosity represents the quantity of gas stored in pores appearing during the degradation or initially present in the composite. It is defined as the volume fraction of void in each porous medium. The porosity ϕ_i ($\mathrm{m}^3\,\mathrm{m}^{-3}$) is computed from each species bulk density as:

$$\phi_i = 1 - \frac{\bar{\rho}_i}{\bar{\rho}_{i,0}} \tag{6.9}$$

where $\bar{\rho}_{i,0}$ corresponds to the effective density of the non-porous phase i over the control volume. Finally, the total porosity is given by:

$$\bar{\phi} = \sum_{i=1}^{N} X_i \phi_i \tag{6.10}$$

The temperature dependence of c_p and λ can be defined with a polynomial interpolation as:

$$\bar{\mathbb{P}}_i(T) = \sum_j C_{ij} T^j \tag{6.11}$$

where C_{ij} is the jth polynomial coefficient of the ith thermo-physical property. The parameters C_{ij} are then chosen empirically to fit experimental data representing the property $\bar{\mathbb{P}}_i$ as a function of temperature. Once the temperature-dependent properties of each phase have been calculated, the *effective* thermo-physical properties of the entire control volume can be computed with mass (c_p) or volume fraction (λ, ρ, ϕ, M, emissivity ϵ (-)).

Modeling of the degradation rate

Consider a system of reactions composed of N_r equations including N_i different species, occurring in the sample during fire exposure

$$\sum_{i=1}^{N_i} \theta'_{ij} S_i = \sum_{i=1}^{N_i} \theta''_{ij} S_i + q_j \tag{6.12}$$

where the θ_{ij} are the mass stoichiometric coefficients and S_i the different species. The reaction rate k_j of each reaction j is computed according to:

$$k_j = (\bar{\rho}_0 - \bar{\rho}_\infty) \left[\frac{\bar{\rho} - \bar{\rho}_\infty}{\bar{\rho}_0 - \bar{\rho}_\infty} \right]^{n_j} A_j \exp\left(-\frac{E_j}{RT} \right) \tag{6.13}$$

where n_j is the reaction order and $\bar{\rho}_0$ and $\bar{\rho}_\infty$ respectively refer to the initial and final (after degradation) densities of the reacting phase.

Mathematical model

The thermo-chemical model consists of simultaneously modeling the conservation of solid species, gas phase mass, gaseous species and energy in a one-dimensional domain:

$$\frac{\partial \bar{\rho}_i}{\partial t} = \sum_{j=1}^{N_r} \theta_{ij} k_j \tag{6.14a}$$

$$\frac{\partial \rho_g \bar{\phi}}{\partial t} + \frac{\partial \dot{m}_g}{\partial x} = \sum_{i=1}^{N_g} \sum_{j=1}^{N_r} \theta_{ij} k_j \tag{6.14b}$$

$$\bar{\phi} \rho_g \frac{\partial Y_{i,g}}{\partial t} + \dot{m}_g \frac{\partial Y_{i,g}}{\partial x} = \frac{\partial}{\partial x} \left(\bar{\phi} \rho_g D \frac{\partial Y_{i,g}}{\partial x} \right) + \sum_{j=1}^{N_r} \theta_{ij} k_j \tag{6.14c}$$

$$\bar{\rho} \bar{c_p} \frac{\partial T}{\partial t} + \dot{m}_g \bar{c_{pg}} \frac{\partial T}{\partial x} = \frac{\partial}{\partial x} \left(\bar{\lambda} \frac{\partial T}{\partial x} \right) + \sum_{j=1}^{N_r} k_j q_j \tag{6.14d}$$

where N_r is the number of chemical reactions and ρ_g the gas density ($\mathrm{kg\,m^{-3}}$). The heat is assumed to be transmitted only by convection from the flame to the composite [26]. As the material temperature increases, it also loses heat by radiation. The heat flux on the hot face of the material is given by:

$$j_{q,hot} = h_{c,hot}(T_{bl} - T_{hot}) - \sigma \epsilon_{hot}(T_{hot}^4 - T_0^4) \tag{6.15}$$

where $h_{c,hot}$ is the convective heat transfer coefficient between the pilot flame and the solid surface ($\mathrm{W\,K^{-1}\,m^{-2}}$), σ the Stefan-Boltzmann constant ($\mathrm{W\,m^{-2}\,K^{-4}}$) and T_{hot} the hot face temperature. T_0 is the temperature of the surroundings and also the initial material temperature. The heat flux measurement with a heat gauge on the composite surface yields $h_{c,hot} = 108.5\ \mathrm{W\,m^{-2}\,K^{-1}}$ close to the stagnation point. In this work, the material emissivity is assumed to be 0.85 [210]. T_{bl} denotes the temperature immediately outside of the boundary layer in the gas phase close to the composite hot surface. The key concept of this coupled approach is to use different values of T_{bl} over time. At the beginning of the fire test, when the pyrolysate flow is not significant, T_{bl} is equal to the pilot flame temperature T_b. The effective temperature for the heat transfer across the boundary layer next to the sample surface T_{bl} is then taken as the highest temperature between T_b and the temperature computed by the counterflow diffusion flame sub-model T_{fl}. The radiative heat feedback from the pyrolysate

ignition is neglected, when compared to the convective heat transfer from the impinging flame. On the cold face, the material is assumed to be subjected to natural convection and radiation heat losses such that:

$$j_{q,cold} = -h_{c,cold}(T_{cold} - T_0) - \sigma\epsilon_{cold}(T_{cold}^4 - T_0^4) \tag{6.16}$$

where $h_{c,cold}$ and T_{cold} are respectively the convection coefficient and material temperature on the cold face. $h_{c,cold}$ is computed with the McAdams correlation for natural convection [211]. The initial density of the gaseous species in the solid, as well as the initial flux of gaseous species on each boundary, are set to zero. The mass flow rate $\dot{m}_g$ is computed by integrating Equation 6.14b:

$$\dot{m}_g = \int_{x_{cv}}^{L} \left(\sum_{i=1}^{N_g} \sum_{j=1}^{N_r} \theta_{ij} k_j - \frac{\partial \rho_g \bar{\phi}}{\partial t} \right) dx \tag{6.17}$$

where L is the composite thickness. By analogy with heat transfers, Robin boundary conditions are assumed on each face to compute the mass fraction $Y_{i,g}$ as:

$$j_Y = \frac{h_c}{\bar{c}_{pg}} \left(Y_{i,g}|_\infty - Y_{i,g} \right) \tag{6.18}$$

Finite Element Formulation

The system of coupled differential equations 6.14a to 6.14d is modeled with the Finite Element approach [143]. The temperature $T(x,t)$ and mass fractions $Y_{i,g}$ are discretized over the entire computational domain, divided into n elements. Each element is constituted of two nodes to which a value of T and $Y_{i,g}$ are assigned. In the following, a simple bar under a letter indicates a vector and a double bar a matrix. Between two nodes, the variables are approximated on each element Ω^e by a linear interpolation represented by an approximation function $\underline{\boldsymbol{\psi}}^e(x)$ as:

$$T(x,t) = \underline{\boldsymbol{\psi}}^e(x)\underline{\boldsymbol{T}}^e(t) = \sum_{j=1}^{2} \psi_j^e(x) T_j^e(t) \tag{6.19}$$

$$Y_{i,g}(x,t) = \underline{\boldsymbol{\psi}}^e(x)\underline{\boldsymbol{Y}}_{i,g}^e(t) = \sum_{j=1}^{2} \psi_j^e(x) Y_{ij,g}^e(t) \tag{6.20}$$

with:

$$\underline{\boldsymbol{\psi}}^e(x) = \begin{bmatrix} \dfrac{l-x}{l} & \dfrac{x}{l} \end{bmatrix} \tag{6.21a}$$

$$\frac{\partial \underline{\boldsymbol{\psi}}^e(x)}{\partial x} = \begin{bmatrix} \dfrac{-1}{l} & \dfrac{1}{l} \end{bmatrix} \tag{6.21b}$$

where l is the length of one element (m). The Bubnov-Galerkin method is applied to Equations 6.14c and 6.14d and all the terms are regrouped [143], providing the *finite element model*:

$$\underline{\underline{\boldsymbol{C}}}_Y^e \underline{\dot{\boldsymbol{Y}}}_{i,g}^e + (\underline{\underline{\boldsymbol{K}}}_{Y,1}^e + \underline{\underline{\boldsymbol{K}}}_{Y,2}^e)\underline{\boldsymbol{Y}}_{i,g}^e = \underline{\boldsymbol{F}}_{Y,1}^e - \underline{\boldsymbol{F}}_{Y,2}^e \tag{6.22}$$

With:

$$\underline{\underline{\boldsymbol{C}}}_Y^e = \int_0^l \underline{\boldsymbol{\psi}}^{eT} \bar{\phi}^e \rho_g^e \underline{\boldsymbol{\psi}}^e \, dx \tag{6.23a}$$

$$\underline{\underline{\boldsymbol{K}}}_{Y,1}^e = \int_0^l \underline{\boldsymbol{\psi}}^{eT} \dot{m}_g^e \frac{\partial \underline{\boldsymbol{\psi}}^e}{\partial x} \, dx \tag{6.23b}$$

$$\underline{\underline{\boldsymbol{K}}}_{Y,2}^e = \int_0^l \frac{\partial \underline{\boldsymbol{\psi}}^{eT}}{\partial x} \bar{\phi}^e \rho_g^e D^e \frac{\partial \underline{\boldsymbol{\psi}}^e}{\partial x} \, dx \tag{6.23c}$$

$$\underline{\boldsymbol{F}}_{Y,1}^e = \begin{bmatrix} -j_{Y,0} \\ j_{Y,l} \end{bmatrix} \tag{6.23d}$$

$$\underline{\boldsymbol{F}}_{Y,2}^e = \int_0^l \underline{\boldsymbol{\psi}}^{eT} \sum_{j=1}^{N_r} \theta_{ij} k_j \, dx \tag{6.23e}$$

$$\underline{\underline{\boldsymbol{C}}}_T^e \underline{\dot{\boldsymbol{T}}}^e + (\underline{\underline{\boldsymbol{K}}}_{T,1}^e + \underline{\underline{\boldsymbol{K}}}_{T,2}^e)\underline{\boldsymbol{T}}^e = \underline{\boldsymbol{F}}_{T,1}^e - \underline{\boldsymbol{F}}_{T,2}^e \tag{6.24}$$

With:

$$\underline{\underline{\boldsymbol{C}}}_T^e = \int_0^l \underline{\boldsymbol{\psi}}^{eT} \bar{\rho}^e \bar{c}_p^e \underline{\boldsymbol{\psi}}^e \, dx \tag{6.25a}$$

$$\underline{\underline{\boldsymbol{K}}}_{T,1}^e = \int_0^l \underline{\boldsymbol{\psi}}^{eT} \dot{m}_g^e \bar{c}_{p,g}^e \frac{\partial \underline{\boldsymbol{\psi}}^e}{\partial x} \, dx \tag{6.25b}$$

$$\underline{\underline{\boldsymbol{K}}}_{T,2}^e = \int_0^l \frac{\partial \underline{\boldsymbol{\psi}}^{eT}}{\partial x} \bar{\lambda}^e \frac{\partial \underline{\boldsymbol{\psi}}^e}{\partial x} \, dx \tag{6.25c}$$

$$\underline{\boldsymbol{F}}_{T,1}^e = \begin{bmatrix} -j_{q,0} \\ j_{q,l} \end{bmatrix} \tag{6.25d}$$

$$\underline{\boldsymbol{F}}_{T,2}^e = \int_0^l \underline{\boldsymbol{\psi}}^{eT} \sum_{j=1}^{N_r} k_j q_j \, dx \tag{6.25e}$$

Finally, the elemental matrices are assembled to calculate the global matrices [143]. It is worth noting that the element matrices $\underline{\underline{\boldsymbol{C}}}$, $\underline{\underline{\boldsymbol{K}}}$ and $\underline{\boldsymbol{F}}$ depend on the element properties, which in turn depend most of time on the variables Y and T. Therefore, their terms are computed with estimated variables and the convergence is investigated in an iterative process with the fixed point method.

The duration of the fire test is divided into m discrete time steps and the duration of an interval is $\Delta t = t^{n+1} - t^n$, where n indicates the time step number. The variation of T in

one time step is described by the Crank-Nicholson approach [143]:

$$\frac{\partial \underline{\boldsymbol{T}}^a}{\partial t} = \frac{\underline{\boldsymbol{T}}^{n+1} - \underline{\boldsymbol{T}}^n}{\Delta t} \tag{6.26a}$$

$$\underline{\boldsymbol{T}}^a = (1-\Theta)\underline{\boldsymbol{T}}^n + \Theta \underline{\boldsymbol{T}}^{n+1} \tag{6.26b}$$

where the superscript a denotes the approximation of T used to compute the element matrices and $\Theta = 0.5$. A similar procedure is used to compute the temporal variation of $Y_{i,g}$. Finally, Figure 6.4 represents the code algorithm.

6.5 Material characterization

An aerospace-grade carbon-fiber epoxy pre-preg (procured from Solvay - formerly CYTEC - Tulsa, OK, USA) is selected as the base material to validate the proposed approach. This material system (carbon reinforcement: HTS40 E13 3K PW) is based on an Out-of-Autoclave (OOA) toughened epoxy. An 8-ply quasi-isotropic laminate $[0°, +45°, 0°, -45°]_S$ is prepared following the manufacturer's recommended cure and post-cure cycles.

6.5.1 Physical properties

Both solid and gaseous species co-exist in the sample exposed to fire, as the degradation degree progresses. The different phases making up the material are referred to here by the index m for the matrix, f for the fibers, ch for the char and g for the gaseous species (pyrolysis and oxidation products, air, combustion exhaust gases, etc).
At least two samples of the same material are required for a full characterization of the phases: a virgin composite sample (containing only matrix and fibers) and a fully pyrolyzed composite sample (containing only char and fibers). To prepare the fully pyrolysed sample, a virgin composite is placed into a furnace tube (Carbolite Gero STF) with an inert argon flow. The sample is then heated at 3 K/min until reaching 1300 K, then kept at a constant temperature for one hour. The mass of the samples is reduced by $26.5\% \pm 0.43\%$ after pyrolyzation. With this method, the fully pyrolyzed sample contains only non-oxidized fibers and char. The density of a virgin sample is measured using the Archimedean principle at 297.65 K (24.5 °C). This method yields a density for the virgin composite of $\rho_v = 1460.27 \pm 1.5\%$ kg m^{-3}, where the index v refers to a virgin sample. The density of the pyrolyzed composite is computed using the mass loss previously measured and assuming constant volume, yielding $\rho_p = 1073.3$ kg m^{-3}, where the index p refers to a pyrolyzed sample. For each sample, the composite density is

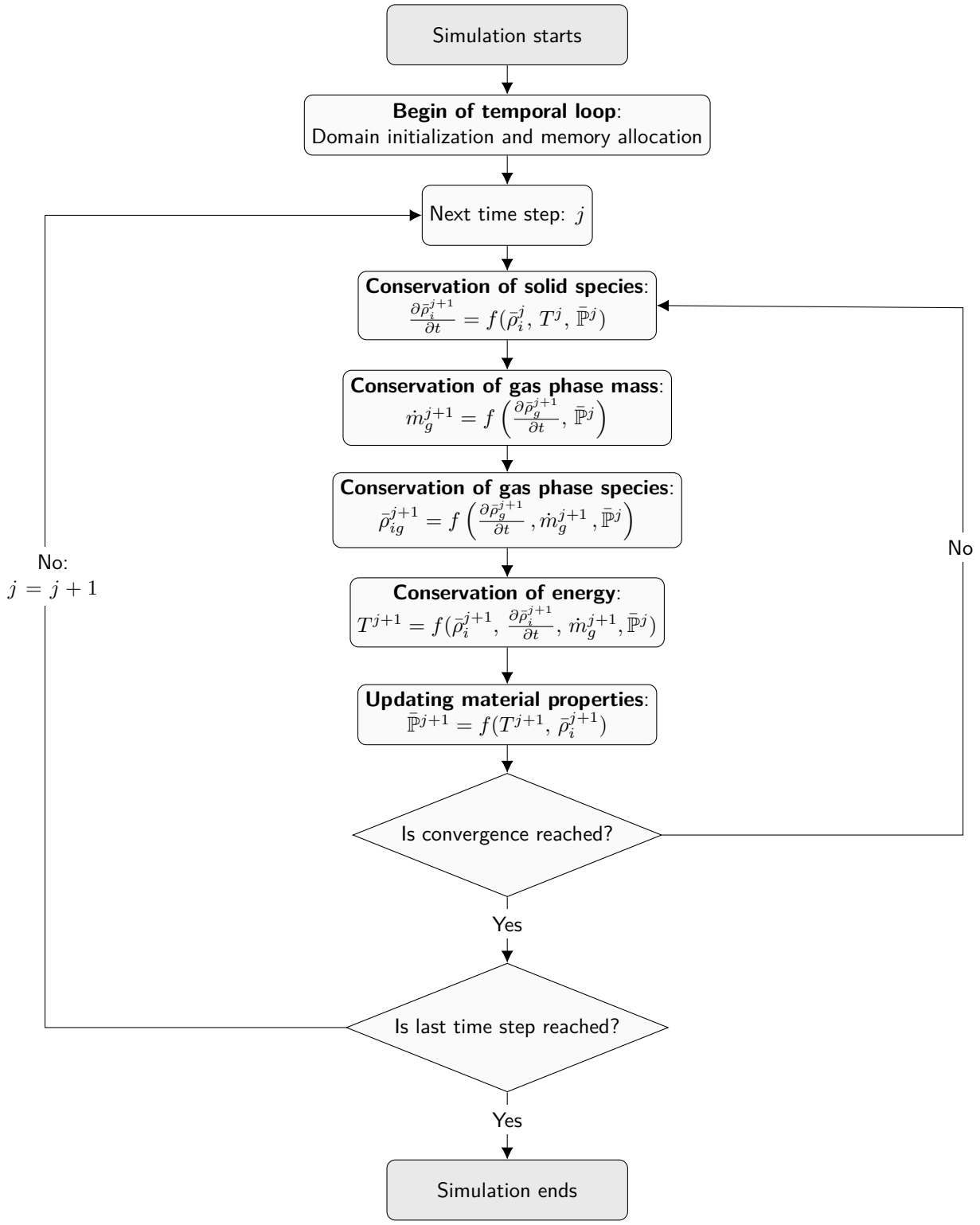

Figure 6.4 Algorithm representing the simulation steps.

expressed as a function of the phase densities and volume fraction as:

$$\bar{\rho}_v = X_m\rho_m + X_f\rho_f = \bar{\rho}_m + \bar{\rho}_f \quad (6.27)$$

$$\bar{\rho}_p = X_m[\phi_{ch}\rho_g + (1-\phi_{ch})\rho_{ch}] + X_f\rho_f \quad (6.28)$$

Considering the matrix and fiber densities provided by the material supplier and neglecting the porosity of the virgin composite, the matrix and fiber volume fractions can be obtained through Equation 6.27 and are listed in Table 6.3. Similarly, Equation 6.28 can be used to estimate the porosity if ρ_{ch} is known, which is crucial for calculating the thermal conductivity. However, the char density is challenging to measure independently. For this reason, the char density of another epoxy resin (M21, Hexcel) measured by Biasi [52] is used in the following to compute ϕ_{ch}.

6.5.2 Thermal properties

Heat capacity

Figure 6.5 represents the heat capacities of the virgin and pyrolyzed samples measured by DSC (NETZSCH DSC 204F1 Phoenix) from 260 to 475 K. The heat flow of the samples is compared to that of a sapphire sample with similar mass and diameter, under inert atmosphere and at a heating rate of 20 $\mathrm{K\,min^{-1}}$. The composite heat capacity is computed with a mixture rule weighed by the mass fraction of each phase. The determination of the heat capacity of each sub-phase from the global measurement requires the knowledge of thermal properties for at least one of the phases, for instance the carbon fibers which are common to both samples. To the best of our knowledge, the material system's reinforcement (HTS40 fiber) used in this work lacks publicly-available thermal properties. However, other polyacyrlonitrile (PAN)-based commercial fibers have similar tensile strength and modulus. The AS4 carbon fibers which have been characterized between 280 and 680 K by other re-

Phase	ρ_i ($\mathrm{kg\,m^{-3}}$)	Virgin sample		Pyrolyzed sample	
		$X_{i,v}$ ($\mathrm{m^3/m^3}$)	$Y_{i,v}$ (kg/kg)	$X_{i,p}$ ($\mathrm{m^3/m^3}$)	$Y_{i,p}$ (kg/kg)
Matrix	1180 [212]	0.5168	0.4176	-	-
Fibers	1760 [212]	0.4832	0.5824	0.4832	0.7924
Char	1488.7 [52]	-	-	0.1494	0.2073
Pyrolysates	1.017 [52]	-	-	0.3674	3.480×10^{-4}

Table 6.3 Physical properties of the carbon/epoxy composite.

searchers [213], are used in this work. With these properties for the HTS40 carbon fibers, the matrix and char heat capacities can be determined from the DSC measurements carried out. Results and range of validity are shown in Table 6.4.

Thermal conductivity

Figure 6.6 represents the material thermal diffusivity measured in vacuum with a Linseis XFA 600 system. The temperature programs ranged from 300 to 500 K, and 300 to 780 K for virgin and fully pyrolyzed samples, respectively. The thermal diffusivity of the fully pyrolyzed sample is lower than that of the virgin material, most likely because of the high level of porosity that hinders heat transfer.
The material conductivity is subsequently computed within an elementary control volume containing matrix, fibers, char and gas in three steps. First, the conductivity of the porous char layer $\lambda_{ch,porous}$ is computed as a function of the char and gas conductivities with the Maxwell's model [163]:

$$\lambda_{ch,porous} = \lambda_{ch}\left[\frac{\lambda_g + 2\lambda_{ch} + 2\phi_{ch}(\lambda_g - \lambda_{ch})}{\lambda_g + 2\lambda_{ch} - \phi_{ch}(\lambda_g - \lambda_{ch})}\right] \tag{6.29}$$

Then, the conductivity of the degraded matrix is computed as a function of the porous char and matrix conductivities with a rule of mixture following Reuss model, as the char is first formed on the hot side of the control volume. A similar method is used to compute the conductivity of the oxidized fibers as a function of the fibers and gas conductivities as:

$$\lambda_{m,degr} = \left(\frac{X_m}{\lambda_m} + \frac{X_{ch,porous}}{\lambda_{ch,porous}}\right)^{-1} \tag{6.30}$$

$$\lambda_{f,degr} = \left(\frac{X_f}{\lambda_f} + \frac{\phi_f}{\lambda_g}\right)^{-1} \tag{6.31}$$

Finally, the conductivity of the complete composite is computed as a function of the degraded matrix and fibers conductivities with the Clayton model [164]:

$$\bar{\lambda} = \frac{\lambda_{m,degr}}{4}\left[\sqrt{(1-X_f)^2\left(\frac{\lambda_{f,degr}}{\lambda_{m,degr}} - 1\right)^2 + \frac{4\lambda_{f,degr}}{\lambda_{m,degr}}} - (1-X_f)\left(\frac{\lambda_{f,degr}}{\lambda_{m,degr}} - 1\right)\right]^2 \tag{6.32}$$

With a value for the thermal conductivity of the carbon fibers extracted from the literature, the thermal properties of all the phases are presented in Table 6.4. The radial thermal conductivity of the carbon fibers λ_f can be calculated from the axial one λ_{fa} with the orthotropy ratio $F = \lambda_{fa}/\lambda_f$ [214]. An orthotropy ratio of 6.10 has been estimated from the

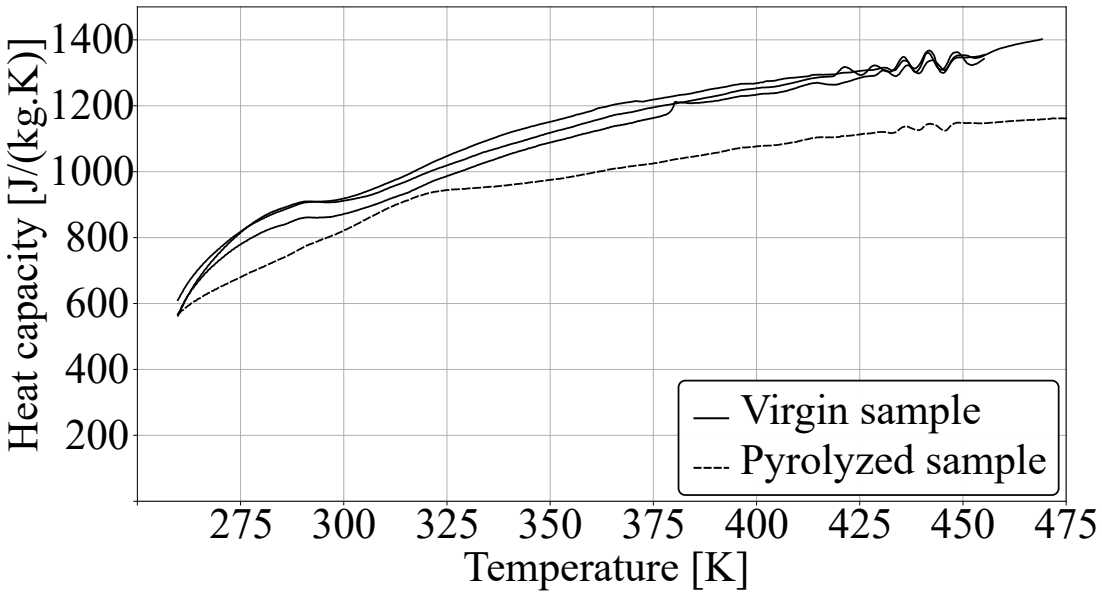

Figure 6.5 Heat capacity of the virgin and pyrolyzed carbon/epoxy obtained by DSC.

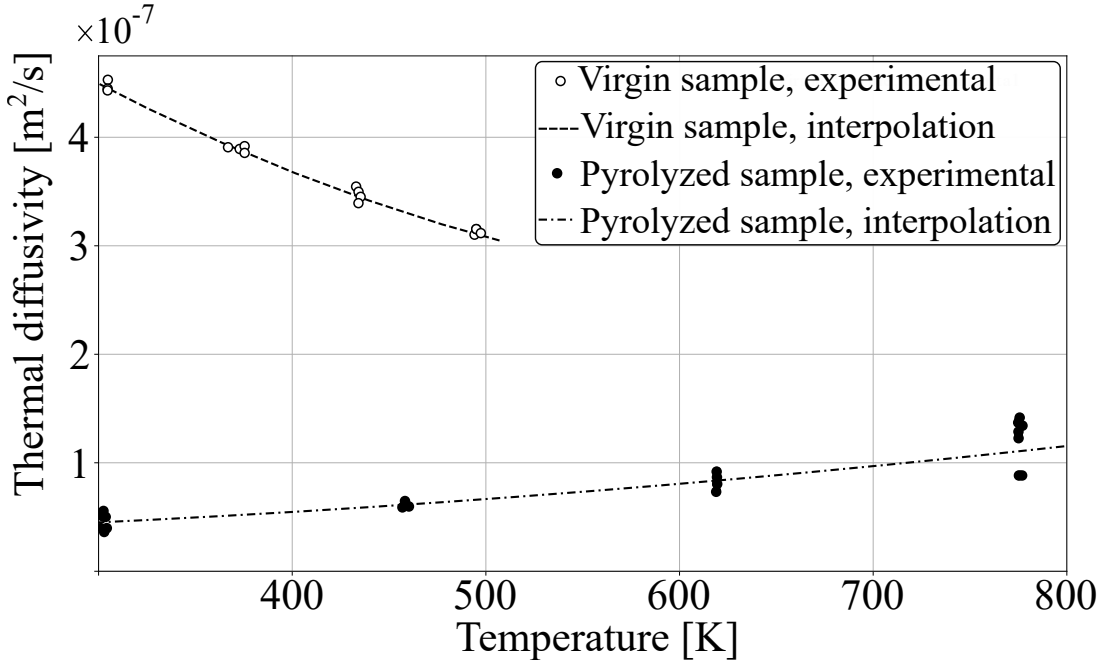

Figure 6.6 Thermal diffusivity of the virgin and pyrolyzed carbon/epoxy obtained by XFA. The dashed lines are polynomial interpolations.

properties of a AS4/3501-6 carbon/epoxy composite [214], similar to the material used here.

6.5.3 Chemical properties

The kinetic triplet (A_j, E_j, n_j) describing reaction j in a thermal degradation model can be inferred experimentally from TGA measurements [47]. Carbon/epoxy samples are exposed to three different heating rates, i.e. 5, 10, and 25 $\mathrm{K\,min^{-1}}$, under inert (N_2) and oxidative atmospheres. The pilot flame releases several species, such as O_2, H_2O, CO_2, CO, O, OH that are likely to oxidize the carbon species contained in the composite. However, the exact composition of the exhaust gases from the pilot flame presented in Table 6.2 cannot be replicated in TGA experiments. For this reason, a standard method based on oxidation in air has been preferred in this work, following the procedures commonly used in the literature.
Isoconversional methods are used to obtain the values of the kinetic triplet for matrix pyrolysis, char oxidation and fiber oxidation, assuming single-step degradation [215]. The parameters describing the chemical degradation of the material are reported in Table 6.5, as well as the char yield θ_j ($\mathrm{kg\,kg^{-1}}$), that represents the quantity of char produced per kilogram of matrix pyrolyzed. Finally, the heat of reaction measured in [128] for an epoxy resin and in [52] for char and carbon fiber oxidation is used to quantify the heat absorbed or released by the material degradation.
The outgassing from char and carbon fibers oxidation is assumed to be composed only of CO_2. The modeling of pyrolysate ignition being strongly influenced by their composition, more research is needed to measure quantitatively the composition of pyrolysate exhaust gases as a function of the material temperature and/or degradation degree.

6.6 Results and discussions

6.6.1 Gas phase reactions and heat feedback

The predictions of the model for the temporal evolution of the heat flux received by the material, the pyrolysate mass flow rate, the composite hot face temperature and the boundary layer temperature are shown in Figure 6.7. To assess the effect of pyrolysate ignition, two predictions are compared: a case with ignition, modeled with the coupled architecture introduced in Section 6.4.1, and a case without ignition, modeled with the pyrolysis model only (no coupling with Cantera). According to the results of Figure 6.7b), matrix pyrolysis and emissions of pyrolysates from the hot face starts after 8 seconds of fire exposure. Then, the pyrolysate mass flow increases with the matrix degradation rate, until a critical value is

Phase	$c_{p,i}$ ($\mathrm{J\,K^{-1}\,kg^{-1}}$)	Range (K)
Matrix	$-5156 + 30.68T$ $-0.0442T^2 + 2.071 \times 10^{-5}T^3$	260-475
Fibers	$2367 - 8.212T$ $+0.01615T^2 - 8.529 \times 10^{-6}T^3$	272-672 [213]
Char	$-1.219 \times 10^4 + 66.42T$ $-0.106T^2 + 5.302 \times 10^{-5}T^3$	260-475
Pyrolysates	$1972.5 + 1.45T$ $+9.59 \times 10^{-4}T^2 + 3.47 \times 10^{-7}T^3$	300-1000 [52]
Phase	λ_i ($\mathrm{W\,m^{-1}\,K^{-1}}$)	Range (K)
Matrix	$-1.1 + 9.084 \times 10^{-3}T$ $-1.838 \times 10^{-5}T^2 + 1.159 \times 10^{-8}T^3$	260-475
Fibers	$0.5638 + 0.002561T$	272-672 [213]
Char	$-0.08318 + 6.528 \times 10^{-4}T$ $-9.002 \times 10^{-7}T^2 + 7.662 \times 10^{-10}T^3$	300-800
Pyrolysates	$2.88 \times 10^{-2} + 7.74 \times 10^{-5}T$	300-1000 [52]

Table 6.4 Thermal properties of the carbon/epoxy composite determined from DSC and XFA experiments. Where a reference is provided, values were extracted from the literature for similar carbon fiber/epoxy composites.

Reaction	E_j ($\mathrm{kJ\,mol^{-1}}$)	A_j ($\mathrm{s^{-1}}$)	n_j (-)	θ_j ($\mathrm{kg\,kg^{-1}}$)	q_j ($\mathrm{kJ\,g^{-1}}$)
Pyrolysis	193	2.20×10^{13}	3.03	0.3678	-2.5 [128]
Char oxidation	112	1.7×10^4	1.76	0	3.43 [52]
Fiber oxidation	260	4.93×10^{10}	4.83	0	8.94 [52]

Table 6.5 Reaction mechanism of a carbon/epoxy composite. Data inferred from TGA with different heating rates $5, 10, 25\ \mathrm{K\,min^{-1}}$.

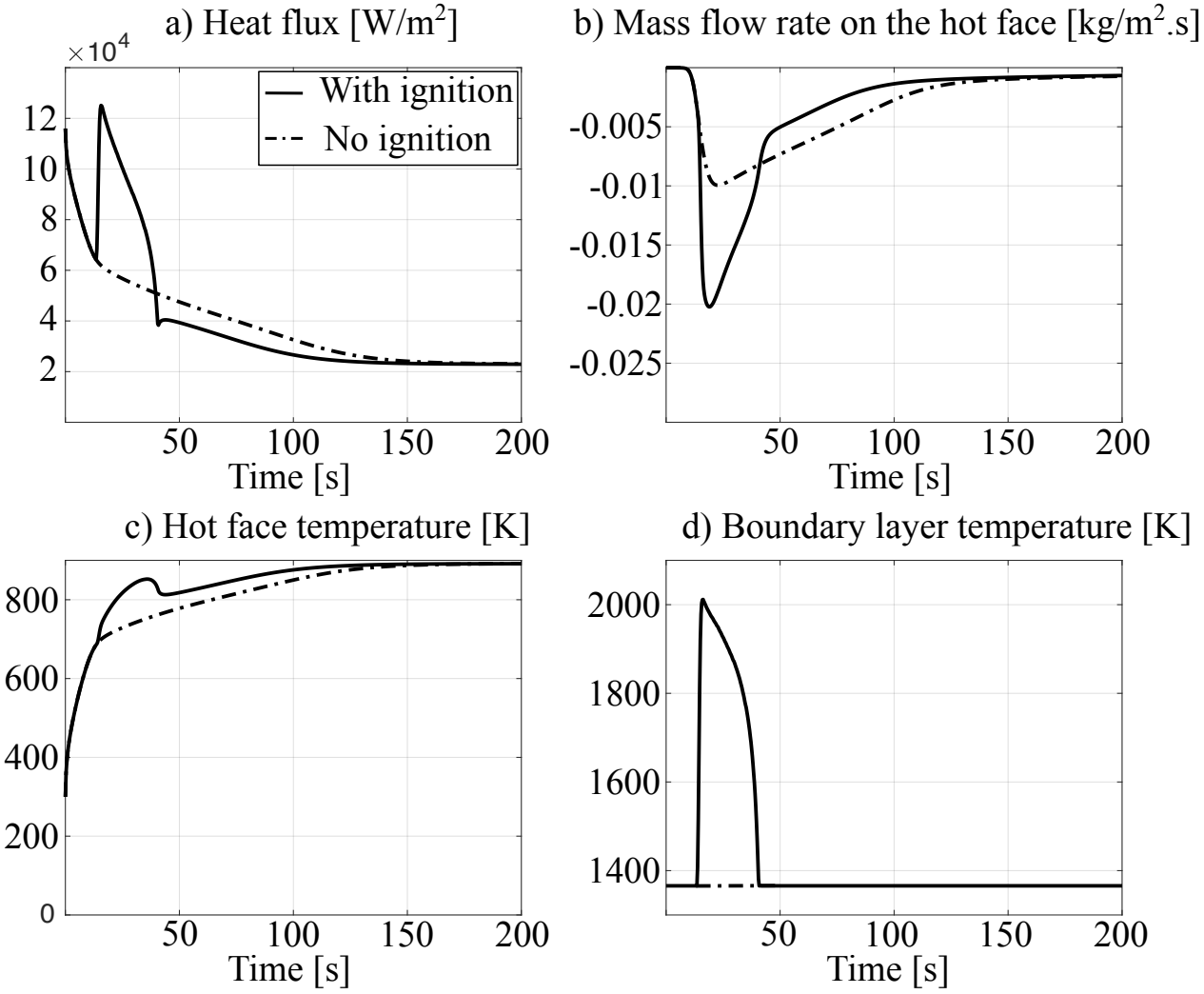

Figure 6.7 Temporal evolution of a) the heat flux received by the material $j_{q,hot}$, b) the pyrolysate mass flow rate $\dot{m}_{g,pyr}$, c) the hot face temperature of the material $T_{g,pyr}$, d) and the boundary layer temperature T_{bl}.

reached corresponding to the ignition conditions in the boundary layer. After a flame exposure time of 14.1 s, the model predicts a boundary layer temperature that exceeds the pilot flame temperature. This threshold is selected as the criterion defining outgassing ignition, consistent with experimental observations of flames onset on the hot face of the composite after 9 to 11 s of fire exposure in our small-scale tests. After pyrolysate ignition, the heat flux received by the material approximately doubles, increasing the material temperature and further promoting its degradation. At that point, a self-sustained combustion could be established; however, the formation of a porous layer of char mixed with carbon fiber and the endothermicity of the pyrolysis reduce greatly the heat transfer to the matrix remaining deeper in the sample. The pyrolysate mass flow rate starts to decrease, after a flame exposure time of approximately 19 s, causing finally the flame extinction at approximately 41 s. The positive heat feedback from pyrolysate ignition is compensated after extinction, when compared to a case without ignition, by higher radiative heat losses and reduced convective heat transfer to the sample, again from the higher surface temperature. After 200 s, the hot face temperature is the same with and without pyrolysate ignition.

6.6.2 Solid phase degradation

Figure 6.8 shows the numerically predicted and experimentally measured evolution of the composite cold face temperature over a 10 minutes fire test, and Figure 6.9 presents the evolution calculated by our model for the composite temperature, density, porosity and diffusivity throughout its thickness, for different fire exposure times. For comparison purposes, a case without ignition has also been modeled and is shown on Figure 6.8. The initial exposure of the material to the flame, *i.e* between 0 and 11 s on Figure 6.8, corresponds to the heating of the material purely by conductive heat transfer within the solid phase, prior to thermal degradation onset. Figure 6.9b shows that the matrix starts to degrade significantly at $t = 11$ s and the mass loss is very rapid because of the high reactivity of the epoxy resin. As seen on Figure 6.7b, most of the pyrolysates are emitted between 14 and 40 s, leading to material ignition. Model predictions show that the pyrolysis is complete after approximately 100 s, with the maximum temperature $T = 800$ K reached later, at $t = 166$ s. The temperature profile tends toward a steady state, slowly decreasing until the end of the certification test. This slow decrease can be explained by the reduction of the material thermal diffusivity because the carbon fiber and char oxidation increases the material porosity, as represented on Figure 6.9c and d. This effect is especially important on the hot face of the material where the temperature is maximum, reducing the heat flux received from the flame.

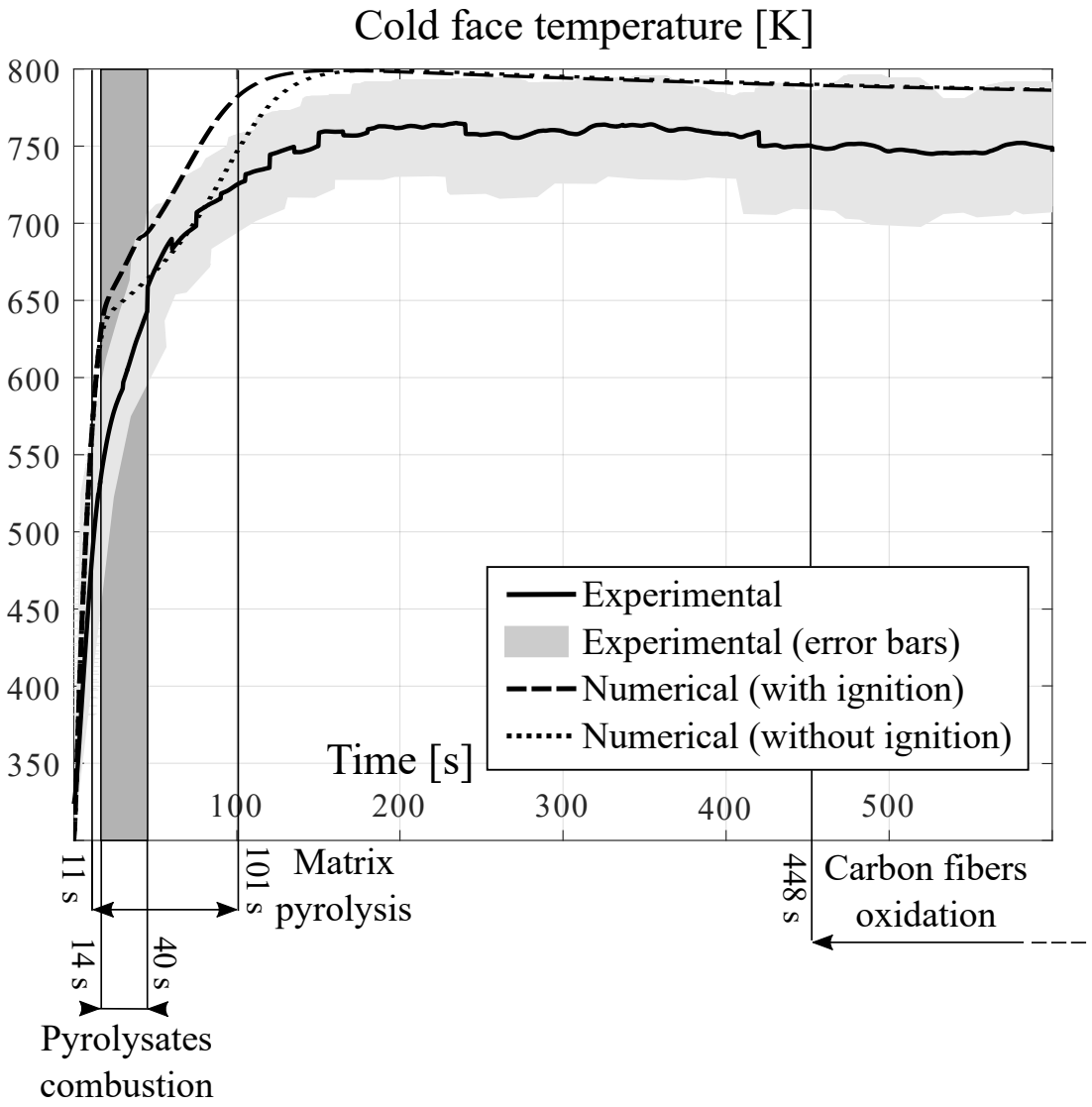

Figure 6.8 Numerical and experimental evolution over time of the composite back face temperature. The light grey zone shows the 95% Confidence Interval considering Student's t-distribution of experimental data. The dark grey zone represents the duration of pyrolysate combustion.

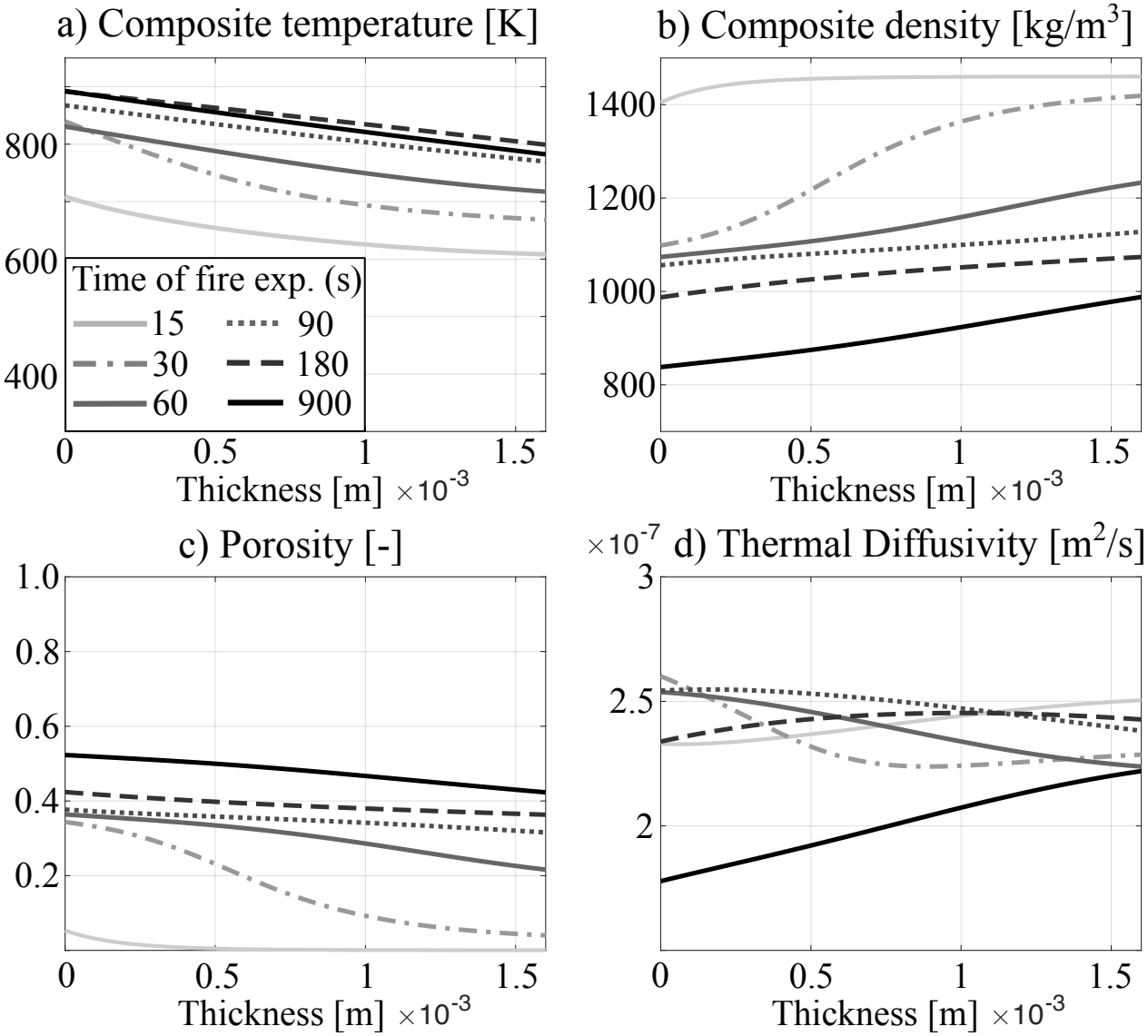

Figure 6.9 Prediction of the evolution over the thickness of the a) composite temperature, b) density, c) porosity and d) thermal diffusivity after 15, 30, 60, 90, 180 and 900 s of fire exposure.

6.6.3 Sensitivity Analysis

A sensitivity analysis is done to investigate the relative influence of input parameters variations on the pyrolysate combustion. In the solid phase, the material thermal diffusivity ($m^2\,s^{-1}$), the kinetic triplet (E, A, n) and heat of reaction q describing the material pyrolysis have been varied by $\pm 30\%$. In the gas phase, the burner mass flow rate $\dot{m}_b$, mole fraction of O_2 in the exhaust gases from the pilot flame and mole fraction of fuel contained in the pyrolysate (H_2 and C_2H_2) are also varied by $\pm 30\%$. The relative proportions of the other species of Table 6.1 and 6.2 are kept constant. The variations of the time-to-ignition, maximum boundary layer temperature and maximum heat flux received by the material are reported in Figure 6.10.

In the solid phase, results show that the material thermal diffusivity has a relatively weak influence on the model response. A reduction of $\lambda/(\rho C_p)$ lessens the amount of heat transmitted to the material and therefore delays the onset of matrix pyrolysis, which explains why the time-to-ignition is slightly more important ($+4.25\%$) when the diffusivity decreases. The effect on the boundary layer temperature is even more limited (-1.65%) and is bound to the hypothesis of local thermal equilibrium, which implies that the pyrolysate temperature is equal to the material hot face temperature. However, it appears that pyrolysate combustion is mainly driven by the activation energy (E) of the matrix pyrolysis. This parameter represents the amount of heat necessary to degrade the material and is therefore directly associated to the production of pyrolysates. A variation of $+30\%$ of E can totally prevent the ignition, and a deviation of -30% decreases the time-to-ignition by 75%. The effect on the boundary layer temperature and heat flux is less important, although still dominant when compared to the influence of other input parameters ($+10\%$ and $+26\%$, respectively). Fluctuations in the char yield also have an impact on the three parameters describing the pyrolysate combustion, as it directly influences the quantity of pyrolysates produced by the pyrolysis. Therefore, a diminution of the char yield increases the mass flow rate of pyrolysates, reducing the time-to-ignition while increasing the heat feedback. This effect is however quite limited when compared to the impact of activation energy and gas-phase reactions.

The sensitivity analysis for the gas-phase reactions is especially valuable considering the high uncertainty in the model input data. A diminution of 30% of the fraction of fuel in pyrolysates and oxidizer in the pilot flame exhaust changes the time-to-ignition by $+10.6\%$ and -2.12%, respectively. These observations can be explained by considering that at the beginning of pyrolysis, the quantity of pyrolysate emitted in the environment is very low when compared to the quantity of oxidizer available. Therefore, a reduction of the mole fraction of oxidizer or an augmentation of the mole fraction of fuel helps the mixture to reach its lower flammability limit. An increase of the fuel and oxidizer mole fractions promotes the heat feedback in

similar proportions (+9%). An augmentation of the mass flow rate of exhaust gases increases the strain rate in the gas phase and therefore delays the time-to-ignition (+2.12%), although its effect is modest for all three parameters when compared to variations in pyrolysates or exhaust gases composition.

6.6.4 Discussions

The model slightly overestimates the material temperature during the fire test compared to experimental data, particularly during matrix pyrolysis. The origin of this error could not be clearly identified, because of the large number of processes interacting during pyrolysis. One likely explanation is however the swelling and delamination of the material, which are not considered in the model but observed in the experiments. The delamination process is a deconsolidation phenomenon of the fibrous structure, which is caused by the softening and subsequent degradation of the matrix as well as the associated gas migration [65]. Moreover, the fiber crimp of woven architectures plays an important role in this process as it promotes spring-out. The presence of additional internal gas layers not considered in the model reduces again the heat transfer to the composite, which could explain the error observed during the fire test. However, it is worth noting that swelling is restrained in our case by the clamping of the sample on each extremity. The overestimation reaches 50 K at $t = 115$ s, which corresponds to an error of 6.7%, and increases at the later stages of the fire test. A better estimation of the heat released or absorbed by pyrolysis could also help to improve the agreement. Nevertheless, the qualitative agreement remains very good as the time to reach the maximum temperature and the overall shape of the curve are correctly predicted.

The temperature variation after the maximum has been reached at $t \approx 200$ s on Figure 6.8 reveals that oxidation reactions are not negligible. Oxidation reactions are slow, when compared to other processes such as pyrolysis and swelling, which are completed once the steady state is reached. Therefore, the decrease of temperature observed experimentally on the cold face is likely to be due to a reduction of the thermal diffusivity on the hot face, from carbon fiber and char oxidation that increases porosity. However, oxidation reactions are most of the time neglected in previous models found in the literature [35, 58].

The error in temperature prediction with experimental data increases as the steady state is approached after 200 s, until reaching an overestimation of approximately 35 K at the end of the fire test (4.7% of the total temperature increase). This increased error is likely due to an underestimation of the carbon fiber oxidation. As a reminder, the composite oxidation has been characterized by TGA in an oxidative (air) atmosphere, containing approximately 20% of oxygen. However, the combustion exhaust gases of the pilot flame contain only 12% oxygen, but also contain H_2O, CO_2 and combustion radicals, notably OH, that can have a

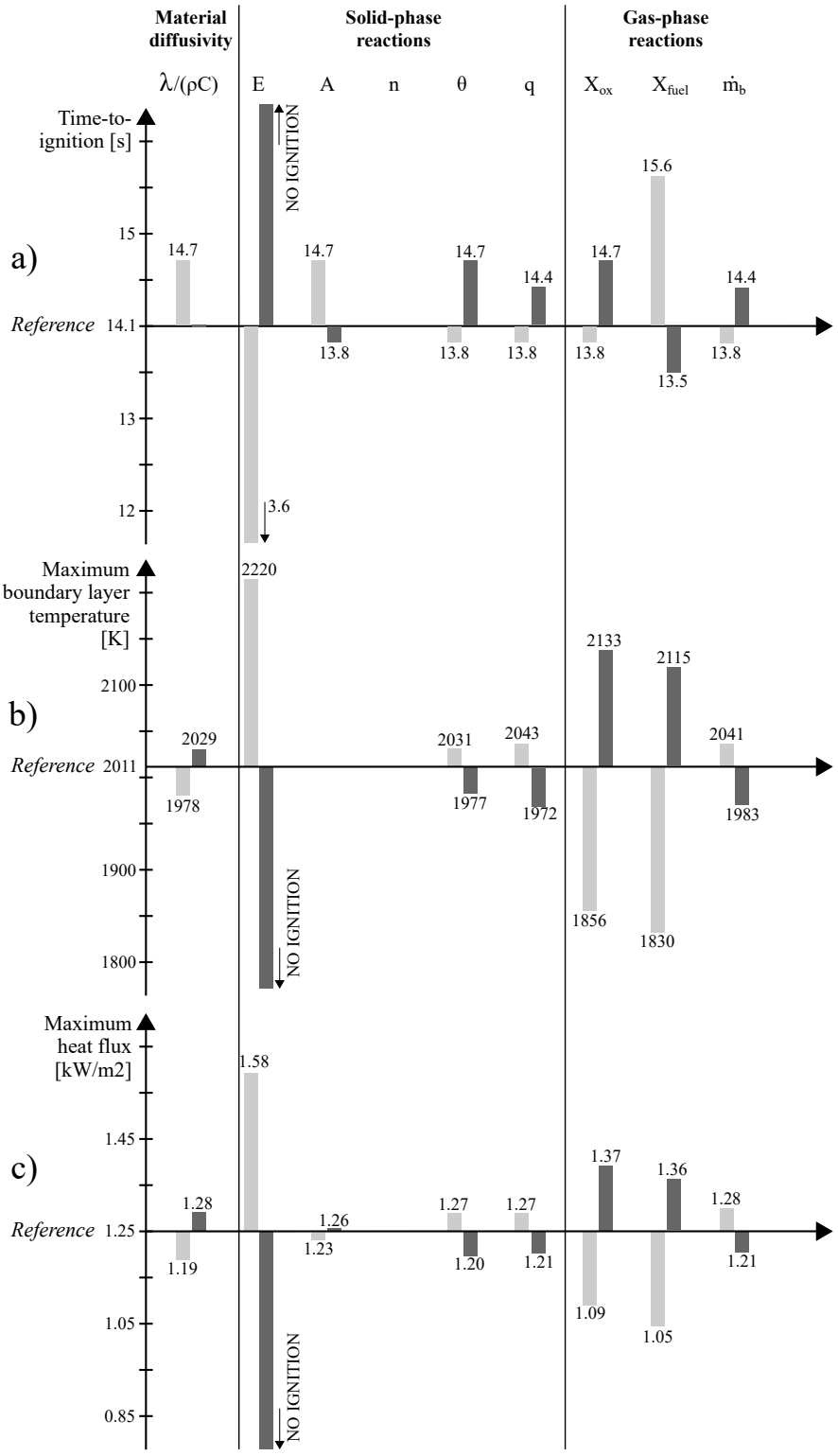

Figure 6.10 Effect of variations in input parameters ((▭): −30%, (▬): +30%) to predict a) the time-to-ignition of pyrolysates, b) the maximum boundary layer temperature and c) the maximum heat feedback from pyrolysate combustion. The time-to-ignition has been predicted with a time-step of 0.3 s.

major impact on solid carbon oxidation [71]. The effect of such species is not considered in this work. The kinetic triplets characterizing graphite oxidation by these species have already been measured in the literature and could be adapted to epoxy-derived char and carbon fibers in a future work [66]. Results show that modeling the composite under fire test conditions using air flow-derived kinetic triplets is inaccurate, although it can provide a reasonable baseline in the absence of more appropriate source data.

It is also worth noting that the gases emitted by the fire test are evacuated by a ventilation system that can contribute to cooling the composite backface, as represented on Figure 6.1. This exhaust provides an additional weak forced convection term that has not been considered in the simulation results presented, in which the sample is cooled by natural convection only. Simulations with forced convection on the cold face have shown that an air velocity of 1 $\mathrm{m\,s^{-1}}$ reduces the temperature overestimation at the end of the test to approximately 26 K, instead of 35 K, showing that the ventilation has a limited influence on the composite temperature.

A comparison between modeling with and without ignition reveals that ignition momentarily increases the material backface temperature, but this effect has vanished after 150 s. Although including pyrolysate ignition does not significantly change the backside temperature evolution on the long term, the heat feedback it yields to the sample is significant and the diffusion flame modeling approach implemented here provides a novel way to quantify it. During the time pyrolysate outgassing burns at the surface of the sample, the heat flux it receives approximately doubles, as shown in Figure 6.7a, an effect that should be considered when the temporal evolution of material properties or flame spread over the sample surface are of interest.

The comparison between numerical and experimental data reveals that this coupled approach is able to predict the time-to-ignition of a sample exposed to fire with good accuracy, without having to use optimization of material thermal properties against experimental data or empirical formula. The time-to-ignition is slightly overestimated (14 s numerically versus 10 s experimentally), but this modeling is performed close to the stagnation point, where the strain rate can be very important because of the high radial velocity gradient of the exhaust gases from the burner. This could delay or even prevent the pyrolysate ignition [59]. The non-ignited pyrolysate could thus be advected away and may ignite at some radial distance away from the stagnation point, in locations with a lower strain rate and higher fuel concentration. A two-dimensional modeling of the same physical processes in both gas and solid phases would be required to investigate this phenomena.

However, the pyrolysate composition is considered constant during the fire test but in reality, the outgasses composition is temperature-dependent and most of the combustible gases

are released at a specific pyrolysis temperature. This could also influence the prediction of the time-to-ignition. An independent modeling of each gaseous species with temperature-dependent source terms would allow to model a variable pyrolysate composition at the surface of the composite, providing more accurate results. However, the effect of such a modeling is expected to be quite limited as the pyrolysis is not homogeneous along the material thickness because of temperature gradients. Nevertheless, the coupled modeling approach presented here, with detailed chemistry in the gas phase used to model ignition of the pyrolysate and heat feedback to the sample is comprehensive and can be extended by for instance variable outgassing composition or more detailed pyrolysis models in the solid phase.
Results from the sensitivity analysis show that pyrolysate combustion is mainly controlled by the activation energy of the matrix pyrolysis. However, variations of the composition of pyrolysates or exhaust gases from the pilot flame also have a significant effect on the gas-phase reactions. In particular, fluctuations in the mole fraction of oxygen in the exhaust gases affect both the time-to-ignition and heat feedback from pyrolysates combustion. Yet, the fraction of oxidizer contained in the flame exhaust is directly related to the burner operation parameters, such as the type of fuel and calibration method.

6.7 Conclusion

Pyrolysis models are used in the industry to predict the outcome of fire certification tests. Our results revealed that these predictive tools are very sensitive to the ignition of the pyrolysates emitted by the matrix degradation, which provides an additional and non-controlled heat feedback at the surface of the material. Most of the time, the pyrolysate ignition is modeled with empirical parameters specific to each material and fire test conditions, or with simplified chemical kinetics that are not representative of the complexity of the processes at play. There is therefore a need to develop new theoretical approaches able to model the pyrolysate ignition regardless of the material or fire test conditions.
This research presents a new numerical approach to model the heat feedback and time-to-ignition at the surface of a composite exposed to fire test, that does not require empirical parameters specific to each test or material. This method relies on the coupling of several sub-models accounting for the thermal, chemical and physical processes in both gas and solid phases. The approach is implemented and compared against experimental data for a carbon fiber epoxy matrix composite, whose thermal, physical and chemical properties have been measured experimentally through simple and standardized experiments (Archimedean principle, DSC, XFA and TGA). The comparison between modeling results and experimental data obtained in a small-scale fire test facility reproducing the conditions of certification

demonstrates the ability of the model to predict the composite backface temperature with a maximal error of 6.7% (50 K) in realistic test conditions. In particular, the prediction of the time for increased heat release in the boundary layer due to pyrolysate ignition (14s in the model) is consistent with the time-to-ignition measured experimentally in the fire test ($9-11$s). Results also shows that the heat flux received by the material approximately doubles just after the onset of pyrolysate combustion, although such ignition is often neglected in the literature. However, pyrolysate ignition has no significant influence on the composite thermal degradation if the fire test lasts more than 200 s. A sensitivity analysis showed that uncertainty in the pyrolysate combustion is mainly affected by changes in the activation energy of the matrix pyrolysis, which indicates that this parameter must be thoroughly measured to ensure the predictive capabilities of the model. Moreover, the composition of exhaust gases from the pilot flame have a significant influence on the pyrolysate ignition. As, this composition is directly related to the burner operation parameters, these results suggest that the calibration method has an impact on the composite thermal degradation.
This test-case demonstrates the ability of the numerical tool to predict theoretically crucial parameters such as time-to-ignition and heat feedback from pyrolysate combustion, without relying on empirical parameters. In a future work, the authors intend to apply this numerical approach to model several fire tests, involving different materials and pilot flames to demonstrate the capacity of the architecture to be adaptable to different conditions.
Desirable improvements to the model could include a better quantitative measurement of pyrolysate composition, including time dependence of each gaseous species as a function of the matrix temperature and degradation degree. A two-dimensional modeling could also allow to investigate pyrolysate ignition at some radial distance from the stagnation point, in locations with higher pyrolysate concentration and lower strain rate. Moreover, the same coupled architecture could be applied on the cold face of the material to predict the backside ignition, which is an important failure criterion in aerospace materials certification [15].

Acknowledgments

We are grateful for the assistance and financial support from the Natural Sciences and Engineering Research Council of Canada (NSERC/CRSNG), through grant no. CRDPJ 478687-15, from the Government Department for Formation and Research (Germany), through grant Jülich (PTJ) 03INT504BB and the partners from CRIAQ ENV-708 project is acknowledged. One of the authors (PCG) is grateful to the National Science and Technology Council of Mexico (CONACYT) for his doctoral scholarship.

CHAPTER 7 GENERAL DISCUSSIONS

The objective of this thesis was to model the thermal response of a composite material exposed to fire test. A coupled architecture has been developed to model heat and mass transfers in both solid and gas phases and validated against a small-scale fire test. The temperature-dependent properties of the material, as well as parameters describing the solid phase chemical reactions, have been measured through independent experiments.

On the solid phase, the influence of the nature and number of intermediate reactions on the resin pyrolysis has been investigated with a phenomenological approach. The results indicate that a mechanism can provide a very good agreement against mass loss rate data and be simultaneously unable to model the variation of residual mass with heating rate. This suggests that in some cases, the activation energy and pre-exponential factor can be optimized at the expense of the char yield. However, both parameters (E/A and char yield) have an influence on the thermal response of the material, although the extent of this influence depends on the nature of the material considered. There is therefore a need to investigate the impact of optimizing the activation energy at the extent of the char yield for several classes of materials. A possible method to achieve that would be to implement several reaction schemes of different nature in a pyrolysis model to investigate their effects on the thermal response of the material. In this work, the equipment necessary to measure the heat absorbed or released by the chemical reaction in the solid phase was not available. As a consequence, the heat of reaction associated with epoxy pyrolysis had to be found in the literature. This data is available for a single-step reaction only, which explains the use of such a reaction scheme in Chapter 6, although more complex reaction schemes are suggested in Chapter 5. Further research is needed to optimize simultaneously mass loss rate and heat of reaction associated to complex reaction schemes.

The thermal properties of the composite were measured as a function of temperature to be used as input parameters in the model. In order to have a generalized model applicable to various types of matrix/fiber combinations for fast-testing purposes, the thermal properties have been measured independently for each phase instead of relying on the global properties of the composite. The results suggest that the properties obtained, and particularly the thermal conductivity, are not *absolutely* valid but rather valid relatively to the hypothesis and geometrical models used to infer them (Voigt, Reuss, Maxwell, Clayton model, etc), which in turn depend on the composite architecture and must therefore be thoroughly chosen. Moreover, due to equipment limitations, these properties have been measured over a narrowed range of temperatures, which is only partially representative of the temperature

range encountered in fire tests. Further work is needed to measure these properties over a wider range of temperatures.

The thermal response of a composite material to fire test has been modeled with a coupled architecture. This approach avoids the use of empirical formulations to predict the pyrolysate combustion as it was commonly done in the literature so far. The implementation of a very detailed reaction scheme (GRI-Mech 3.0) allowed to predict the time-to-ignition and heat feedback with a theoretical approach, adaptable to various fire test conditions, materials and burner operation parameters. Predictions of the time-to-ignition and backface temperature were in good agreement with experimental data obtained from a small-scale fire test, which is proof of concept of this approach. A sensitivity analysis indicated that the time-to-ignition is mostly driven by the activation energy, but that the atmosphere and pyrolysate composition also play a role. This suggests that the burner fuel and calibration method used to reach the certification requirements could have an impact on the thermal response of the composite, even if this effect is rather limited in our results when compared to other factors such as solid-phase reactions. In a future work, it would be interesting to model the effect of varying the fuel and calibration methods on the material thermal response. The validation should also be extended to other variables, such as the through-thickness temperature of the composite, and temperature reached by the pyrolysate combustion.

CHAPTER 8 CONCLUSION AND RECOMMENDATIONS

8.1 Summary of the work

The goal of this research is to model numerically the thermal degradation of an aerospace composite undergoing a fire certification test, with ultimately the objective of reducing the number of tests necessary to certify materials and therefore accelerating the development process of new fire resistant composites.

To address these objectives, a new numerical method was developed and applied on a carbon-epoxy aerospace composite. First, the thermo-chemical response of a composite material to a heat source was modeled with the Finite Element Method in Chapter 4. The chemical reactions leading to the composite degradation were characterized in Chapter 5. A novel coupling architecture was proposed in Chapter 6 to model pyrolysate ignition and combustion on the surface of the composite during a fire test. The global methodology was validated by comparing the model predictions to the outcomes of an experimental small scale fire test. The thermal properties of the carbon-epoxy composite were thoroughly measured as a function of temperature through independent experiments and used as input parameters in the model.

An improvement in the methodologies used to model polymer chemical decomposition is achieved with the characterization of epoxy pyrolysis in Chapter 5. Several reactions schemes with a variable number of reactions of different nature are considered and compared with a phenomenological approach. Results show that on one hand, the addition of parallel or consecutive reactions enhances the accuracy of the mass loss rate prediction against TGA data, but cannot account for the variation of residual mass observed when the heating rate is changed. On the other hand, adding competitive reactions does not change significantly the accuracy of mass loss rate prediction but is the only reaction scheme able to account for the observed variable residual mass. This research demonstrates that contrary to what is commonly done in the literature, adding consecutive or parallel intermediate reactions is not always representative of the material chemical behavior, even if it allows a better quality of fit of the predicted mass loss rate against TGA data.

A new perspective in the modeling of pyrolysate combustion is achieved with the coupling of a gas-phase chemical kinetics software to a solid-phase thermo-chemical model. This innovative coupled architecture is able to simulate chemical reactions occurring in both solid and gas phases simultaneously. The complexity of the reaction scheme used to model gas-phase reactions (GRI-Mech 3.0) allows to model the time-to-ignition and heat feedback from pyrolysate combustion as a function of the composition of pyrolysates and exhaust gases

from the pilot flame. Results show that the heat flux received by the material approximately doubles when pyrolysate burn close to the surface, although this additional heat source is often neglected in the literature. Moreover, this approach is able to model the composite ignition without using empirical parameters specific to each material and fire test conditions. This original architecture opens up new possibilities in the development of new fire-resistant materials as it allows to test more rapidly several composite systems, without having to infer empirical parameters every time the conditions of the fire test are changed.

8.2 Limitations and future research

Although this work addressed some of the gaps identified in the literature, several topics require more investigation.

The three-dimensional equations governing the gas phase modeling are reduced to a single dimension through the use of similarity solution. This type of one-dimensional configuration was used successfully in previous work to model similar three-dimensional configurations of impinging gas jet. However, it would be interesting to model the fire test in at least two-dimensions to investigate if the non-ignited pyrolysate at the beginning of the fire test could be advected away and ignite at some distance from the fire test, where the strain rate is lower. As the chemical kinetics software used in this study is only available in one-dimension, the coupling of a two-dimensional CFD code including GRI-Mech 3.0 or similar kinetic mechanisms in a two-dimensional pyrolysis model of the solid and gaseous phases could help to address this issue.

The coupled architecture developed here to model pyrolysate ignition is only applied on the hot face on the composite, on which the pilot flame impinges, as most of the pyrolysates migrate in this direction. In theory, this architecture could also be applied on the cold face, which would be very interesting as burn-through is often a failure criteria in certification tests. The pressure solver developed in Chapter 4 is intended to model pyrolysates migration towards the cold face as well, but could not be used for this purpose in Chapter 6 because of its dependence on the composite permeability and the lack of time and resources to conduct the experiments to characterize this parameter. Further work is thus necessary to model the composite permeability as a function of its degradation.

The coupled architecture developed here is based on a quantitative knowledge of the pyrolysate composition. However, these data are challenging to measure and are to date very scarce in the literature. Moreover, an average composition has been used in this work but the pyrolysate composition is known to be time and temperature-dependent. It is therefore desirable to gather more data on the pyrolysate composition and enhance the repeatability

of the measurements techniques.

The composition of exhaust gases from the pilot flame includes many oxidative species and is obviously very different from ambient air composition. As it was not possible to reproduce such an environment in a TGA, it has been decided in this work to characterize composite oxidation in an air flow, as it is usually done in the literature. As a result, the oxidation predicted in the composite is most likely underestimated. Reaction mechanisms representing the oxidation of graphite by a wide range of oxidative species are available in the literature and could be implemented in a future work to account for fiber and char oxidation. However, the surface of the composite exposed to oxidative species must be available as an input parameters in these models. This surface remains difficult to measure and model as it includes not only the surface of the composite exposed to the flame, but also the surface of the porosity inside the material, in which the oxidative species may diffuse. A model of pore growth accounting for the variation of pores diameters as a function of decomposition degree is therefore necessary to implement more realistic oxidation mechanisms on solid surfaces.

Although the method developed here is able to model pyrolysate ignition in various atmospheres, only one calibrated methane burner was available for the pilot flame at the time the thesis was written. In a future work, a kerosene burner will be developed and calibrated to investigate the impact of the fuel composition and calibration method on the time-to-ignition of the composite.

REFERENCES

[1] J. Lelieveld, A. Pozzer, U. Pöschl, M. Fnais, A. Haines, and T. Münzel, "Loss of life expectancy from air pollution compared to other risk factors: a worldwide perspective," *Cardiovascular Research*, 2020.

[2] ICAO, "ICAO Environmental Report 2016, aviation and climate change," *Environmental report 2016*, p. 250, 2016.

[3] M. A. Cameron, M. Z. Jacobson, S. R. Barrett, H. Bian, C. C. Chen, S. D. Eastham, A. Gettelman, A. Khodayari, Q. Liang, H. B. Selkirk, N. Unger, D. J. Wuebbles, and X. Yue, "An intercomparative study of the effects of aircraft emissions on surface air quality," *Journal of Geophysical Research*, vol. 122, no. 15, pp. 8325–8344, 2017.

[4] B. Graver, K. Zhang, and D. Rutherford, "CO2 emissions from commercial aviation, 2018," *International Council on Clean Transportation, 2019*, no. September, p. 13, 2019.

[5] EIA, "Petroleum & Other liquids," 2020. [Online]. Available: https://www.eia.gov/petroleum

[6] Alioth Finance, "Inflation Calculator," 2020. [Online]. Available: https://www.in2013dollars.com/us/inflation/https://www.officialdata.org/us/inflation/

[7] L. Nicolais, M. Meo, and E. Milella, *Composite materials: A Vision for the Future*, springer ed., L. Nicolais, E. Milella, and M. Meo, Eds., 2011.

[8] A. Négrier and J.-C. Rigal, "Présentation des matériaux composites," *Techniques de l'Ingénieur*, no. A7790v1, 1991.

[9] D. Bettebghor, J. Morlier, S. Grihon, D. B. Onera, S. Grihon, and J. Morlier, "Bilevel optimization of large composite structures based on lamination parameters and post-optimal sensitivities. Part 1: Theoretical aspects," no. May, 2018. [Online]. Available: https://www.researchgate.net/publication/324918713

[10] G. Ferrer, C. Chamfroy, and S. S. Dupouy, "A350 XWB composite repairs," *Airbus technical magazine*, vol. 57, pp. 16–21, 2016.

[11] FAA, "http://www.fire.tc.faa.gov/research/summary.stm."

[12] A. Mouritz, "Fire Safety of Advanced Composites for Aircraft," Australian Transport Safety Bureau, Tech. Rep. B2004/0046, 2006. [Online]. Available: https://www.atsb.gov.au/media/32739/

[13] ISO5660, "Reaction-to-fire tests — Heat release, smoke production and mass loss rate," ISO: Geneva, Switzerland, Tech. Rep., 2015.

[14] FAA, "Powerplant Installation and Propulsion System Component Fire Protection Test Methods, Standards, and Criteria," Tech. Rep., 2005.

[15] ISO2685:1998(E), "Aircraft - Environmental Test Procedure for Airborne Equipment - Resistance to Fire in Designated Fire Zones," *the International Organization for Standardization (ISO): Geneva, Switzerland*, 1998.

[16] R. I. Ochs, "Federal Aviation Administration Development of a Next- Generation Burner for Testing Thermal Acoustic Insulation Burnthrough Resistance," 2008.

[17] J. Hamp and S. Caulfeild, "Fireproof Testing of Pressurized Acoustic Organic Composite Sandwich Structures," *62nd CASI Aeronautics Conference and AGM 3rd GARDN Conference*, vol. 7500, no. 905, pp. 1–9, 2015.

[18] A. Mouritz, S. Feih, E. Kandare, Z. Mathys, A. Gibson, P. Des Jardin, S. Case, and B. Y. Lattimer, "Review of fire structural modelling of polymer composites," *Composites Part A: Applied Science and Manufacturing*, vol. 40, no. 12, pp. 1800–1814, 2009. [Online]. Available: http://dx.doi.org/10.1016/j.compositesa.2009.09.001

[19] Statista.com, "Annual growth in global air traffic passenger demand from 2006 to 2020," 2020. [Online]. Available: https://www.statista.com/statistics/193533/growth-of-global-air-traffic-passenger-demand/

[20] T. Kashiwagi, "Polymer combustion and flammability-Role of the condensed phase," *Symposium (International) on Combustion*, vol. 25, no. 1, pp. 1423–1437, 1994.

[21] C. Di Blasi, "The state of the art of transport models for charring solid degradation," *Polymer International*, vol. 49, no. 10, pp. 1133–1146, 2000.

[22] B. Moghtaderi, "The state-of-the-art in pyrolysis modelling of lignocellulosic solid fuels," *Fire and Materials*, vol. 30, no. 1, pp. 1–34, 2006.

[23] A. Mouritz and A. Gibson, *Fire Properties of polymer composite materials*, springer ed., G. Gladwell, Ed., 2006.

[24] M. W. Beckstead, K. Puduppakkam, P. Thakre, and V. Yang, "Modeling of combustion and ignition of solid-propellant ingredients," *Progress in Energy and Combustion Science*, vol. 33, no. 6, pp. 497–551, 2007.

[25] L. Shi and M. Y. L. Chew, "A review of fire processes modeling of combustible materials under external heat flux," *Fuel*, vol. 106, pp. 30–50, 2013.

[26] C. Baukal and B. Gebhart, "A review of semi-analytical solutions for flame impingement heat transfer," *International Journal of Heat and Mass Transfer*, vol. 39, no. 14, pp. 2989–3002, 1995.

[27] J. Beér and N. Chigier, "Impinging jet flames," *Combustion and Flame*, vol. 12, no. 6, pp. 575–586, 1968.

[28] H. Martin, "Heat and Mass Transfer between Impinging Gas Jets and Solid Surfaces," *Advances in Heat Transfer*, 1977.

[29] K. J. Hammad and I. Milanovic, "Flow Structure in the Near-Wall Region of a Submerged Impinging Jet," *Journal of Fluids Engineering*, 2011.

[30] R. Viskanta, "Heat Transfer to Impinging Isothermal Gas and Flame Jets," *Experimental Thermal and Fluid Science*, vol. 6, pp. 111–134, 1993.

[31] N. Zuckerman and N. Lior, *Jet impingement heat transfer: Physics, correlations, and numerical modeling*. Elsevier Masson SAS, 2006, vol. 39, no. C. [Online]. Available: http://dx.doi.org/10.1016/S0065-2717(06)39006-5

[32] P. S. Shadlesky, "Stagnation Point Heat Transfer for Jet Impingement to a Plane Surface," *AIAA Journal*, vol. 21, no. 8, pp. 1214–1215, 1982.

[33] J. M. Bergthorson, D. Goodwin, and P. Dimotakis, "Experiments and Modeling of Impinging Jets and Premixed (Article)," *15th Australian Fluid Mechanics Conference*, 2004.

[34] E. M. Stuland, "Computation of impinging gas jets," Master of Science, Norwegian University of Science and Technology, 2008.

[35] D. Sikoutris, D. Vlachos, V. Kostopoulos, S. Jagger, and S. Ledin, "Fire burnthrough response of CFRP aerostructures. Numerical investigation and experimental verification," *Applied Composite Materials*, vol. 19, no. 2, pp. 141–159, 2012.

[36] J. Kreuder, X. Gao, and A. Kirkpatrick, "Computation of Heat Transfer from an Impinging Flame Jet to a Plane Surface," *51st AIAA Aerospace Sciences Meeting including the New Horizons Forum and Aerospace Exposition*, pp. 1–11, 2013. [Online]. Available: http://arc.aiaa.org/doi/abs/10.2514/6.2013-605

[37] N. Grange, K. Chetehouna, N. Gascoin, and S. Senave, "Numerical investigation of the heat transfer in an aeronautical composite material under fire stress," *Fire Safety Journal*, vol. 80, pp. 56–63, 2016.

[38] M. Aadmi, M. Karkri, L. Ibos, and M. E. Hammouti, "Effective thermal conductivity of random two-phase composites," *Journal of Reinforced plastics and composites*, vol. 33, no. 1, pp. 69–80, 2014.

[39] J. Eshelby, "The determination of the elastic field of an ellipsoidal inclusion, and related problems," *Proceedings of the Royal Society of London. Series A. Mathematical and Physical Sciences*, vol. 241, no. 1226, pp. 376–396, 1957.

[40] T. Mori and K. Tanaka, "Average stress in matrix and average elastic energy of materials with misfitting inclusions," *Acta Metallurgica*, vol. 21, no. 5, pp. 571–574, 1973.

[41] R. C. Progelhof, J. L. Throne, and R. R. Ruetsch, "Methods for predicting the thermal conductivity of composite systems: A review," *Polymer Engineering and Science*, vol. 16, no. 9, pp. 615–625, 1976. [Online]. Available: http://doi.wiley.com/10.1002/pen.760160905

[42] Y. I. Dimitrienko, "Thermomechanical behaviour of composite materials and structures under high temperatures: 1. Materials," *Composites Part A: Applied Science and Manufacturing*, vol. 28, no. 5, pp. 453–461, 1997.

[43] C. Lautenberger and A. Fernandez-Pello, "Generalized pyrolysis model for combustible solids," *Fire Safety Journal*, vol. 44, no. 6, pp. 819–839, 2009. [Online]. Available: http://dx.doi.org/10.1016/j.firesaf.2009.03.011

[44] M. Looyeh, P. Bettess, and A. Gibson, "A one-dimensional finite element simulation for the fire-performance of GRP panels for offshore structures," *International Journal of Numerical Methods for Heat & Fluid Flow*, vol. 7, pp. 609–625, 1997.

[45] J. Florio, J. Henderson, F. Test, and R. Hariharan, "A study of the effects of the assumption of local-thermal equilibrium on the overall thermally-induced response of a decomposing, glass-filled polymer composite," *International Journal of Heat and Mass Transfer*, vol. 34, no. 1, pp. 135–147, 1991.

[46] S. Vyazovkin, K. Chrissafis, M. L. Di Lorenzo, N. Koga, M. Pijolat, B. Roduit, N. Sbirrazzuoli, and J. J. Suñol, "ICTAC Kinetics Committee recommendations for collecting experimental thermal analysis data for kinetic computations," *Thermochimica Acta*, vol. 590, pp. 1–23, 2014.

[47] S. Vyazovkin, A. K. Burnham, J. M. Criado, L. A. Pérez-Maqueda, C. Popescu, and N. Sbirrazzuoli, "ICTAC Kinetics Committee recommendations for performing kinetic computations on thermal analysis data," *Thermochimica Acta*, vol. 520, no. 1-2, pp. 1–19, 2011. [Online]. Available: http://dx.doi.org/10.1016/j.tca.2011.03.034

[48] S. Vyazovkin, A. K. Burnham, L. Favergeon, N. Koga, E. Moukhina, L. A. Pérez-Maqueda, and N. Sbirrazzuoli, "ICTAC Kinetics Committee recommendations for analysis of multi-step kinetics," *Journal of the Neurological Sciences*, p. 116544, 2020. [Online]. Available: https://doi.org/10.1016/j.tca.2020.178597

[49] J. A. Parker and D. A. Kourtides, "New Fireworthy Composites for Use in Transportation Vehicles," *Journal of Fire Sciences*, vol. 1, no. 6, pp. 432–458, 1983. [Online]. Available: http://jfs.sagepub.com/cgi/doi/10.1177/073490418300100604

[50] C. Di Blasi, "Modeling and simulation of combustion processes of charring and non-charring solid fuels," *Progress in Energy and Combustion Science*, vol. 19, no. 1, pp. 71–104, 1993.

[51] K. A. Trick and T. E. Saliba, "Mechanisms of the pyrolysis of phenolic resin in a carbon/phenolic composite," *Carbon*, vol. 33, no. 11, pp. 1509–1515, 1995.

[52] V. Biasi, "Modelisation Thermique de la Dégradation d'un Matériau Composite Soumis au Feu," Thèse de Doctorat, Université de Toulouse, 2014. [Online]. Available: http://www.theses.fr/2014ESAE0034

[53] P. Tranchard, F. Samyn, S. Duquesne, B. Estèbe, and S. Bourbigot, "Modelling behaviour of a carbon epoxy composite exposed to fire: Part I-Characterisation of thermophysical properties," *Materials*, vol. 10, no. 5, 2017.

[54] C. Law, *Combustion Physics*. Cambridge University Press, 2006.

[55] C. Lautenberger, "Title: A Generalized Pyrolysis Model for Combustible Solids," PhD Thesis, University of California, Berkeley, 2007. [Online]. Available: http://escholarship.org/uc/item/7wz5m7dg

[56] N. Tian and A. Zhou, "An ignition criterion for combustible solids integrating surface temperature and heating rate," *Fire and materials*, no. August 2008, p. 4B, 2014.

[57] A. Gibson, T. Browne, S. Feih, and A. Mouritz, "Modeling composite high temperature behavior and fire response under load," *Journal of Composite Materials*, vol. 46, no. 16, pp. 2005–2022, 2012.

[58] P. Tranchard, F. Samyn, S. Duquesne, B. Estèbe, and S. Bourbigot, "Modelling behaviour of a carbon epoxy composite exposed to fire: Part ii-comparison with experimental results," *Materials*, vol. 10, no. 5, 2017.

[59] C. Lautenberger, Y. Zhou, and A. Fernandez-Pello, "Numerical Modeling of Convective Effects on Piloted Ignition of Composite Materials," *Combustion Science and Technology*, vol. 177, no. 5-6, pp. 1231–1252, 2006. [Online]. Available: http://www.tandfonline.com/doi/abs/10.1080/00102200590927058

[60] W. Xie and P. DesJardin, "An embedded upward flame spread model using 2D direct numerical simulations," *Combustion and Flame*, vol. 156, pp. 522–530, 2009. [Online]. Available: www.elsevier.com/locate/combustflame

[61] A. Kacem, M. Mense, Y. Pizzo, G. Boyer, S. Suard, P. Boulet, G. Parent, and B. Porterie, "A fully coupled fluid/solid model for open air combustion of horizontally-oriented PMMA samples," *Combustion and Flame*, vol. 170, pp. 135–147, 2016. [Online]. Available: http://dx.doi.org/10.1016/j.combustflame.2016.04.009

[62] G. Boyer, "Fully coupled CFD simulation of the pyrolysis of non-charring polymers: A predictive approach," *Fire Safety Journal*, pp. 1–10, 2017. [Online]. Available: http://linkinghub.elsevier.com/retrieve/pii/S0379711217301650

[63] U. Sorathia, "Flammability and Fire Safety of Composite Materials," in *Proceedings of the 1st International Workshop on Composite Materials for Offshore Operations*, 1993, pp. 309–317.

[64] A. Snegirev, V. Talalov, V. Stepanov, and J. Harris, "A new model to predict pyrolysis, ignition and burning of flammable materials in fire tests," *Fire Safety Journal*, vol. 59, pp. 132–150, 2013.

[65] A. L. Brown, "The Decomposition Behavior of Thermoset Carbon Fiber Epoxy Composites in the Fire Environment," in *Combustion Institute Joint US Sections Meeting May 19-22*, 2013, pp. 1–18.

[66] R. Acharya and K. K. Kuo, "Effect of pressure and propellant composition on graphite rocket nozzle erosion rate," *Journal of Propulsion and Power*, vol. 23, no. 6, pp. 1242–1254, 2007.

[67] ——, "Effect of Chamber Pressure and Propellant Composition on Erosion Rate of Graphite Rocket Nozzle," *Journal of Propulsion and Power*, vol. 23, no. 6, pp. 1242–1254, 2007. [Online]. Available: http://arc.aiaa.org/doi/10.2514/1.24011

[68] D. Bianchi, F. Nasuti, and E. Martelli, "Coupled Analysis of Flow and Surface Ablation in Carbon-Carbon Rocket Nozzles," *Journal of Spacecraft and Rockets*, vol. 46, no. 3, pp. 492–500, 2009. [Online]. Available: http://arc.aiaa.org/doi/10.2514/1.40197

[69] D. Bianchi, A. Turchi, F. Nasuti, and M. Onofri, "Chemical Erosion of Carbon-Phenolic Rocket Nozzles with Finite-Rate Surface Chemistry," *Journal of Propulsion and Power*, vol. 29, no. 5, pp. 1220–1230, 2013. [Online]. Available: http://arc.aiaa.org/doi/10.2514/1.B34791

[70] D. Bianchi and F. Nasuti, "Numerical Analysis of Nozzle Material Thermochemical Erosion in Hybrid Rocket Engines," *Journal of Propulsion and Power*, vol. 29, no. August, pp. 1–12, 2013. [Online]. Available: http://arc.aiaa.org/doi/abs/10.2514/1.B34813

[71] H. K. Chelliah, A. Makino, I. Kato, N. Araki, and C. K. Law, "Modeling of graphite oxidation in a stagnation-point flow field using detailed homogeneous and semiglobal heterogeneous mechanisms with comparisons to experiments," *Combustion and Flame*, vol. 104, no. 4, pp. 469–480, 1996.

[72] G. La Delfa, J. W. Luinge, and a. G. Gibson, "Integrity of composite aircraft fuselage materials under crash fire conditions," *Plastics, Rubber and Composites*, vol. 38, no. 2, pp. 111–117, 2009. [Online]. Available: http://openurl.ingenta.com/

[73] J. B. Henderson, J. A. Wiebelt, and M. R. Tant, "A Model for the Thermal Response of Polymer Composite Materials with Experimental Verification," *Journal of Composite Materials*, vol. 19, no. 6, pp. 579–595, 1985.

[74] J. G. Quintiere, "A simulation model for fire growth on materials subject to a room-corner test," *Fire Safety Journal*, vol. 20, no. 4, pp. 313–339, 1993.

[75] M. Looyeh and P. Bettess, "A finite element model for the fire-performance of GRP panels including variable thermal properties," *Finite Elements in*

Analysis and Design, vol. 30, no. 4, pp. 313–324, 1998. [Online]. Available: http://www.sciencedirect.com/science/article/pii/S0168874X98000365

[76] S. I. Stoliarov and R. Lyon, "Thermo-kinetic model of burning for pyrolyzing materials," *Fire Safety Science - Proceedings of the ninth international symposium*, pp. 1141–1152, 2008.

[77] R. J. Asaro, B. Y. Lattimer, C. Mealy, and G. Steele, "Thermo-physical performance of a fire protective coating for naval ship structures," *Composites Part A: Applied Science and Manufacturing*, vol. 40, no. 1, pp. 11–18, 2009. [Online]. Available: http://dx.doi.org/10.1016/j.compositesa.2008.07.015

[78] M. Tsoi, J. Zhuge, R.-H. Chen, and J. Gou, "Modeling and experimental studies of thermal degradation of glass fiber reinforced polymer composites," *Fire and Materials*, vol. 38, pp. 247–263, 2014.

[79] M. Mckinnon, Y. Ding, S. I. Stoliarov, S. Crowley, and R. E. Lyon, "Pyrolysis model for a carbon fiber/epoxy structural aerospace composite," *Journal of Fire Sciences*, vol. 1, 2016.

[80] H. C. Kung, "A mathematical model of wood pyrolysis," *Combustion and Flame*, vol. 18, no. 2, pp. 185–195, 1972.

[81] E. J. Kansa, H. E. Perlee, and R. F. Chaiken, "Mathematical model of wood pyrolysis including internal forced convection," *Combustion and Flame*, vol. 29, no. C, pp. 311–324, 1977.

[82] C. D. Blasi, "Physico-chemical processes occurring inside a degrading two-dimensional anisotropic porous medium," *International Journal of Heat and Mass Transfer*, vol. 41, no. 24, pp. 4139–4150, 1998.

[83] M. E. Metochianakis and D. W. Netzer, "Modeling Solid-Fuel Ramjet Combustion, Including Radiation to the Fuel Surface," *J. Spacecraft*, no. August, pp. 405–406, 1983.

[84] A. R. Kerstein, "Percolation model of polydisperse composite solid propellant combustion," *Combustion and Flame*, vol. 69, no. 1, pp. 95–112, 1987.

[85] T. L. Jackson, "Modeling of Heterogeneous Propellant Combustion: A Survey," *AIAA Journal*, vol. 50, no. 5, pp. 993–1006, 2012. [Online]. Available: http://arc.aiaa.org/doi/10.2514/1.J051585

[86] J. Quintiere and M. Harkleroad, "New Concepts for Measuring Flame Spread Properties," *Fire Safety: Science and Engineering*, pp. 239–267, 1985.

[87] B. Karlsson, "Models for calculating flame spread on wall lining materials and the resulting heat release rate in a room," *Fire Safety Journal*, vol. 23, no. 4, pp. 365–386, 1994.

[88] M. A. Dietenberger, "Ignitability analysis using the cone calorimeter and LIFT apparatus," *Proceedings of the International Conference on Fire Safety*, no. January 1996, pp. 189–197, 1996.

[89] E. G. Brehob, C. I. Kim, and A. K. Kulkarni, "Numerical model of upward flame spread on practical wall materials," *Fire Safety Journal*, vol. 36, no. 3, pp. 225–240, 2001.

[90] T. Kuang-Chung and D. Drysdale, "Using cone calorimeter data for the prediction of fire hazard," *Fire Safety Journal*, vol. 37, no. 7, pp. 697–706, 2002.

[91] T. Keller, C. Tracy, and A. Zhou, "Structural response of liquid-cooled GFRP slabs subjected to fire – Part I: Thermo-chemical and thermo-mechanical modeling," *Composites Part A: Applied Science and Manufacturing*, vol. 37, no. 9, pp. 1286–1295, 2006.

[92] ——, "Structural response of liquid-cooled GFRP slabs subjected to fire – Part II: Thermo-chemical and thermo-mechanical modeling," *Composites Part A: Applied Science and Manufacturing*, vol. 37, no. 9, pp. 1296–1308, 2006.

[93] Y. Bai, T. Vallée, and T. Keller, "Modeling of thermo-physical properties for FRP composites under elevated and high temperature," *Composites Science and Technology*, vol. 67, no. 15-16, pp. 3098–3109, 2007.

[94] C. A. Griffis, R. A. Masumura, and C. I. Chang, "Thermal Response of Graphite Epoxy Composite Subjected to Rapid Heating," *Journal of Composite Materials*, vol. 15, no. 5, pp. 427–442, 1981.

[95] L. McManus and D. Coyne, "A digital computer program for calculating the response of mechanically and thermally loaded aircraft structures to the thermal radiation of a nuclear explosion or high-energy laser," Tech. Rep., 1982.

[96] J. Chen, C. Sun, and C. Chang, "Failure analysis of a graphite/epoxy laminate subjected to combined thermal and mechanical loading," *Journal of Composite Materials*, vol. 19, no. 5, pp. 216–235, 1985.

[97] Y. Bai, T. Keller, and T. Vallée, "Modeling of stiffness of FRP composites under elevated and high temperatures," *Composites Science and Technology*, vol. 68, no. 15-16, pp. 3099–3106, 2008. [Online]. Available: http://dx.doi.org/10.1016/j.compscitech.2008.07.005

[98] B. J. McCaffrey, J. G. Quintiere, and M. F. Harkleroad, "Estimating room temperatures and the likelihood of flashover using fire test data correlations," *Fire Technology*, vol. 17, no. 2, pp. 98–119, 1981.

[99] M. E. Kim, "Parameter Estimation Methods for Comprehensive Pyrolysis Modeling," PhD Thesis, Worcester Polytechnic Institute, 2014.

[100] N. Tian, "A general thermal thickness model and a heating rate related ignition criterion for combustible solids," PhD Thesis, The University of North California at Charlotte, 2013.

[101] C. H. Bamford, J. Crank, and D. H. Malan, "The combustion of wood. Part I," *Mathematical Proceedings of the Cambridge Philosophical Society*, vol. 42, no. 2, pp. 166–182, 1946.

[102] T. Munson and R. Spindler, "Transient thermal behavior of decomposing materials," Tech. Rep., 1961.

[103] K. A. Murty and P. L. Blackshear, "Pyrolysis effects in the transfer of heat and mass in thermally decomposing organic solids," *Symposium (International) on Combustion*, vol. 11, no. 1, pp. 517–523, 1967.

[104] T. Kashiwagi, "A radiative ignition model of a solid fuel," *Combustion Science and Technology*, vol. 8, no. 5-6, pp. 225–236, 1973.

[105] C. A. Miller and K. N. Ramohalli, "A Theoretical Heterogeneous Model of Wood Pyrolysis," *Combustion Science and Technology*, vol. 46, no. 3-6, pp. 249–265, 1986.

[106] B. Fredlund, "A model for heat and mass transfer in timber structures during fire: a theoretical, numerical and experimental study," *Report LUTVDG (TVBB-1003)*, 1988.

[107] J. Henderson, M. Tant, G. Moore, and J. Wiebelt, "Determination of kinetic parameters for the thermal decomposition of phenolic ablative materials by a multiple heating rate method," *Thermochimica Acta*, vol. 44, pp. 253–264, 1981.

[108] J. Henderson, J. Wiebelt, M. Tant, and G. Moore, "A method for the determination of the specific heat and heat of decomposition of composite materials," *Thermochimica Acta*, vol. 57, no. 2, pp. 161–171, 1982. [Online]. Available: http://www.sciencedirect.com/science/article/pii/0040603182800579

[109] M. A. Zanoni, J. L. Torero, and J. I. Gerhard, "The role of local thermal non-equilibrium in modelling smouldering combustion of organic liquids," *Proceedings of the Combustion Institute*, vol. 000, pp. 1–9, 2018. [Online]. Available: https://doi.org/10.1016/j.proci.2018.05.177

[110] J. Milke and A. Vizzini, "Thermal Response of Fire-Exposed Composites," *Journal of Composites, Technology and Research*, vol. 13, no. 3, pp. 145–151, 1991.

[111] M. R. Tant, J. B. Henderson, and C. T. Boyer, "Measurement and modelling of the thermochemical expansion of polymer composites," *Composites*, vol. 16, no. 2, pp. 121–126, 1985.

[112] J. B. Henderson, M. R. Tant, M. P. Doherty, and E. F. O'Brien, "Characterization of the high-temperature behaviour of a glass-filled polymer composite," *Composites*, vol. 18, no. 3, pp. 205–215, 1987.

[113] R. Sullivan and N. Salamon, "A finite element method for the decomposition of thermochemical decomposition of polymeric materials - I. Theory," *International Journal of Engineering Sciences*, vol. 30, no. 4, pp. 431–441, 1992.

[114] M. Looyeh, "Finite element simulation of heat flow in decomposing polymer composites," PhD Thesis, Durham University, 1999. [Online]. Available: http://etheses.dur.ac.uk/4566/

[115] M. Looyeh, A. Samanta, S. Jihan, and J. McConnachie, "Modelling of reinforced polymer composites subject to thermo-mechanical loading," *International Journal for Numerical Methods in Engineering*, vol. 63, no. 6, pp. 898–925, 2005.

[116] M. Looyeh, K. Rados, and P. Bettess, "Thermochemical responses of sandwich panels to fire," *Finite Elements in Analysis and Design*, vol. 37, no. 11, pp. 913–927, 2001.

[117] A. Galgano, C. Di Blasi, C. Branca, and E. Milella, "Thermal response to fire of a fibre-reinforced sandwich panel: Model formulation, selection of intrinsic properties and experimental validation," *Polymer Degradation and Stability*, vol. 94, no. 8, pp. 1267–1280, 2009. [Online]. Available: http://dx.doi.org/10.1016/j.polymdegradstab.2009.04.007

[118] Y. I. Dimitrienko, "Thermal stresses and heat-mass transfer in ablating composite materials," *International Journal of Heat and Mass Transfer*, vol. 38, no. 1, pp. 139–146, 1995.

[119] ——, "Thermomechanical behaviour of composite materials and structures under high temperatures: 2. Structures," *Composites Part A: Applied Science and Manufacturing*, vol. 28, no. 5, pp. 463–471, 1997.

[120] Y. Dimitrienko, "Thermomechanical behaviour of composites under local intense heating by irradiation," *Composites Part A*, vol. 31, no. 6, pp. 591–598, 2000.

[121] A. Gibson, Y. Wu, H. Chandler, J. Wilcox, and P. Bettess, "Model for the thermal performance of thick composite laminates in hydrocarbon fires," *Revue de l'Institute Francais du Petrole*, vol. 50, no. 1, pp. 69–74, 1995.

[122] A. Gibson, P. Wright, Y. Wu, A. Mouritz, Z. Mathys, and C. Gardiner, "Modelling residual mechanical properties of polymer composites after fire," *Plastics, Rubber and Composites*, vol. 32, no. 2, pp. 81–90, 2003. [Online]. Available: http://www.ingentaselect.com/

[123] A. G. Gibson, P. N. H. Wright, Y. S. Wu, A. P. Mouritz, Z. Mathys, and C. P. Gardiner, "The Integrity of Polymer Composites during and after Fire," *Journal of Composite Materials*, vol. 38, no. 15, pp. 1283–1307, 2004.

[124] A. G. Gibson, Y. S. Wu, J. T. Evans, and A. P. Mouritz, "Laminate Theory Analysis of Composites under Load in Fire," *Journal of Composite Materials*, vol. 40, no. 7, pp. 639–658, 2006.

[125] N. Dodds, A. G. Gibson, D. Dewhurst, and J. M. Davies, "Fire behaviour of composite laminates," *Composites Part A: Applied Science and Manufacturing*, vol. 31, no. 7, pp. 689–702, 2000.

[126] S. Feih, Z. Mathys, A. G. Gibson, and A. P. Mouritz, "Modelling the compression strength of polymer laminates in fire," *Composites Part A: Applied Science and Manufacturing*, vol. 38, no. 11, pp. 2354–2365, 2007.

[127] ——, "Modelling the tension and compression strengths of polymer laminates in fire," *Composites Science and Technology*, vol. 67, no. 3-4, pp. 551–564, 2007.

[128] J. A. Quintiere, R. N. Walters, and S. Crowley, "Flammability Properties of Aircraft Carbon-Fiber Structural Composite," Federal Aviation Administration, Tech. Rep. October, 2007.

[129] M. McGurn, P. E. Desjardin, and A. B. Dodd, "Numerical simulation of expansion and charring of carbon-epoxy laminates in fire environments," *International Journal of Heat and Mass Transfer*, vol. 55, no. 1-3, pp. 272–281, 2012. [Online]. Available: http://dx.doi.org/10.1016/j.ijheatmasstransfer.2011.09.013

[130] R. D. Chippendale, I. O. Golosnoy, and P. L. Lewin, "Numerical modelling of thermal decomposition processes and associated damage in carbon fibre composites," *Journal of Physics D: Applied Physics*, vol. 47, no. 38, 2014.

[131] B. Y. Lattimer, J. Ouellette, and J. Trelles, "Thermal Response of Composite Materials to Elevated Temperatures," *Fire Technology*, vol. 47, no. 4, pp. 823–850, 2011.

[132] N. Grange, P. Tadini, K. Chetehouna, N. Gascoin, I. Reynaud, and S. Senave, "Determination of thermophysical properties for carbon-reinforced polymer-based composites up to 1000C," *Thermochimica Acta*, vol. 659, no. October 2017, pp. 157–165, 2018. [Online]. Available: https://doi.org/10.1016/j.tca.2017.11.014

[133] P. Krysl, W. T. Ramroth, L. K. Stewart, and R. J. Asaro, "Finite element modelling of fibre reinforced polymer sandwich panels exposed to heat," *International Journal for Numerical Methods in Engineering*, vol. 61, no. 1, pp. 49–68, 2004.

[134] S. I. Stoliarov, N. Safronava, and R. Lyon, "The effect of variation in polymer properties on the rate of burning," *Fire and Materials*, vol. 33, pp. 257–271, 2009.

[135] M. Chaos, "Application of sensitivity analyses to condensed-phase pyrolysis modeling," *Fire Safety Journal*, vol. 61, pp. 254–264, 2013. [Online]. Available: http://dx.doi.org/10.1016/j.firesaf.2013.09.016

[136] B. Batiot, "Étude et modélisation de la cinétique de décomposition thermique des matériaux solides." Ph.D. Dissertation, École Nationale Supérieure de Mécanique et d'Aérotechnique, 2014.

[137] G. Rein, C. Lautenberger, A. C. Fernandez-Pello, J. L. Torero, and D. L. Urban, "Application of genetic algorithms and thermogravimetry to determine the kinetics of polyurethane foam in smoldering combustion," *Combustion and Flame*, vol. 146, no. 1-2, pp. 95–108, 2006.

[138] E. Kim, N. Dembsey, and S. Shivkumar, "Evaluating effects of applying different kinetic models to pyrolysis modeling of fiberglass-reinforced polymer composites," *Fire and Materials*, vol. 39, pp. 153–173, 2015.

[139] P. Tranchard, S. Duquesne, F. Samyn, B. Estèbe, and S. Bourbigot, "Kinetic analysis of the thermal decomposition of a carbon fibre-reinforced epoxy resin laminate," *Journal of Analytical and Applied Pyrolysis*, vol. 126, no. May, pp. 14–21, 2017. [Online]. Available: http://dx.doi.org/10.1016/j.jaap.2017.07.002

[140] K. Mcgrattan, S. Hostikka, R. Mcdermott, J. Floyd, C. Weinschenk, and K. Overholt, "Fire Dynamics Simulator User's Guide," 2016. [Online]. Available: http://dx.doi.org/10.6028/NIST.SP.1019

[141] S. I. Stoliarov, I. T. Leventon, and R. E. Lyon, "Two-dimensional model of burning for pyrolyzable solids," *Fire and Materials*, 2014.

[142] C. Lautenberger and C. Fernandez-Pello, "Optimization Algorithms for Material Pyrolysis Property Estimation," *Fire Safety Science*, vol. 10, no. 3, pp. 459–470, 2011. [Online]. Available: http://www.iafss.org/publications/fss/10/459

[143] J. Reddy and D. Gartling, *The Finite Element Method in Heat Transfer and Fluid Dynamics, 3rd edition*, taylor & f ed. CRC Press, 2010.

[144] H.-B. Wang, "Heat transfer analysis of components of construction exposed to fire," Ph.D. Dissertation, University of Salford, 1995. [Online]. Available: http://usir.salford.ac.uk/14780/

[145] J. Lua, J. O'Brien, C. Key, Y. Wu, and B. Lattimer, "A temperature and mass dependent thermal model for fire response prediction of marine composites," *Composites Part A*, vol. 37, pp. 1024–1039, 2006.

[146] B. Fredlund, "Modelling of heat and mass transfer in wood structures during fire," *Fire Safety Journal*, vol. 20, no. 1, pp. 39–69, 1993.

[147] T. Morgado, J. Correia, A. Moreira, F. Branco, and C. Tiago, "Experimental study on the fire resistance of GFRP pultruded tubular columns," *Composites Part B: Engineering*, vol. 69, pp. 201–211, 2014.

[148] J. Zhang, M. A. Delichatsios, T. Fateh, M. Suzanne, and S. Ukleja, "Characterization of flammability and fire resistance of carbon fibre reinforced thermoset and thermoplastic composite materials," *Journal of Loss Prevention in the Process Industries*, vol. 50, no. October, pp. 275–282, 2017. [Online]. Available: https://doi.org/10.1016/j.jlp.2017.10.004

[149] H. L. McManus and G. S. Springer, "High Temperature Thermomechanical Behavior of Carbon-Phenolic and Carbon-Carbon Composites, I. Analysis," *Journal of Composite Materials*, vol. 26, no. 2, pp. 206–229, 1992.

[150] ——, "High Temperature Thermomechanical Behavior of Carbon-Phenolic and Carbon-Carbon Composites, II. Results," *Journal of Composite Materials*, vol. 26, no. 2, pp. 230–255, 1992.

[151] C. Luo, W. Xie, and P. DesJardin, "Fluid-Structure Simulations of Composite Material Response for Fire Environments," *Fire Technology*, vol. 47, no. 4, pp. 887–912, 2011.

[152] D. M. Marquis, E. Guillaume, A. Camillo, T. Rogaume, and F. Richard, "Existence and uniqueness of solutions of a differential equation system modeling the thermal decomposition of polymer materials," *Combustion and Flame*, vol. 160, no. 4, pp. 818–829, 2013. [Online]. Available: http://dx.doi.org/10.1016/j.combustflame.2012.12.008

[153] T. Pelzmann, M. Kelly, S. Hind, M. Lévesque, and E. Robert, "The BTU Heat Transfer Device: Adapting a Standard Tool in Aircraft Fire Testing to Small Scale Experiments," *Ninth Triennial International Fire & Cabin Safety Research Conference of FAA*, 1996.

[154] G. P. Smith, D. M. Golden, M. Frenklach, N. W. Moriarty, B. Eiteneer, M. C. Goldenberg, T. Bowman, R. K. Hanson, S. Song, W. C. Gardiner, V. V. Lissianski, and Z. Qin, "GRI-Mech." [Online]. Available: http://combustion.berkeley.edu/gri-mech/

[155] P. Dagaut and M. Cathonnet, "The ignition, oxidation, and combustion of kerosene: A review of experimental and kinetic modeling," *Progress in Energy and Combustion Science*, vol. 32, no. 1, pp. 48–92, 2006.

[156] J. Luche, "Obtention de modèles cinétiques réduits de combustion - Application à un mécanisme du kérosène," PhD Thesis, Université d'Orléans, 2003.

[157] H. Wang, E. Dames, B. Sirjean, D. Sheen, R. Tango, A. Violi, J. Lai, F. Egolfopoulos, D. Davidson, R. Hanson, C. Bowman, C. Law, W. Tsang, N. Cernansky, D. Miller, and R. Lindstedt, "A high-temperature chemical kinetic model of n-alkane (up to n-dodecane), cyclohexane, and methyl-, ethyl-, n-propyl and n-butyl-cyclohexane oxidation at high temperatures," 2010. [Online]. Available: http://web.stanford.edu/group/haiwanglab/JetSurF/JetSurF2.0/index.html

[158] W. P. Law and J. Gimbun, "Thermal performance enhancement of non-premixed syngas combustion in a partial combustion unit by winged nozzle: Experimental

and CFD study," *Energy*, vol. 182, pp. 148–158, 2019. [Online]. Available: https://doi.org/10.1016/j.energy.2019.06.040

[159] Z. Mei, J. Mi, F. Wang, and C. Zheng, "Dimensions of CH4-jet flame in hot O2/CO2 coflow," *Energy and Fuels*, vol. 26, no. 6, pp. 3257–3266, 2012.

[160] D. Goodwin, H. Moffat, and R. Speth, "Cantera: An Object-oriented Software Toolkit for Chemical Kinetics, Thermodynamics, and Transport Processes," *http://www.cantera.org, 2017. Version 2.3.0.*, 2017.

[161] J. Bear, S. Kakaç, B. Kilkis, and F. A. Kulacki, "Modelling transport phenomena in porous media," in *Convective Heat and Mass Transfer in Porous Media*, 1991, ch. 1, pp. 7–71.

[162] D. A. Nield, *Convection in Porous Media*, 4th ed., Springer, Ed., 2013. [Online]. Available: http://www.springerlink.com/index/10.1007/0-387-33431-9

[163] J. Maxwell, *A treatise on Electricity and Magnetism*, 1954.

[164] W. Clayton, "Constituent and composite thermal conductivities of phenolic-carbon and phenolic- graphite ablators," *AIAA Paper 71-380*, 1971.

[165] F. M. White, *Fluid Mechanics*, 4th ed. McGraw-Hill, 2001.

[166] S. V. Patankar, *Numerical heat transfer and fluid flow.* Taylor & Francis, 1980.

[167] J. O. Hirschfelder, C. F. Curtiss, and R. B. Bird, *Molecular theory of gases and liquids*, 1964.

[168] J. C. Paterson-Jones, "The mechanism of the thermal degradation of aromatic amine-cured glycidyl ether-type epoxide resins," *Journal of Applied Polymer Science*, vol. 19, no. 6, pp. 1539–1547, 1975.

[169] K. S. Chen and R. Z. Yeh, "Pyrolysis kinetics of epoxy resin in a nitrogen atmosphere," *Journal of Hazardous Materials*, vol. 49, no. 2-3, pp. 105–113, 1996.

[170] S. Montserrat, J. Málek, and P. Colomer, "Thermal degradation kinetics of epoxy–anhydride resins: I." *Thermochimica Acta*, vol. 313, no. 1, pp. 83–95, 1998.

[171] L. A. Burns, S. Feih, and A. Mouritz, "Fire-Under-Load Testing of Carbon Epoxy Composites," *Aerospace Engineering*, vol. 222, pp. 1–10, 2009.

[172] C. Branca, C. Di Blasi, A. Galgano, and E. Milella, "Thermal and kinetic characterization of a toughened epoxy resin reinforced with carbon fibers," *Thermochimica Acta*, vol. 517, no. 1-2, pp. 53–62, 2011. [Online]. Available: http://dx.doi.org/10.1016/j.tca.2011.01.034

[173] P. Tadini, N. Grange, K. Chetehouna, N. Gascoin, S. Senave, and I. Reynaud, "Thermal degradation analysis of innovative PEKK-based carbon composites for high-temperature aeronautical components," *Aerospace Science and Technology*, vol. 65, pp. 106–116, 2017. [Online]. Available: http://dx.doi.org/10.1016/j.ast.2017.02.011

[174] E. Moukhina, "Determination of kinetic mechanisms for reactions measured with thermoanalytical instruments," *Journal of Thermal Analysis and Calorimetry*, vol. 109, no. 3, pp. 1203–1214, 2012.

[175] C. Lautenberger and C. Fernandez-pello, "A model for the oxidative pyrolysis of wood," *Combustion and Flame*, vol. 156, no. 8, pp. 1503–1513, 2009. [Online]. Available: http://dx.doi.org/10.1016/j.combustflame.2009.04.001

[176] M. Olave, A. Vanaerschot, S. Lomov, and D. Vandepitte, "Internal Geometry Variability of Two Woven Composites and Related Variability of the Stiffness," *Polymer Composites*, vol. 33, pp. 1335–1350, 2012.

[177] F. Gommer, A. Endruweit, and A. C. Long, "Quantification of micro-scale variability in fibre bundles," *Composites Part A: Applied Science and Manufacturing*, vol. 87, pp. 131–137, 2016. [Online]. Available: http://dx.doi.org/10.1016/j.compositesa.2016.04.019

[178] S. S. Park, D. K. Seo, S. H. Lee, T. U. Yu, and J. Hwang, "Study on pyrolysis characteristics of refuse plastic fuel using lab-scale tube furnace and thermogravimetric analysis reactor," *Journal of Analytical and Applied Pyrolysis*, vol. 97, pp. 29–38, 2012. [Online]. Available: http://dx.doi.org/10.1016/j.jaap.2012.06.009

[179] K. Le Manquais, C. Snape, J. Barker, and I. McRobbie, "TGA and drop tube furnace investigation of alkali and alkaline earth metal compounds as coal combustion additives," *Energy and Fuels*, vol. 26, no. 3, pp. 1531–1539, 2012.

[180] J. Zsakó, "Remarks on "A new equation for modelling nonisothermal reactions"," *Journal of Thermal Analysis*, vol. 34, no. 5-6, pp. 1489–1494, 1988.

[181] M. J. Starink, "The determination of activation energy from linear heating rate experiments: A comparison of the accuracy of isoconversion methods," *Thermochimica Acta*, vol. 404, no. 1-2, pp. 163–176, 2003.

[182] H. E. Kissinger, "Variation of peak temperature with heating rate in differential thermal analysis," *Journal of Research of the National Bureau of Standards*, vol. 57, no. 4, p. 217, 1956.

[183] T. Ozawa, "A New Method of Analyzing Thermogravimetric Data," *Bulletin of the Chemical Society of Japan*, vol. 38, no. 11, pp. 1881–1886, 1965. [Online]. Available: http://www.journal.csj.jp/doi/10.1246/bcsj.38.1881

[184] J. Flynn and L. Wall, "A quick, direct method for the determination of activation energy from thermogravimetric data," *Polymer letters*, vol. 322, no. 1211, pp. 379–400, 1966.

[185] R. Lyon, "An integral method of non-isothermal kinetic analysis," Federal Aviation Administration, Tech. Rep., 1996.

[186] J. H. Flynn, "The "temperature integral" - Its use and abuse," *Thermochimica Acta*, vol. 300, no. 1-2, pp. 83–92, 1997.

[187] N. Sbirrazzuoli, "Determination of pre-exponential factors and of the mathematical functions f(α) or G(α) that describe the react ion mechanism in a model-free way," *Thermochimica Acta*, vol. 564, pp. 59–69, 2013. [Online]. Available: http://dx.doi.org/10.1016/j.tca.2013.04.015

[188] R. Iacocca and D. Duquette, "The catalytic effect of platinum on the oxidation of carbon fibres," *Journal of Materials Science*, vol. 28, pp. 1113–1119, 1993.

[189] A. Adumitroaie and E. J. Barbero, "Beyond plain weave fabrics - II. Mechanical properties," *Composite Structures*, vol. 93, no. 5, pp. 1449–1462, 2011. [Online]. Available: http://dx.doi.org/10.1016/j.compstruct.2010.11.016

[190] A. De Fenzo, C. Formicola, V. Antonucci, M. Zarrelli, and M. Giordano, "Effects of zinc-based flame retardants on the degradation behaviour of an aerospace epoxy matrix," *Polymer Degradation and Stability*, vol. 94, no. 9, pp. 1354–1363, 2009. [Online]. Available: http://dx.doi.org/10.1016/j.polymdegradstab.2009.05.020

[191] N. Rose, M. Le Bras, S. Bourbigot, R. Delobel, and B. Costes, "Comprehensive study of the oxidative degradation of an epoxy resin using the degradation front model," *Polymer Degradation and Stability*, vol. 54, no. 2-3, pp. 355–360, 2002.

[192] "Carbon Fiber Production using a PAN Precursor," in *Carbon Fibers and their Composites*, P. Morgan, Ed. Taylor & Francis, 2005.

[193] M. K. Ismail, "On the reativity, structure, and porosity of carbon fibers and fabrics," *Carbon*, vol. 29, no. 6, pp. 777–792, 1991.

[194] M. C. Halbig, J. D. McGuffin-Cawley, A. J. Eckel, and D. N. Brewer, "Oxidation Kinetics and Stress Effects for the Oxidation of Continuous Carbon Fibers within a Microcracked C/SiC Ceramic Matrix Composite," *Journal of the American Ceramic Society*, vol. 91, no. 2, pp. 519–526, 2008.

[195] M. Newville and T. Stensitzki, "Non-Linear Least-Squares Minimization and Curve-Fitting for Python," 2018.

[196] K. V. Pochiraju, G. Tandon, and G. A. Shoeppner, *Long-Term Durability of Polymeric Matrix Composites*, 2012.

[197] W. Li, H. Huang, and X. Xu, "A coupled thermal/fluid/chemical/ablation method on surface ablation of charring composites," *International Journal of Heat and Mass Transfer*, vol. 109, pp. 725–736, 2017. [Online]. Available: http://dx.doi.org/10.1016/j.ijheatmasstransfer.2017.02.052

[198] Y. Chen, M. Motevalli, and M. A. Delichatsios, "Material Pyrolysis Properties, Part I: An Integral Model for One-Dimensional Transient Pyrolysis of Charring and Non-Charring Materials," *Combustion Science and Technology*, vol. 88, no. 5-6, pp. 309–328, 1993.

[199] E. Kim and N. Dembsey, "Engineering Guide for Estimating Material Pyrolysis Properties for Fire Modeling," *Project final Report*, no. September, p. 382, 2012.

[200] V. K. Sin and T. Y. Tong, "Comparison of numerical simulation of 2-D stagnation-point flow with similarity solution," *AIP Conference Proceedings*, vol. 1048, no. 2008, pp. 763–766, 2008.

[201] W. R. Smith and R. W. Missen, *Chemical Reaction Equilibrium Analysis: Theory and Algorithms*, reprint ed. Krieger Pub Co, 1991.

[202] A. Dasgupta, R. K. Agarwal, and S. M. Bhandarkar, "Three-dimensional modeling of woven-fabric composites for effective thermo-mechanical and thermal properties," *Composites Science and Technology*, vol. 56, no. 3, pp. 209–223, 1996.

[203] X. Maldague and S. Marinetti, "Pulse phase infrared thermography," *Journal of Applied Physics*, vol. 79, no. 5, pp. 2694–2698, 1996.

[204] N. Grange, K. Chetehouna, N. Gascoin, A. Coppalle, I. Reynaud, and S. Senave, "One-dimensional pyrolysis of carbon based composite materials using FireFOAM," *Fire Safety Journal*, vol. 97, no. April 2017, pp. 66–75, 2018. [Online]. Available: http://linkinghub.elsevier.com/retrieve/pii/S0379711217303053

[205] G. Jiang, S. J. Pickering, G. S. Walker, N. Bowering, K. H. Wong, and C. D. Rudd, "Soft ionisation analysis of evolved gas for oxidative decomposition of an epoxy resin/carbon fibre composite," *Thermochimica Acta*, vol. 454, no. 2, pp. 109–115, 2007.

[206] T. Ahamad and S. M. Alshehri, "Thermal degradation and evolved gas analysis of epoxy (DGEBA)/ novolac resin blends (ENB) during pyrolysis and combustion," *Journal of Thermal Analysis and Calorimetry*, vol. 111, pp. 445–451, 2013.

[207] B. Schartel, A. I. Balabanovich, U. Braun, U. Knoll, J. Artner, M. Ciesielski, M. Döring, R. Perez, J. K. W. Sandler, V. Altstädt, T. Hoffmann, and D. Pospiech, "Pyrolysis of Epoxy Resins and Fire Behavior of Epoxy Resin Composites Flame-Retarded with 9,10-Dihydro-9- oxa-10-phosphaphenanthrene-10-oxide Additives," *Journal of Applied Polymer Science*, vol. 104, no. 7, pp. 2260–2269, 2007.

[208] T. Fateh, J. Zhang, M. Delichatsios, and T. Rogaume, "Experimental investigation and numerical modelling of the fire performance for epoxy resin carbon fibre composites of variable thicknesses," *Fire and Materials*, no. June 2016, pp. 307–322, 2016.

[209] E. Robert, "Mass spectrometer calibration over wide concentration ranges in multicomponent gas mixtures," *Measurement Science and Technology*, vol. 21, no. 2, p. 025102, 2009. [Online]. Available: http://iopscience.iop.org/0957-0233/21/2/025102

[210] J. A. Hubbard, A. L. Brown, A. B. Dodd, S. Gomez-vasquez, and C. J. Ramirez, "Carbon fiber composite characterization in adverse thermal environments," Sandia National Laboratory, Tech. Rep., 2011.

[211] J. R. Welty, C. E. Wicks, R. E. Wilson, and G. L. Rorrer, *Fundamentals of Momentum, Heat, and Mass Transfer*, 2008.

[212] Y. Ng, J. Tomblin, and E. Lian, "Medium Temperature, Out-of-Autoclave, Oven-Vacuum-Bag Cure Expoxy Resin Impregnated Fiber Reinforced Composite Materials, Type 36, Class 2, Grade 193, Style 3k-70-PW," National Center for Advanced Materials Performance - NIAR Wichita State University, Tech. Rep., 2017.

[213] A. Kollmannsberger, R. Lichtinger, F. Hohenester, C. Ebel, and K. Drechsler, "Numerical analysis of the temperature profile during the laser-assisted automated fiber

placement of CFRP tapes with thermoplastic matrix," *Journal of Thermoplastic Composite Materials*, vol. 31, no. 12, pp. 1563–1586, 2018.

[214] S. Hind, "Predicting and Measuring Thermal Conductivity in Carbon/Epoxy Unidirectional Tape and Textile Reinforced Composites," Ph.D. dissertation, 2010.

[215] J. Langot, P. Chavez-Gomez, M. Levesque, and E. Robert, "Modeling the thermal degradation and residual mass of a carbon fiber epoxy matrix composite with a phenomenological approach: effect of the reaction scheme," *Submitted to Fire and Materials*, pp. 1–21, 2020.

[216] ATAG, "Air Transport Action Group - Facts and Figures," 2020. [Online]. Available: https://www.atag.org/facts-figures.html

[217] S. R. Barrett, R. E. Britter, and I. A. Waitz, "Global mortality attributable to aircraft cruise emissions," *Environmental Science and Technology*, vol. 44, no. 19, pp. 7736–7742, 2010.

[218] M. Burzlaff, "Aircraft Fuel Consumption - Estimation and Visualization," Tech. Rep., 2017. [Online]. Available: http://www.fzt.haw-hamburg.de/

[219] "Bureau of Transportation Statistics," 2018. [Online]. Available: https://www.bts.dot.gov/newsroom/2018-traffic-data-us-airlines-and-foreign-airlines-us-flights

[220] L. Gornet, "Généralités sur les matériaux composites," *HAL*, 2011. [Online]. Available: https://cel.archives-ouvertes.fr/cel-00470296v1

APPENDIX A THE IMPACT OF AIRCRAFT WEIGHT REDUCTION ON MORTALITY ATTRIBUTABLE TO AIR POLLUTION

According to a recent study by Lelieveld *et al.* [1], air pollution is responsible of 8.8 million of death every year through cardiovascular and respiratory diseases, in particular due to exposition to fine particle matters (diameter ≤ 2.5 μm) and O_3. The objective of this appendix is to provide a rough estimation of the number of casualties caused by aircraft transport only, and how many lives could be spared every year if the airplane weight was reduced by 1% with the use of new lightweight materials.

Figure A.1 from Lelieveld *et al.* [1] provides an estimation of the excess mortality in the world due to air pollution. Their research showed that anthropogenic emissions from the use of fossil fuels only are responsible of 3239×10^3 deaths per year, which represents a loss of life expectancy of 1.1 years per person. It is commonly admitted that the aeronautic sector only is at the origin of 2.4% of all CO_2 emissions [4, 216]. The part of aircraft transport in surface ozone and particle matters emission is more difficult to estimate, but an order of magnitude of 1% seems reasonable according to the recent literature [2, 3]. Obviously, the location at which emissions are produced also have an influence on the hazardousness of exhaust gases. Nevertheless, emissions of aeronautic transport are potentially at the origin of $8800 \times 10^3 \times 0.01 = 88000$ deaths every year. It is worth noting that another study from 2010 [217] estimated the number of premature death per year because of aircraft operations to 8000, but it is based on an estimation of 0.8 million deaths because of anthropogenic air pollution, much lower than the casualties estimated in by Lelieveld *et al.* [1].

An aircraft fuel consumption depends, among other, on the aircraft weight and range. Figure A.2 from [218] displays the fuel consumption per payload as a function of the aircraft range. It can be read that for a range of 1600 km, which is the average non-stop flight length in 2018 [219], the fuel consumption is close to 0.3 kg of fuel for 1 kg of payload. Therefore, a reduction of 1% of aircraft weight through the use of new lightweight materials could reduce the emissions of 0.3% on this type of flight and spare 264 lives per year, which represents 3275 lives spared over the next decade with an expected traffic growth of 4.6% per year [19].

	Mortality ($\times 10^3$/year)	Deaths per 100 000 (year^{-1})	YLL ($\times 10^6$/year)	LLE (years)	Avoidable LLE (years)	Avoidable mortality ($\times 10^3$/year)	Mortality for disease categories ($\times 10^3$/year)					
							LRI	COPD	LC	CEV	IHD	Other NCD
Africa	957	81	40.0	3.1	0.7	230	378	36	7	113	224	199
East Asia	3112	196	67.4	3.9	3.0	2403	204	511	300	738	779	580
South Asia	2809	119	83.6	3.3	1.9	1660	478	509	61	383	981	397
West Asia	544	94	14.6	2.3	1.0	241	50	27	19	76	292	80
Europe	790	133	14.3	2.2	1.7	608	54	49	54	64	313	256
Australia	14	47	0.3	0.8	0.2	3	0.6	0.8	0.9	0.6	4	7
North America	360	74	7.5	1.4	1.1	294	24	40	24	14	112	146
South America	207	42	5.3	1.0	0.5	115	30	14	6	14	63	80
World	8793	120	233	2.9	1.7	5554	1218	1187	472	1403	2768	1745

Avoidable LLE and mortality were calculated by removing anthropogenic emissions in the model. Australia also includes other islands of Oceania. Data for all countries, including 95% uncertainty intervals, are given in the Supplementary material online, *Tables* (overall uncertainty about ±50%).
CEV, cerebrovascular disease; COPD, chronic obstructive pulmonary disease; IHD, ischaemic heart disease; LC, lung cancer; LLE, loss of life expectancy; LRI, lower respiratory infections; NCD, non-communicable diseases; YLL, years of life lost.
[a]Excess mortality expresses the number of deaths over a given period that would not occur in the absence of exposure.

Figure A.1 Excess mortality attributable to ambient air pollution (from [1])

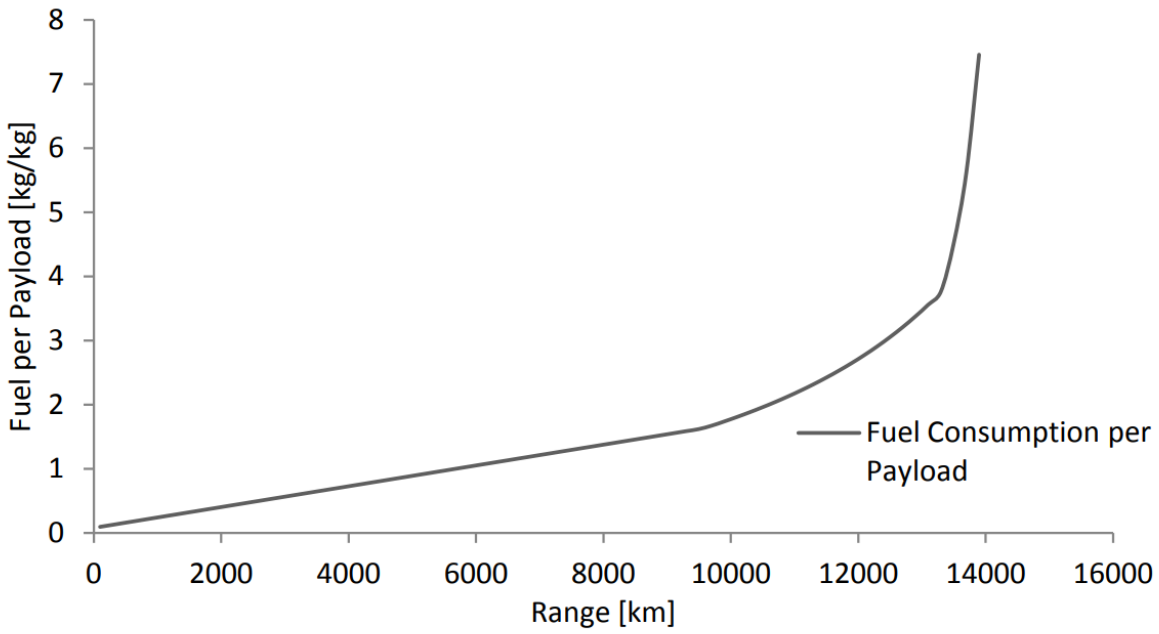

Figure A.2 Fuel consumption per aircraft payload as a function of flight range [218]

APPENDIX B INTRODUCTION TO COMPOSITE MATERIALS

A composite is a combination of at least two non-miscible materials, usually a matrix and a reinforcement. The main advantage of composites is the possibility to tailor their properties to a specific need through the choice and assembly of the different phases, yielding properties very different to those of each phase alone. The matrix surrounds the other materials and ensures the cohesion of the composite. Figure B.1 presents the different categories of matrices. Composites can be classified according to their matrix: polymer- (PMC), metal- (MMC) or ceramic-based (CMC). On one hand, MMC and CMC are generally heavier, brittler and more expensive than PMC and as such are mostly used in niche applications. On the other hand, PMCs are the most popular given their versatility and easier manufacturing processes and can advantageously be used in an airplane fuselage. For this reason, this thesis focuses on PMCs. The resins used in PMCs can be divided in thermosets (mostly amorphous) and thermoplastics (semi-crystalline and amorphous). The main difference between them lies in the method to build the polymer from the monomer. A thermoset resin is made of macromolecular three-dimensional compounds irreversibly created by the curing of a viscous resin. They cannot be reshaped once hardened. On the contrary to thermosets, thermoplastic-based composites are not created by a chemical reaction but by the reversible melting of a resin at high temperature. They can be melted to be reshaped [220].

The reinforcement is chosen to improve particular properties. It often consists in fibers, whose orientation is often chosen to enhance a property in a specific direction. The main types of fibers are carbon, glass, aramid, aromatic polyamides (Kevlar) and metal fibers, as represented in Figure B.2.

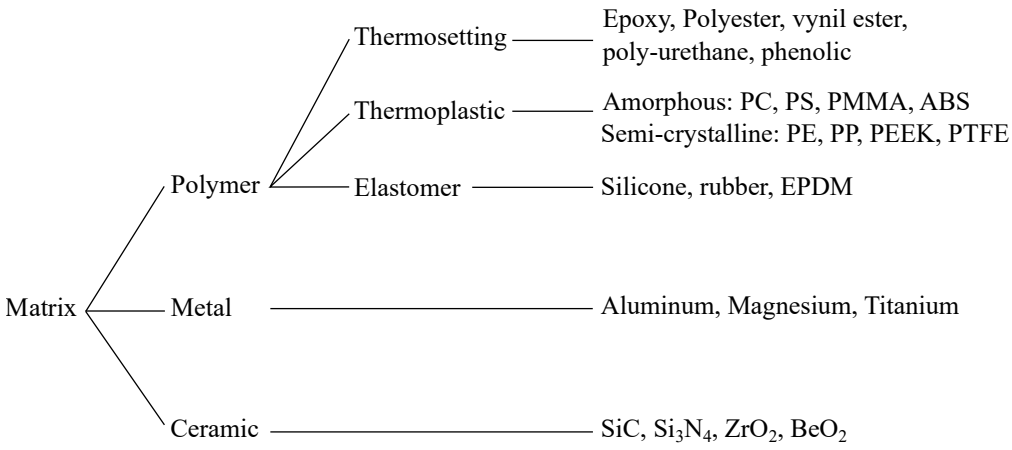

Figure B.1 Categories of matrices.

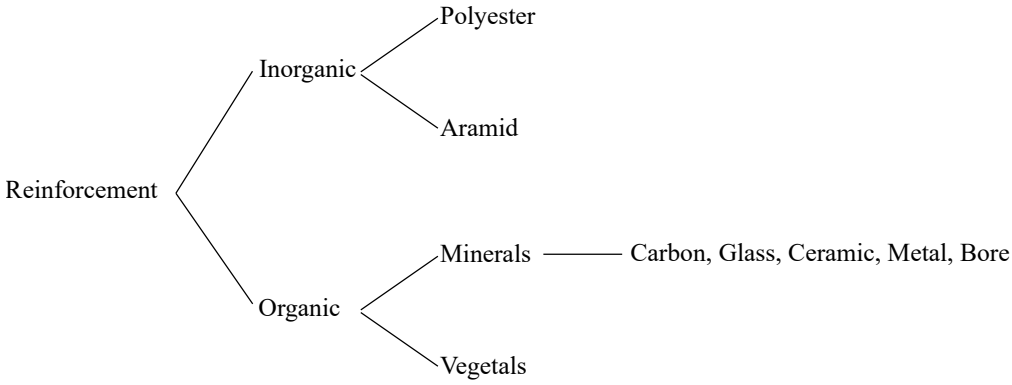

Figure B.2 Categories of fibers (adapted from [220]).

APPENDIX C MULTI-COMPONENTS APPROACH: EXAMPLE OF APPLICATION

Figure C.1 represents a control volume filled with three different phases A, B and C. The phases A and C are porous, so they contain a solid subphase (the squares containing filled circles, each of them representing 10 kg) and gas subphase (the squares containing empty circles, each of them representing 1 kg). Each small square represents $1\,m^3$. Figure C.1 is intended to be a mathematical illustration of the multi-components approach and the dimensions/masses have been chosen to ease calculation, but are of course not realistic from a physical point of view. This conceptual view advantageously provides an illustration of Equations 4.1 to 4.10 and allows to compute the parameters X_i, $\bar{\rho_i}$, $\bar{\rho}$, Y_i, ϕ_i and $\bar{\phi}$ on the control volume depicted on Figure C.1:

1. **Volume fraction**:

$$X_i = \frac{V_i}{V_{tot}} \tag{C.1}$$

$$X_{ip,p} = \frac{V_{ip}}{\sum_{i=1}^{N_p} V_{ip}} \tag{C.2}$$

The volume fraction of the solid and gaseous phases with respect to the control volume, respectively denoted by X_{is} and X_{ig}, are computed by counting the squares containing filled or empty circles in each color and dividing it by the total number of squares in the control volume, providing:

Phase	X_{is}	X_{ig}	$X_{is,s}$	$X_{ig,g}$	$X_i = X_{is} + X_{ig}$
A	4/16	2/16	4/11	2/5	6/16
B	2/16	0/16	2/11	0/5	2/16
C	5/16	3/16	5/11	3/5	8/16

It is easy to verify that $\sum_{i=1}^{N} X_i = 16/16 = 1$.

2. **Weighted bulk density**:

$$\bar{\rho_i} = \rho_i X_i \tag{C.3}$$

The weighted bulk densities of the gaseous and solid phases $\bar{\rho_{ig}}$ and $\bar{\rho_{is}}$ are computed from their volume fractions and "absolute" densities. For instance, the "absolute"

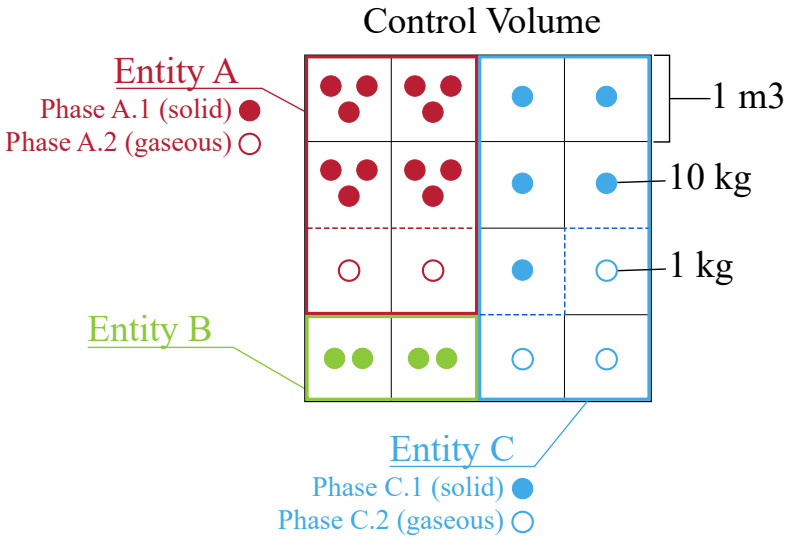

Figure C.1 Example of a control volume containing 3 phases. A square represents $1\,\mathrm{m}^3$, a filled circle 10 kg and an empty circle 1 kg

density of the solid phase As here is $\rho_{As} = 30\,\mathrm{kg\,m^{-3}}$ (because there are 3 filled red circles in one small square), providing $\bar{\rho}_{As} = \rho_{As} X_{As} = 30 \times 4/16 = 120/16\,\mathrm{kg\,m^{-3}}$. This result can be easily checked by counting the number of filled red circle and dividing it by the total volume, $16\,\mathrm{m}^3$. This method can be applied to the other phases:

Phase	$\bar{\rho}_{is}$ ($\mathrm{kg\,m^{-3}}$)	$\bar{\rho}_{ig}$ ($\mathrm{kg\,m^{-3}}$)	$\bar{\rho}_i = \bar{\rho}_{is} + \bar{\rho}_{ig}$
A	120/16	2/16	122/16
B	40/16	0/16	40/16
C	50/16	3/16	53/16

Then, the total density can be computed as:

$$\bar{\rho} = \sum_{i=1}^{N} X_i \rho_i = \sum_{i=1}^{N} \bar{\rho}_i = \frac{215}{16} \tag{C.4}$$

$$\bar{\rho}_g = \sum_{i=1}^{N_g} \bar{\rho}_{ig} = \frac{5}{16} \tag{C.5}$$

$$\bar{\rho}_s = \sum_{i=1}^{N_s} \bar{\rho}_{is} = \frac{210}{16} \tag{C.6}$$

$$\tag{C.7}$$

3. **Mass fraction**

$$Y_i = X_i \frac{\rho_i}{\bar{\rho}} \tag{C.8}$$

$$Y_{ip,p} = X_{ip} \frac{\rho_{ip}}{\bar{\rho}_p} \tag{C.9}$$

The mass fraction is computed from the volume fraction and absolute density of phase i, and total effective density. For instance, $Y_{As} = X_{As}\rho_{As}/\bar{\rho} = 4/16 \times 30 \times 16/215 = 120/215$. The mass fraction of other phases is:

Phase	Y_{is}	$Y_{is,s}$	Y_{ig}	$Y_{ig,g}$	$Y_i = Y_{is} + Y_{ig}$
A	120/215	120/210	2/215	2/5	122/215
B	40/215	40/210	0/215	0/5	40/215
C	50/215	50/210	3/215	3/5	53/215

It is worth noting that $\sum_{i=1}^{N} Y_i = 1$.

4. **Porosity**:

$$\phi_i = 1 - \frac{\bar{\rho}_{is}}{\bar{\rho}_{is,0}} = \frac{X_{ig}}{X_i} \tag{C.10}$$

where $\bar{\rho}_{i0}$ is the effective density of the non-porous phase i over control volume, that is the density of the solid subphase if it totally filled the volume occupied by phase i. It is given by $\bar{\rho}_{is,0} = \bar{\rho}_{is}X_i/X_{is}$. It provides:

Phase	ϕ_i
A	2/6
B	0
C	3/8

The porosity of each phase can be estimated directly from Figure C.1 by dividing the number of squares containing an empty circle by the total number of squares contained in the phase, which allows to check the results.
Finally, the total effective porosity of the control volume is given by:

$$\bar{\phi} = \sum_{i=1}^{N} X_i \phi_i = \sum_{i=1}^{N} X_{ig} = \frac{5}{16} \tag{C.11}$$

APPENDIX D APPLICATION OF THE CONSERVATION EQUATION TO THE CONTROL VOLUME

This appendix illustrates the control volumes used to derive the conservation equations developed in Section 4.2.1. The conservation equation are reminded at the top of each table. The figures on the left depict the control volume and in red the phase(s) on which the conservation equation is applied, according to the convention introduced in Figure C.1. The terms corresponding to the general conservation equation 4.33 are identified on the right side. The first table is the general conservation equation and the control volume on which it is applied.

General conservation equation of the intensive property β:

$$\frac{\partial \rho\beta}{\partial t} + \frac{\partial \rho v\beta}{\partial x} = \frac{\partial}{\partial x}\left(\Gamma_\beta \frac{\partial \beta}{\partial x}\right) + S_\beta$$

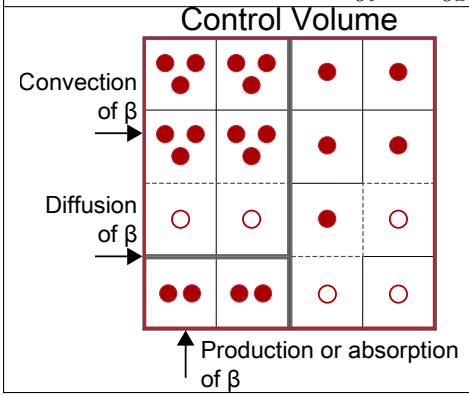

- $\rho = \rho$
- $m = m$
- $B = B$
- $\beta = \frac{\partial B}{\partial m}$

Conservation of solid species:

$$\frac{\partial \bar{\rho_{is}}}{\partial t} = \sum_{j=1}^{N_r} \theta_{ij} k_j$$

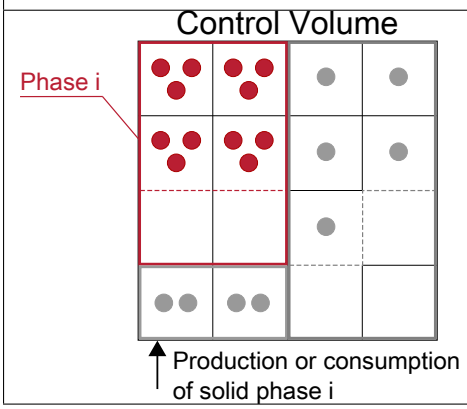

- $\rho = \bar{\rho}_s$
- $m = m_s$
- $B = m_{is} = Y_{is,s} m_s$
- $\beta = \frac{\partial B}{\partial m} = Y_{is,s}$

Conservation of gas phase:

$$\frac{\partial \rho_g \bar{\phi}}{\partial t} + \frac{\partial \rho_g \bar{\phi} v}{\partial x} = \sum_{i=1}^{N_p} \sum_{j=1}^{N_r} \theta_{ij} k_j$$

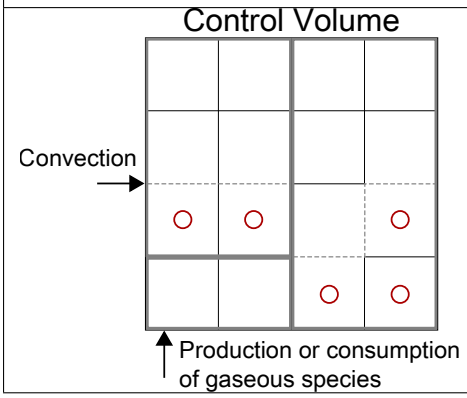

- $\rho = \bar{\rho}_g$
- $m = m_g$
- $B = m_g$
- $\beta = \frac{\partial B}{\partial m} = 1$

Conservation of gas species:

$$\bar{\phi} \rho_g \frac{\partial Y_{ig,g}}{\partial t} + \dot{m}_g \frac{\partial Y_{ig,g}}{\partial x} = \frac{\partial}{\partial x} \left(\bar{\phi} \rho_g D \frac{\partial Y_{ig,g}}{\partial x} \right) + \sum_{j=1}^{N_r} \theta_{ij} k_j$$

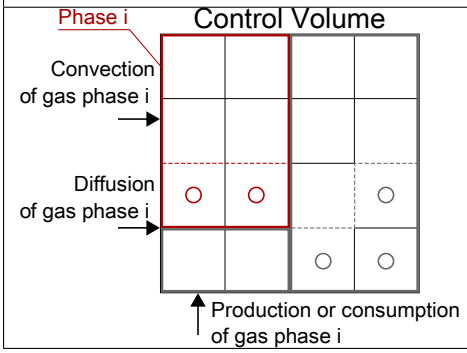

- $\rho = \bar{\rho}_g$
- $m = m_g$
- $B = m_{ig} = m_g Y_{ig,g}$
- $\beta = \frac{\partial B}{\partial m} = Y_{ig,g}$

Conservation of energy:

$$\bar{\rho}\bar{c_p}\frac{\partial T}{\partial t} + \dot{m}_g \bar{c_{pg}}\frac{\partial T}{\partial x} = \frac{\partial}{\partial x}\left(\bar{\lambda}\frac{\partial T}{\partial x}\right) + \sum_{j=1}^{N_r} k_j q_j$$

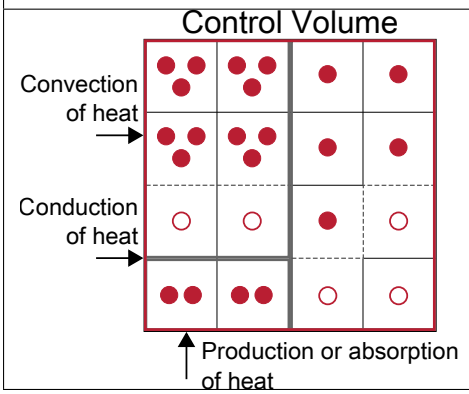

- $\rho = \bar{\rho}$
- $m = m_{cv}$
- $B = m_{cv}\bar{c_p}T$
- $\beta = \bar{c_p}T$

APPENDIX E CALCULATION OF THE ELEMENT MATRICES FOR EACH CONSERVATION EQUATION

1. **General conservation equation**:

$$\rho\frac{\partial\beta}{\partial t}+\rho v\frac{\partial\beta}{\partial x}=\frac{\partial}{\partial x}\left(\Gamma_\beta\frac{\partial\beta}{\partial x}\right)+S_\beta \tag{E.1}$$

Interpolation function:

$$\underline{\boldsymbol{\psi}}^{eT}(x) = \begin{bmatrix}\frac{l-x}{l} & \frac{x}{l}\end{bmatrix} \tag{E.2}$$

$$\frac{\partial\underline{\boldsymbol{\psi}}^{eT}(x)}{\partial x} = \begin{bmatrix}-\frac{1}{l} & \frac{1}{l}\end{bmatrix} \tag{E.3}$$

Element matrices:

$$\underline{\underline{\boldsymbol{C}}}^e=\int_0^l \underline{\boldsymbol{\psi}}_e^T(x)\rho\underline{\boldsymbol{\psi}}_e(x)\,dx=\frac{\rho l}{3}\begin{bmatrix}1 & 1/2\\ 1/2 & 1\end{bmatrix} \tag{E.4}$$

$$\underline{\underline{\boldsymbol{K}}}_1^e=\int_0^l \underline{\boldsymbol{\psi}}_e^T(x)\dot{m}_g\frac{\partial\underline{\boldsymbol{\psi}}_e(x)}{\partial x}\,dx=\frac{\dot{m}_g}{2}\begin{bmatrix}-1 & 1\\ -1 & 1\end{bmatrix} \tag{E.5}$$

$$\underline{\underline{\boldsymbol{K}}}_2^e=\int_0^l \frac{\partial\underline{\boldsymbol{\psi}}_e^T(x)}{\partial x}\Gamma_\beta\frac{\partial\underline{\boldsymbol{\psi}}_e(x)}{\partial x}\,dx=\frac{\Gamma_\beta}{l}\begin{bmatrix}1 & -1\\ -1 & 1\end{bmatrix} \tag{E.6}$$

$$\underline{\boldsymbol{F}}_2^e=\int_0^l \underline{\boldsymbol{\psi}}_e^T(x)S_\beta\,dx=\frac{S_\beta l}{2}\begin{bmatrix}1\\ 1\end{bmatrix} \tag{E.7}$$

2. **Conservation of gaseous species**:

$$\bar{\phi}\rho_g\frac{\partial Y_{ig,g}}{\partial t}+\dot{m}_g\frac{\partial Y_{ig,g}}{\partial x}=\frac{\partial}{\partial x}\left(\bar{\phi}\rho_g D\frac{\partial Y_{ig,g}}{\partial x}\right)+\sum_{j=1}^{N_r}\theta_{ij}k_j \tag{E.8}$$

Element matrices:

$$\underline{\underline{\boldsymbol{C}}}^e = \frac{\phi\rho_g l}{3}\begin{bmatrix} 1 & 1/2 \\ 1/2 & 1 \end{bmatrix} \tag{E.9}$$

$$\underline{\underline{\boldsymbol{K}}}_1^e = \frac{\dot{m}_g}{2}\begin{bmatrix} -1 & 1 \\ -1 & 1 \end{bmatrix} \tag{E.10}$$

$$\underline{\underline{\boldsymbol{K}}}_2^e = \frac{\bar{\phi}\rho_g D}{l}\begin{bmatrix} 1 & -1 \\ -1 & 1 \end{bmatrix} \tag{E.11}$$

$$\underline{\boldsymbol{F}}_2^e = \frac{l}{2}\sum_{j=1}^{N_r}\theta_{ij}k_j\begin{bmatrix} 1 \\ 1 \end{bmatrix} \tag{E.12}$$

3. **Conservation of energy**:

$$\bar{\rho}\bar{c_p}\frac{\partial T}{\partial t} + \dot{m}_g\bar{c_{pg}}\frac{\partial T}{\partial x} = \frac{\partial}{\partial x}\left(\bar{\lambda}\frac{\partial T}{\partial x}\right) + \sum_{j=1}^{N_r}k_j q_j \tag{E.13}$$

Element matrices:

$$\underline{\underline{\boldsymbol{C}}}^e = \frac{\bar{\rho}\bar{c_p}l}{3}\begin{bmatrix} 1 & 1/2 \\ 1/2 & 1 \end{bmatrix} \tag{E.14}$$

$$\underline{\underline{\boldsymbol{K}}}_1^e = \frac{\dot{m}_g\bar{c_{pg}}}{2}\begin{bmatrix} -1 & 1 \\ -1 & 1 \end{bmatrix} \tag{E.15}$$

$$\underline{\underline{\boldsymbol{K}}}_2^e = \frac{\bar{\lambda}}{l}\begin{bmatrix} 1 & -1 \\ -1 & 1 \end{bmatrix} \tag{E.16}$$

$$\underline{\boldsymbol{F}}_2^e = \frac{l}{2}\sum_{j=1}^{N_r}k_j q_j\begin{bmatrix} 1 \\ 1 \end{bmatrix} \tag{E.17}$$

4. **Conservation of gas phase momentum**:

$$\frac{\partial\frac{P\bar{M}\bar{\phi}}{RT}}{\partial t} = \frac{\partial}{\partial x}\left(\frac{\bar{\kappa}}{\nu}\frac{\partial P}{\partial x}\right) + \sum_{i=1}^{N_p}\sum_{j=1}^{N_r}\theta_{ij}k_j \tag{E.18}$$

Element matrices:

$$\underline{\underline{\boldsymbol{C}}}^e = \frac{\bar{M}\bar{\phi}l}{3RT}\begin{bmatrix} 1 & 1/2 \\ 1/2 & 1 \end{bmatrix} \tag{E.19}$$

$$\underline{\underline{\boldsymbol{K}}}_2^e = \frac{\bar{\kappa}}{\nu l}\begin{bmatrix} 1 & -1 \\ -1 & 1 \end{bmatrix} \tag{E.20}$$

$$\underline{\boldsymbol{F}}_2^e = \frac{l}{2}\sum_{i=1}^{N_p}\sum_{j=1}^{N_r}\theta_{ij}k_j\begin{bmatrix} 1 \\ 1 \end{bmatrix} \tag{E.21}$$